

# **Coral calcification response to ocean warming and acidification in the southern Great Barrier Reef**

**Jung Ok Kang**

October 2013

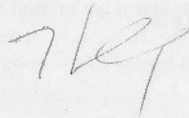
A thesis submitted for the degree of Doctor of  
Philosophy of The Australian National University



**Australian  
National  
University**

## **Declaration**

The work presented in this thesis was carried out at the Research School of Earth Sciences, The Australian National University. I certify that this thesis contains no material that has been accepted for the award of any degree or diploma at any other university. All data, interpretation and conclusions are my own, except where otherwise acknowledged.



Jung Ok Kang  
October 2013



---

## Acknowledgements

---

Most of all, I give thanks and glory to God for giving me an ability and wisdom of carrying out this thesis.

There are many of the individuals to whom I am grateful, for advise, assistance, and support throughout the PhD. Without them, I would not be able to complete this thesis.

First of all, I wish to thank my supervisor Malcolm McCulloch for his guidance, inspiration, patience, and support during my PhD at the ANU. He gave me this invaluable opportunity to enter paleoclimate world and shared his vision of coral geochemistry with me. I also would like to express my gratitude to my supervisor, Steve Eggins, for his encouragement, ideas, and trust in my work. I could have belief in my data by his friendly praise and positive feedbacks all the time. I also would like to acknowledge Michael Gagan for providing access to his famous stable isotope facilities, welcoming attitude whenever I visited him. My thanks go to my official advisory panel, Patrick De Deckker and Bradley Opdyke, for their helps.

Thanks to amazing technical support by many people, I could get the basis of this thesis (i.e. geochemical data). Graham Mortimer generously and patiently guided me for precise PTIMS boron isotope analysis, the outcome of his endless endeavor, and offered me whatever I want in the lab (not only column and solutions but also answers for my questions). Les Kinsley always kindly contributed his extensive knowledge and experience of LA-ICPMS and TIMS. It was the most comfortable time for me during my PhD when I sat down in front of the machines thanks to him. Joe Cali, Heather Scott-Gagan, Joan Cowley and Linda McMorrow have all been willing to share and teach their knowledge and put my convenience first.

There are two individuals that I must truly express my gratitude for their wonderful friendship that made my PhD pleasant: Juan Pablo D'Olivo Codero and Heejin Jeon. Without a doubt, Juan Pablo incredibly helped me to become a coral person by his entertaining mature guide to the basic interpretation of coral records at the beginning

and many challenging discussions at the end. Heejin was the only person who could encourage and comfort with girls' talk in Korean and the time we spending together in RSES and Prague would be never forgotten.

I wish to offer special thanks to Julie Trotter who shared her boron-pH equation and spent her precious time for checking my boron-pH data and comments. My special thanks also go to Chantal Alibert for her insightful comments and instrumental information derived by an unbelievable data searching ability. For the field trip to the southern GBR there are numerous of you to thank, in particular Julie and Stewart Fallon. There is a big thank to Jennie Mallela for her proofreading of my manuscripts and friendship. A special thank you also goes to Stacy Jupiter for generous providing two southern Great Barrier Reef coral samples and even her hard drive filled with all her precious work.

I would also like to broadly thank the Earth Environment group, the members of marine biogeochemistry team (easily Steve and Michael Ellwood's group) for opportunities presenting my coral research and also experiencing new marine carbonate area like forams and deeper area like deep-sea corals. Plus I would like to show my thanks to Susanne Hutchinson, Robyn Petch and Maree Coldrick for their endless administrative helps.

I would like to thank my first officemate, Jill Sutton, who was a best mentor at the beginning of my PhD, and the second officemate Yunxing Xue, whom suffered from my keenness during my thesis writing. Thanks to both of them, my office could have perfect atmosphere for the study. Many thanks to all those at the RSES for their smiles, encouragement, and inspiration on Earth Sciences: Julie, Kate, Anja, Charlotte, Andrea, Améé, Rebecca, Ryan, and Irina with Sasha.

My best friends in the Northern Hemisphere, Jeawon and Yunhee, deserve my gratitude for their continuous encouragement and friendship. Their enthusiastic and future-oriented life in Korea motivated me to achieve better results during my PhD. Also I would like to thank to Sang-Tea Kim who introduced me into the isotope world and guide me based on his own PhD and PostDoc experiences.

Finally, my biggest thank you goes to my family: Mom, Dad, my sisters (Jung Eun and Jung Hwa), parents-in-law, and other family members. They have been always there for me with love and support, and the belief that I could do it. In particular, I would like to thank my wonderful husband and fellow, Jung-Woo Park, whom shared the best and worst moments in Canberra. He provided everything what I need during my PhD including; encouragement, and academic advice, and tennis skill for my health. His genialness, praise, and love could overwhelm my annoyance and madness, and hence make this thesis exist.

---

## Abstract

---

The current unprecedented rate of increase in atmospheric greenhouse gases levels is resulting in rapid warming and acidification of the surface ocean. The effect that these changes have had and will continue to have on marine calcifiers is poorly constrained. In particular, calcification on high latitude coral reefs which lie near the limit for reef growth could be expected to respond first to changes in ocean pH and temperature. Accordingly, this study aims to determine to what extent rising temperatures and increasing ocean acidity have and will affect coral calcification in the southern Great Barrier Reef (GBR). To address this aim, long-term multiple proxy records of temperature and seawater pH were measured along with corresponding calcification rates from four *Porites sp.* corals for the period of 1834-2008.

Seasonally resolved coral proxy records reveal the significant physiological modification of temperature proxy signals and reef water chemistry during calcification process. Reconstructions of SST based on Sr/Ca and  $\delta^{18}\text{O}$  show suppressed variation compared to instrumental SST. This can be attributed to an attenuation of SST records in coral skeleton by the “bio-smoothing effect” of the living tissue layer, particularly during winter when coral growth slows. The seasonal reef water pH derived from coral  $\delta^{11}\text{B}$  is characterized by higher acidity in summer than winter with greater pH variations relative to the open ocean. This reflects changes in local reef water pH mainly due to a build-up  $\text{CO}_2$  as a result of higher coral calcification and lower wind-driven flushing efficiency in summer.

The long coral proxy records generated in this study provide direct evidence for significant ocean warming and acidification of reef waters in the southern GBR over the last 170 years. Ocean warming has occurred at a rate of  $0.055 \pm 0.052^\circ\text{C}$  per decade equivalent to  $1.0^\circ\text{C}$  over the past 170 years, and the warming rate is consistent with the global average surface temperature increase since 1850. Southern GBR reef waters have become 0.21 pH units more acidic over the same period, which is approximately a factor of two more rapid than the global surface ocean acidification rate. These long-term changes are overprinted with decadal-scale variability that is associated with ocean-atmosphere anomalies (e.g. Pacific Decadal Oscillation) in the southern GBR and the southwest Pacific.

Despite the significant increase in ocean acidity over the past 170 years, coral calcification has increased by 12% due to a concurrent increase in seawater temperature. An estimate of cumulative impact of the two competing influences on coral calcification shows that an increase in SST is a dominant factor that is controlling changes in coral calcification as atmospheric  $\text{pCO}_2$  increases. Future coral calcification in the southern GBR, based on modeled trajectories of reef water  $\text{pH}_T$  and seawater temperature changes under the IPCC  $\text{CO}_2$  emission scenarios, is projected to remain approximately constant or possibly undergo a slight decrease by the end of this century. This study provides evidence, subject to future emission scenarios, that ocean acidification has the potential to cause a sufficiently large decrease in seawater saturation state that may overwhelm the ability of corals to up-regulate the pH in their calcifying fluid and kinetic enhancement of calcification due to ocean warming.

---

## Table of Contents

---

Acknowledgements .....	i
Abstract.....	iii
Table of Contents .....	v
<b>Chapter 1. Introduction.....</b>	<b>1</b>
1.1 The aims and approach of this study .....	1
1.2 Ocean warming and acidification due to anthropogenic CO <sub>2</sub> emissions .....	2
1.3 Threats on coral reefs by ocean warming and acidification.....	3
1.4 Corals as a source of paleoclimate records .....	4
1.5 Southern Great Barrier Reef.....	6
1.6 Structure of this thesis .....	6
<b>Chapter 2. Seasonally-Resolved Coral Proxy Records of Seawater Temperature     and pH from the Southern Great Barrier Reef .....</b>	<b>9</b>
2.1 Introduction .....	9
2.2 Materials and methods .....	12
2.2.1 Coral samples and study area .....	12
2.2.2 Core treatment for geochemical analysis .....	14
2.2.3 Coral geochemistry.....	17
2.2.3.1 Trace element analyses .....	17
2.2.3.2 Coral carbon and oxygen isotope compositions .....	18
2.2.3.3 Boron isotope methods and systematics .....	18
2.2.4 Sea surface temperature (SST) .....	21
2.3. Results .....	22
2.3.1 Coral chronology construction .....	22
2.3.2 Seasonal variations of coral proxies .....	25
2.3.3 Correlation of geochemical proxies.....	27
2.4. Discussion .....	30

2.4.1 Seasonal amplitude of coral trace element records .....	30
2.4.2 Calibration of Sr/Ca- and $\delta^{18}\text{O}$ -sea surface temperature proxies .....	33
2.4.3 Seawater pH .....	40
2.5 Conclusion .....	43
<b>Chapter 3. Ocean warming in the southern Great Barrier Reef.....</b>	<b>47</b>
3.1 Introduction .....	47
3.2 Methods.....	50
3.2.1 Coral sampling .....	50
3.2.2 Geochemical analysis.....	50
3.2.3 Sea surface temperature (SST).....	52
3.2.4 Establishing chronology.....	55
3.2.5 Data manipulation .....	60
3.3 Results and discussion .....	61
3.3.1 Variations in Sr/Ca and $\delta^{18}\text{O}$ .....	61
3.3.2 Calibration of coral Sr/Ca and $\delta^{18}\text{O}$ thermometers .....	65
3.3.3 Natural and anthropogenic ocean warming in the southern GBR.....	67
3.4 Conclusion .....	72
<b>Chapter 4. Ocean acidification in the southern Great Barrier Reef.....</b>	<b>75</b>
4.1 Introduction.....	75
4.2 Materials and methods .....	79
4.2.1 Coral samples and study area.....	79
4.2.2 Core treatment for geochemical analysis .....	81
4.2.3 Coral geochemistry .....	82
4.2.3.1 Coral carbon isotope compositions .....	82
4.2.3.2 Boron isotope methods and systematics.....	82
4.2.4 Data manipulation .....	85
4.3 Results and discussion .....	86
4.3.1 $\delta^{13}\text{C}$ variation in southern GBR corals.....	86
4.3.2 $\delta^{11}\text{B}$ coral records and $\delta^{11}\text{B}$ -derived seawater pH from the southern GBR .....	91
4.3.3 The relationship between $\delta^{13}\text{C}$ and $\delta^{11}\text{B}$ coral records from the southern GBR .....	95
4.3.4 Evidence for uptake of anthropogenic $\text{CO}_2$ in the southern GBR corals .....	97
4.3.5 Natural variability in the pH of reef waters of the Coral Sea and GBR.....	103
4.3.5.1 Physical modification of reef water properties .....	103
4.3.5.2 Biological controls on interdecadal variability in seawater $\text{pH}_T$ .....	107
4.4 Conclusions.....	108
<b>Chapter 5. Coral calcification in the southern Great Barrier Reef .....</b>	<b>111</b>
5.1 Introduction.....	111
5.1.1 Coral calcification, ocean warming and acidification.....	112
5.1.1.1 Rising temperature of the ocean and coral calcification.....	112
5.1.1.2 Ocean acidification and coral calcification.....	115

5.1.1.3 Combined effects of increasing temperature and decreasing pH due to increasing $pCO_{2atm}$ on coral calcification.....	121
5.1.2 Adapting to rising temperature and ocean acidification.....	122
5.2 Methods.....	123
5.2.1 Coral sampling and geochemical analysis.....	123
5.2.2 Coral calcification rate .....	123
5.2.2.1 Buoyant-weighting methods .....	126
5.2.2.2 Skeletal 'bulk density' .....	126
5.2.2.3 Skeletal 'micro-density'.....	128
5.2.2.4 Reproducibility of coral skeletal density measurements .....	131
5.2.3 Annual extension rate .....	132
5.2.4 Data manipulation .....	133
5.3 Results	133
5.4 Discussion .....	139
5.5 Conclusion.....	147
<b>Chapter 6. Coral calcification response to increasing ocean temperature and acidity in the southern Great Barrier Reef .....</b>	<b>151</b>
<b>References.....</b>	<b>165</b>
<b>Appendices.....</b>	<b>185</b>
Appendix A. Details of all collected coral cores from the southern GBR.....	187
Appendix B. Positive X-radiography of coral slabs.....	190
Appendix C. Boron isotope as a proxy for seawater pH.....	195
Appendix D. Coral geochemical records .....	200
Appendix E. Measured density, extension rate, and calcification records in the southern GBR.....	213



---

## Chapter 1.

### Introduction

---

#### 1.1 The aims and approach of this study

The primary aims of this study are to determine the extent of temperature increase and ocean acidification in the southern Great Barrier Reef (GBR), and how these changes have and are likely to affect coral calcification in this region. The southern GBR is expected to be highly sensitive to the effects of warming and acidification, as it is located near the low temperature and seawater pH limits for reef growth. The aims of this study are addressed by generating high-resolution, multi-proxy records of past changes in seawater pH (using  $\delta^{11}\text{B}$ ) and sea surface temperature (using Sr/Ca and  $\delta^{18}\text{O}$ ) as a means of quantifying the changes in ocean acidification and sea surface temperature that have been already experienced by corals. The proxy records are further integrated with changing rates of coral calcification, based on density and linear extension rate measurements, to examine the relationships between changing rates of coral calcification, temperature and seawater pH over inter-annual to centennial time scales.

To address the aims of this study massive corals of the genus *Porites* were sampled by taking multiple moderately long (50 to 150 cm) cores from living colonies at various reefs in the southern GBR. *Porites* corals were targeted for their longevity and because the trace element and isotopic compositions of their skeletons are

proven and widely used tools for detecting and reconstructing past environmental changes. Moreover, changes in the calcification rates of these corals can be readily estimated from measurement of their density and extensions rates, and in turn linked directly to geochemical proxy records of changes in temperature (Sr/Ca and  $\delta^{18}\text{O}$ ), salinity ( $\Delta\delta^{18}\text{O}$ ) and pH ( $\delta^{11}\text{B}$ ) recorded by in the same parts of the coral skeleton. Any changes in coral growth or reconstructed environment conditions can further be linked to the reliable growth chronologies that are preserved in these corals and, in turn, these records can be compared to and calibrated using instrumental records of environmental change.

This study has specifically sought to determine the long-term response of coral calcification to seawater temperature, and to seawater pH and aragonite saturation state. In the absence of long (more than several decade) instrumental records of ocean pH, this has entailed application of the boron isotope-seawater pH proxy using a state-of-the-art PTIMS (positive ion thermal ionization mass spectrometry) method to reconstruct seawater pH changes at sub-annual through annual to decadal timescale spanning the last 170 years.

## **1.2 Ocean warming and acidification due to anthropogenic CO<sub>2</sub> emissions**

Since the mid-eighteenth century, atmospheric carbon dioxide levels have increased by nearly 40%, from preindustrial levels of approximately 280 ppmv (parts per million volume) to 395 ppmv in 2012 (Tans and Keeling, 2013, NOAA/ESRL, [www.esrl.noaa.gov/gmd/ccgg/trends/](http://www.esrl.noaa.gov/gmd/ccgg/trends/)). This rate of CO<sub>2</sub> increase (a major greenhouse gas) can be attributed to the human activities of fossil fuel combustion and deforestation, and is at least an order of magnitude faster than has occurred for millions of years (Doney & Schimel, 2007). The present atmosphere concentration of CO<sub>2</sub> (i.e. 400 ppmv) is higher than that experienced for at least the past 800,000 years (Luthi et al., 2008). The current rate of annual mean CO<sub>2</sub> increase at Mauna Loa Observatory in Hawaii is even greater and is nearly three times faster now than in 1959 (Tans and Keeling, 2013).

In recent years global warming and climate changes due to the enhanced greenhouse effect produced by rising CO<sub>2</sub> in the atmosphere has received considerable global attention. There is now a clear scientific consensus that increasing levels of CO<sub>2</sub> in the atmosphere have caused global mean surface temperatures to rise by nearly 0.6°C over the last 140 years (IPCC, 2007a).

Approximately one third of anthropogenic carbon emissions to the atmosphere have been absorbed by the oceans (Caldeira and Wickett, 2005; Sabine et al., 2004). This is causing reduction in pH and alterations of seawater chemistry that is commonly referred to as ocean acidification. The surface ocean has become acidified by nearly 0.1 pH units below pre-industrial pH levels, which is equivalent to a 30% increase in hydrogen ion concentration (Caldeira and Wickett, 2005; IPCC, 2007b; Feely et al., 2009).

### **1.3 Threats on coral reefs by ocean warming and acidification**

Coral reefs are one of the most biologically diverse and economically important ecosystems on Earth. They occupy approximately 600,000 km<sup>2</sup> of the world's oceans, within a relatively narrow zone of tropical and subtropical oceans (Veron, 2000). Reef-building corals reside in warm and shallow waters, and are provided extra energy by the photosynthetic symbiotic algae. Coral reef growth requires higher rates of calcification than the rates of dissolution and erosion, and under the appropriate conditions are able to construct a physical framework upon which is developed an extensive underwater ecosystem. The development of calcium carbonate (CaCO<sub>3</sub>) of tropical and subtropical reefs plays a major role in the global carbon cycle with an average deposition rate of  $2.0 \times 10^{13}$  mol CaCO<sub>3</sub> yr<sup>-1</sup> over the past 5 ka (Opdyke and Walker, 1992).

Marine organisms are by definition adapted to their environment, however, changes in surface water conditions, especially rapid modifications such as ocean warming

and acidification, can have substantial direct and indirect effects on these organisms and the ecosystems in which they live. Rising concentrations of CO<sub>2</sub> in the atmosphere has two major direct impacts on corals and the reefs they build. Firstly, rising sea surface temperature (SST) due to an enhanced greenhouse effect alters the thermal conditions under which both corals and their symbiotic dinoflagellates live, resulting in changes to coral calcification rates (Coles and Jokiel, 1978). Secondly, the changes in ocean carbonate chemistry associated with ocean acidification reduce the saturation state of aragonite ( $\Omega_{\text{arag}}$ ), the principal crystalline form of calcium carbonate precipitated by corals, which is likely to cause a decline in coral calcification (Kleypas et al., 1999a; Langdon et al., 2000) and hence an overall decline in net carbonate accretion rates on coral reefs.

An understanding of the chemical processes involved when CO<sub>2</sub> is absorbed from the atmosphere and dissolves in seawater is well established. However, much less is known about the impact of rising SST and ocean acidification on coral growth and coral reef development, in particular over long-time scales.

#### **1.4 Corals as a source of paleoclimate records**

The spatial and temporal variability of seawater temperature and acidity and the potential to threaten marine ecosystems by those changes are poorly known. This is because the instrumental records of SST and particularly seawater pH are short and have poor spatial coverage. The longest available records of seawater pH span less than three decades and exist at only three sites in the world. None are available for the Great Barrier Reef.

Corals are invaluable as a source of paleoclimate records as they provide high-resolution, continuous records of ocean surface climate records ranging from several decades to centuries. Several characteristics of corals make corals ideal tools for the reconstruction of changes in environmental conditions as they have: (1) annual skeletal density bands that can provide accurate chronologies, (2) high growth rates

of around 1-2 cm a year in case of *Porites* which provide annual to subannual resolution, (3) long growth histories for individual colonies reaching up to several hundred years or longer, and (4) calcium carbonate skeletons that incorporate a range of geochemical tracer element and isotopic tracers which can be used to reconstruct local environmental conditions (Johns et al., 2009).

The ability to reconstruct past environmental changes from coral geochemical proxy records remains complicated by the need to calibrate and verify coral geochemical changes against long-term instrumental and environmental measurement records. For these reasons, this is problematic for many coral reef locations. Furthermore, trace metal and isotopic tracers can respond to a number of environmental variables at different timescales, and often the climate-related mechanisms responsible for producing changes in the coral skeleton's geochemical composition are uncertain. For example, temperature and salinity are tightly coupled on seasonal to interannual timescales, with high SST driving increased atmospheric convection and accompanying heavy rainfall in the western and central equatorial Pacific warm pool region (Johns et al., 2009). Limited understanding of the biological mechanisms for coral skeleton formation (calcification) results in additional uncertainty. These biological processes may modify how geochemical proxies for paleoclimate reconstruction are incorporated into the skeleton.

Corals have been used to make significant contributions to our understanding of natural and human-induced causes of climate change and variability in the tropical oceans. However, most published coral proxy time-series records are based on single coral cores. There is a pressing need to provide and establish the extent of replication of proxy records from specific sites and regions in order to identify the presence/absence of artifacts in individual coral core records, and to identify site and region wide environmental signals that occur in different coral core proxy records. Finally, given the rarity and difficulty of obtaining long, centennial-scale coral core records, it is essential that efforts be made to replicate records using more readily available cores that span the last several decades.

## 1.5 Southern Great Barrier Reef

To date, concern about climate and ocean chemistry changes due to rising atmospheric CO<sub>2</sub> has focused on the fate of tropical corals, with less attention given to subtropical corals which grow near the temperature, salinity, light availability, and aragonite saturation limits of coral reef development. It is possible that subtropical coral reefs may be instrumental to the survival of coral reefs through geological time as they may act as refuges for tropical corals under hotter climate regimes. It follows that understanding the sensitivity of subtropical corals to current and future environmental changes may provides insights into the future of coral reefs that could become marginal in tropical settings under future climate scenarios.

A relatively cold water environment (as low as ~20°C in August) occurs in this region due to constriction of the East Australian Current (EAC) by densely packed reefs and persistent upwelling (Kleypas and Burrage, 1994). According to a recent study at Lady Elliot Island in the southernmost GBR, intra-lagoonal seawater pH varies over a wide range on diurnal timescales from as low as 7.6 in summer to as high as 8.6 in winter, with large associated changes in  $\Omega_{\text{arag}}$  from 1.1 to 6.5 (Shaw et al., 2012). Thus the southern GBR coral study will allow investigating coral growth responses to the environmental changes under already marginal conditions for growth (i.e. below optimum temperatures, in more acidic seawater pH, and below lower aragonite saturation state due to the increased solubility of carbonates at lower temperature).

## 1.6 Structure of this thesis

This thesis comprises five main chapters. Chapter 2 summarizes intra-annual variation of high-resolution coral geochemical proxies. This includes novel seasonal variations in seawater pH reconstructed from coral skeletal boron isotopes, which are compared to local *in situ* surface ocean pH data. Chapter 3 examines the effect of increasing atmospheric pCO<sub>2</sub> on sea surface temperatures in the southern GBR over

the last 170 years through the direct comparison of instrumental and geochemical proxy data. Chapter 4 reports ocean acidification in the southern GBR and discriminates natural atmospheric-ocean influences on reef water carbon chemistry from trends in ocean chemistry due to anthropogenic influences. Chapter 5 presents changes in coral calcification rates in the southern GBR with an emphasis on methods of measuring coral calcification. Chapter 6 combines all the coral records measured in this thesis to evaluate the response of corals in the southern GBR to anthropogenic climate change and ocean acidification over the past two centuries. These responses are used to make predictions of future seawater pH change based on observation from the coral boron isotope proxy. Finally future coral calcification in the southwest Pacific is projected using the modeled seawater pH and SST based on IPCC CO<sub>2</sub> emission scenarios out to 2100.





---

## **Chapter 2.**

# **Seasonally-Resolved Coral Proxy Records of Seawater Temperature and pH from the Southern Great Barrier Reef**

---

### **2.1 Introduction**

Understanding the nature and cause of interannual, decadal and longer-term climate variability requires extension of available, relatively short, instrumental records of climate (Lough, 2004). This can be achieved through development of high-resolution, climate reconstruction from various paleoclimatic archives including tree rings, ice cores and corals. A range of different proxies have been applied to reconstruct past climate, however, none have provided a clear and consistent interpretation of past climate. Accordingly, it has become critical to develop and verify well calibrated reconstructions of relevant climate indices which are also accurately dated and of defined reliability, from which the seasonality and frequency responses can be clearly identified (Lough, 2004).

Scleractinian corals can grow continuously for many centuries and in doing so record changes in oceanographic conditions over these periods as variations in the isotopic and trace element compositions of their aragonite skeletons. Moreover, due to their high growth rates, corals can record short-term climate events (e.g. El Niño-Southern Oscillation (ENSO); Gagan et al., 2000; Linsley et al., 2004; McCulloch et al., 1994) at subannual and often seasonal resolution (Fallon et al., 2003; Fallon et al., 1999; Gagan et al., 1998). Seasonal variability of sea surface temperature, salinity, and pH

in surface reef waters is greater than in the open ocean (Dore et al., 2009). These relatively large intra-annual variations have the potential to provide important information about the response of coral growth to ocean acidification and climate change.

Oxygen isotope compositions ( $\delta^{18}\text{O}$ ) and strontium/calcium ratios (Sr/Ca) in corals have been extensively used as a source of high temporal resolution paleotemperature information over the last several decades (Alibert and McCulloch, 1997; Gagan et al., 1998; Gagan et al., 2000). However, major uncertainties surround the interpretation of these proxies due to a lack of replication and the limited understanding of the influence of biological mechanisms on them (reviewed in Lough (2004) and Jones et al. (2009)). For example, some studies have demonstrated close reproducibility of coral  $\delta^{18}\text{O}$  and Sr/Ca proxy records within the same colony or between nearby colonies (e.g. Alibert and McCulloch, 1997; Gagan et al., 1998) whereas others have revealed major disagreement (e.g. de Villers et al., 1995; Linsely et al., 1999). Such discrepancies highlight the need for improving coral-based paleoclimate records, which can be achieved by improving the reliability of coral geochemical records and by distinguishing the influence of non-climatic artifacts (e.g. physiological processes) from climatic factors through increased replication.

Boron isotope ( $\delta^{11}\text{B}$ ) systematics in marine carbonates have been used to investigate natural variation in past surface seawater pH through the glacial-interglacial cycle (Foster, 2008; Hönisch et al., 2009; Pelejero et al., 2010) and the effects of ocean acidification over centennial timescales (Pelejero et al., 2010; Pelejero et al., 2005; Wei et al., 2009). In comparison only two studies have investigated seasonal variations in coral skeleton  $\delta^{11}\text{B}$ , the results of which are inconsistent (Hemming et al., 1998; Pelejero et al., 2005). The study of seasonal  $\delta^{11}\text{B}$  variation by Hemming et al. (1998) showed  $\delta^{11}\text{B}$  isotopic enrichment during summer over 2 years of coral growth at Fanning Island. The elevated  $\delta^{11}\text{B}$  that coincides with high carbon isotope ( $\delta^{13}\text{C}$ ) was attributed to the uptake of  $\text{CO}_2$  by photosynthetic symbionts during summer high insolation. Later, Hönisch et al. (2004) reinterpreted the Fanning Island

coral records and concluded that changes in seasonal carbonate chemistry of seawater by oceanic current systems account for the seasonal variation in  $\delta^{11}\text{B}$ . In contrast, seasonal  $\delta^{11}\text{B}$  variation across one year of coral growth at Flinders Reef in the Coral Sea showed low  $\delta^{11}\text{B}$  values in summer and high  $\delta^{11}\text{B}$  in winter, and covariation with wind speed (Pelejero et al., 2005). Pelejero et al. (2005) suggested that stronger winds correlated with higher  $\delta^{11}\text{B}$  values and seawater pH in winter, and that weaker winds correlated with lower seawater pH in summer at Flinders Reef. This was interpreted as reflecting increased wind driven flushing of reef-lagoon high  $\text{pCO}_2$  waters due to coral calcification within the reef complex (Pelejero et al., 2005). Both studies are limited to single colony investigations and time spans of only 1-2 years.

Studies that employ high-resolution proxy records require chronological accuracy to allow reliable comparisons with synchronous records. Dendrochronology is a common method used in the reconstruction of coral chronology whereby calendar years are assigned to seasonal density bands. In counting density bands, it is critical to resolve the initial age, especially in the presence of indistinct or stress induced density banding. Luminescent banding, which signals terrestrial runoff events, has proved useful in cross-dating with density band age models (Hendy, 2003). However, luminescent banding is of limited application as it is restricted to inshore corals which experience significant periodic river runoff events. The matching of seasonal cycles in coral temperature proxies (e.g. Sr/Ca and  $\delta^{18}\text{O}$ ) to instrumental temperature records is an important method for high temporal resolution (subannual) paleoenvironmental studies, which can provide resolution down to a weekly/fortnightly scale (Alibert and McCulloch, 1997; Fallon et al., 1999). The current study establishes absolute chronologies for coral cores from the southern Great Barrier Reef (GBR) through a combination of dendrochronology and continuous high-resolution (<weekly) variations in trace element ratios.

In this study, we investigated Sr/Ca, Mg/Ca ratios and C and O isotope compositions in four southern Great Barrier Reef (GBR) corals to determine how these trace elements and isotopic compositions serve as indicators of the substantial seasonal

surface water changes in this region. In order to also better understand seasonal pH variation in natural reef water, this study reports multiple 5-year long, seasonally resolved coral  $\delta^{11}\text{B}$  records of seawater pH from four different coral colonies from southern GBR. The large seasonal variability observed allow the determination of how *in situ* physiological processes during calcification and seasonal climatic conditions in a natural coral reef have influence on varying seasonal coral proxy records in a skeleton and carbonate chemistry of the reef water in this region.

## 2.2 Materials and methods

### 2.2.1 Coral samples and study area

Living massive corals of the genus *Porites* were sampled from the southern GBR using underwater drilling techniques developed at the Australian National University (ANU; Alibert and McCulloch, 1997; Fallon et al., 2003; Wei et al., 2009). Two coral cores were obtained from the Pompey complex (Middle Pompey and Little Kindermar reefs) in March 2006 and two cores were collected from Lady Musgrave Island and Fitzroy Reef in October 2008 (sample sites and core details are summarized in Table 2.1; Fig. 2.1). These particular reefs are not affected by terrestrial runoff as they are well offshore; 139 km and 126 km from Mackay in the case of Middle Pompey and Little Kindermar samples, and 94 km and 116 km from Gladstone in the case of Fitzroy Reef and Lady Musgrave Island.

**Table 2.1** Description of the coral cores used in this study.

Reef	Sample ID	Latitude (°S)	Longitude (°E)	Core collecting depth (m)	Core length (cm)	Date collected	Sampling location of reef lagoon
Middle Pompey	PSC	20.99	150.51	5	150	10/03/2006	outside
Little Kindermar	PSA	21.10	150.40	5	186	9/03/2006	outside
Fitzroy Reef	FYR08-D	23.37	152.10	0.5	96.5	24/10/2008	inside
Lady Musgrave Is.	LMI08-H	23.54	152.25	7.9	143	22/10/2008	inside

The southern GBR, located between 20°S and 24°S, is one of the most topographically complex continental-shelf regions in Australia (Middleton, 1994). Part of this complexity is due to the extensive offshore reefs, which impede the flow across the outer shelf (Middleton, 1994). The continental shelf widens north of about 23°S from 80 km to more than 200 km, leaving a substantial gap between the reefs that is named the Capricorn Channel.

The Capricorn Channel separates the southern GBR into two distinct reef systems with different geomorphologies (Fig. 2.1A). To the north of the channel the Pompey complex and Swain Reefs form a broad (> 200 km east-west), densely packed reef tract. To the south of the channel the Capricorn and Bunker Reefs form a line of reefs near the outer edge of a narrow shelf (70 km; Kleypas and Burrage, 1994).

The circulation of seawater in the southern GBR is complicated by the interaction between the East Australian Current (EAC) and the shelf waters of the Capricorn Channel. The meandering of the EAC in this area develops into a cyclonic mesoscale (~100 km) eddy, and associated smaller (~10 km) eddies (Kleypas and Burrage, 1994).

#### *Pompey Complex: Middle Pompey and Little Kindermar Reefs*

The two cores sampled from the Pompey Complex were collected from the fore-reefs of the crescent shaped Middle Pompey and Little Kindermar reefs. These two reefs lie 20 km landward of and are separated from the main Pompey complex (Fig. 2.1B-1) which extends parallel to the shelf edge over a distance of 140 km. The narrow channels that cut through the Pompey Reefs reach depths exceeding 100 m.

The southeast of Middle Pompey and Little Kindermar reefs is exposed to the prevailing wind and sea conditions found within the lagoon of the GBR. The reef slope is steep, dropping off to a moderate sloping reef base composed mainly of sand, rubble and reef framework. According to the Australian Institute of Marine Science

(AIMS) Reef survey (2006-2012; <http://www.aims.gov.au/docs/data-centre/reef-monitoring-surveys.html>, hereafter referred to as the AIMS Reef survey), the benthic community is dominated by coralline/turf algae, but hard and soft corals were also common. The dominant coral form is sub-massive, but other forms such as massive, digitate, encrusting and foliose corals were also present in decreasing order of abundance.

*Capricorn-Bunker Group: Fitzroy Reef and Lady Musgrave Island*

The two cores from the Capricorn-Bunker Group were collected from intra-lagoon sites at Fitzroy Reef (Fig. 2.1B-2) and Lady Musgrave Island (Fig. 2.1B-3). Fitzroy Reef is the largest reef (36.5 km<sup>2</sup>) in the Capricorn Bunker Group and has a large and deep (6-10 m) lagoon that harbors well-developed coral communities that include a large community of branching corals on the lagoon floor (Great Barrier Reef Marine Park Authority, GRMPA, <http://www.gbrmpa.gov.au/zoning-permits-andplans/sitespecific-management/fitzroy-reef>). Although no cay is present at Fitzroy reef, an intermittent sand body often appears at low tide on the southwest end of the reef.

Lady Musgrave Island is an outer shelf lagoonal reef that covers an area of 12.5 km<sup>2</sup> (Hopley et al., 2007) and has a permanent sand cay at its southwest end. The southern and eastern perimeter of Lady Musgrave Island reef are exposed to the prevailing wind and sea conditions within the Coral Sea while the northwestern margin of this reef is sheltered from these conditions (AIMS Reef survey).

**2.2.2 Core treatment for geochemical analysis**

The 55 mm diameter coral cores from the southern GBR were sliced length-wise into 7 mm thick slabs. Those with minimal evidence of bioerosion were X-rayed to assign chronologies based on annual density banding (additional information in Appendix Table A-1 and Figs B-1 to B-4 and an example of bioerosion is shown by Appendix



Fig. B-5). The slabs were then cut along with the axes of maximum growth into lengths up to 95 mm and widths of 25 mm for laser ablation inductively coupled plasma mass spectrometry (LA-ICPMS) analysis. These coral slices were cleaned ultrasonically in ultrapure Milli-Q water and dried overnight at 40°C prior to LA-ICPMS analysis.

Coral slabs from Pompey complex, Fitzroy Reef and Lady Musgrave Island were milled along the maximum growth axes in 2-month intervals to assess seasonal variation of coral geochemical proxies (Sr/Ca, Mg/Ca,  $\delta^{18}\text{O}$ ,  $\delta^{13}\text{C}$ , and  $\delta^{11}\text{B}$ ) for the recent five years of each core; 2000-2006 in case of Middle Pompey, 2001-2006 in case of Little Kindermar, and 2003-2008 in case of Fitzroy Reef and Lady Musgrave Island. The 2-month interval samples were estimated from the distance between successive winter maximums (i.e. August to August) based on LA-ICPMS geochemical profiles (details of age modeling is in section 2.3.1). Milling of the slab surface to a depth of 0.25 mm was undertaken to clean samples prior to collecting samples for analysis by further milling to a depth of 2.5 mm. Two different drill bits were used depending on the annual extension rate of the cores, in order to obtain sufficient coral powder for all stable isotope measurements (i.e. >100 mg); a 4 mm bit for Middle Pompey, Fitzroy Reef and Lady Musgrave Island which have high annual extension rates and a 6 mm bit for Little Kindermar which has a low extension rate (see Appendix Figs B-1 to B-4).

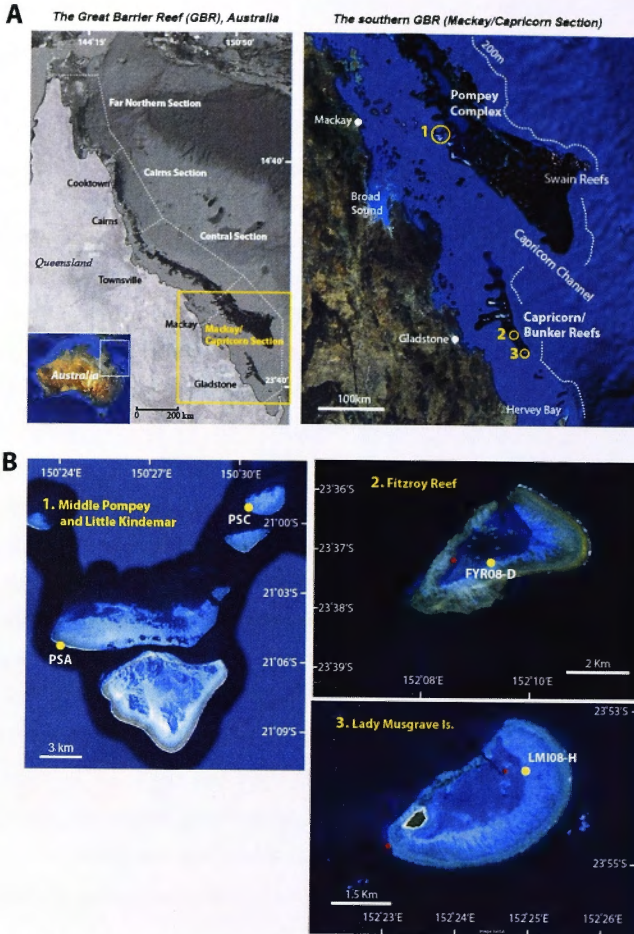


**Fig. 2.1** (A) Map of northeastern Australia showing the locations of the Great Barrier Reef (GBR) in Australia (left) and the southern GBR or Mackey/Capricorn Section (right). (B) Maps showing the location of *Porites* coral core sampling sites in the southern GBR. Yellow circles in the main map are enlarged and exhibit (1) Middle Pompey and Little Kindemar in Pompey Complex, (2) Fitzroy Reef, and (3) Lady Musgrave Island. Yellow dots represent coral collection sites and red dots show seawater-sampling sites. Images are from Google maps.

## **2.2.3 Coral geochemistry**

### **2.2.3.1 Trace element analyses**

The compositions of selected elements (Li, B, Mg, Ca, Mn, Sr, Y, Cd, Ba, and U) were determined over the full-length of the coral cores using LA-ICPMS, following the analytical protocols described in Fallon et al. (1999) and Sinclair et al. (1998). Laser ablation ICPMS was conducted using an ANU HelEx laser ablation system, comprising an ArF excimer laser (193 nm) coupled to a Varian 820 ICPMS via a custom-built laser ablation cell that is designed to hold two 95 mm lengths of coral core. The laser was pulsed at 5 Hz with an applied fluence of  $\sim 4 \text{ J cm}^{-2}$  and was scanned across the coral core using a rectangular ablation field ( $40 \times 400 \mu\text{m}$ ) to minimize the effect of surface morphology. A pre-ablation has undertaken to remove potential surface contamination using a 10 Hz laser pulse rate and slightly wider  $40 \times 500 \mu\text{m}$  rectangular ablation field. The scan speed was  $40 \mu\text{m s}^{-1}$  for the analysis and  $100 \mu\text{m s}^{-1}$  for pre-ablation. SRM NIST 612 glass was used for tuning the ICPMS sensitivity and for instrument calibration. Drift correction was undertaken using both SRM NIST 614 and an in-house pressed coral power, measured before and after each coral sample.

Mg, Ca, and Sr compositions of milled coral samples were measured using a Varian Vista simultaneous axial atomic emission spectrometry (ICP-AES). About 2 mg of coral powder was dissolved in 10 ml of 2% nitric acid and measured using the method of standard-sample-standard bracketing method following the protocol of Schrag (1999) and Wei et al. (2007) and measuring optimum analytical lines for Sr (407.771 nm), Mg (285.213 nm), and Ca (315.887 nm). A synthetic 'coral' reference solution was used for instrument calibration and drift correction. Repeat measurements of the reference solution indicate a reproducibility for Sr/Ca and Mg/Ca determinations over the course of this study of 0.15% RSD and 0.30% RSD respectively. Aliquots of the Davies coral in-house standard (Fallon et al., 1999) were measured every 5 unknowns to ascertain the accuracy and precision of the method. The average measured ratios for Sr/Ca ( $8.994 \pm 0.034 \text{ mmol mol}^{-1}$ ,  $1\sigma$ ) and

Mg/Ca ( $4.680 \pm 0.034 \text{ mmol mol}^{-1}$ ,  $1\sigma$ ) were determined from 125 measurements of the Davies coral powder, and agree well with the previously reported ratio values determined by isotope dilution analysis (Sr/Ca =  $8.86 \pm 0.02 \text{ mmol mol}^{-1}$  using TIMS and Mg/Ca =  $4.43 \pm 0.05 \text{ mmol mol}^{-1}$  using solution ICP-MS; Fallon et al., 1999).

### ***2.3.3.2 Coral carbon and oxygen isotope compositions***

Analyses of  $\delta^{18}\text{O}$  and  $\delta^{13}\text{C}$  were carried out following the methods described by Hendy et al. (2002) and Gagan et al. (1998). Powdered coral samples weighing 180–220  $\mu\text{g}$  were analyzed using a Kiel carbonate device connected to a dual-inlet Finnigan MAT 251 isotope ratio mass spectrometer (IRMS). The samples were reacted with 105% phosphoric acid at  $90^\circ\text{C}$ , and the  $\text{CO}_2$  generated from the reaction was purified by freezing and then vaporizing it in a double trap system using liquid nitrogen and heating lines. Primary calibration was made using National Bureau of Standards NBS 19 ( $-2.30\text{‰}$  for  $\delta^{18}\text{O}$  and  $+1.95\text{‰}$  for  $\delta^{13}\text{C}$ ), and a secondary correction was then made to Vienna Peedee belemnite (V-PDB). The standard deviation ( $1\sigma$ ) of the analysed NBS 19 standard was  $0.03\text{‰}$  for  $\delta^{18}\text{O}$  and  $0.05\text{‰}$  for  $\delta^{13}\text{C}$  ( $n = 84$ ).

### ***2.3.3.3 Boron isotope methods and systematics***

#### ***Boron Isotope analysis***

Boron purification was undertaken following chemical pretreatment to remove organic matter by reacting  $\sim 20 \text{ mg}$  of coral samples with 30%  $\text{H}_2\text{O}_2$  for at least 24 hr. The samples were then dissolved in 3 M HCl and diluted to 0.1 M with ultrapure water (Milli-Q).  $\sim 0.5 \text{ mL}$  AG50W-X8 cation exchange resin was then used to capture most of the  $\text{Ca}^{2+}$  as the digested coral solutions passed through the column. During this boron-matrix separation the solution was maintained above pH 9 to

minimize boron loss (Wei et al., 2009). Eluant from the first column was buffered with concentrated  $\text{NH}_4\text{OH}$  and then passed through an anion exchange column containing  $\sim 0.05$  mL Amberlite IRA 743 B-specific resin.  $\sim 0.2$  mL aliquots of the sample solution were loaded incrementally to allow equilibration between aliquots. The columns were then washed using 0.5 mL Milli-Q and 0.25 mL of 0.6 M NaCl ( $\text{pH} = 8$ ), and the boron released with 0.5 mL of 0.1 M HCl. As a final step, residual  $\text{Na}^+$  in the eluted boron samples was removed using  $\sim 0.1$  mL AG50W-X8 cation resin with  $\text{H}_2\text{O}$  (Trotter et al., 2011).

$\text{CsOH}$  and mannitol were added to the boron extract and then dried down at  $40\text{--}50^\circ\text{C}$  on a hotplate or under a heat lamp. Finally, the residues were dissolved in 2  $\mu\text{L}$  of 0.1 M HCl and loaded onto degassed and graphite-coated single tantalum filaments, and completely dried under a ceramic heat lamp prior to positive-ion TIMS analysis.

Boron isotope compositions of coral samples were analyzed using a Finnigan TRITON thermal ionization mass spectrometer (TIMS) by the positive-ion TIMS method. Two high mass isotopologues of B were measured at masses 309 ( $^{133}\text{Cs}_2^{11}\text{BO}^{2+}$ ) and 308 ( $^{133}\text{Cs}_2^{10}\text{BO}^{2+}$ ) in static multi-collector mode using a double Faraday cup (details of the Faraday cup setup can be found in Trotter et al. (2011)). Data collection was commenced when ion beams reached at least 300 mV, after which between 1 and 3 blocks comprising  $200 \times 3$  second cycles were measured. Following correction for the  $^{17}\text{O}$  interference on mass 309  $\text{Cs}_2\text{BO}^{2+}$  (Spivack and Edmond, 1986), the B isotope ratio ( $^{11}\text{B}/^{10}\text{B}$ ) was converted into standard  $\delta^{11}\text{B}$  notation by reference to the NIST SRM 951 boric acid composition. Analytical precision was assessed by repeat measurement of NIST SRM 951 and an in-house NEP coral powder standard. The measured  $^{11}\text{B}/^{10}\text{B}$  ratios of SRM 951 were  $4.0537 \pm 0.0004$  ( $2\sigma_{\text{mean}}$ ,  $n = 51$ ) which corresponds to a  $\delta^{11}\text{B}$  value of  $0.02 \pm 0.09\text{‰}$  ( $2\sigma_{\text{mean}}$ ). This matches the  $^{11}\text{B}/^{10}\text{B}$  ratio of  $4.0540 \pm 0.0003$  ( $2\sigma$ ) measured by N-TIMS in the same ANU laboratory (Fig. 2.2A; Wei et al., 2009). The measured  $\delta^{11}\text{B}$  of the NEP coral standard when subjected to full column processing was  $4.1592 \pm 0.0004$  ( $2\sigma_{\text{mean}}$ ,  $n = 49$ ), which corresponds to a  $\delta^{11}\text{B}$  value of  $26.06 \pm 0.11\text{‰}$  ( $2\sigma_{\text{mean}}$ , Fig. 2.2B). A seawater sample collected from the southern GBR in 2008 gave a  $\delta^{11}\text{B}$  value of

$39.75 \pm 0.11\text{‰}$  ( $2\sigma_{\text{mean}}$ ,  $n = 2$ ), which is slightly higher than the accepted  $\delta^{11}\text{B}$  for modern seawater ( $39.5\text{‰}$ ).

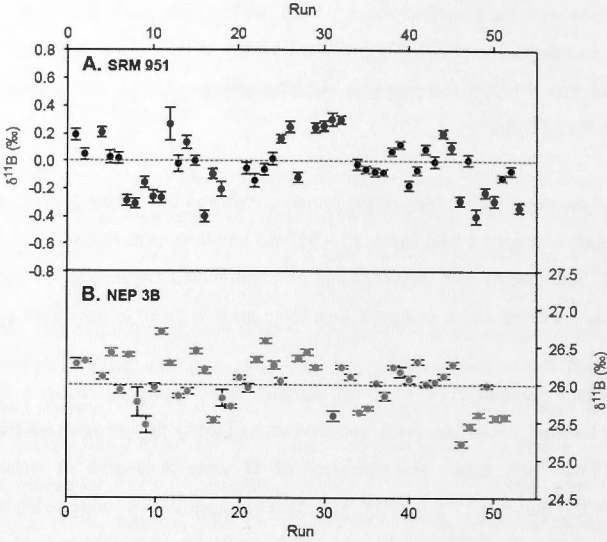


**Fig. 2.2** Analyses of  $\delta^{11}\text{B}$  of (A) international boron standard, SRM 951 following direct loading and (B) NEP 3B internal coral standard passed through all column chemistry same to coral samples during measurement using TRITON PTIMS. Dashed lines show accepted values and error bars show the analytical precision of individual analyses ( $\pm 2\sigma_{\text{mean}}$ ,  $n \geq 200$ , PTIMS cycle measurements).

### Calibration seawater pH from boron isotopic composition in coral

Measured  $\delta^{11}\text{B}$  from coral skeleton was converted to pH of calcification ( $\text{pH}_{\text{cf}}$ ) using the relationship;

$$\text{pH}_{\text{cf}} = \text{p}K_{\text{B}}^* - \log \left[ \frac{\delta^{11}\text{B}_{\text{sw}} - \delta^{11}\text{B}_{\text{carb}}}{\alpha_{\text{B3-B4}} \delta^{11}\text{B}_{\text{carb}} - \delta^{11}\text{B}_{\text{sw}} + 10^3 (\alpha_{\text{B3-B4}} - 1)} \right] \quad (2-1)$$



where  $\delta^{11}\text{B}_{\text{sw}}$  and  $\delta^{11}\text{B}_{\text{carb}}$  are the  $\delta^{11}\text{B}$  measured compositions of seawater (i.e. 39.75‰) and coral samples respectively. A  $\alpha_{\text{B}_3\text{-B}_4}$  value of 1.0272 (Klochko et al., 2006) was used and the dissociation constant of boric acid ( $\text{p}K_{\text{B}}$ ; 8.597 at 25°C and 35 PSU; Dickson, 1990) was adjusted to the ambient seawater temperature (data from AIMS *in situ* SST) and salinity reconstructed from the Sr/Ca and  $\delta^{18}\text{O}$  temperature (temperature-salinity dependent proxies) following Gagan et al. (1998; 2000) (DOE, 1994; Zeebe and Wolf-Gladrow, 2001). The calibrated  $\text{pH}_{\text{cf}}$  of seawater scale was then converted to the total scale.

The  $\delta^{11}\text{B}$  composition of coral could be modified from the  $\delta^{11}\text{B}$  values of borate ion in ambient seawater by the up-regulation of pH at the coral calcification site (Trotter et al., 2011). The  $\delta^{11}\text{B}$ -seawater pH proxy can be adjusted to account for this effect using the relationship between measured ambient seawater pH ( $\text{pH}_{\text{T}}$ ) and the assumption that the pH at the site of calcification ( $\text{pH}_{\text{cf}}$ ) is given by coral skeletal  $\delta^{11}\text{B}$  values. The ambient seawater pH ( $\text{pH}_{\text{T}}$ ) was estimated based on the relationship,  $\text{pH}_{\text{T}} = (\text{pH}_{\text{cf}} - 4.7242)/0.4664$  for *Porites cylindrica* that was fit by Trotter et al. (2011) using earlier experimental results reported by Hönisch et al. (2004) (A detailed discussion of the physiological modification of coral  $\delta^{11}\text{B}$ -seawater pH proxy is given in Chapter 4).

#### 2.2.4 Sea surface temperature (SST)

The *in situ* SST data for East Cay (152.3°E, 21.2°S) from the Australian Institute of Marine Science (AIMS; <http://www.aims.gov.au/docs/data-centre/seatemperatures.html>) was applied to the Middle Pompey and Little Kindermar coral cores. The weekly resolution record spans from November 1995 to March 2006 and ranges in temperature from 21.2 to 29.4°C. In the case of Fitzroy Reef and Lady Musgrave Island, the *in situ* SST data for Heron Island (151.5°E, 23.2°S), which ranges from 1995 to 2008 but excludes 2002 and 2003, was also taken from AIMS archives. The updated global SST from Reynold et al. (2002) was obtained at weekly resolution for the location centred at 152.5°E and 23.5°S to cover the gap in the *in situ* SST data



from 2002 to 2003 (NOAA NCDC ERSST version 3, extended Reconstructed Sea Surface Temperature Dataset centered at 152°E, 23°S; <http://www.esrl.noaa.gov/psd/data/gridded/data.noaa.ersst.html>). The Heron Island weekly SST record varies from 19.8 to 28.7°C (Fig. 2.3).

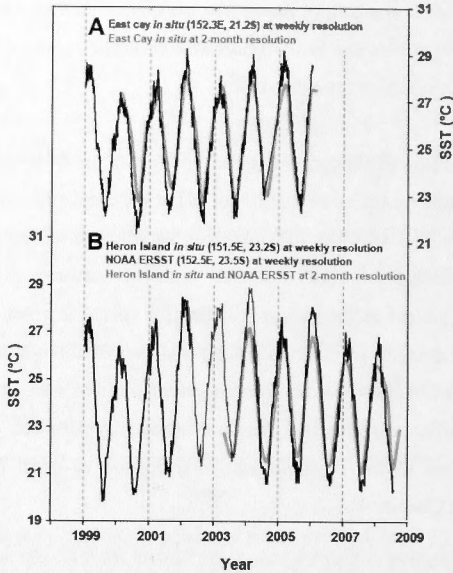


Fig. 2.3 Sea Surface temperature from (A) East Cay *in situ* data logger and (B) Heron Island *in situ* data logger and NOAA ERSST. 2-month resolution SST records are plotted for the time period when geochemical proxies are obtained at the same resolution.

## 2.3. Results

### 2.3.1 Coral chronology construction

Sr/Ca, U/Ca and B/Ca ratios measured by LA-ICPMS exhibit seasonal cycles along the full length of the coral records from the southern GBR. These cycles were used to

convert distance along the growth axis to time by matching Sr/Ca maximums to minimum SST values (assumed to correspond to mid-August) and minimum Sr/Ca to maximum SST values (assumed to correspond to mid-January) using AnalySeries 2.0 (Paillard et al., 1996). This method is based on the assumptions that Sr/Ca incorporation into coral is predominantly controlled by temperature and that coral growth is linear between these 'marker' points in time (Fallon et al., 1999).

The methodology described above produced a very good correlation between Sr/Ca and SST in the last 5-years of growth of both the Fitzroy Reef and Lady Musgrave Island cores ( $r > 0.7$ ; Figs 2.4C and D). However, the Sr/Ca cycles from Middle Pompey and Little Kindermar cores show an offset (up to 3 months) from the SST record (Figs 2.4A and B). Such offsets are typically caused by seasonal variations in growth rate which can result in a greater density of data points in summer due to faster growth than during winter (slow growth; Alibert and McCulloch, 1997; Barnes et al., 1995; Quinn et al., 1996). Similar seasonal asymmetry in coral growth is reported to have a major effect on records from high latitude corals, for example Japanese reefs at 32°N where winter temperature falls below 18°C (Fallon et al., 1999). It is generally considered to have a minor effect on coral records growing under more optimal conditions, such as the central GBR (Alibert and McCulloch, 1997; Gagan et al., 1994) or the Galápagos (Wellington et al., 1996).

In order to assess the signal distortion that might be caused by varying seasonal growth, comparisons of best fit for Sr/Ca and SST versus time were developed using the different assumptions of constant annual growth and faster summer growth (Fig. 2.4). The high-resolution Sr/Ca records from the four southern GBR corals show a non-linear growth with bias on the time axis between Sr/Ca and SST cycles. In the case of the Little Kindermar coral records, the correlation between Sr/Ca and SST becomes more significant under the assumption of faster summer growth ( $r = -0.72$ ,  $p < 0.001$ ) than constant summer and winter growth ( $r = -0.16$ ,  $p = 0.057$ ; Fig. 2.4B). The time-corrected coral trace element records based on faster summer growth were then linearly interpolated to provide measurements in equally spaced time intervals using the AnalySeries 2.0 (Paillard et al., 1996).

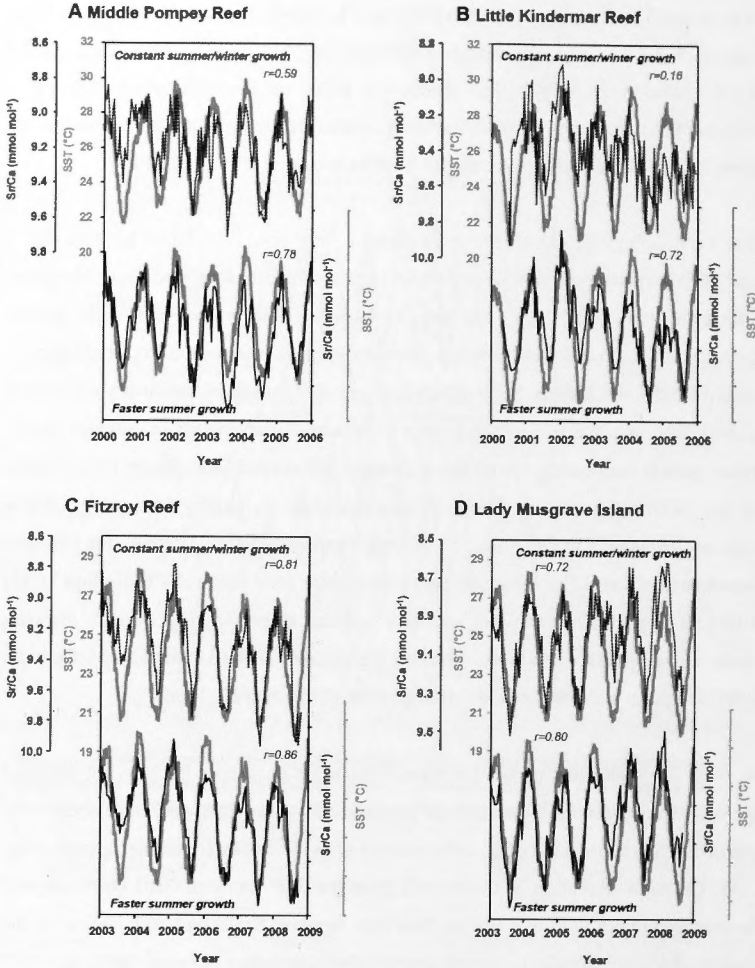


**Fig. 2.4** Sr/Ca and *in situ* SSTs vs. time for (A) Middle Pompey, (B) Little Kindermar, (C) Fitzroy Reef, and (D) Lady Musgrave Island. Datasets have been calculated using two different assumptions: uniform growth and faster growth in summer than in winter. Statistical fits for datasets based on faster summer growth show higher correlation coefficient ( $r$ ) than assumed constant growth over a year. All data are shown at 2-week resolution.

### 2.3.2 Seasonal variations of coral proxies

The isotopic compositions ( $\delta^{13}\text{C}$ ,  $\delta^{18}\text{O}$ , and  $\delta^{11}\text{B}$ ) and trace element ratios (Sr/Ca and Mg/Ca) from four *Porites* coral samples were analyzed at 2-month resolution to investigate the presence of synchronous subannual variation among the proxies and to assess the influence of environmental and physiological factors on the coral proxy records. A comparison of each of the measured proxies is shown in Fig. 2.5 and summarized in Table 2.2 (the full list of the data is presented in appendix Table D-1).

**Table 2.2** Mean proxy compositions and their standard deviations ( $1\sigma$ ) for four *Porites* cores from the southern GBR. Values have been determined for the common period (April 2003–December 2005) in all cores.

Proxies	Middle Pompey Reef	Little Kindermar Reef	Fitzroy Reef	Lady Musgrave Island
$\delta^{13}\text{C}$ (‰)	$-2.08 \pm 0.20$	$-1.92 \pm 0.31$	$-2.61 \pm 0.30$	$-2.22 \pm 0.37$
$\delta^{18}\text{O}$ (‰)	$-4.66 \pm 0.22$	$-4.38 \pm 0.21$	$-4.53 \pm 0.26$	$-4.39 \pm 0.36$
Sr/Ca (mmol mol <sup>-1</sup> )	$9.08 \pm 0.07$	$9.09 \pm 0.06$	$9.08 \pm 0.12$	$9.23 \pm 0.13$
Mg/Ca (mmol mol <sup>-1</sup> )	$4.30 \pm 0.15$	$4.52 \pm 0.32$	$4.43 \pm 0.30$	$4.55 \pm 0.26$
$\delta^{11}\text{B}$ (‰)	$24.25 \pm 0.74$	$24.48 \pm 0.59$	$23.64 \pm 0.59$	$24.25 \pm 0.50$
Seawater pH <sub>T</sub>	$8.09 \pm 0.14$	$8.11 \pm 0.11$	$8.03 \pm 0.12$	$8.11 \pm 0.11$

All geochemical temperature proxy profiles exhibit clear and synchronous annual cycles for the four coral records.  $\delta^{18}\text{O}$ , Sr/Ca and Mg/Ca co-vary with SST (Figs 2.5B to D), however, Mg/Ca shows elevated values in the uppermost part of the coral core (i.e. in the tissue zone). This likely reflects a biological influence on Mg/Ca values due to the presence of the tissue layer.  $\delta^{13}\text{C}$  and  $\delta^{11}\text{B}$  profiles display relatively poor seasonal cycles compared to the temperature proxies (Figs 2.5A and E). Seasonal variation in the  $\delta^{11}\text{B}$  records is common to the four corals with a consistent pattern of lower values in summer and higher values in winter (Fig. 2.5E). The  $\delta^{11}\text{B}$  compositions of the four coral profiles have average values of  $23.30 \pm 0.54$  ‰ ( $1\sigma$ ,  $n = 21$ ) for seasonal minima and  $24.76 \pm 0.32$  ‰ ( $1\sigma$ ,  $n = 21$ ) for seasonal maxima over the observation periods. The amplitude of these seasonal variations is consistent with previously reported data (Hemming et al., 1998) and with decadal

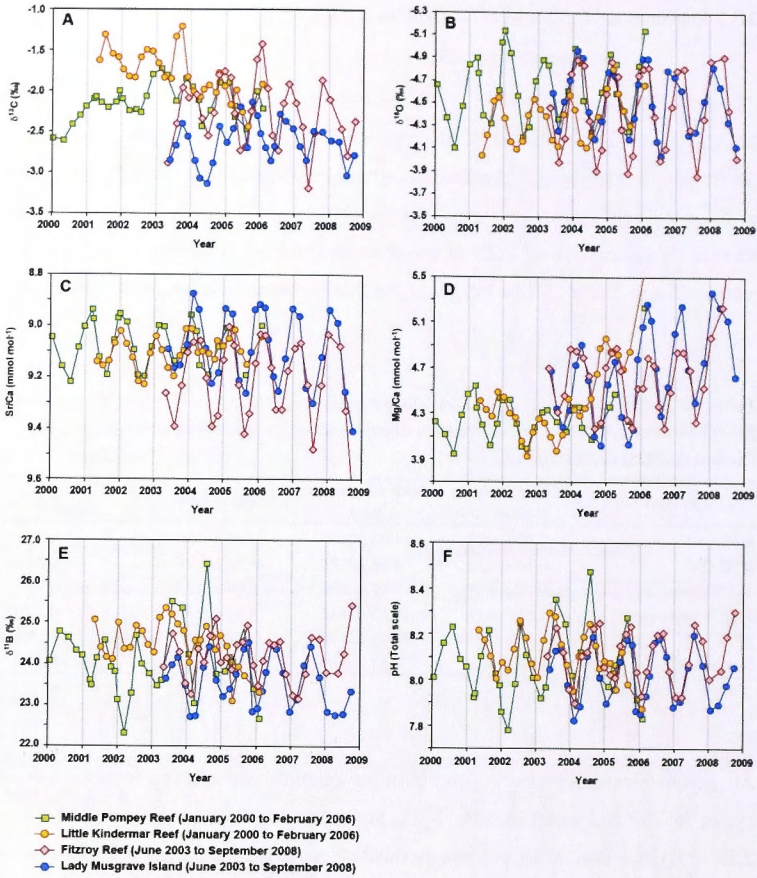


Fig. 2.5 Seasonal time series variation of coral environmental proxies from 2000 to 2008; (A)  $\delta^{13}\text{C}$ , (B)  $\delta^{18}\text{O}$ , (C) Sr/Ca, (D) Mg/Ca, (E)  $\delta^{11}\text{B}$ , and (F) seawater pH (total scale). All data points represent approximately 2-month growth intervals. Note that Sr/Ca values higher than  $9.6 \text{ mmol mol}^{-1}$  and Mg/Ca values higher than  $5.5 \text{ mmol mol}^{-1}$  which likely reflect a biological influence due to tissue layer have been omitted.  $\delta^{18}\text{O}$  and Sr/Ca axes are inverted.

scale variability (Pelejero et al., 2005). The average  $\delta^{18}\text{O}$ , Sr/Ca, and  $\delta^{11}\text{B}$  compositions of the four *Porites* corals are similar, but there are significant differences in their mean  $\delta^{13}\text{C}$  and Mg/Ca compositions (Figs 2.5A and D). The Sr/Ca and Mg/Ca profiles from Fitzroy Reef and Lady Musgrave Island show seasonal variations that are almost twice as large as those observed for the Pompey complex corals (Figs 2.5C and D), whereas the amplitude of seasonal isotopic variations of  $\delta^{18}\text{O}$  and  $\delta^{11}\text{B}$  is comparable among the colonies except for the smaller variability of the Little Kindermar  $\delta^{18}\text{O}$  record.

### **2.3.3 Correlation of geochemical proxies**

Correlations between all the geochemical proxies for all the southern GBR cores and individual corals are shown as scatterplots in Fig. 2.6. The correlation coefficients ( $r$ ) and  $p$ -values for the common periods (April 2003-December 2005) are listed in Table. 2.3.

The highest correlations ( $r \geq 0.9$ ) occur between  $\delta^{18}\text{O}$  and Sr/Ca from the composite southern GBR data and from individual locations except for the Little Kindermar coral records. Little Kindermar shows a lower correlation between  $\delta^{18}\text{O}$  and Sr/Ca than the other cores but the correlation is still significant with  $r = 0.68$ .  $\delta^{18}\text{O}$  and Sr/Ca correlate significantly with SST in the composite southern GBR and individual corals ( $r \geq -0.8$ ) but a much lower correlation is observed for Little Kindermar compared to other records ( $r = -0.60$  for  $\delta^{18}\text{O}$ ;  $r = -0.57$  for Sr/Ca) and similar relationships are observed between  $\delta^{18}\text{O}$  and Sr/Ca. This is consistent with the Sr/Ca and  $\delta^{18}\text{O}$  compositions of corals being influenced predominantly by temperature. Significant negative correlations exist between  $\delta^{18}\text{O}$  and Mg/Ca for all observed coral records ( $r = -0.60$  to  $-0.89$ ) and also between Sr/Ca and Mg/Ca with exception of the Pompey Complex coral records (ca.  $r = -0.4$ ). Positive relationships between Mg/Ca and SST are observed in all coral records except for Little Kindermar.



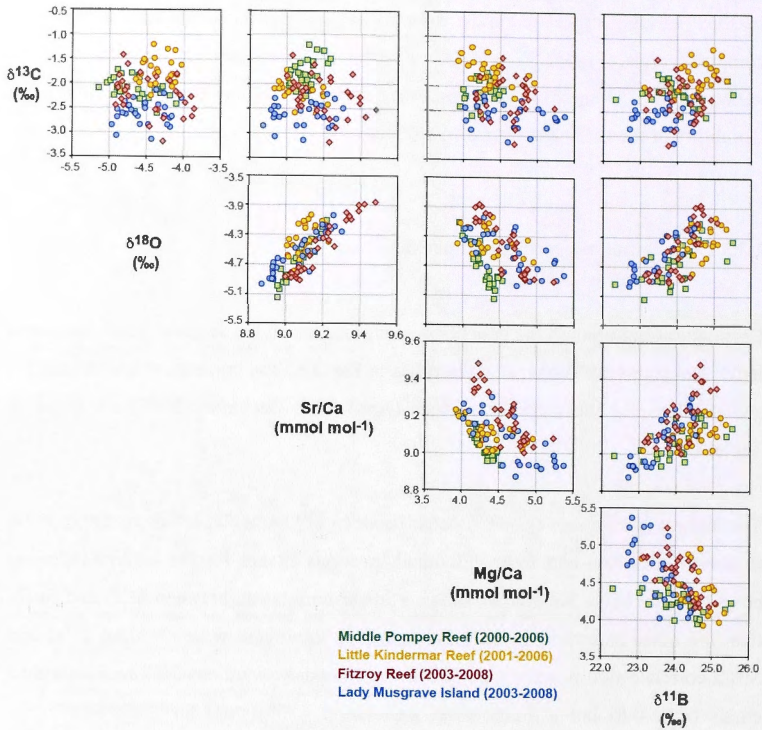


Fig. 2.6 Scatterplot matrix of proxy relationships. Statistical significance in the relationships is in Table 2.3. All data points are at 2-month resolution.

**Table 2.3** Coral proxy cross-correlations for all dataset from the southern GBR and individual reef cores based on the common period (April 2003-December 2005). The composite southern GBR data are the average of individual coral proxy records. The correlations and significance were determined using Pearson Product-moment correlation at 95% confidential level. All correlation coefficients are given as *r*-values and all statistically significant values are shown in italics where  $p < 0.05$  and in bold text where  $p < 0.01$ . Correlation that are not significant are shown with *p*-values in brackets.

	$\delta^{18}\text{O}$	Sr/Ca	Mg/Ca	$\delta^{11}\text{B}$	pH <sub>T</sub>	SST
<i>All southern GBR (n=15)</i>						
$\delta^{13}\text{C}$	-0.19 (0.49)	-0.16 (0.58)	0.00 (1.0)	0.13 (0.64)	-0.09 (0.76)	0.34 (0.21)
$\delta^{18}\text{O}$	-	<b>0.96</b>	<b>-0.86</b>	<b>0.78</b>	<b>0.91</b>	<b>-0.97</b>
Sr/Ca	-	-	<b>-0.83</b>	<b>0.77</b>	<b>0.89</b>	<b>-0.93</b>
Mg/Ca	-	-	-	<b>-0.85</b>	<b>-0.87</b>	<b>0.81</b>
$\delta^{11}\text{B}$	-	-	-	-	<b>0.95</b>	<b>-0.77</b>
pH	-	-	-	-	-	<b>-0.92</b>
<i>Middle Pompey Reef (n=15)</i>						
$\delta^{13}\text{C}$	-0.54	-0.61	0.10 (0.72)	-0.14 (0.61)	-0.27 (0.32)	0.48 (0.07)
$\delta^{18}\text{O}$	-	<b>0.92</b>	-0.59	<b>0.66</b>	<b>0.81</b>	<b>-0.92</b>
Sr/Ca	-	-	-0.39 (0.15)	<b>0.51</b>	<b>0.65</b>	<b>-0.82</b>
Mg/Ca	-	-	-	-0.57	-0.60	0.60
$\delta^{11}\text{B}$	-	-	-	-	<b>0.97</b>	<b>-0.63</b>
pH	-	-	-	-	-	<b>-0.77</b>
<i>Little Kindermar Reef (n=15)</i>						
$\delta^{13}\text{C}$	0.22 (0.44)	0.24 (0.39)	-0.62	0.60	0.48 (0.07)	-0.04 (0.87)
$\delta^{18}\text{O}$	-	<b>0.68</b>	<b>-0.63</b>	0.40 (0.14)	0.60	-0.60
Sr/Ca	-	-	-0.43 (0.11)	0.49 (0.06)	<b>0.71</b>	-0.57
Mg/Ca	-	-	-	<b>-0.64</b>	<b>-0.63</b>	0.31 (0.27)
$\delta^{11}\text{B}$	-	-	-	-	<b>0.82</b>	-0.12 (0.67)
pH	-	-	-	-	-	<b>-0.66</b>
<i>Fitzroy Reef (n=15)</i>						
$\delta^{13}\text{C}$	-0.35 (0.21)	-0.35 (0.20)	0.02 (0.94)	-0.12 (0.68)	-0.31 (0.25)	0.55
$\delta^{18}\text{O}$	-	<b>0.96</b>	<b>-0.89</b>	<b>0.78</b>	<b>0.90</b>	<b>-0.91</b>
Sr/Ca	-	-	<b>-0.91</b>	<b>0.75</b>	<b>0.87</b>	<b>-0.89</b>
Mg/Ca	-	-	-	<b>-0.82</b>	<b>-0.86</b>	<b>0.76</b>
$\delta^{11}\text{B}$	-	-	-	-	<b>0.95</b>	<b>-0.72</b>
pH	-	-	-	-	-	<b>-0.89</b>
<i>Lady Musgrave Island (n=15)</i>						
$\delta^{13}\text{C}$	0.21 (0.46)	0.16 (0.58)	-0.36 (0.18)	0.17 (0.53)	0.09 (0.76)	0.06 (0.83)
$\delta^{18}\text{O}$	-	<b>0.94</b>	<b>-0.81</b>	<b>0.85</b>	<b>0.89</b>	<b>-0.88</b>
Sr/Ca	-	-	<b>-0.86</b>	<b>0.84</b>	<b>0.89</b>	<b>-0.87</b>
Mg/Ca	-	-	-	<b>-0.80</b>	<b>-0.75</b>	0.58
$\delta^{11}\text{B}$	-	-	-	-	<b>0.98</b>	<b>-0.82</b>
pH	-	-	-	-	-	<b>-0.92</b>



The individual coral core and the composite records for the southern GBR produce significant positive correlations between  $\delta^{18}\text{O}$  and  $\delta^{11}\text{B}$  ( $r \geq 0.7$ ) and between Sr/Ca and  $\delta^{11}\text{B}$  ( $r \geq 0.5$ ).  $\delta^{11}\text{B}$  also shows a significant negative correlation with SST ( $r = -0.63$  to  $-0.82$ ) for the individual coral core records in the southern GBR. Again, no significant correlation occurs between the variables in the Little Kindermar record. The positive correlation between  $\delta^{11}\text{B}$  and Sr/Ca is similar to the seasonal variability observed in a single year record reported previously for Flinders Reef in the Coral Sea (Pelejero et al., 2005). The coupling between  $\delta^{11}\text{B}$  and both SST proxies ( $\delta^{18}\text{O}$  and Sr/Ca) suggests a physical and/or biological effect on  $\delta^{11}\text{B}$  that may be related to seasonal temperature variation.

The statistical significance of correlations between  $\delta^{11}\text{B}$ -seawater  $\text{pH}_T$  and  $\delta^{18}\text{O}$  ( $r \geq 0.8$ ) and between the seawater  $\text{pH}_T$  and Sr/Ca ( $r \geq 0.7$ ) is greater than the correlation between  $\delta^{11}\text{B}$  and the temperature proxies. The correlation of reconstructed seawater  $\text{pH}_T$  with the temperature proxies is statistically significant for the Little Kindermar coral ( $r = 0.60$  for  $\delta^{18}\text{O}$ ;  $r = 0.71$  for Sr/Ca) in contrast to the poor correlations observed between the temperature proxies and  $\delta^{11}\text{B}$  for this core. Seawater  $\text{pH}_T$  and SST also correlate strongly and have negative values ( $r = -0.66$  to  $-0.92$ ).

## 2.4. Discussion

### 2.4.1 Seasonal amplitude of coral trace element records

The annual cycles in the geochemical proxies of the four southern GBR cores, in particular the Sr/Ca and Mg/Ca records, show significant inter-colony differences in the amplitude of their seasonal fluctuations (Figs 2.5C and D). For example, the seasonal amplitude of Sr/Ca observed at Middle Pompey (and Little Kindermar) is 2 to 3 times larger than for Lady Musgrave Island (and Fitzroy Reef). This contrasts with the *in situ* weekly temperature records near the various coral core locations which show very similar seasonal variations (equivalent to about  $9^\circ\text{C}$ ; Fig. 2.2). It follows that SST variability by itself does not account the differences between the

geochemical records. Identical sampling and measurement procedures were applied to the four southern GBR coral cores so these differences are unlikely due to analysis and/or sampling artifacts (cf. Mitsuguchi et al., 2003). Mg/Ca offsets in coral records are generally considered to result from biological/metabolic differences between *Porites* colonies (Inoue et al., 2007; Mitsuguchi et al., 1996; Mitsuguchi et al., 2003; Sinclair, 2005). Several possible factors could play a role in producing the observed differences in seasonal amplitude in the different coral Sr/Ca records including other environmental variables such as salinity and pH, vital effects such as growth rate (Cohen et al., 2001; de Villiers et al., 1995; Sinclair, 2005), and the activity of symbionts (Cohen et al., 2002).

Differences in salinity and/or pH between the different coral core sites could account for the differences in seasonal amplitudes of Sr/Ca. This would necessarily produce additional variation in  $\delta^{18}\text{O}$  compositions which is a function of both temperature and salinity, and/or of  $\delta^{11}\text{B}$  which is a function largely of a seawater pH. However, no significant differences are observed in the seasonal amplitude of  $\delta^{18}\text{O}$  and  $\delta^{11}\text{B}$  variation for the all southern GBR cores, indicating similar salinity and pH variations at these different sites (Figs 2.5B and E). This implies no significant influences of salinity and seawater pH on Sr/Ca in the southern GBR cores.

Kinetic factors linked to differences in growth rate between the cores could also lead to the observed differences in the amplitude of seasonal Sr/Ca ratio variation. The extent of the kinetic effect could be related to the depths of their core heads, as might offsets between local instrumental SST and seawater temperature at these depths. However, the variation in the depths of the cored coral heads is not related to the observed variation in the seasonal amplitude in this study (Table 2.1). For example, samples obtained from depths of 0.5 m and 7.5 m show similar seasonal variations for the Fitzroy Reef and Lady Musgrave Island coral records. The Sr/Ca ratio can also be controlled kinetically by a Rayleigh distillation process between the precipitating skeleton and calcifying fluid (Cohen et al., 2006; Gaetani and Cohen, 2006; Sinclair, 2005) as well as by  $\text{Ca}^{2+}$ -ATPase pump activity (Inoue et al., 2007; Sinclair, 2005). Both mechanisms can produce lower Sr/Ca compositions with higher

growth rate (Gactani and Cohen, 2006; Sinclair, 2005), and a negative relationship between Sr/Ca and extension rates is observed for the Middle Pompey and Fitzroy Reef coral records over the common period (Fig. 2.7A). However, the results of this study do not lend support these kinetic process models as there is a positive relationship between Sr/Ca and extension rate (Fig. 2.7A) for the Lady Musgrave Island core and the four southern GBR records. There is also no difference in seasonal amplitude between Fitzroy Reef and Lady Musgrave Island corals which show up to two times differences in their growth rates. Therefore, it is unlikely that kinetic effects contribute to the variation in amplitude of the seasonal coral proxy cycles.

Cohen et al. (2002) observed the annual range of Sr/Ca variation in coral skeletons to be greater in the presence of algal symbionts. This was attributed to enhanced calcium deposition relative to strontium during active symbiont photosynthesis, thereby linking enhanced Sr/Ca variations to an increase in calcification rate (Cohen et al., 2002). As Sr/Ca ratios from the southern GBR corals do not appear to be related to extension or calcification rate (Fig. 2.7), and thus such a metabolic effect is unlikely to account for the different Sr/Ca seasonal amplitude in the different colonies.

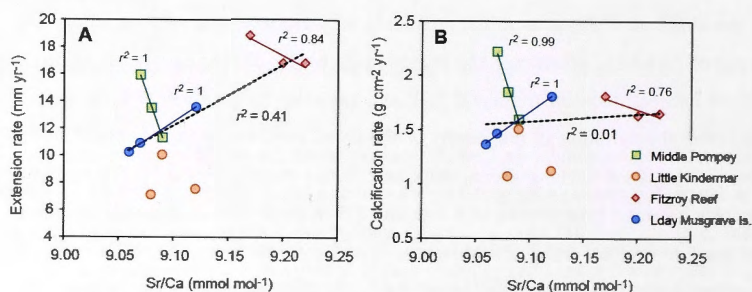


**Fig. 2.7** Annual average coral Sr/Ca compared to annual extension rates (A) and calcification rates (B) for the common time periods, April 2003–December 2005. Statistically significant regressions for each core are shown with the same color to symbols. Dashed lines are the regression fits for the composite southern GBR coral records. Details of extension and calcification rate rate calculations are given in Chapter 5.

Lastly, it is also possible that the different seasonal amplitude of Sr/Ca (and Mg/Ca) variation in the different corals might be attributed to species-specific variability within the genus *Porites*. Specimens of *Porites* are rarely identified to the species level (e.g. *P. lobata*, *P. lutea*, *P. solida*, and *P. australiensis*) due to the similar skeletal structures found in their massive colonies (Veron, 2000). Geochemical differences have been identified between the *Porites* species including differences due to reproductive behavior (McCulloch et al., 1994), effective tissue thickness and skeletal density (Lough and Barnes, 2000). These differences could generate different metabolic isotopic fractionation in  $\delta^{13}\text{C}$  while not affecting Sr/Ca variability (Alibert and McCulloch, 1997). However, the lack of any systematic seasonal change in  $\delta^{13}\text{C}$  and large differences in Sr/Ca seasonality may indicate that species-specific effects are insufficient to cause the seasonal cycle differences of Sr/Ca observed in this study.

In summary, it is not clear what factor(s) is(are) causing the different seasonal amplitude of temperature proxies (i.e. Sr/Ca) between the coral core sites. Possible influences include environmental variables such as salinity and pH, the growth-rate-related kinetic effects, the metabolic effects of symbionts photosynthesis, and the species-specific variability. None of these factors by themselves can account for the discrepancy in seasonal amplitude of coral trace element records from the southern GBR. Recently, Gagan et al. (2012) proposed that the living tissue layer produces a physiological smoothing effect that could explain the varying seasonal amplitude in the coral temperature proxy records. This smoothing effect will be discussed along with the proxy-SST calibration in the next section.

#### 2.4.2 Calibration of Sr/Ca- and $\delta^{18}\text{O}$ -sea surface temperature proxies

Sr/Ca and  $\delta^{18}\text{O}$  records are converted in practice to SST using individual empirical temperature slope calibrations. Moreover, Sr/Ca ratios ( $\text{SST}_{\text{Sr/Ca}}$ ) have often been used for  $\delta^{18}\text{O}$ -SST calibration because instrumental temperature records are limited or unavailable. In this study, three separate calibrations have been used to reconstruct

SST and are summarized in Table 2.4.

**Table 2.4** Summary of Sr/Ca-SST,  $\delta^{18}\text{O}$ -SST, and  $\delta^{18}\text{O}$ -SST<sub>Sr/Ca</sub> regressions. SST<sub>Sr/Ca</sub> is SST derived from Sr/Ca values. Calibrations are of the form,  $y = \text{intercept} + \text{slope} \times x$  ( $^{\circ}\text{C}$ ), where  $r$  is the correlation coefficient, and  $n$  is the number of points used in the regression. All data have been derived at 2-month resolution and the time period over which the analysis has been conducted is indicated for each cores.

y	x	Slope ( $\pm 1\sigma$ )	Intercep ( $\pm 1\sigma$ )	r	n	p
<i>Middle Pompey Reef (2000-2006)</i>						
Sr/Ca (mmol mol <sup>-1</sup> )	SST	-0.035 (0.003)	9.983(0.080)	0.91	28	< 0.0001
$\delta^{18}\text{O}$ (‰)	SST	-0.115 (0.008)	-1.615 (0.223)	0.93	30	< 0.0001
$\delta^{18}\text{O}$ (‰)	SST <sub>Sr/Ca</sub>	-0.108 (0.006)	-1.793 (0.163)	0.96	28	< 0.0001
<i>Little Kindermar (2001-2006)</i>						
Sr/Ca (mmol mol <sup>-1</sup> )	SST	-0.016 (0.004)	9.512 (0.094)	0.66	26	< 0.005
$\delta^{18}\text{O}$ (‰)	SST	-0.046 (0.013)	-3.195 (0.328)	0.58	26	< 0.005
$\delta^{18}\text{O}$ (‰)	SST <sub>Sr/Ca</sub>	-0.027 (0.009)	-3.677 (0.232)	0.51	26	< 0.01
<i>Fitzroy Reef (2003-2008)</i>						
Sr/Ca (mmol mol <sup>-1</sup> )	SST	-0.066 (0.006)	10.788 (0.137)	0.91	30	< 0.0001
$\delta^{18}\text{O}$ (‰)	SST	-0.168 (0.016)	-4.431 (0.391)	0.89	30	< 0.0001
$\delta^{18}\text{O}$ (‰)	SST <sub>Sr/Ca</sub>	-0.164 (0.010)	-4.534 (0.237)	0.95	30	< 0.0001
<i>Lady Musgrave Island (2003-2008)</i>						
Sr/Ca (mmol mol <sup>-1</sup> )	SST	-0.062 (0.007)	10.553 (0.160)	0.87	28	< 0.0001
$\delta^{18}\text{O}$ (‰)	SST	-0.113 (0.017)	-1.823 (0.402)	0.79	28	< 0.0001
$\delta^{18}\text{O}$ (‰)	SST <sub>Sr/Ca</sub>	-0.119 (0.011)	-1.671 (0.268)	0.90	28	< 0.0001

All three SST reconstructions show excellent correlations with *in situ* SST ( $r \geq 0.8$ ) aside from the Little Kindermar records (Fig. 2.8). The Sr/Ca-SST calibration generated the best correlation ( $r \geq 0.9$ ) with the instrumental SST of the three proxy-SSTs. There is still no single accepted coral Sr/Ca-SST calibration in the literature due to the use of different coral species, analytical methods, and instrumental SST datasets. However, the reported calibration equations for *Porites* are remarkably similar to the average regression fit obtained from multiple studies on *Porites*, that is  $\text{Sr/Ca (mmol mol}^{-1}) = 10.553 (\pm 0.585) - 0.0607 (\pm 0.0178) \times \text{SST (}^{\circ}\text{C)} (\pm 2\sigma, n = 38; \text{Corr\`ege, 2006)}$ . Interestingly, the slope values found in the Fitzroy Reef and Lady Musgrave Island coral records are within the uncertainty of this general *Porites* calibration equation, whereas Little Kindermar and Middle Pompey do not fall within the 95% probability limits of the global data set. The accuracy of the *Porites*



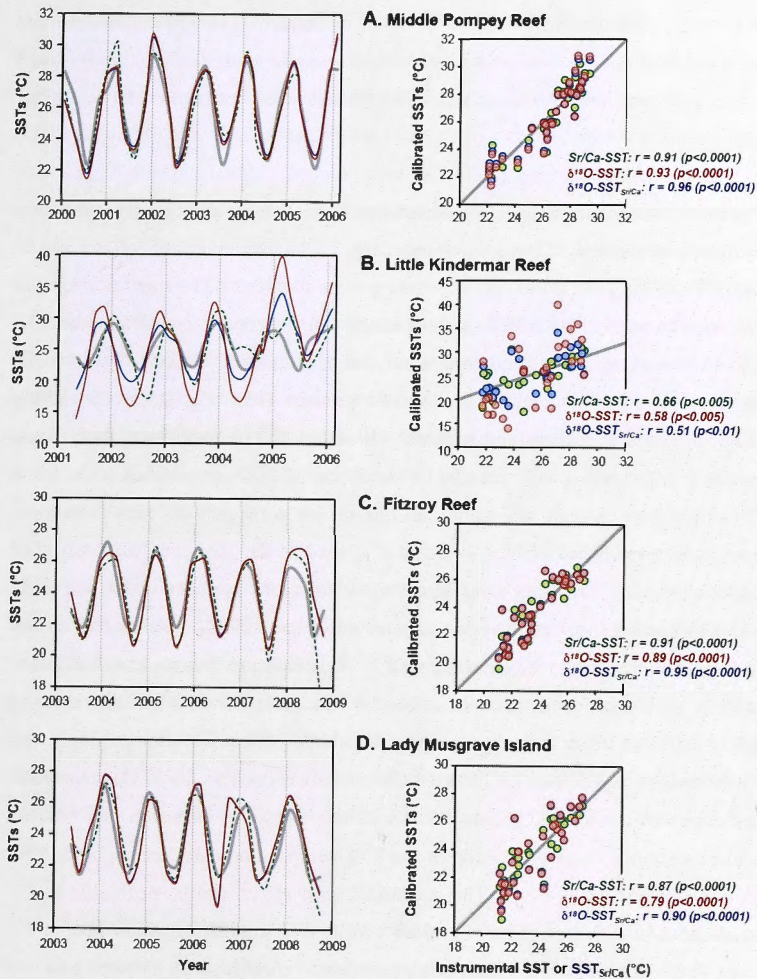


**Fig. 2.8** Comparisons of Sr/Ca- and  $\delta^{18}\text{O}$ -derived SSTs with instrumental seasonal SST records (left) and scatter plots of calibrated and measured SSTs (right); (A) Middle Pompey, (B) Little Kindermar, (C) Fitzroy Reef, and (D) Lady Musgrave Island. Sr/Ca-SST and  $\delta^{18}\text{O}$ -SST are represented by green dashed lines and red lines, and instrumental records are shown by thick grey lines.  $\delta^{18}\text{O}$  calibration incorporating Sr/Ca-derived SST ( $\delta^{18}\text{O}$ -SST<sub>Sr/Ca</sub>) is also compared with *in situ* SST (blue lines). The symbol colors used in the scatter plots are as in left figures and the grey line is the 1:1 relationship. Daily *in situ* measured SST for East Cay (21.2°S, 152.3°E; plotted with Middle Pompey (A) and Little Kindermar (B) coral records) and Heron Island (23.2°S, 151.5°E; plotted with Fitzroy Reef (C) and Lady Musgrave Island (D) coral records) from AIMS have been averaged to match the 2-month proxy resolution. The proxy-SST calibration equations obtained from each sample's empirical relationship for  $\delta^{18}\text{O}$  and Sr/Ca over the observation periods are presented in Table 3.4. The correlation ( $r$ ) obtained between the proxy-SST estimates and the instrumental SST values are also shown.

Sr/Ca-SST calibration and little variation of seawater  $\delta^{18}\text{O}$  composition (average  $\Delta\delta^{18}\text{O}$  of  $-0.01 \pm 0.13$ ,  $1\sigma$ ) in the southern GBR results in high correlation ( $r \geq 0.8$ ) between instrumental SST records and SST reconstructed from Sr/Ca and  $\delta^{18}\text{O}$  (Fig. 2.8).

The Little Kindermar proxy-SST calibrations are notable for their poorer correlation with the instrumental SST measurements (Fig. 2.7B). The ranges of the Sr/Ca-SST and  $\delta^{18}\text{O}$ -SST<sub>Sr/Ca</sub> estimates are 1.5 times greater than the SST range measured *in situ*, and the range of  $\delta^{18}\text{O}$ -SST values is almost 2 times greater. In addition, the  $\delta^{18}\text{O}$  composition of the Little Kindermar coral core is consistently heavier by 0.4 ‰ in summer than the other coral records from the southern GBR (Fig. 2.5B). Given little or no influence of salinity and seawater pH on the  $\delta^{18}\text{O}$  composition, kinetic and metabolic effects potentially account for the abnormal  $\delta^{18}\text{O}$  composition of the Little Kindermar core. Kinetic disequilibrium due to fast coral growth leads to isotopic fractionation and hence skeletal  $\delta^{18}\text{O}$  and  $\delta^{13}\text{C}$  become depleted simultaneously. The Little Kindermar coral records, however, show more enriched  $\delta^{18}\text{O}$  and  $\delta^{13}\text{C}$  compositions compared to the other core records despite indistinguishable extension rates from Lady Musgrave Island (Table 2.5). This indicates that the kinetic effect is unlikely to be a major factor in the unusual  $\delta^{18}\text{O}$  signals from Little Kindermar and that other mechanisms are required. Metabolic disequilibrium produced by photosynthesis and respiration, as a possibility, only influences the  $\delta^{13}\text{C}$  composition and depletion of the  $\delta^{13}\text{C}$  should occur with an increase in extension rate because active respiration causes depletion in the  $\delta^{13}\text{C}$  composition (McConnaughey, 1989; McConnaughey et al., 1997). This metabolic must effect also be negligible as the most enriched and depleted  $\delta^{13}\text{C}$  values appear with similar extension rate in the Little Kindermar and in the Lady Musgrave Island coral records. These results are consistent with the lack of a significant influence from kinetic and/or metabolic effects on the seasonal amplitude of Sr/Ca in different coral colonies from the southern GBR.

Gagan et al. (2012) recently explained the SST proxy records in coral skeletons by a “bio-smoothing effect” that is produced by the living tissue layer. According to a

calcification model for *Porites* (Barnes et al., 1995; Taylor et al., 1993), approximately 50% of aragonite precipitation occurs at the upper surface of a coral while the remaining 50% is distributed over the thickness of the tissue layer. As a result, the amplitudes of seasonal signals recorded in a coral skeleton are mixed and accordingly attenuated as the forming coral skeleton passes through the region of aragonite accumulation within the living tissue layer (Gagan et al., 2012). The major consequence of this “bio-smoothing” is that the sensitivities of the *Porites* coral  $\delta^{18}\text{O}$  and Sr/Ca thermometers based on regression analysis of seasonal signals are suppressed, with the effect varying between (and within) colonies depending on the relationship between skeletal growth rate, tissue layer thickness, and the distribution of skeletal mass accumulation within the tissue layer (Gagan et al., 2012). Gagan et al. (2012) demonstrated 4-65% and 4-48% attenuation of  $\delta^{18}\text{O}$ -SST and Sr/Ca-SST sensitivities (hence amplitude of variation) for different *Porites* colonies due to this bio-smoothing effect.

The time period over which the bio-smoothing effect operates is related to the effective tissue thickness (in months) which can be estimated from the ratio of the tissue thickness to the extension rate. The effective tissue thickness of the four southern GBR corals in this study was estimated to vary between 4.3 and 7.4 months (Table 2.5) and is within the established range for *Porites* in the GBR (3 to 11 months; Gagan et al., 2012). The relationship between the recorded signal amplitude and the effect of bio-smoothing on coral  $\delta^{18}\text{O}$ -SST and Sr/Ca-SST are shown in Fig. 2.9.

The  $\delta^{18}\text{O}$ -SST sensitivities found in this study are attenuated relative to a more typical sensitivity of  $-0.23\text{‰ }^{\circ}\text{C}^{-1}$ , and are only about 50% of this value for Middle Pompey, 80% for Fitzroy Reef, and 20% for Little Kindermar (Fig. 2.9A). Similarly, the observed Sr/Ca-SST sensitivities are reduced by 50% for Middle Pompey, 20% for Fitzroy Reef, and 85% for Little Kindermar corals compared to the values observed in the absence of a bio-smoothing effect (i.e.  $-0.084 \text{ mmol mol }^{\circ}\text{C}^{-1}$ ). These observations indicate bio-smoothing has a similar effect on the sensitivities of both the  $\delta^{18}\text{O}$ -SST and Sr/Ca-SST proxies. The Lady Musgrave Island coral records show



a 20% offset of the smoothing effect between the  $\delta^{18}\text{O}$ -SST and Sr/Ca-SST sensitivities (~50% and 80% respectively). This could be attributed to the similarity between the signal attenuation period of the Lady Musgrave Island and Middle Pompey corals in the case of signal attenuation of  $\delta^{18}\text{O}$ -SST (~4-5 months; Table 2.5) or to the similar regional temperature changes corresponding to Sr/Ca-SST sensitivity of the Lady Musgrave Island and Fitzroy Reef corals.

**Table 2.5** Southern GBR core mean annual extension rate, tissue thickness, and effective tissue thickness.

Reefs	Mean linear extension (mm yr <sup>-1</sup> ) <sup>a</sup>	Tissue thickness (mm) <sup>b</sup>	Effective tissue thickness (months) <sup>c</sup>
Middle Pompey	14.59 ± 2.42	5.5	4.2
Little Kindernar	8.63 ± 1.66	7.4	10.3
Fitzroy Reef	16.66 ± 0.90	4.3	4.2
Lady Musgrave Island	9.79 ± 0.92	5.9	5.3

<sup>a</sup> Means reported with standard deviation (1 $\sigma$ ) over the observation periods of each core. Determined by the LA-ICPMS Sr/Ca profiles for Middle Pompey, Fitzroy Reef and Lady Musgrave Island coral cores, whereas B/Ca profiles were used for Little Kindernar Reef core.

<sup>b</sup> Determined by the LA-ICPMS Mg/Ca profiles

<sup>c</sup> Determined by dividing tissue thickness by extension rate (Gagan et al., 2012)

It seems plausible that the differences in amplitude of the seasonal  $\delta^{18}\text{O}$  and Sr/Ca cycles result from a combination of differing growth rates and relative tissue thickness. The largest amplitude variability occurred in  $\delta^{18}\text{O}$  cycles from Fitzroy Reef and similar variations are observed in seasonal Sr/Ca records from Fitzroy Reef and Lady Musgrave Island (Figs 2.5B and C) which have the lowest attenuation or bio-smoothing of the proxy records in their skeleton (~20%). In particular, the Little Kindernar coral displays the greatest sensitivity attenuation for both the  $\delta^{18}\text{O}$ -SST and Sr/Ca-SST. The  $\delta^{18}\text{O}$ -SST and Sr/Ca-SST amplitude recorded in this coral is only ~20% of the estimated unattenuated signal because of its low extension rate and thick tissue layer which corresponds to a very long bio-smoothing period of 10 months (Table 2.5). This degree of smoothing is sufficient to dampen the records of  $\delta^{18}\text{O}$  and Sr/Ca variability and preclude their use as sensitive thermometers.

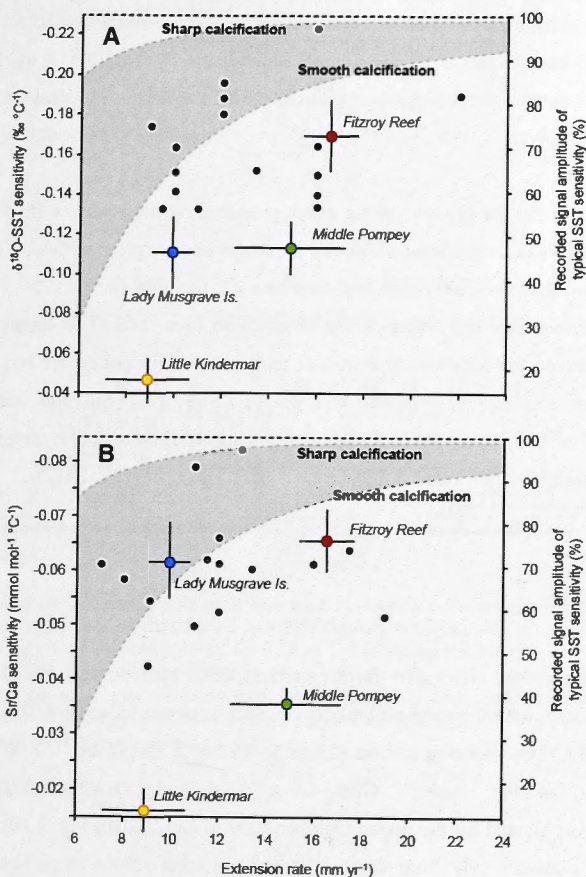


**Fig. 2.9** Modeled attenuation of an annual environmental cycle by the “bio-smoothing effect” and the impact on coral (A)  $\delta^{18}\text{O}$ -SST and (B) Sr/Ca-SST sensitivities modified from Gagan et al. (2012). Black symbols represent published  $\delta^{18}\text{O}$ -SST and Sr/Ca-SST sensitivities and the details are in Gagan et al. (2012). Color symbols indicate data from this study and error bars represent  $\pm 1\sigma$ . Dashed lines on the top of the diagrams indicate the accepted sensitivity of  $-0.23 \text{ ‰ } ^\circ\text{C}^{-1}$  for  $\delta^{18}\text{O}$  (A) and  $-0.084 \text{ mmol mol}^{-1} \text{ } ^\circ\text{C}^{-1}$  for Sr/Ca (B).

Moreover, comparisons of *in situ* SST and coral proxy SSTs from the southern GBR show greater offsets in winter than summer by a factor of two (Fig. 2.8). This suggests that the most smoothing may occur in the winter when the coral growth (extension rate) slows.

This study shows that the bio-smoothing effect produced by the effective thickness of the tissue layer has a significant impact on paleotemperature proxies. Gagan et al. (2012) indicated that two calibration end-members are required for coral  $\delta^{18}\text{O}$  and Sr/Ca paleothermometry depending on the observation time-scale. The suppressed sensitivities derived from individual empirical temperature calibrations are required for the reconstruction of seasonal changes in SST, whereas the revised sensitivities of  $\delta^{18}\text{O}$ -SST and Sr/Ca-SST calibration are required to derive centennial to millennial-scale changes in mean SST (e.g. Chapter 3; Gagan et al., 2012).

### 2.4.3 Seawater pH

The mean reconstructed  $\text{pH}_T$  values for the southern GBR cores is  $8.07 \pm 0.12$  ( $1\sigma$ ) which is consistent with the measured modern surface seawater value of  $8.07 \pm 0.03$  ( $1\sigma$ ) at the MAPCO<sub>2</sub> mooring station (23.46°S, 151.47°E, deployed ~38 km off Heron Island) in the southern GBR (data from <http://www.pmel.noaa.gov/co2/story/Heron+Island> for the period October 2009 to April 2010; Fig. 2.10). The reconstructed seawater  $\text{pH}_T$  from coral  $\delta^{11}\text{B}$  compositions shows large seasonal fluctuations ranging from 7.78 to 8.47. This is notable for being much larger than the measured seawater  $\text{pH}_T$  variation, the MAPCO<sub>2</sub> mooring data for the southern GBR (i.e.  $\text{pH}_T$  of 8.04-8.10; Fig. 2.10), by a factor of approximately ten. It is also considerably more variable than open ocean pH variability measured at three long time-series stations:  $\text{pH}_T$  values 8.08-8.12 for the Hawaii Ocean Time-Series (HOT, 23°N, 158°W; 1988-2007; Dore et al., 2009) in the North Pacific, 8.01-8.06 for the European Station Time-series in the Ocean (ESTOC, 29°N, 15°W; 1995-2004; Santana-Casiano et al., 2007) in the North Atlantic, and 8.03-8.18 for the Bermuda Atlantic Time-series Study (BATS, 31-32°N, 64°W, 1983-2009; Bates, 2009; Bates



et al., 2010). Also, unlike temperature proxies (Sr/Ca and  $\delta^{18}\text{O}$ ), the amplitude of seasonal  $\delta^{11}\text{B}$  isotopic variations is comparable among the colonies which may suggest little or no biological artifact on the reconstruction of seawater pH from  $\delta^{11}\text{B}$  between the different colonies.

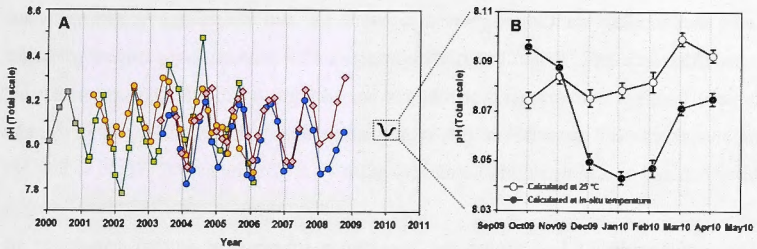


**Fig. 2.10** (A) Seasonal cycles of  $\delta^{11}\text{B}$ -derived seawater  $\text{pH}_T$  from this study and calculated pH from the mooring data from a MAPCO<sub>2</sub> system deployed off Heron Island (23.46°S, 151.47°E) from October 2009 to April 2010. Color-coding and symbols as in the previous figures. (B) Enlarged time-series of *in situ* pH records over 7 months. Monthly mean surface ocean *in situ* pH was calculated from  $f\text{CO}_2$  and total alkalinity at *in situ* temperature (solid symbols) and at 25°C (open symbols). Vertical error bars represent  $\pm 2$  standard error of mean ( $\pm 2\sigma_{\text{mean}}$ ).

The  $\delta^{11}\text{B}$ -seawater  $\text{pH}_T$  records from each coral core site show much clearer seasonal cycles than the primary  $\delta^{11}\text{B}$  variations due to temperature correlation to *in situ* SST (Figs 2.5E and F). The coral records are characterized by more acidity (i.e. lower  $\text{pH}_T$ ) in summer than winter. This sense of change is consistent with  $\delta^{11}\text{B}$  coral record reported for Flinders Reef in the Coral Sea (Pelejero et al., 2005) and the *in situ*  $\text{pH}_T$  data for the southern GBR (Fig. 2.10). The clear seasonality that occurs in the reconstructed seawater  $\text{pH}_T$  is indicated by the high correlation coefficients ( $r \geq \pm 0.8$ ) between  $\text{pH}_T$  and the various temperature proxies and the *in situ* SST (Table 2.3).

Dore et al. (2009) reported low pH in summer and high pH in winter over an *in situ* temperature range of 23.5-26.5°C for Station HOT in the North Pacific consistent with this study. However, when the seawater pH values were calculated at a fixed temperature (25°C), the opposite pattern was obtained. This can be attributed to seasonal variation in the magnitude of vertical mixing in the Hawaiian region. In contrast, the reconstructed  $\text{pH}_T$  data and *in situ*  $\text{pH}_T$  measurements for the southern GBR maintain the same pattern at both the *in situ* and standardized temperatures, with dampening on the original  $\text{pH}_T$  trend (*in situ*  $\text{pH}_T$  data) occurring when standardized to 25°C (Fig. 2.10B). This suggests that seasonal temperature variation (winter cooling and summer warming) is not enough to produce the seasonality of reconstructed reef water pH in this region as changes in surface temperature could have induced an additional pH variability of only ~0.02 units per °C.

Shaw et al. (2012) has shown the occurrence of extreme diurnal variability in carbonate chemistry within a reef flat in the southern GBR (the pH range of 7.6-8.4). This was attributed to biological activity which is enhanced at low tide when reef flat waters become isolated from the surrounding open ocean. An increase in biological production accompanying enhanced light intensity in summer leads to higher calcification rates and/or respiration (Cohen and Holcomb, 2009; Reynaud-Vaganay et al., 2001). While zooxanthellae photosynthesis is a sink for  $\text{CO}_2$ , calcifying corals act as a source of  $\text{CO}_2$ , and hence increase  $\text{pCO}_2$  and decrease the pH of reef waters. The observed strong negative correlations of  $\delta^{11}\text{B}$ -seawater  $\text{pH}_T$  and temperature tracers (and SST) appear to be consistent with this biological modulation of reef water and ocean chemistry in summer in the southern GBR (Table 2.3). The interaction of sources and sinks of  $\text{pCO}_2$  in reef water is indicated with around a 2-month offset between the maximum of temperature proxies and coral  $\text{pH}_T$  in the case of Middle Pompey and Little Kindermar corals (Figs 2.5C and F), as the strongest solar irradiance occurs from November to January (Cayan, 1992) and could reduce the concentration of  $\text{CO}_2$  in seawater through enhanced photosynthesis during this period.

Furthermore, a stronger regional ocean current (East Australian Current, EAC) occurs from May to July in the southern GBR due to the higher wind speed in austral autumn (Taft and Kessler, 1991). The water chemistry of the southern GBR, therefore, can be expected to shift toward lower  $p\text{CO}_2$  and higher  $\text{pH}_T$  due to the inflow of less acidic tropical water during this time. Moreover,  $\delta^{11}\text{B}$  derived-seawater  $\text{pH}_T$  variation represented by lower values in summer and higher in winter suggests the mechanism of refreshment of  $\text{CO}_2$  accumulated reef water by strong winds in austral autumn-winter (Pelejero et al., 2005). The enhanced stratification of surface water during the summer due to warmer temperature and weaker winds may intensify this process and cause the large seasonal amplitude of seasonal reef water  $\text{pH}_T$ . In summary, the greater seasonal  $\text{pH}_T$  variations in reef waters ( $\sim 0.4$  pH units) relative to the open ocean ( $\sim 0.1$  pH units) is attributed to changes in local reef water pH and a build-up of  $\text{CO}_2$  due to higher coral calcification rates and lower wind-driven flushing efficiency in summer.

Large natural pH variations occur in the southern GBR coral reefs over interannual time scales. The average seasonal range in reef water pH in the southern GBR ( $\sim 0.4$  pH units) itself is already close to that which is predicted to occur due to anthropogenic carbon emissions of 0.3-0.5 units by the end of this century (Caldeira and Wickett, 2005). It follows that the anthropogenic changes in seawater chemistry (ocean acidification) to date are relatively small compared to the observed interannual variability, and that understanding future impact of the shifting baseline pH will require a thorough understanding of the underlying natural variability.

## 2.5 Conclusion

High-resolution analyses of various geochemical proxies ( $\delta^{13}\text{C}$ ,  $\delta^{18}\text{O}$ ,  $\delta^{11}\text{B}$ , Sr/Ca and Mg/Ca) in four *Porites* coral cores from the southern GBR all show clear seasonality effects. Changes in coral  $\delta^{18}\text{O}$ , Sr/Ca, and Mg/Ca reflect seasonal SST variations showing the strong correlations between *in situ* SST and both  $\delta^{18}\text{O}$  and Sr/Ca aside from Little Kindermar coral records. Although Sr/Ca and  $\delta^{18}\text{O}$  variability

was tightly linked to *in situ* SST in all colonies, none of the tracer calibrations to SST provide an absolute SST estimate. The  $\delta^{18}\text{O}$ -SST and Sr/Ca-SST estimates from Little Kindermar based on regression analysis of seasonal signals, in particular, show significant offsets with instrumental SST. This is attributed to an attenuation of SST records in coral skeleton by the “bio-smoothing effect” of the living tissue layer. The reduced temperature sensitivities of  $\delta^{18}\text{O}$  and Sr/Ca and suppressed amplitude of temperature annual cycles found in all southern GBR coral records are due to the long time period of the smoothing effect (~4-5 months), in particular in Little Kindermar (~10 months). The greater offset between instrumental SST and coral proxy SSTs in winter than summer further suggests that the greater smoothing occurs in winter when coral growth slows.

The mean reconstructed seawater  $\text{pH}_T$  from coral  $\delta^{11}\text{B}$  compositions is 8.07 with a large seasonal cycle ranging from 7.78 to 8.47. The coral  $\text{pH}_T$  records are importantly characterized by higher acidity (i.e. lower  $\text{pH}_T$ ) in summer than winter. The greater seasonal pH variation in reef waters (~0.7 pH units) relative to the open ocean (~0.1 pH units) mainly reflects the build-up of  $\text{CO}_2$  in local reef water as a result of higher coral calcification and lower wind-driven flushing efficiency in summer. This result highlights seawater carbon chemistry in coral reef environments changes in response to a complex set of biological, physical and chemical processes, including horizontal water mixing, photosynthesis and calcification. Therefore, an understanding of the response of different natural coral reef communities to seawater chemistry and an understanding of why the different systems show different responses will be required in order to make quantitative global predictions about coral reef responses to ocean acidification.









---

## Chapter 3.

# Ocean warming in the southern Great Barrier Reef

---

### 3.1 Introduction

Increasing anthropogenic CO<sub>2</sub> and other greenhouse gases (GHGs) concentrations in the atmosphere are a major cause of the accelerating global-mean air temperature and sea surface temperature (SST) rises since the industrial revolution, and both temperature are projected to warm further (IPCC, 2007a). The spatial pattern of SST increase is significant for changing climate variability around the world as it can be linked to changes in the atmospheric circulation and patterns of precipitation (Hoerling et al., 2004; Pfeiffer et al., 2006). For example, the influence of SST within the Pacific Basin contributes to changes in the El Niño-Southern Oscillation (ENSO), which is centered in ocean-atmospheric dynamics of the tropical Pacific with teleconnections to other parts of the tropics and some higher latitude locations, and which have long-lasting climatic effects over the entire globe, due to changes in the intensity of trade winds and the transition of the equatorial thermocline (Collins et al., 2010).

Coral reefs are particularly sensitive to the rapid changing, and projected further changes, in their physical environment, primarily SST and also increased stratification, acidification, salinity (Hughes et al., 2003; Hoegh-Guldberg et al., 2007). Tropical corals have already demonstrated their sensitivity to warmer

temperatures, for example, large-scale mass coral bleaching in recent years (e.g. during the 1997–1998 El Niño) and more frequent outbreaks of coral diseases (Bruno et al., 2007).

The spatial warming patterns are regionally variable. Global projections provide, however, little regional detail on the magnitude of warming for Australian coastal seas. Commonwealth Scientific and Industrial Research Organisation and Australian Bureau of Meteorology (CSIRO and ABOM; 2007) and Lough (2008b) have found substantial warming already around Australia, especially off the far southeastern and southwestern coasts. Annual SST averaged through 10.5–29.5°S of the Australian coast has significantly warmed from 1950 to 2007 by 0.12°C/decade (Lough, 2008b) and, as a result, the coastal marine climatic zones (as defined by average annual SST) along the eastern Australian coast have been shifted southward between 63 km (11.5°S) and 313 km (23.5°S) between 1950–1969 and 1988–2007 (Lough, 2008b). This study also observed faster warming in the southern GBR and suggested ~0.5°C warmer for northern GBR SST and 1.5–2.0°C warmer for southern GBR SSTs within the next 100 years based on extrapolation of current warming trends. In addition, Lough (2012) showed that coral reefs which occupy 10% of the tropical oceans tend to occur 1.8°C warmer than non-reefs over the period 1951–2011.

Historical SST datasets including the Global Sea Ice and Sea Surface Temperature dataset (GISST2; Rayner et al., 1996), the Hadley Center Sea Ice and Sea Surface Temperature (HadISST; Rayner et al., 2003), and the Extended Reconstructed Sea Surface Temperature (ERSST; Smith and Reynolds, 2003) are often used for the determination of decadal ocean temperature changes due to the lack of long-term *in situ* SST records. However, significant inconsistencies exist between these instrumental SST records, which lead to difficulties in the accurate identification of trends in SST in particular regions. For example, the ERSST record in the Pacific exhibits a warming of SST since 1900, which is stronger along in equatorial regions than in the subtropics. On the other hand, the SST from the HadISST record shows a cooling in the equatorial region and a warming in the subtropics (Zhu and Liu, 2009).

Long-term warming trends are rather difficult to discern in the surface Pacific Ocean because of the strong interannual and decadal variability and the relatively short length of the observational records, particularly in the Southern Hemisphere. The high-resolution paleoclimate information that is archived within multi-decadal to centuries-old massive corals has the potential to resolve these uncertainties in temperature variability. Strontium/calcium (Sr/Ca) and oxygen isotope ratios ( $\delta^{18}\text{O}$ ) in the coral skeletons are a widely used source of high temporal resolution paleotemperature information and have proven fidelity in recording seasonal to interannual SST variability (Gagan et al., 2000; Delong et al., 2012). The Sr/Ca ratios of *Porites spp.* corals have been used to successfully reconstruct SSTs in the Pacific and Indian Oceans and applied to paleoclimatic studies (Alibert and McCulloch, 1997; Ayling et al., 2006; Corrège, 2006; Delong et al., 2012; de Villiers et al., 1994; Gagan et al., 2000; Gagan et al., 1998; Linsley et al., 2000; Linsley et al., 2004; McCulloch et al., 1994; McCulloch et al., 1999). The most recent study by Delong et al. (2012) reconstructed twentieth-century SST variability in the southwest Pacific using coral Sr/Ca records from New Caledonia using five coral cores. Their coral Sr/Ca-SST reconstruction is significantly correlated with *in situ* SST and exhibits a warming trend of  $\sim 0.6^\circ\text{C}$  for the period 1900-1999. Many coral studies have also utilized measurements of oxygen isotope compositions ( $\delta^{18}\text{O}$ ) of coral skeletons as a paleothermometer because  $\delta^{18}\text{O}$  is readily measured and relatively straightforward to interpret (Gagan et al., 2000). However, the SST component of the coral  $\delta^{18}\text{O}$  variation needs to be evaluated from Sr/Ca measurements as the coral skeletal  $\delta^{18}\text{O}$  records both SST and salinity variability in seawater (Corrège, 2006).

Given the lack of SST information in the southern GBR, this study examines how the southern GBR has warmed to date and how rates of change compare with average global warming. The contribution of natural variability was differentiated from the anthropogenic warming as it relates to climate prediction. This study uses multiple Sr/Ca and oxygen isotope ( $\delta^{18}\text{O}$ ) records to reconstruct SST changes from four coral cores for the period 1834-2008.

## 3.2 Methods

### 3.2.1 Coral sampling

Four long cores of *Porites* used in this study were collected from Middle Pompey, Little Kindermar, Fitzroy Reefs and Lady Musgrave Island, all offshore reefs in the southern GBR (see Chapter 2 for details of core locations). The Middle Pompey and Little Kindermar cores were collected from outside their reef lagoons, whereas the Fitzroy Reefs and Lady Musgrave Island cores were collected from inside their reef lagoons. The coral cores were sampled by drilling a 55mm diameter core along the primary vertical growth axis of the coral colony and then these cores were sliced vertically to 7 mm thick slabs. Annual density bands visible on X-rays of these slabs were used to determine sampling paths (Appendix Figs A1 to A4). The slabs were cut along with the axes of maximum growth into lengths up to 95 mm and widths of 25 mm for laser ablation inductively coupled plasma mass spectrometry (LA-ICPMS) analysis. Coral slabs from Middle Pompey, Fitzroy Reef, and Lady Musgrave Island were milled for analyses of  $\delta^{18}\text{O}$  isotope along the maximum growth axes, winter to winter (i.e. August to August) in annual intervals. Meanwhile, the coral slabs from Little Kindermar were powdered in annual increments from 2000 back to 1940, and in 5-year intervals from 1939 to 1834. The annual coral samples were obtained from using the distance between successive winter maximums (i.e. August to August) based on LA-ICPMS geochemical profiles.

### 3.2.2 Geochemical analysis

High-resolution compositions of selected elements (Li, B, Mg, Ca, Mn, Sr, Y, Cd, Ba, and U) were determined over the full-length of corals using LA-ICPMS at the Australian National University, an ANU HelEx laser ablation system comprising an ArF excimer laser (193 nm) coupled to a Varian 820 ICPMS via a custom-built laser ablation cell designed to hold two 95 mm lengths of a coral core, following the

analytical protocols described in Fallon et al. (1999) and Sinclair et al. (1998) (Details are given in Chapter 2). These high-resolution geochemical profiles are used to reconstruct chronology and estimate precise annual milling lengths for individual coral cores.

Elemental ratio (Sr/Ca) and stable isotopic ( $\delta^{18}\text{O}$ ) measurements were made from splits of the homogenized coral sample using instrumentation at the Australian National University. Sr/Ca measurements were made using a Varian Vista simultaneous axial atomic emission spectrometry (ICP-AES) using the drift correction method described by Schrag (1999). Coral powder samples (~2 mg) were diluted in a volume of 2% nitric acid and measured using the following analytical lines 407.771 nm for Sr and 315.887 nm for Ca. The overall analytical precision of a synthetic 'coral' reference solution used for instrument calibration and drift correction was 0.15% RSD based on measurements before and after each sample. An additional estimate of precision was determined using a homogenized powder of the Davies coral in-house standard, which was analyzed every fifth sample. The average measured ratios of Sr/Ca ( $8.994 \pm 0.034 \text{ mmol mol}^{-1}$ ,  $1\sigma$ ) determined from 125 measurements of the Davies coral powder agree well with the previously reported ratio values determined by isotope dilution analyses (Sr/Ca =  $8.86 \pm 0.02 \text{ mmol mol}^{-1}$  using thermal ionization mass spectrometry (TIMS); Fallon et al., 1999).

Stable isotope was measured using a Kiel carbonate device connected to a dual-inlet Finnigan MAT 251 isotope ratio mass spectrometer (IRMS) using the methods described by Hendy et al. (2002) and Gagan et al. (1998). Coral powder (180-220  $\mu\text{g}$ ) was reacted with 105% phosphoric acid at 90°C in the Kiel device to release  $\text{CO}_2$  gas for analysis in the mass spectrometer. The overall analytical precision determined by analysis of the National Bureau of Standards NBS 19 run in conjunction with coral samples was 0.03%. Isotopic ratios are reported in delta ( $\delta$ ) notation relative to Vienna Pee Dee belemnite (V-PDB).

### 3.2.3 Sea surface temperature (SST)

The daily *in situ* SST data from the Australian Institute of Marine Science (AIMS) and weekly- and monthly-reconstructed records from NOAA SST (NOAA ERSST version 3, Reynolds et al., 2002; Smith and Reynolds, 2003) were used to investigate changes in SST in the southern GBR over the period 1854 to 2008. The details of the data sources and time span that was used for this study are summarized in Table 3.1.

A comparison between satellite-derived data (the 1° gridded, centered on 20.5–21.5°S, 150°E) and weekly *in situ* SST from East Cay (21.2°S, 152.3°E), the closest monitoring station to Middle Pompey and Little Kindermar Reefs, is shown in Fig. 3.1A. A very strong correlation exists between the two datasets with only slight offset between the two (Fig. 3.1C). The *in situ* SST shows lower values than NOAA data in summer 2003 and 2004 and in winter 1996, which is likely due to the satellite-derived SST being measured at lower latitude than the *in situ* dataset. A combination of both datasets is used for developing the chronology and interpretation of Middle Pompey and Little Kindermar Reef records.

The comparison of NOAA satellite-derived SST (the 1° gridded, centered on 23.5°S, 152.5°E) and *in situ* weekly datasets from Heron Island (23.2°S, 151.5°E), the nearest monitoring station to Fitzroy Reef and Lady Musgrave Island, is shown in Fig. 3.1B. At Heron Island, the *in situ* SST was up to 1.5°C below the NOAA SST record. The offset was greatest in winter, possibly due to local upwelling in this region at this time. To account for this offset, the satellite SST was corrected using the equation,  $\text{in situ SST (}^{\circ}\text{C)} = 1.0524 \times \text{NOAA ERSST (}^{\circ}\text{C)} - 2.0693$  (Fig. 3.1D). The calibrated NOAA SST record correlates well with the *in situ* SST data (Fig. 3.1B) and therefore these two combined datasets are used for interpretation of Fitzroy Reef and Lady Musgrave Island records.

**Table 3.1** Summary of applied instrumental sea surface temperatures (SSTs) in this study

Site		Middle Pompey Reef (150.51°E, 20.99°S)	Little Kindermar Reef (150.40°E, 21.10°S)	Fitzroy Reef (152.09°E, 23.37°S)	Lady Musgrave Island (152.25°E, 23.54°S)
Daily	Source	East Cay (152.3°E, 21.2°S; AIMS <sup>1</sup> )		Heron Island (151.°5E, 23.2°S; AIMS)	
	Time span	November 1995 - March 2006		November 1995 - October 2008 (except 2002 - 2003)	
Weekly	Source	NOAA satellite-derived SST (150°E, 20.5°S; Reynolds et al., 2002 <sup>2</sup> )	NOAA satellite-derived SST (150°E, 21.5°S; Reynolds et al., 2002)	NOAA satellite-derived SST (152.5°E, 23.5°S; Reynolds et al., 2002)	
	Time span	November 1981 - March 2006		November 1981 - October 2008	
Monthly	Source	NOAA NCDC ERSST version 3 <sup>3</sup> (2° × 2° boxes centered at 150°E, 20°S)		NOAA NCDC ERSST version 3 (2° × 2° boxes centered at 152°E, 23°S)	
	Time span	January 1854 - March 2006		January 1854 - October 2008	

<sup>1</sup> Australian Institute of Marine Science; <http://www.aims.gov.au/docs/data-centre/seatemperatures.html><sup>2</sup> [http://iridl.ldeo.columbia.edu/SOURCES/NOAA/NCEP/EMC/CMB/GLOBAL/Reyn\\_SmithOlv2/weekly/sst/](http://iridl.ldeo.columbia.edu/SOURCES/NOAA/NCEP/EMC/CMB/GLOBAL/Reyn_SmithOlv2/weekly/sst/)<sup>3</sup> Extended Reconstructed Sea Surface Temperature Dataset; <http://iridl.ldeo.columbia.edu/SOURCES/NOAA/NCDC/ERSST/version3/sst/>



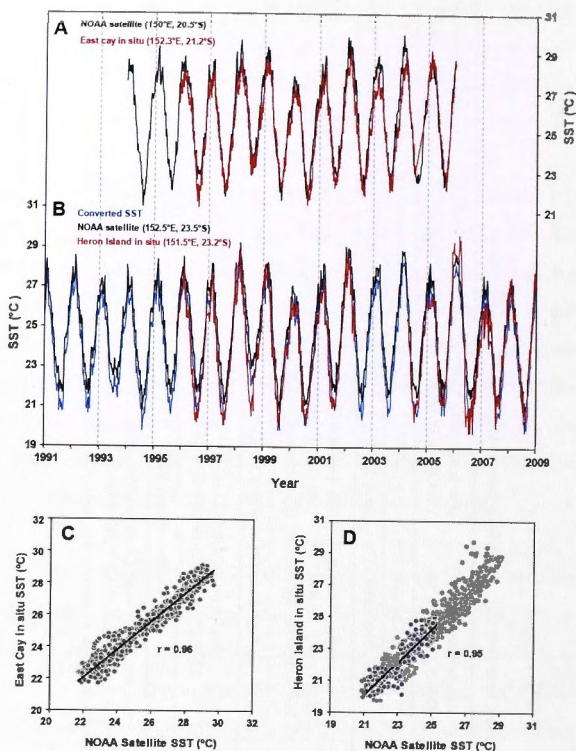


Fig. 3.1 Sea surface temperature from (A) East Cay *in situ* data logger and NOAA satellite and (B) Heron Island *in situ* data logger and NOAA satellite. Comparisons between satellite SST and *in situ* SST from (C) East Cay and (D) Heron Island. In case the Heron Island (higher latitude), *in situ* data shows notably lower values (about 1°C) in austral winter periods than the records from satellite; thus SST was converted using the equation from regression line in (D) and is represented by the blue line in (B). All data are at weekly resolution.

### **3.2.4 Establishing chronology**

Two methods were employed to establish the age model for the individual coral records: counting annual density bands on the coral X-rays and aligning coral Sr/Ca, U/Ca and B/Ca variations to a SST record. The conversion from distance to time domain was achieved by matching coral trace element ratio maxima (minima) to SST minima (maxima) for each annual cycle using AnalySeries 2.0 (Paillard et al., 1996). In order to maximize alignment between records, additional tie points were utilized to match summer points between trace element/Ca and SST records. The geochemical and distance records were linearly resampled to even monthly intervals using AnalySeries 2.0 (Paillard et al., 1996) and the monthly distance record was used to calculate annual extension rate.

Cross dating was employed to create the master chronology and to verify the chronology of the individual records. Advantages of cross dating include improved alignment between discontinuous sampling paths and the ability to assess locally absent years between core sections (Appendix Figs A1 to A4). Each core section was aligned to the SST record using a best guess assignment determined from the density band chronology, next each core section was visually aligned with concurrent core sections, and then the age assignments were adjusted accordingly. The master chronology was generated after all the cores were aligned and gaps between core sections were assessed for locally absent years. The final age model for each core was verified against the annual density bands and SST record. The completed chronology using the cross dating from the southern GBR cores are shown in Fig. 3.2 and Appendix Figs A1 to A4.

The time periods derived from the completed age models are July 1907-March 2006 for Middle Pompey, September 1833-March 2006 for Little Kindermar, December 1949-October 2008 for Fitzroy Reef, November 1889-October 2008 for Lady Musgrave Island (LHI08-H), and October 1955-October 2008 for Lady Musgrave Island (LHI08-C-a). The Sr/Ca ratios have the most apparent seasonal cycles and have been used to reconstruct chronologies for all southern GBR coral records except

for the Little Kindermar coral. The correlation coefficients ( $r$ ) between weekly SST and the Sr/Ca ratios were obtained from linear regression analysis for the whole time series of each coral record ( $r = 0.54$ ,  $p < 0.0001$ ,  $n = 5188$  for Middle Pompey,  $r = 0.77$ ,  $p < 0.0001$ ,  $n = 3065$  for Fitzroy Reef,  $r = 0.74$ ,  $p < 0.0001$ ,  $n = 6184$  for Lady Musgrave Island (LMI08-H), and  $r = 0.68$ ,  $p < 0.0001$ ,  $n = 2788$  for Lady Musgrave Island (LMI08-C-a)). These correlations between SST and Sr/Ca are higher than in a previous study in the GBR (Fallon et al., 2003) despite much longer time spans (5-10 years vs. 50-100 years).

The trace elements from the Little Kindermar coral show different characteristics from the other southern GBR cores. B/Ca is the only element having seasonal cycles whereas Sr/Ca and U/Ca, which are considered to be the most temperature dependent elements, do not show any correlation with the SST over long-term time scales. Accordingly, the reconstruction of chronology for this coral was performed using B/Ca ratios (Fig. 3.2E). Monthly B/Ca compositions display seasonal cycles with a correlation of  $r = 0.41$  ( $p < 0.0001$ ,  $n = 2039$ ).

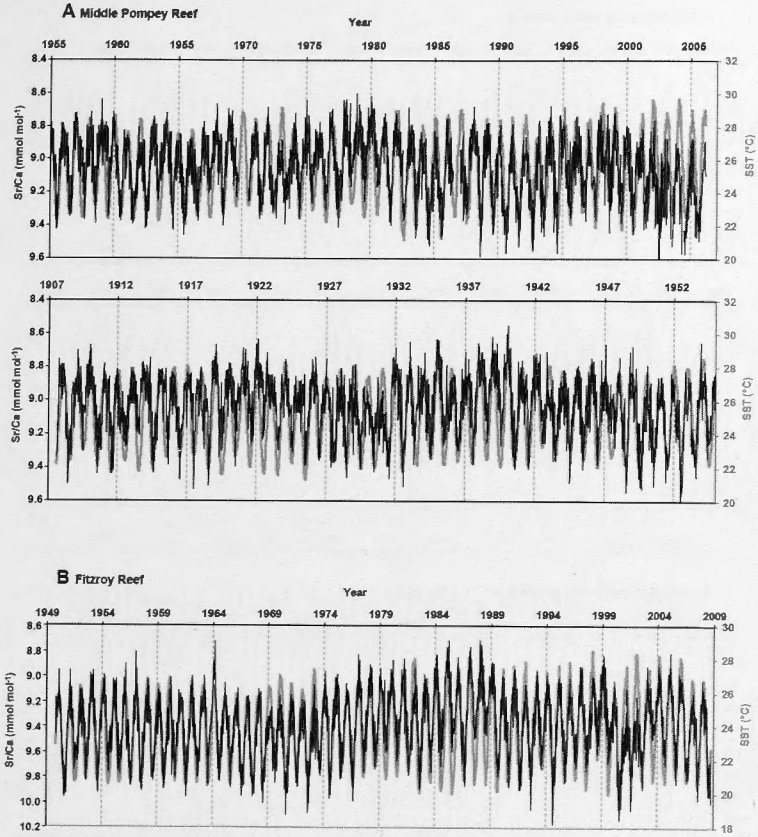


Fig. 3.2 Whole time series of Sr/Ca or B/Ca (black line) and SSTs (grey line) from (A) Middle Pompey Reef, (B) Fitzroy Reef, (C) Lady Musgrave Island (LMI08-H), (D) Lady Musgrave Island (LMI08-C-a), and (E) Little Kindermar corals. Chronology was carried out assuming faster growth in summer than in winter. Sr/Ca and B/Ca axes are inverted and signals caused by glue were deleted. All data are at weekly resolution, whereas Little Kindermar coral records (E) are shown in 1-month intervals.

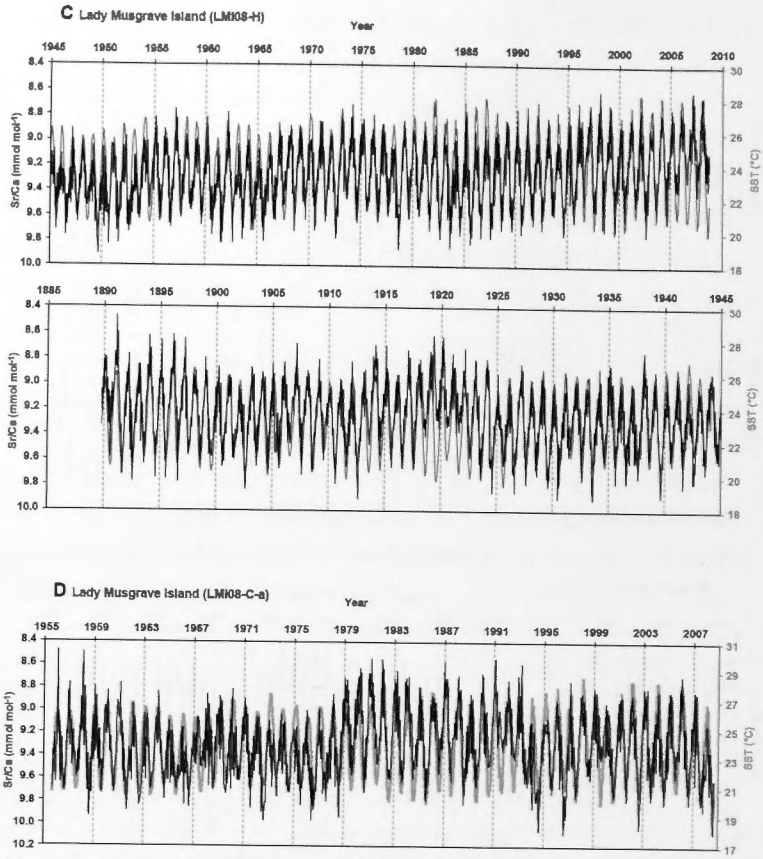


Fig. 3.2 (Continued)

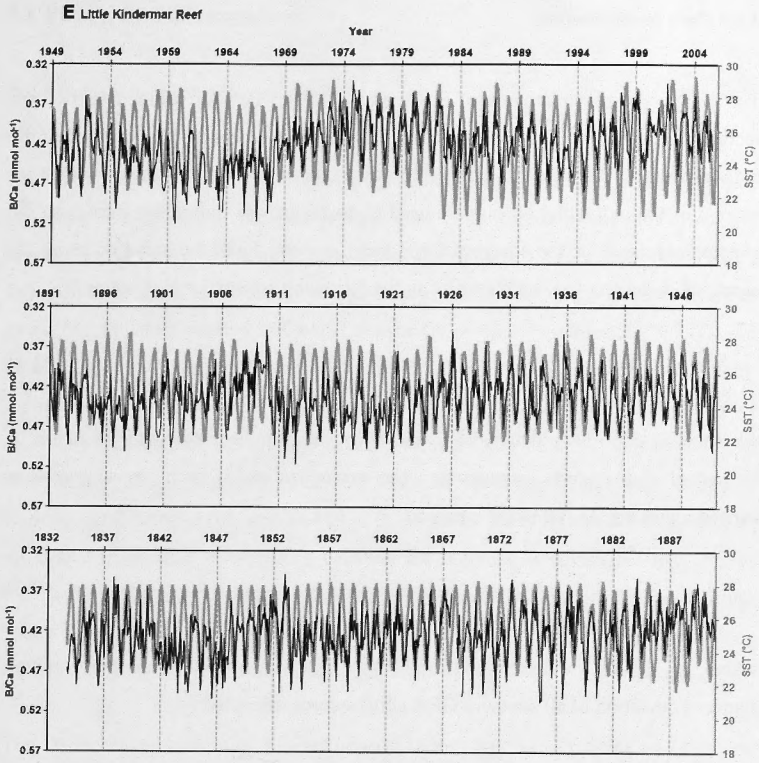


Fig. 3.2 (Continued)

### 3.2.5 Data manipulation

The composite master records of Sr/Ca and  $\delta^{18}\text{O}$  for the four southern GBR core records are calculated as the mean of the individual records after normalization of the coral records to the shared period of all cores (i.e. 1950-2005). Standard scores (z-scores) of the individual cores were used to normalize the individual records to the average obtained for the southern GBR coral records. First, the standard score (z-score) of each core was calculated using the following conventional equation.

$$z = (x - \bar{x}) / \sigma \quad (3-1)$$

where,  $x$  is a primary data, and  $\bar{x}$  and  $\sigma$  are a mean and standard deviation of individual core records respectively. The normalization of each record was then carried out using the following equation.

$$x_{normalized} = \bar{x}_{sGBR} + z \times \sigma_{sGBR} \quad (3-2)$$

where,  $x_{normalized}$  is the normalized coral record and  $\bar{x}_{sGBR}$  and  $\sigma_{sGBR}$  are the mean and standard deviation of all southern GBR coral records respectively.

Weighted least square linear regressions of the composite record are used to estimate the rate of variations of the Sr/Ca and  $\delta^{18}\text{O}$  time series due to the different number of samples in each year by means of IBM SPSS (IBM Corp., 2011). The 95% of confidence interval values are employed as weighting variables and the maximum values of these confidence intervals for each parameter are used for periods when only one record exists (i.e. the period of 1834-1891).



### 3.3 Results and discussion

#### 3.3.1 Variations in Sr/Ca and $\delta^{18}\text{O}$

The Sr/Ca records from the four cores are plotted in Fig. 3.3A. With the exception of the mean Sr/Ca value of the Fitzroy Reef core ( $9.25 \pm 0.05 \text{ mmol mol}^{-1}$ ,  $1\sigma$ ), the average Sr/Ca values of the other three cores are identical ( $9.14 \pm 0.05 \text{ mmol mol}^{-1}$ ,  $1\sigma$ ). Although there is an apparent temperature difference of  $1.4^\circ\text{C}$  between these two different values given a Sr/Ca-SST sensitivity of  $-0.084 \text{ mmol mol}^{-1} \text{ }^\circ\text{C}^{-1}$  (Gagan et al., 2012), similar differences have been observed elsewhere (e.g. a colony replication study in the GBR by Hendy (2003)). Fig. 3.4A compares the four  $\delta^{18}\text{O}$  records which exhibit an average relative standard deviation of 2.8% ( $-4.556 \pm 0.098\text{‰}$  for Middle Pompey,  $-4.277 \pm 0.096\text{‰}$  for Little Kindermar,  $-4.355 \pm 0.146\text{‰}$  for Fitzroy Reef, and  $-4.419 \pm 0.136\text{‰}$  for Lady Musgrave Island). The difference in average  $\delta^{18}\text{O}$  values between the colonies is equivalent to  $1.2^\circ\text{C}$  ( $-0.23\text{‰ }^\circ\text{C}^{-1}$  of  $\delta^{18}\text{O}$  sensitivity; Gagan et al., 2012), which is within the range of the values reported from colonies elsewhere within the GBR and with intercept values reported for  $\delta^{18}\text{O}$ -SST relationships (Gagan et al., 1998).

The different annual and 5-year interval coral Sr/Ca and  $\delta^{18}\text{O}$  records are significantly correlated in the case of Middle Pompey and Little Kindermar for both Sr/Ca and  $\delta^{18}\text{O}$  variations, whereas SST shows significant relationships only in the case of Little Kindermar and Lady Musgrave Island for Sr/Ca and in the case of Middle Pompey and Lady Musgrave Island for  $\delta^{18}\text{O}$  (Tables 3.1 and 3.2). The reason why Middle Pompey and Little Kindermar Sr/Ca and  $\delta^{18}\text{O}$  variations are well correlated is possibly that the sampling locations of Middle Pompey and Little Kindermar reef cores are closer than those of Fitzroy reef and Lady Musgrave Island, and both cores derive from similar conditions as outside their reef lagoons (see Table 2.1 in Chapter 2). Gagan et al. (2004) also showed that inter-colony reproducibility appears to be greatly improved when corals are sampled at high-resolution rather than bulk samples. Therefore, less significant correlations between individual coral



core records could be contributed to the relatively low-resolution sampling (annual) than weekly- to monthly-resolution samples.

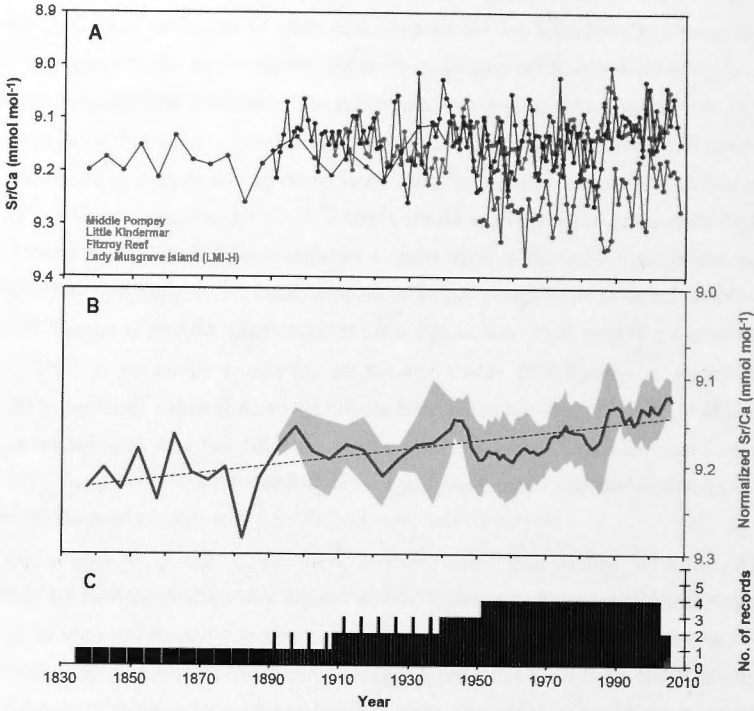


**Fig. 3.3** Time series of all Sr/Ca records in the southern GBR. (A) Absolute Sr/Ca compositions are annual values except Little Kindermar which is given at 5-year intervals before 1940. (B) Composite Sr/Ca master record with 95% confidence envelope calculated from 5-year running averages of individual coral records after normalization to the period of 1950-2005. The weighted linear regression line for the master Sr/Ca record is shown with the green dotted line. (C) Number of cores contributing to the Sr/Ca master record from each annual or 5-year period. Note that the axes values for Sr/Ca are inverted.

A stronger relationship between coral Sr/Ca and  $\delta^{18}\text{O}$  variations with SST was found for the composite southern GBR coral records compared to the correlations of individual coral records (Tables 3.1 and 3.2). This may reflect the individual corals additionally capturing the local and/or physiological influences in regard to SST variability which may lead to lower correlations between different coral Sr/Ca and  $\delta^{18}\text{O}$  variations. In the case of all Fitzroy Reef, the correlation between Sr/Ca,  $\delta^{18}\text{O}$  and SST are not significant, possibly due to small number of observations.

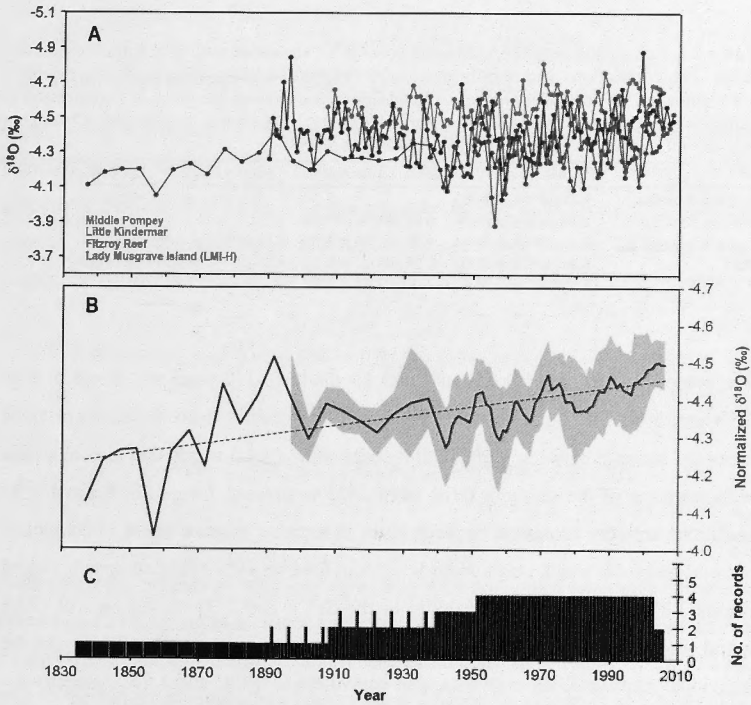


**Fig. 3.4** Time series of all  $\delta^{18}\text{O}$  records in the southern GBR. (A) Absolute  $\delta^{18}\text{O}$  compositions are annual values except Little Kindermar which is given at 5-year intervals before 1940. (B) Composite  $\delta^{18}\text{O}$  master records with 95% confidence envelope calculated from 5-year running averages of individual coral records normalized to the period of 1950-2005. The weighted linear regression line for the master  $\delta^{18}\text{O}$  record is shown with the purple dotted line. (C) Number of cores contributing to the  $\delta^{18}\text{O}$  master record from each annual or 5-year period. Note that the axes values for  $\delta^{18}\text{O}$  are inverted.

**Table 3.1** Correlation between individual coral Sr/Ca variations and SST from the southern GBR. The correlations and significance were determined using Pearson Product-moment correlation at 95% confidential level. All correlation coefficients are given as  $r$ -values and all statistically significant values at 95% confidential level are shown in bold text. Correlation that are not significant are shown with  $p$ -values in brackets.

	Middle Pompey	Little Kindermar	Fitzroy Reef	Lady Musgrave Is.
Little Kindermar	<b>0.34</b> (df=71, p<0.01)			
Fitzroy Reef	0.13 (df=54, p=0.34)	-0.12 (df=54, p=0.37)		
Lady Musgrave Is.	0.20 (df=71, p=0.09)	<b>0.34</b> (df=74, p<0.01)	0.18 (df=57, p=0.16)	
SST	<b>-0.35</b> (df=71, p<0.01)	<b>-0.47</b> (df=81, p<0.01)	-0.21 (df=57, p=0.11)	<b>-0.22</b> (df=77, p<0.05)

**Table 3.2** Correlation between individual coral  $\delta^{18}\text{O}$  variations and SST from the southern GBR. The correlations and significance were determined using Pearson Product-moment correlation at 95% confidential level. All correlation coefficients are given as  $r$ -values and all statistically significant values at 95% confidential level are shown in bold text. Correlation that are not significant are shown with  $p$ -values in brackets.

	Middle Pompey	Little Kindermar	Fitzroy Reef	Lady Musgrave Is.
Little Kindermar	<b>0.36</b> (df=71, p<0.01)			
Fitzroy Reef	0.06 (df=54, p=0.68)	0.01 (df=54, p=0.94)		
Lady Musgrave Is.	<b>0.29</b> (df=71, p<0.05)	0.16 (df=74, p=0.18)	0.18 (df=57, p=0.18)	
SST	<b>-0.46</b> (df=71, p<0.01)	<b>-0.29</b> (df=81, p<0.01)	-0.13 (df=57, p=0.34)	-0.14 (df=77, p=0.21)

The composite records of Sr/Ca and  $\delta^{18}\text{O}$  for the last ~170 years are shown in Figs 3.3B and 3.4B. Although absolute Sr/Ca and  $\delta^{18}\text{O}$  values from the southern GBR cores are variable between reefs, both records show robust trends that are consistent with warming of the southern GBR from 1835 to present. Overall Sr/Ca and  $\delta^{18}\text{O}$  variations are very consistent between cores in terms of relative trends to composite records, and on average, single records account for over 40% of the composite record (Table 3.3). The long-term variability in the Sr/Ca and  $\delta^{18}\text{O}$  master records (0.18 mmol mol<sup>-1</sup> and 0.42‰ respectively) are higher than the average variability of the individual southern GBR core data, and equivalent to 2.1°C and 1.8°C respectively. This indicates other factors influence the coral Sr/Ca and  $\delta^{18}\text{O}$  records in addition to the offsets derived from colonies.

**Table 3.3** Individual coral Sr/Ca and  $\delta^{18}\text{O}$  records compared with composite Sr/Ca and  $\delta^{18}\text{O}$  records from the southern GBR. The correlations and significance were determined using Pearson Product-moment correlation at 95% confidential level. All correlation coefficients are given as  $r$ -values

	Sr/Ca			$\delta^{18}\text{O}$		
	$r$	$p$	$df$	$r$	$p$	$df$
Middle Pompey	0.68	< 0.001	71	0.69	< 0.001	71
Little Kindermar	0.75	< 0.001	85	0.72	< 0.001	85
Fitzroy Reef	0.49	< 0.001	57	0.53	< 0.001	57
Lady Musgrave Is.	0.69	< 0.001	77	0.67	< 0.001	77

### 3.3.2 Calibration of coral Sr/Ca and $\delta^{18}\text{O}$ thermometers

Coral Sr/Ca and  $\delta^{18}\text{O}$  thermometers are generally calibrated using relationships between Sr/Ca and  $\delta^{18}\text{O}$  compositions and instrumental SST over seasonal cycles. Bimonthly Sr/Ca and  $\delta^{18}\text{O}$  vs. SST comparisons for the most recent 5 years show good agreement apart from the Little Kindermar cores (see Chapter 2). The average calibration equations obtained for Sr/Ca-SST and  $\delta^{18}\text{O}$ -SST are:

$$\text{Sr/Ca (mmol mol}^{-1}\text{)} = 10.204 (\pm 0.571) - 0.045 (\pm 0.024) \times \text{SST (}^{\circ}\text{C)}$$

$$(r = 0.84, p < 0.0001) \quad (3-3)$$

$$\delta^{18}\text{O (}\text{‰}\text{)} = -1.766 (\pm 1.133) - 0.111 (\pm 0.050) \times \text{SST (}^{\circ}\text{C)}$$

$$(r = 0.80, p < 0.0001) \quad (3-4)$$

Although these calibration equations agree well with previously reported calibrations (summarized in Ayling et al. (2006) and Corrège (2006)), a recent study has shown suppression of the *Porites* Sr/Ca and  $\delta^{18}\text{O}$  thermometer sensitivities by up to 65% due to the bio-smoothing effect (described in Chapter 2; Gagan et al., 2012). The seasonal variation of Sr/Ca and  $\delta^{18}\text{O}$  in coral records is attenuated by this bio-smoothing and as a result coral Sr/Ca and  $\delta^{18}\text{O}$  thermometer calibrations can overestimate changes in mean SST over decadal timescales (Gagan et al., 2012). Accordingly, they suggested two types of proxy-SST calibration scales for coral paleothermometry; an attenuated *Porites*-specific thermometer sensitivity for studies

of seasonal to interannual change in SST and the rescaled Sr/Ca and  $\delta^{18}\text{O}$  sensitivities for studies of 20th-century trends and millennial-scale changes in mean SST (Gagan et al., 2012).

The Sr/Ca-SST and  $\delta^{18}\text{O}$ -SST sensitivities derived from comparisons of seasonal signals in this study are a factor of two lower than those reported by Gagan et al. (2012; Sr/Ca-SST and  $\delta^{18}\text{O}$ -SST sensitivities of  $-0.23 \text{‰ } ^\circ\text{C}^{-1}$  and  $-0.084 \text{ mmol mol}^{-1} \text{ } ^\circ\text{C}^{-1}$  respectively) as a result of the significant bio-smoothing effect. Therefore, annual to 5-year resolution Sr/Ca and  $\delta^{18}\text{O}$  records in this study were converted to SST using revised temperature sensitivities of  $-0.23 \text{‰ } ^\circ\text{C}^{-1}$  and  $-0.084 \text{ mmol mol}^{-1} \text{ } ^\circ\text{C}^{-1}$  respectively after Gagan et al. (2012) to calibrate the tissue layer bio-smoothing effect in *Porites*. The intercept values for Sr/Ca-SST and  $\delta^{18}\text{O}$ -SST calibrations in this study were estimated using the instrumental SST records of each site and these calibrations are summarized in Table 3.4. Both  $\delta^{18}\text{O}$  and Sr/Ca composite records have been converted to SST and verified against the composite NOAA NCDC ERSST (Smith and Reynolds, 2003) at  $20^\circ\text{S}$ ,  $150^\circ\text{E}$  and at  $23^\circ\text{S}$ ,  $152^\circ\text{E}$  which has been corrected to *in situ* SST data from Heron Island at  $23.2^\circ\text{S}$ ,  $151.5^\circ\text{E}$ . This accounts for an offset between the *in situ* SST (or “sea-truth” data; Castillo and Lima, 2010) and the satellite-based reconstructed SST datasets (resampled to 5-year running averages, 1854 to 2006; Fallon et al., 2003). These results are shown in Fig. 3.5.

**Table 3.4** Sr/Ca and  $\delta^{18}\text{O}$  versus SST calibration equations for the southern GBR *Porites* corals using the revised temperature sensitivity (Gagan et al., 2012).

Sample	Sr/Ca-SST calibration
Middle Pompey Reef	$\text{Sr/Ca}_{\text{mean}} \text{ (mmol mol}^{-1}\text{)} = -0.084 \times \text{SST}_{\text{mean}} \text{ (}^\circ\text{C)} + 11.272$
Little Kindermar Reef	$\text{Sr/Ca}_{\text{mean}} \text{ (mmol mol}^{-1}\text{)} = -0.084 \times \text{SST}_{\text{mean}} \text{ (}^\circ\text{C)} + 11.280$
Fitzroy Reef	$\text{Sr/Ca}_{\text{mean}} \text{ (mmol mol}^{-1}\text{)} = -0.084 \times \text{SST}_{\text{mean}} \text{ (}^\circ\text{C)} + 11.255$
Lady Musgrave Island	$\text{Sr/Ca}_{\text{mean}} \text{ (mmol mol}^{-1}\text{)} = -0.084 \times \text{SST}_{\text{mean}} \text{ (}^\circ\text{C)} + 11.119$
Sample	$\delta^{18}\text{O}$ -SST calibration
Middle Pompey Reef	$\delta^{18}\text{O}_{\text{mean}} \text{ (}\text{‰}\text{)} = -0.23 \times \text{SST}_{\text{mean}} \text{ (}^\circ\text{C)} + 1.288$
Little Kindermar Reef	$\delta^{18}\text{O}_{\text{mean}} \text{ (}\text{‰}\text{)} = -0.23 \times \text{SST}_{\text{mean}} \text{ (}^\circ\text{C)} + 1.575$
Fitzroy Reef	$\delta^{18}\text{O}_{\text{mean}} \text{ (}\text{‰}\text{)} = -0.23 \times \text{SST}_{\text{mean}} \text{ (}^\circ\text{C)} + 1.133$
Lady Musgrave Island	$\delta^{18}\text{O}_{\text{mean}} \text{ (}\text{‰}\text{)} = -0.23 \times \text{SST}_{\text{mean}} \text{ (}^\circ\text{C)} + 1.007$

Sea surface salinity (SSS) was estimated from the residual  $\delta^{18}\text{O}$  signal record ( $\Delta\delta^{18}\text{O}$ ) after removing the SST component of  $\delta^{18}\text{O}$  using the Sr/Ca-SST value obtained for each sample. The  $\Delta\delta^{18}\text{O}$  is defined as follows (Gagan et al., 1998);

$$\Delta\delta^{18}\text{O} = \alpha\delta^{18}\text{O}/\alpha\text{SST} (\text{SST}_{\delta^{18}\text{O}} - \text{SST}_{\text{Sr/Ca}}) \quad (3-5)$$

where,  $\alpha\delta^{18}\text{O}/\alpha\text{SST}$  is the empirically derived temperature-dependent oxygen isotope fractionation for *Porites* investigated in this study ( $-0.12\text{‰ } ^\circ\text{C}^{-1}$ ; cf.  $-0.18\text{‰ } ^\circ\text{C}^{-1}$  in Gagan et al., 1998).  $\text{SST}_{\delta^{18}\text{O}}$  and  $\text{SST}_{\text{Sr/Ca}}$  represent the  $\delta^{18}\text{O}$ -derived SST and Sr/Ca-derived SST respectively. The SSS is finally calculated with the following equation (Gagan et al., 2000);

$$\text{SSS} (\text{‰}) = 35.2 + (\Delta\delta^{18}\text{O}/0.27) \quad (3-6)$$

### 3.3.3 Natural and anthropogenic ocean warming in the southern GBR

The dominant trends of decreasing Sr/Ca and  $\delta^{18}\text{O}$  in both master records reflect a long-term warming pattern in the southern GBR region. Weighted linear regressions of the SST composite records reconstructed from Sr/Ca ratios and  $\delta^{18}\text{O}$  compositions show very good agreement with instrumental SST over the period of 1890-2006 ( $r = 0.59$ ,  $p < 0.001$ ,  $n = 114$  for Sr/Ca-SST and  $r = 0.62$ ,  $p < 0.001$ ,  $n = 114$  for  $\delta^{18}\text{O}$ -SST). The rate of surface ocean warming derived from the composite Sr/Ca-SST and  $\delta^{18}\text{O}$ -SST records are consistent at  $0.055 \pm 0.052^\circ\text{C}$  per decade ( $1\sigma$ ) and are comparable to the warming rate of NOAA NCDC ERSST of  $0.056 \pm 0.064^\circ\text{C}$  per decade ( $1\sigma$ , 1875-2006; Fig. 3.5).



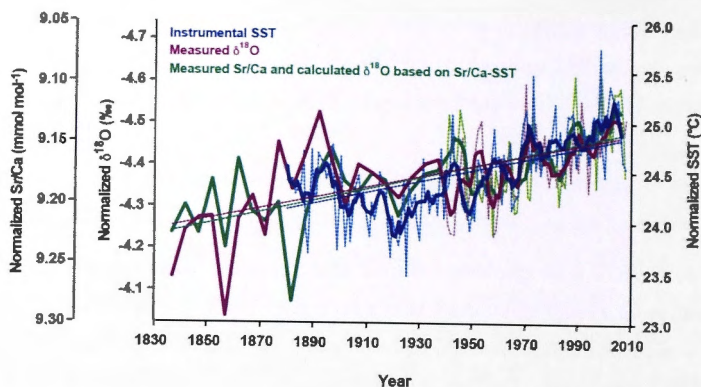


Fig. 3.5 Comparison of averages of measured  $\delta^{18}\text{O}$ , calculated  $\delta^{18}\text{O}$  based on Sr/Ca-derived SST, and instrumental SST master records after normalization of the four sites. Dotted lines are annual variation and bold lines are the variability of 5-year running averages for each record. Reconstructed  $\delta^{18}\text{O}$  was calculated from Sr/Ca-SST with  $\delta^{18}\text{O} (\text{‰}) = -0.2300 \times \text{Sr/Ca-SST} (\text{°C}) + 1.2508$  assuming a zero seawater  $\delta^{18}\text{O}$  composition and adapting the slope reported by Gagan et al (2012). The Intercept was calculated as the mean of intercepts of the four  $\delta^{18}\text{O}$ -SSTs from each core. The results of equivalent SSTs to Sr/Ca and  $\delta^{18}\text{O}$  are shown on the right SST axis. Weighted linear regressions of each master record are shown with the same color-coding and as dotted lines.

Although the  $\delta^{18}\text{O}$  warming trend shows excellent agreement with the instrumental and Sr/Ca-derived SST trends, coral skeletal  $\delta^{18}\text{O}$  can be affected by salinity in addition to SST. The influence of evaporation or precipitation on the  $\delta^{18}\text{O}$  proxy records has been evaluated using the residual  $\delta^{18}\text{O}$  signal record ( $\Delta\delta^{18}\text{O}$ ), which was quantified by removing the SST component of  $\delta^{18}\text{O}$  based on the Sr/Ca-SST record following the methods of Gagan et al. (1998).

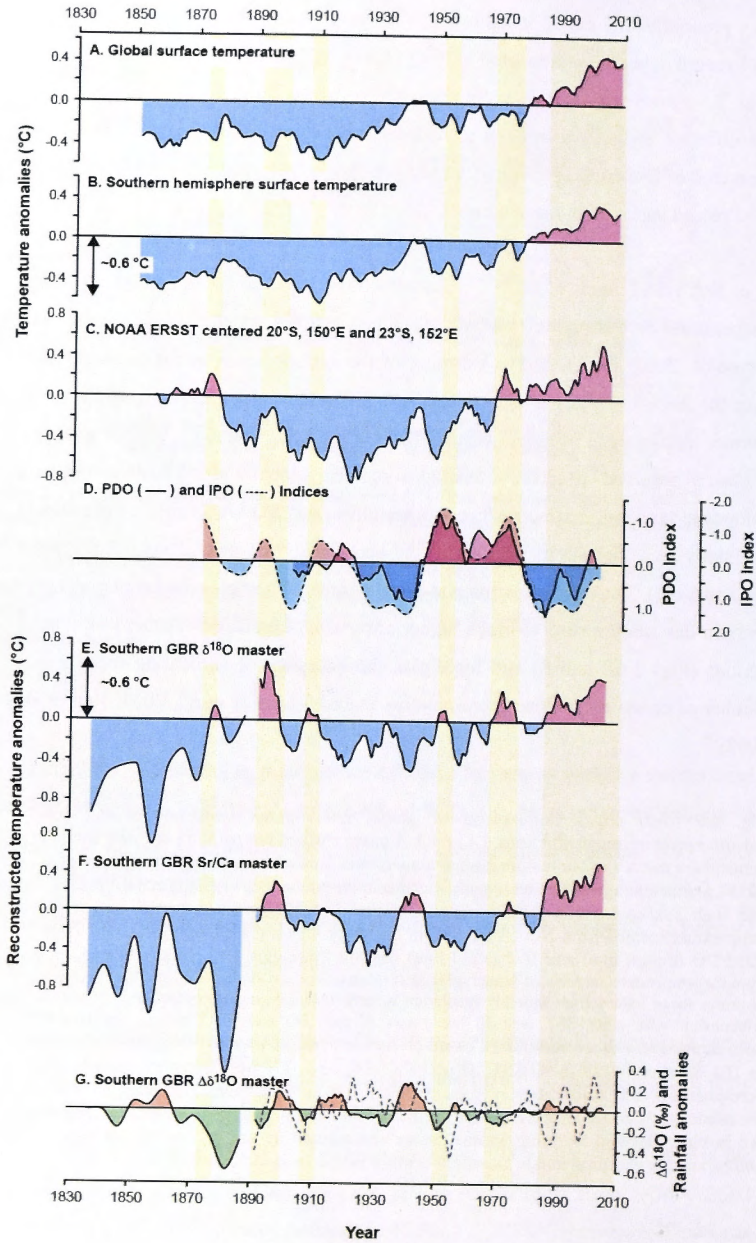
The average  $\Delta\delta^{18}\text{O}$  value is zero across the observation period and the average range of  $\Delta\delta^{18}\text{O}$  variation is less than 0.1‰ except for the period (1887-1835) when there was only one core sampled at 5-year resolution. A variation of 0.1‰ corresponds to a salinity change of  $\sim 0.3\text{‰}$  (Fig. 3.6G; Gagan et al., 2000) and is well within the seasonal salinity change (0.4‰) observed in this region (data from NOAA EMC CMB Pacific GODAS salinity centered at 149.5°E, 20.5°S). Given the  $\delta^{18}\text{O}$  records



vary predominantly due to temperature,  $\delta^{18}\text{O}$  values were reconstructed from Sr/Ca-SST record using the relationship of  $\delta^{18}\text{O} (\text{‰}) = -0.2300 \times \text{Sr/Ca-SST } (^\circ\text{C}) + 1.2508$  (Fig. 3.5 shown with a green solid line). These results show identical trends among the different SST reconstruction techniques and between the calculated and actual measured  $\delta^{18}\text{O}$  records. This indicates temperature is the primary component of coral  $\delta^{18}\text{O}$  record variation in the southern GBR.

The Sr/Ca-SST and  $\delta^{18}\text{O}$ -SST reconstructions can be compared with other temperature reconstruction records elsewhere (Jones et al., 2011; Smith and Reynolds, 2003; Fig. 3.6). The warming of the surface ocean in the southern GBR over the last ~170 years is approximately 1.2°C and modern SSTs are about 0.6°C warmer than average twentieth century SSTs (Figs 3.6C, E, and F). Smiliar warming is clearly observed in all the temperature records (global and southern hemisphere composite land and marine surface temperatures, and NOAA ERSST centered near this study area) despite differences in the occurrence of warm anomalies (between 1965 to 1980). The low resolution and small number of samples for the period 1835-1887 in this study results in much higher uncertainty compared to other observation periods (Figs 3.6E and F) and highlights the necessity of replicating records in a number of corals to produce representative records (Linsley et al., 2004; Ren et al., 2003).

**Fig. 3.6** (Next page) Comparison of global instrumental temperatures and coral paleotemperature reconstructions. (A) Global mean surface temperature and (B) southern hemisphere mean surface temperature averaged over land and ocean surfaces (Jones et al., 2011). Surface temperatures were normalized relative to the mean of the period 1961-1990 and then averaged for 3-year running intervals. (C) Master instrumental sea surface temperature records from NOAA-ERSST in the study region (Smith and Reynolds, 2003), (D) PDO (dotted line) and IPO (solid line) indices. The annual IPO index is filtered values from the temperature anomaly of January-February-March (Folland et al., 2002) and the PDO index is yearly mean values from monthly resolution records (Mantua and Hare, 2002). To show the relationship with other SST records, the y-axis of the IPO and PDO indices are inverted. Reconstructed records are normalized based on the mean of the period 1950-2005 and shown in (E) Southern GBR  $\delta^{18}\text{O}$ -SST, (F) Sr/Ca-SST, and (G)  $\Delta\delta^{18}\text{O}$  master records with precipitation data from MacKay meteorological station (data from Australian Bureau of Meteorology). Warmer temperature anomalies are in red and cooler temperature anomalies are in blue. Decadal warming anomalies are represented by the yellow shaded area and anthropogenic warming in late twentieth century is shown in the orange shaded area.



The warming rates derived from the southern GBR coral  $\delta^{18}\text{O}$ -SST and Sr/Ca-SST records compare well with the instrumental temperature records despite the difference in spatial resolution, whereas the more intense warming occurs at the shorter observation periods (Figs 3.6A to C and E to F). The warming rate of the southern GBR coral records from 1835 to present ( $0.055 \pm 0.052^\circ\text{C}$  per decade,  $1\sigma$ ) is consistent with the southern GBR NOAA ERSST ( $0.056 \pm 0.064^\circ\text{C}$  per decade), as well as the southern hemisphere average surface temperatures ( $0.044 \pm 0.029^\circ\text{C}$  per decade), and the global mean surface temperature ( $0.045 \pm 0.031^\circ\text{C}$  per decade). The rate of warming over the last 100 years (1906-2005) is higher than the full 170 year time interval (1835-2008), with decadal rates for this period of  $0.071 \pm 0.029^\circ\text{C}$  for  $\delta^{18}\text{O}$ -SST and  $0.081 \pm 0.084^\circ\text{C}$  for Sr/Ca-SST, which compare to  $0.075 \pm 0.034^\circ\text{C}$  for southern hemisphere surface temperature and  $0.076 \pm 0.037^\circ\text{C}$  for global surface temperature. The coral proxy derived warming rates per decade over the last 50 years are  $0.0896 \pm 0.094^\circ\text{C}$  for  $\delta^{18}\text{O}$ -SST and  $0.147 \pm 0.066^\circ\text{C}$  for Sr/Ca-SST, and compare to  $0.114 \pm 0.037^\circ\text{C}$  for the southern hemisphere surface temperature and  $0.117 \pm 0.049^\circ\text{C}$  for the global surface temperature per decade. All these records show two to three times more intense warming since 1950 than for the whole time period from 1835 to 2008 at both global and regional scales.

Despite the warming trend exhibited by all land and ocean surface temperature records, there are periodic increases in temperature that occur only in the ocean surface temperature records (e.g. 1887-1898 and 1968-1978; Figs 3.6C, E, and F). Interdecadal variability in the instrumental and coral SST records is also stronger than in the southern hemisphere average land and marine temperature record, suggesting oceanographic changes force interdecadal SST changes. Well-documented ocean-atmospheric anomalies, represented by the Interdecadal Pacific Oscillation (IPO) and the Pacific Decadal Oscillation (PDO) indices, have been used to explain these interdecadal variations in SSTs in the tropical and subtropical south Pacific (Calvo et al., 2007; Linsley et al., 2000; Linsley et al., 2004; Mantua and Hare, 2002; Pelejero et al., 2005; Power et al., 1999; Quinn et al., 1993; Ren et al., 2003).

The coral core records from the southern GBR indicate that many of the interdecadal transitions in coral  $\delta^{18}\text{O}$ -SST and Sr/Ca-SST are aligned with each other and with transitions in the PDO and IPO indices (Figs 3.6D, E and F). Consistent warming signals in coral-based SST reconstructions are associated with negative IPO and PDO indices due to the negative correlation of the IPO and PDO indices with southwest Pacific SSTs (yellow shaded area in Fig. 3.6; Calvo et al., 2007; Linsley et al., 2000; Pelejero et al., 2005; Power et al., 1999). Reduced variation in reconstructed  $\Delta\delta^{18}\text{O}$  and the absence of any significant relationship with ocean-atmospheric anomalies or rainfall records (Fig. 3.6G) is consistent with temperature-dominated variation of coral Sr/Ca and  $\delta^{18}\text{O}$  proxies in the southern GBR. Furthermore, positive SST anomalies and enhanced trade winds during negative IPO or PDO phases could be expected to cause increased evaporation rates and be associated with more positive  $\Delta\delta^{18}\text{O}$ . However, the coral  $\Delta\delta^{18}\text{O}$  record shows only weak positive anomalies during the late twentieth century due to large variations in precipitation (Fig. 3.6G). Interestingly, since 1980 instrumental and coral-derived SSTs show warming anomalies and still display the PDO pattern despite positive IPO and PDO indices (orange shaded area in Fig. 3.6). A comparison of the PDO index with the coral proxy-derived SSTs detrended for warming over the last 50 years shows a good correlation, with the natural PDO decadal variation accounting for approximately 30% ( $p = 0.012$ ,  $n = 20$ ) and 54% ( $p < 0.0001$ ,  $n = 22$ ) of the late twentieth century SST variability in the coral Sr/Ca and  $\delta^{18}\text{O}$  records respectively. This indicates both anthropogenic warming and natural SST variations should be considered in future temperature projections as temperature changes due to ocean-atmospheric teleconnections have been until now at least as significant as the GHG warming effect.

### 3.4 Conclusion

A 170-year proxy record of SST has been reconstructed from Sr/Ca and  $\delta^{18}\text{O}$  analyses on four *Porites* from the southern GBR. These reconstructions were carried out using higher sensitivities of Sr/Ca and  $\delta^{18}\text{O}$  thermometers than those derived by

conventional regression against instrumental SST records due to the bio-smoothing effect. They were performed at both annual and 5-year sampling resolution to allow the study of long-term changes and interdecadal variability in the southern GBR. The SST reconstructions from the southern GBR coral proxies record significant ocean warming at a rate of 0.055°C per decade consistent with that observed in the global average land and ocean surface temperatures. Both Sr/Ca-SST and  $\delta^{18}\text{O}$ -SST reconstructions are characterized by warming in the late twentieth century (since 1950) at rates ( $\sim 0.1^\circ\text{C}$  per decade) above these during the nineteenth and early twentieth century. This indicates the importance of choosing appropriate observation periods to estimate decadal scale warming rates and evidence of recent acceleration in warming rate in the southern GBR. Decadal variability in the coral-derived SST reconstructions shows coupling with the ocean and atmospheric anomalies (e.g. IPO and PDO). These coral records document the strong effects of both anthropogenic warming and natural decadal temperature variability in the southwestern Pacific Ocean. This study highlights the need to consider natural SST variations in response to ocean-atmospheric teleconnections when developing projections of future ocean warming due to increased atmosphere  $\text{CO}_2$  levels.







---

## Chapter 4.

### Ocean acidification in the southern Great Barrier Reef

---

#### 4.1 Introduction

The rise in atmospheric carbon dioxide concentration ( $p\text{CO}_{2\text{atm}}$ ) over the past two centuries exceeds any documented rate of change in geological history (Doney and Schimel, 2007). This has contributed to a  $\sim 0.7^\circ\text{C}$  increase in the average temperature of the global ocean over the past hundred years through the effects of  $\text{CO}_{2(\text{g})}$  as a greenhouse gas (IPCC, 2007a). Moreover, approximately one third of anthropogenic  $\text{CO}_2$  emissions to the atmosphere have been absorbed into the ocean via air-sea exchange (Caldeira and Wickett, 2005; Sabine et al., 2004) and, as a consequence, there has been significant acidification of the surface ocean by  $\sim 0.1$  pH units which is equivalent to a 30% increase in hydrogen ion concentration (IPCC, 2007b; Feely et al., 2009). The surface ocean pH is predicted to drop from a preindustrial average value of 8.2 to 7.8 by 2100 contingent on the emission scenarios (Caldeira and Wickett, 2005). These changes in the ocean temperature and chemistry may produce significant feedbacks into the global carbon cycle via changes in biological and chemical reactions and may have major consequences for marine ecosystems (Wootton et al., 2008). The tropical surface oceans are currently supersaturated with respect to aragonite ( $\Omega_{\text{arag}} \approx 4.0 \pm 0.2$ ; Kleypas et al., 1999a), but as the surface ocean pH continues to decrease the degree of supersaturation will also decrease and this may have negative consequences for many calcifying marine biota and coral reefs

(Doney and Schimel, 2007). Studies indicate that net calcium carbonate accretion on coral reefs may become negative at  $\Omega_{\text{arag}} \leq 3.3$  (Kleypas et al., 1999b; Hoegh-Guldberg et al., 2007), a level that will be reached when atmospheric  $\text{CO}_2$  attains 480 ppm, which may occur as soon as 2065 (Hoegh-Guldberg et al., 2007; Raven, 2005)

Despite the changes posed by ocean acidification to marine ecosystems and coral reefs specifically, the natural spatial and temporal variability of seawater pH and its effects on coral calcification remain poorly known (Trotter et al., 2011; Wei et al., 2009). This reflects the lack of long-term instrumental seawater pH records which, unlike temperature records, span less than three decades and exist for only a handful of sites in the central North Pacific (Hawaii Ocean Time-series: HOT, since 1988, [http://hahana.soest.hawaii.edu/hot/hot\\_jgofs.html](http://hahana.soest.hawaii.edu/hot/hot_jgofs.html)), the North Atlantic (Bermuda Atlantic Time-series Study: BATS, since 1984, <http://bats.bios.edu/>), and the eastern North Atlantic (European Station for Time-Series in the Ocean: ESTOC, since 1995, <http://www.estoc.es/en/>).

Assessment of the impacts of ocean acidification on marine biota is also limited by a lack of knowledge of various local and regional controls on the variation of seawater pH over decadal to centennial time-scales. Natural semi-periodic variations are still the most significant component of climate variability and are closely related to ocean chemistry changes. This is especially the case of the El Niño Southern Oscillation (ENSO) which affects the entire Pacific Ocean basin and global changes depending on the intensity of ENSO teleconnections (Mantua and Hare, 2002; Power et al., 1999). Other sources of variability, such as ocean-atmosphere anomalies described by the Interdecadal Pacific Oscillation (IPO) for the whole Pacific and Pacific Decadal Oscillation (PDO) for the North Pacific, also alter atmospheric conditions and can lead to major perturbations in both horizontal and vertical ocean circulation (Linsley et al., 2000; Power et al., 1999). Due to the lack of long-term instrumental data, there is a scarcity of studies trying to decipher the response of ocean chemistry to and the role of anthropogenic versus natural climate variations. This is particularly true of the south Pacific, where continuous *in situ* measurements of surface ocean  $\text{pCO}_2$  and pH have commenced only in 2009 near Heron Island in the southern Great

Barrier Reef (GBR; the MAPCO<sub>2</sub> mooring station located 23.46°S, 151.47°E and deployed ~38 km off Heron Island, data is available from <http://www.pmel.noaa.gov/co2/story/Heron+Island> for the period October 2009 to April 2010).

Seawater carbon chemistry in coral reef environments changes in response to a complex set of biological, physical and chemical processes, including air-sea exchange of CO<sub>2</sub>, horizontal and vertical water mixing, photosynthesis, respiration, and calcification (Kleypas et al., 2011). Large variations in reef water pH and pCO<sub>2</sub> have been reported to occur on diurnal, seasonal, and interdecadal timescales. For example, the diel pH range is from 7.8 to 8.3 in Molokai reef flat, Hawaii (Yates and Halley, 2006) and an even larger pH range from 7.7 to 8.5 has been observed in Heron Island lagoon (Santos et al., 2011) and at Lady Elliot Island (Shaw et al., 2012) in the southern GBR, Australia. Large variations in reef water pH (up to 0.5 pH units) have been reported to occur over decadal time-scales in the central GBR (Wei et al., 2009) and Coral Sea (Pelejero et al., 2005) based on coral boron isotope ( $\delta^{11}\text{B}$ ) compositions, and have been attributed to the accumulation of CO<sub>2</sub> generated from calcification within these coral reef environments.

The reconstruction of past seawater pH values may be valuable for understanding the impacts of varying seawater pH on corals and their resilience to future ocean acidification. Long-term changes in ocean pH can be tracked in principle using the boron isotope ( $\delta^{11}\text{B}$ ) composition of coral skeletons (Hemming and Hanson, 1992; Hönisch et al., 2004; Vengosh et al., 1991; additional information about boron isotope as a proxy for seawater pH is in Appendix C). The boron isotope seawater pH proxy is based on the preferential incorporation into coral aragonite of boron with the pH-dependent  $\delta^{11}\text{B}$  composition of seawater borate (Hemming and Hanson, 1992; Vengosh et al., 1991). However, coral calcification takes place within a physiologically controlled environment that is located in the semi-isolated space between the coral skeleton and the calciblastic ectoderm (Al-Horani et al., 2003; Cohen and McConnaughey, 2003; Cohen and Holcomb, 2009; Ries, 2011). To promote aragonite precipitation (i.e.  $\text{Ca}^{2+} + \text{CO}_3^{2-} \leftrightarrow \text{CaCO}_3$ ) the pH of the

calcifying fluid ( $\text{pH}_{\text{cf}}$ ) is elevated by 0.2-0.5 pH units above that of the ambient seawater (Al-Horani et al., 2003; Venn et al., 2011). This is thought to occur via action of a  $\text{Ca}^{2+}$ -ATPase pump which removes two  $\text{H}^+$  ions from the calcifying fluid in exchange for every  $\text{Ca}^{2+}$  ions (Al-Horani et al., 2003; Cohen and McConnaughey, 2003) which shifts the dissolved inorganic carbon (DIC) equilibrium in favor of  $\text{CO}_3^{2-}$  (relative to  $\text{HCO}^-$ ) and dissolved boron equilibrium toward borate. The  $\delta^{11}\text{B}$  compositions of corals grown under controlled pH conditions indicate the calcification fluid pH is raised by 0.3 to 1.0 pH units relative to the ambient seawater pH, depending on species and ambient seawater pH (Honish et al., 2004; Krief et al., 2010; Trotter et al., 2011). This difference between the calcification and ambient seawater pH can be corrected using calibrated species-dependent linear functions (Trotter et al., 2011) that translate the boron isotopic composition of corals to ambient seawater pH.

The uptake of atmospheric  $\text{CO}_2$  derived from fossil fuel burning is also causing the carbon isotope ( $\delta^{13}\text{C}$ ) of surface ocean DIC to become lighter, a process referred to as the  $^{13}\text{C}$ -Suess effect (Druffel and Benavides, 1986). This trend towards lower DIC  $\delta^{13}\text{C}$  values is reflected in the carbon isotope ( $\delta^{13}\text{C}$ ) composition of coral skeletons and has been reported from the South Pacific Ocean and elsewhere (Druffel and Griffin, 1999; Linsley et al., 1999; Quinn et al., 1998; Swart et al., 2010; Wei et al., 2009). However, it is overprinted by large annual and inter-annual variations in  $\delta^{13}\text{C}$  (Swart et al., 2010) that arise from a combination of physiological mechanisms (Grottoli and Wellington, 1999), kinetic effects (McConnaughey, 1989b; McConnaughey and Whelan, 1997; Omata et al., 2005) and variations in seawater pH (Adkins et al., 2003; Krief et al., 2010).

Concern about climate and ocean chemistry changes due to rising  $\text{pCO}_2$  has focused largely on the fate of tropical corals rather than subtropical ( $20^\circ\text{S}$  to  $35^\circ\text{S}$ ) corals, which grow under lower (below optimum) temperatures, more acidic seawater pH, and lower aragonite saturation state (Lough and Barnes, 2000; Orr et al., 2005). It remains to be established whether subtropical corals will be more or less sensitive than tropical corals to future environmental changes. Accordingly, this study has



generated carbon ( $\delta^{13}\text{C}$ ) and boron ( $\delta^{11}\text{B}$ ) isotopic records for multiple ( $n=4$ ) *Porites* corals from the southern GBR that span the last 170 years as a basis for constraining the influence of anthropogenic forcing and natural climate variability on surface ocean chemistry and coral calcification in this region. These records are compared to and combined with previously determined coral  $\delta^{11}\text{B}$ -seawater pH records from the central GBR (Wei et al., 2009) and the Coral Sea (Pelejero et al., 2005) to establish the long-term variability of surface ocean pH in the region. This study provides evidence for large variation in reef water pH across centennial timescales (Bates et al., 2010; Pelejero et al., 2010; Wei et al., 2009) due to both ocean acidification and natural variation of reef water pH.

## **4.2 Materials and methods**

### **4.2.1 Coral samples and study area**

Living massive corals of the genus *Porites* were sampled from the southern GBR using underwater drilling techniques developed at the Australian National University (ANU; Alibert and McCulloch, 1997; Fallon et al., 2003b; Wei et al., 2009). Two coral cores were obtained from the Pompey complex (Middle Pompey and Little Kindermar reefs) in March 2006 and two cores from Lady Musgrave Island and Fitzroy Reef in October 2008 (Fig. 2.1 in Chapter 2 and Table 4.1). These particular reefs avoid the effects of terrestrial runoff as they are well offshore; 139 km and 126 km from Mackay in the case of Middle Pompey and Little Kindermar, and 94 km and 116 km from Gladstone in the case of Fitzroy Reef and Lady Musgrave Island.

**Table 4.1** Location and time spans of coral cores from the southern GBR

Reef	sample	Latitude (°S)	Longitude (°E)	Core collecting depth (m)	Core length (cm)	Time span	Sampling location of reef lagoon
Middle Pompey	PSC	20.99	150.51	5	150	1907-2006	outside
Little Kindermar	PSA	21.10	150.40	5	186	1834-2006	outside
Fitzroy Reef	FYR08-D	23.37	152.10	0.5	96.5	1950-2008	inside
Lady Musgrave Is.	LMI08-H	23.54	152.25	7.9	143	1890-2008	inside

The southern GBR between 20°S and 24°S comprises two distinct reef systems separated by the Capricorn Channel (Fig. 2.1A in Chapter 2). To the north of the channel the Pompey complex and Swain Reefs form a broad (>200 km east-west), densely packed reef tract. To the south of the channel the Capricorn and Bunker Reefs form a line of reefs near the outer edge of a narrow shelf (~70 km; Kleypas and Burrage, 1994). The circulation of seawater in the southern GBR is complicated by the interaction between the East Australian Current (EAC) and the shelf waters of the Capricorn Channel. The meandering of the EAC in this area develops into a cyclonic mesoscale (~100 km) eddy, and associated smaller (~10 km) eddies (Kleypas and Burrage, 1994).

The two cores sampled from the Pompey Complex were collected from the fore-reefs of the crescent shaped Middle Pompey and Little Kindermar reefs. These two reefs lie 20 km landward of and are separated from the main Pompey complex (Fig. 2.1B-1 in Chapter 2) which extends parallel to the shelf edge over a distance of 140 km. The narrow channels that cut through the Pompey Reefs reach depths exceeding 100 m. The southeast of Middle Pompey and Little Kindermar reefs is exposed to the prevailing wind and sea conditions found within the lagoon of the GBR.

The two cores from the Capricorn-Bunker Group were collected from intra-lagoon sites at Fitzroy Reef and Lady Musgrave Island (Figs 2.1B-2 and 2.1B-3 in Chapter 2). Fitzroy Reef is the largest reef (36.5 km<sup>2</sup>) in the Capricorn Bunker Group, and has a large and deep (6-10 m) lagoon that harbors well-developed coral communities that include a large community of branching corals on the lagoon floor (Great Barrier Reef Marine Park Authority, GRMPA, <http://www.gbrmpa.gov.au/zoning-permits-and-plans/site-specific-management/fitzroy-reef>). Although no cay is present at Fitzroy reef, an intermittent sand body often appears at low tide on the southwest end



of the reef. The Lady Musgrave Island (Fig. 2.1B-3) is an outer shelf lagoonal reef that covers an area of 12.5 km<sup>2</sup> (Hopley et al., 2007) and has a permanent sand cay at its southwest end. The southern and eastern perimeter of Lady Musgrave Island reef are exposed to the prevailing wind and sea conditions within the Coral Sea while the northwestern margin of this reef is sheltered from these conditions (2006-2012; AIMS Reef survey, <http://www.aims.gov.au/docs/data-centre/reef-monitoring-surveys.html>).

#### **4.2.2 Core treatment for geochemical analysis**

The 55 mm diameter cores from the southern GBR were sliced length-wise into 7 mm thick slabs. Those with minimal evidence of bioerosion were X-rayed to assign chronologies based annual density banding. Growth chronologies were validated by cross checking independent chronologies determined from density bands and seasonal trace element ratio cycles measured by laser ablation inductively coupled plasma mass spectrometry (LA-ICPMS) employing the analytical and age modeling protocols described in Fallon et al. (1999; 2003b) and Sinclair et al. (1998). The resulting chronologies along the maximum growth axes are shown in Fig. 3.2 in Chapter 3.

Coral slabs from Pompey complex, Fitzroy Reef and Lady Musgrave Island were milled along the maximum growth axes in annual intervals, winter to winter (i.e. August to August based on LA-ICPMS geochemical profiles), for analysis of stable isotopes ( $\delta^{13}\text{C}$  and  $\delta^{11}\text{B}$ ). The Little Kindermar core was sampled in annual increments from 2000 back to 1940, and in 5-year intervals from 1939 to 1834. Milling of the slab surface to a depth of 0.25 mm was undertaken for the purpose of cleaning, prior to collection of samples by further milling to a depth of 2.5 mm. Two different drill bits were used depending on the annual extension rate of the cores, in order to obtain sufficient coral powder for all stable isotope measurements (i.e. >100 mg); a 4 mm bit for Middle Pompey, Fitzroy Reef and Lady Musgrave Island which

have high annual extension rates and a 6 mm bit for Little Kindermar which has a low extension rate (see appendix Figs B-1 to B-4).

### 4.2.3 Coral geochemistry

#### 4.2.3.1 Coral carbon isotope compositions

Analyses of  $\delta^{13}\text{C}$  were carried out following the methods described by Hendy et al. (2002) and Gagan et al. (1998). Powdered coral samples weighing 180-220  $\mu\text{g}$  were analyzed using a Kiel carbonate device connected to a dual-inlet Finnigan MAT 251 isotope ratio mass spectrometer (IRMS). The samples were reacted with 105% phosphoric acid at  $90^\circ\text{C}$ , and the generated  $\text{CO}_2$  from the reaction was purified by freezing and then vaporizing it in a double trap system using liquid nitrogen and heating lines. Primary calibration was made using NBS 19 (+1.95‰), and a secondary correction then performed against Vienna Peedee belemnite (V-PDB). The standard deviation ( $1\sigma$ ) of the analysed NBS 19 standard was 0.05‰ ( $n = 84$ ).

#### 4.2.3.2 Boron isotope methods and systematics

The same methods of *boron isotope analysis and calibration seawater pH from boron isotopic composition in coral* described in Chapter 2 are used in this study. In this section, we are focusing on the physiological modification of coral  $\delta^{11}\text{B}$ -seawater pH proxy.

#### *Physiological effects on coral $\delta^{11}\text{B}$ -seawater pH proxy*

The measured  $\delta^{11}\text{B}$  composition of coral strictly reflects the pH at the site of calcification ( $\text{pH}_{\text{cf}}$ ) and can be employed to estimate the ambient seawater pH ( $\text{pH}_{\text{T}}$ ) based on the relationships

$$\text{pH}_T = (\text{pH}_{\text{cf}} - 4.7242)/0.4664 \quad (4-1)$$

and

$$\text{pH}_T = (\text{pH}_{\text{cf}} - 5.9545)/0.3200 \quad (4-2)$$

for *Porites cylindrica* and *Porites spp* that have been fit Trotter et al. (2011; Fig. 4.1) and are based on earlier experimental results reported by Hönisch et al. (2004) and Krief et al. (2010).

The  $\delta^{11}\text{B}$  values obtained from the four southern GBR corals range from 22.2‰ to 25.8‰ which correspond to  $\text{pH}_{\text{cf}}$  of 8.35 to 8.61, and seawater  $\text{pH}_T$  values from 7.76 to 8.31 based on equation 4-1 (Fig. 4.1A) and from 7.47 to 8.27 based on equation 4-2 (Fig. 4.1B). The mean  $\text{pH}_T$  values obtained from all for cores for year 2008 were  $8.04 \pm 0.15$  ( $1\sigma$ ) and  $7.87 \pm 0.21$  ( $1\sigma$ ) using equation 4-1 and 4-2 respectively. The  $\text{pH}_T$  values obtained using equation 4-1, which is based on the calibration of Hönisch et al. (2004), are consistent with seawater pH values ( $\text{pH} = 8.07$ ) measured during the period of October 2009-April 2010 at a mooring located near Heron Island in the Capricron-Bunker Group (22.46°S 151.93°E; <http://www.pmel.noaa.gov/co2/story/Heron+Island>). Consequently equation 4-1 has been applied throughout this study.

The seawater  $\text{pH}_T$  values derived from the southern GBR cores fall near the boron isotope-seawater reference curves of  $\alpha_{\text{B3-B4}} = 1.0194$  or  $1.0204$  (Fig. 4.1A), which justified the use of an empirical  $\alpha_{\text{B3-B4}}$  value of  $\sim 1.020$  in earlier  $\delta^{11}\text{B}$ -pH proxy studies that did not take into account the biological modification of the calcification pH (Hönisch et al., 2007; Liu et al., 2009; Wei et al., 2009; Xiao et al., 2006). To account for the application of this empirical  $\alpha_{\text{B3-B4}}$  value in previously published *Porites*  $\delta^{11}\text{B}$  data from the Coral Sea (Pelejero et al., 2005) and the central GBR (Wei et al., 2009), these results from these studies have been converted to  $\text{pH}_T$  using both the conventional calibration method and the new vital effect calibration (Fig. 4.1). The previously reported mean measured seawater  $\text{pH}_T$  values of 8.03 and 8.01

for Flinders Reef and Arlington Reef respectively, compare to recalculated seawater  $\text{pH}_T$  values of 8.07 for Flinders Reef and 7.99 for Arlington Reef. This represents a difference of only 0.02-0.04 pH units between the two calibration approaches possibly due to small difference in temperature and salinity changes at annual to 5-year intervals. However, at subannual and interannual time scale when environmental conditions significantly vary, it is important using the appropriate  $\alpha_{\text{B}_3\text{-B}_4}$  and also need to account for the physiological effect on coral  $\text{pH}$ -up regulation on the  $\delta^{11}\text{B}$ - $\text{pH}$  proxy.

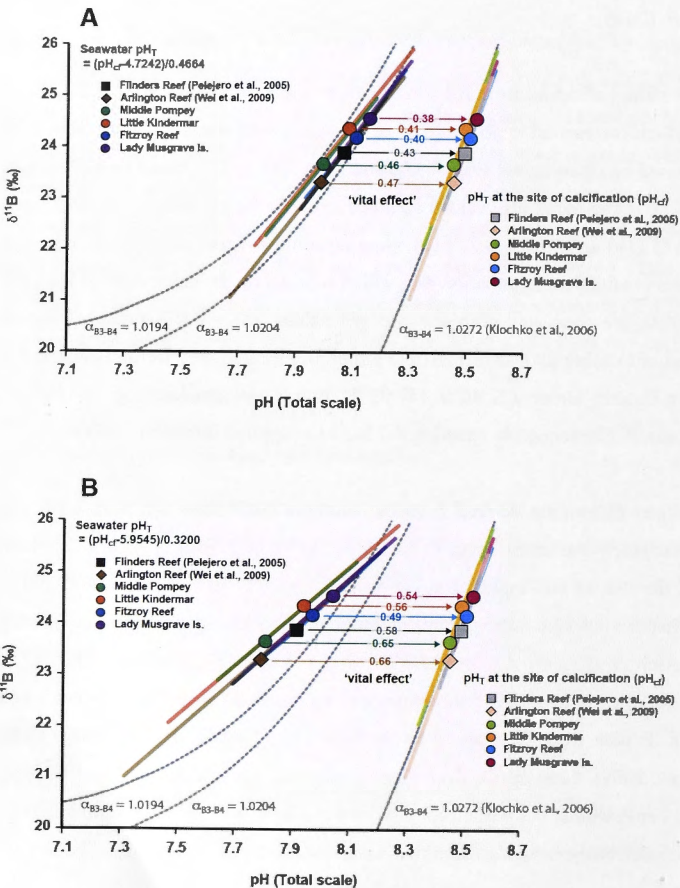


**Fig. 4.1** (*Opposite page*) Measured coral  $\delta^{11}\text{B}$  and reconstructed seawater  $\text{pH}_T$  from the southern GBR. The horizontal offset is the extent of pH up-regulation during coral calcification. The symbols and solid lines represent averaged values and trend lines (or the range of  $\delta^{11}\text{B}$ ) for each coral record, respectively. The color of each trend line corresponds to the colored symbols. Previously published *Porites*  $\delta^{11}\text{B}$  data from Flinders Reef in the Coral Sea (Pelejero et al., 2005) and Arlington Reef in the central GBR (Wei et al., 2009) are also plotted. All  $\delta^{11}\text{B}$ -derived  $\text{pH}_T$  values, including those from previous studies, were calculated with both the conventional  $\delta^{11}\text{B}$ -pH equation ( $\text{pH}_T$  at the site of calcification,  $\text{pH}_{cf}$ ) and the two vital-effect calibrations, equations 4-1 (A) and 4-2 (B).  $\alpha_{\text{B3-B4}}=1.0207$  (Klochko et al., 2006) was used as well as  $pK_B$  adjusted for ambient temperature and salinity for the data from the southern GBR (this study). Fixed values of 25°C and 35 PSU with  $\delta^{11}\text{B}$  of 39.5 ‰ were used for the calculation of published data. The values of  $\text{pH}_{cf}$  compared to modern seawater pH (8.1-8.2) were finally calibrated with respect to the biological pH component by using the approach developed by Trotter et al. (2011). As a result, the seawater pH ( $\text{pH}_T$ ) calibrated for the 'vital effect' shows similar values to modern seawater  $\text{pH}_T$ . Three borate reference curves (dotted gray lines) are calculated assuming a seawater  $\delta^{11}\text{B}$  of 39.7‰, 25°C, and 35 PSU.

#### 4.2.4 Data manipulation

Composite master records of  $\delta^{13}\text{C}$ ,  $\delta^{11}\text{B}$  and  $\delta^{11}\text{B}$ -derived seawater  $\text{pH}_T$  have been calculated for the southern GBR cores by normalizing the individual records to the average obtained for the common analyzed period of the four cores (i.e. 1950-2005). This was achieved by first calculating the standard score value for each core,

$$z = (x - \bar{x}) / \sigma \quad (4-2)$$

where  $x$  is a primary data, and  $\bar{x}$  and  $\sigma$  are a mean and standard deviation of individual core records respectively, and then normalizing each core record using the equation.

$$x_{\text{normalized}} = \bar{x}_{s\text{GBR}} + z \times \sigma_{s\text{GBR}} \quad (4-3)$$

where  $x_{\text{normalized}}$  is the normalized coral record and  $\bar{x}_{s\text{GBR}}$  and  $\sigma_{s\text{GBR}}$  are the mean and standard deviation of all four southern GBR coral records respectively.

An extended composite record of  $\delta^{11}\text{B}$  derived-seawater  $\text{pH}_T$  for the southwest Pacific region has been derived by including the Arlington Reef core record from the central GBR (Wei et al., 2009) and the Flinders Reef core record from the Coral Sea (Pelejero et al., 2005) in addition to the four southern GBR cores analysed in this study. The same methodology has been applied as for the southern GBR composite records, except that annually resolved seawater  $\text{pH}_T$  records from this study and the Arlington Reef core were calculated as 5-year running averages before being normalized in order to circumvent sample resolution differences between the various records. The normalization was again performed over the common period to all cores (i.e. 1950-1990).

Weighted linear regressions of the composite record have been employed to estimate the rate of variation of the southern GBR  $\delta^{13}\text{C}$  and  $\delta^{11}\text{B}$  derived-seawater  $\text{pH}_T$  records to account for the differing number of samples in any one year. Regression statistics were calculated using SPSS (IBM Corp., 2011). The 95% of confidence interval values obtained for each year were employed as weighting variables; else the maximum confidence interval value for each parameter was used for periods where only one record exists (i.e. the period of 1834-1891 for the southern GBR master records and of 1707-1802 for the southwest Pacific  $\text{pH}_T$  master record).

## 4.3 Results and discussion

### 4.3.1 $\delta^{13}\text{C}$ variation in southern GBR corals

The  $\delta^{13}\text{C}$  records of modern *Porites* corals are shown in Fig. 4.2, and the mean values over the full records and the common periods are summarized in Table 4.2.

The average  $\delta^{13}\text{C}$  compositions of the cores are indistinguishable apart from the longest Little Kindermar coral record when averaged over the whole observation period (1834-2008; Table 4.2). In comparison to the long-term average  $\delta^{13}\text{C}$  values, the averages  $\delta^{13}\text{C}$  compositions for the common period (1950-2005) are similar in all



cores in a range of  $\delta^{13}\text{C}$  composition variations ( $1\sigma$ ; Table 4.2). The higher mean  $\delta^{13}\text{C}$  value of the Little Kindermar coral record, compared to the other cores over its whole observation period can be attributed to its higher  $\delta^{13}\text{C}$  during the late nineteenth to early twentieth century.

**Table 4.2** Mean  $\delta^{13}\text{C}$  compositions (‰) and their standard deviations ( $1\sigma$ ) for four *Porites* cores from the southern GBR. Values have been determined for the whole observation period (1837-2008) and the common period (1950-2005).

Sample	Period of record	Mean of full record	Number of samples	Mean of common period record	Number of samples
Middle Pompey	1907-2006	$-1.88 \pm 0.25$	73	$-1.84 \pm 0.23$	56
Little Kindermar	1834-2006	$-1.13 \pm 0.47$	87	$-1.34 \pm 0.42$	56
Fitzroy Reef	1950-2008	$-1.73 \pm 0.42$	59	$-1.70 \pm 0.40$	56
Lady Musgrave Is.	1890-2008	$-2.14 \pm 0.49$	79	$-2.22 \pm 0.52$	56

The  $\delta^{13}\text{C}$  records for the four southern GBR corals all show a progressive depletion with time (Fig. 4.2). Similar long-term  $\delta^{13}\text{C}$  trends have been documented from corals from Arlington Reef in the GBR (Wei et al., 2009), Flinders Reef in the Coral Sea (Pelejero et al., 2005) and Fiji (Dassié et al., 2013) as well as, from coralline sponges from Jamaica and Vanuatu (Böhm et al., 1996; Böhm et al., 2002; Fallon et al., 2003a). The rate of depletion in  $\delta^{13}\text{C}$  with time since 1960 is comparable in all cores regardless of location and latitude;  $-0.0161 \pm 0.0108\% \text{ yr}^{-1}$  ( $1\sigma, p < 0.0001$ ) for Middle Pompey,  $-0.0152 \pm 0.0233\% \text{ yr}^{-1}$  ( $p < 0.0001$ ) for Little Kindermar,  $-0.0185 \pm 0.0222\% \text{ yr}^{-1}$  ( $p < 0.0001$ ) for Fitzroy Reef, and  $-0.0237 \pm 0.0228\% \text{ yr}^{-1}$  ( $p < 0.0001$ ) for Lady Musgrave Island.

Individual coral skeletal  $\delta^{13}\text{C}$  data vary with water depth (Dassié et al., 2013; Grottoli, 1999). Corals growing deeper in the water column have lower (more negative) mean  $\delta^{13}\text{C}$  values than corals growing at shallower water depths. This is because the rates of photosynthetic activity, which increases skeletal  $\delta^{13}\text{C}$  compositions, vary with the amount of light, and light is attenuated with increasing water depth (Dassié et al., 2013; Grottoli, 1999). As a result, more depleted  $\delta^{13}\text{C}$  occurs in the older part of corals and otherwise contributes to enhance the  $\delta^{13}\text{C}$

decline with time. Accordingly, in order to make the composite  $\delta^{13}\text{C}$  record better reflect changes in the regional DIC, the cumulative growth influence from all southern GBR coral  $\delta^{13}\text{C}$  records was calculated and removed for their cumulative extension rates following Dassié et al. (2013; depth or cumulative extension rate (m) =  $-1.4784 - 6.2063 \times \delta^{13}\text{C}$  (‰)) before being composited and detrended (annual extension rate of the four southern GBR corals are in Appendix Table E-7 to E-10). This correction increases the slope of the  $\delta^{13}\text{C}$  against time relationship, resulting in a higher rate of coral  $\delta^{13}\text{C}$  depletion (Fig. 4.2B). The rate of decrease of the growth effect corrected  $\delta^{13}\text{C}$  is very similar to that found for Fiji corals (Dassié et al., 2013) and for direct measurements of DIC in the Pacific (Gruber et al., 1999) for the same observation period (-0.13‰ for this study, -0.19‰ for the Fiji corals and -0.15 ± 0.06‰ for the Tropical Pacific over 1980-1990). These results emphasise the importance of removing the growth (or water depth) influence on the coral  $\delta^{13}\text{C}$  records to reconstruct a more accurate of regional surface water DIC  $\delta^{13}\text{C}$  variability (Dassié et al., 2013).

As seen in Fig 4.2B, all southern GBR  $\delta^{13}\text{C}$  records show a similar long-term trend of increasingly more depleted  $\delta^{13}\text{C}$  values towards the present. To investigate decadal variations about the longer term trend, the  $\delta^{13}\text{C}$  data were detrended using polynomial fits to the depth corrected  $\delta^{13}\text{C}$  records from the southern GBR reef cores over the each observation period. Comparisons of these detrended  $\delta^{13}\text{C}$  records between the southern GBR corals are shown in Table 4.3.

The different coral  $\delta^{13}\text{C}$  records are strongly correlated except for the Middle Pompey and Little Kindermar cores over their common periods (Table 4.3). In contrast, the detrended  $\delta^{13}\text{C}$  records do not show any correlation between individual coral  $\delta^{13}\text{C}$  records for their common period. In other words, the strong correlation between different coral  $\delta^{13}\text{C}$  from the southern GBR is mainly due to the accelerating depletion of  $\delta^{13}\text{C}$  compositions with time. These  $\delta^{13}\text{C}$  variations in the southern GBR are similar to the records from five sites in South Florida (Swart et al., 2010). They found that all corals show the decrease in  $\delta^{13}\text{C}$  towards present with superimposed decadal variations on this decrease of up to 0.5‰. These higher order variations in

$\delta^{13}\text{C}$  were similar in different core records but did not appear to correlate between the records. The decadal variations in detrended  $^{13}\text{C}$  from the southern GBR are as high as reported by Swart et al. (2010) and do not correlate between cores As Swart et al. (2010) noted that the decadal variations in many corals are very complicated deviations from the long-term negative trend and the timing of these variations is not consistent even between corals that are closely located.

**Table 4.3** Correlation between individual coral  $\delta^{13}\text{C}$  variations from the southern GBR for the whole and common observation periods using absolute  $\delta^{13}\text{C}$  compositions and depth effect corrected and detrended  $\delta^{13}\text{C}$  records. The correlations and significance were determined using Pearson Product-moment correlation at 95% confidential level. All correlation coefficients are given as *r*-values and all statistically significant values at 95% confidential level are shown in bold text. Correlation that are not significant are shown with *p*-values in brackets.

	Middle Pompey	Little Kindermar	Fitzroy Reef
<i>Absolute <math>\delta^{13}\text{C}</math> record for the whole period</i>			
Little Kindermar	0.00 (df=71, p=0.10)		
Fitzroy Reef	<b>0.43 (df=54, p&lt;0.01)</b>	<b>0.44 (df=54, p&lt;0.01)</b>	
Lady Musgrave Is.	<b>0.33 (df=71, p&lt;0.01)</b>	<b>0.55 (df=74, p&lt;0.01)</b>	<b>0.68 (df=57, p&lt;0.01)</b>
<i>Absolute <math>\delta^{13}\text{C}</math> record for the common period (1950-2005)</i>			
Little Kindermar	0.24 (df=54, p=0.08)		
Fitzroy Reef	<b>0.43 (df=54, p&lt;0.01)</b>	<b>0.44 (df=54, p&lt;0.01)</b>	
Lady Musgrave Is.	<b>0.49 (df=54, p&lt;0.01)</b>	<b>0.49 (df=54, p&lt;0.01)</b>	<b>0.67 (df=54, p&lt;0.01)</b>
<i>Depth effect corrected and detrended <math>\delta^{13}\text{C}</math> record for the whole period</i>			
Little Kindermar	-0.55 (df=71, p=0.06)		
Fitzroy Reef	0.04 (df=54, p=0.80)	-0.05 (df=54, p=0.72)	
Lady Musgrave Is.	<b>0.26 (df=71, p&lt;0.05)</b>	-0.08 (df=74, p=0.50)	0.21 (df=57, p=0.10)
<i>Depth effect corrected and detrended <math>\delta^{13}\text{C}</math> record for the common period (1950-2005)</i>			
Little Kindermar	-0.16 (df=54, p=0.23)		
Fitzroy Reef	0.04 (df=54, p=0.80)	-0.05 (df=54, p=0.72)	
Lady Musgrave Is.	0.16 (df=54, p=0.25)	-0.12 (df=54, p=0.36)	0.22 (df=54, p=0.11)

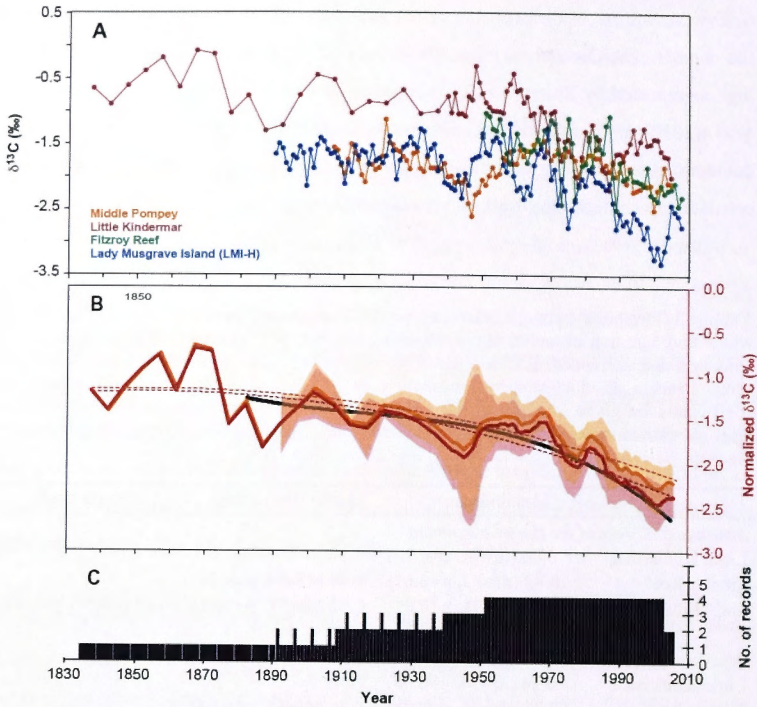


**Fig. 4.2** Time series of all  $\delta^{13}\text{C}$  records in the southern GBR. (A) Absolute  $\delta^{13}\text{C}$  compositions are based on annual records except for Little Kindermar prior to 1940 (5-year intervals). (B) Composite  $\delta^{13}\text{C}$  record (red) and depth effect corrected composite  $\delta^{13}\text{C}$  record (orange) with 95% confidence envelope calculated from 5-year running averages of individual coral records normalized to the period of 1950-2005. Dashed lines represent regression of the composite records indicating accelerated decreasing trend in  $\delta^{13}\text{C}$ . Fiji coral  $\delta^{13}\text{C}$  composite with influence of cumulative growth removed (Dassié et al., 2013) are also shown in a black line. (C) Number of cores contributing to the  $\delta^{13}\text{C}$  composite record from each annual or 5-year period. Weighted linear and non-linear regressions trends for the composite  $\delta^{13}\text{C}$  record are represented by dotted lines over the full observation period. An individual  $\delta^{13}\text{C}$  record accounts for on average 67% of the common variance contained in the master  $\delta^{13}\text{C}$  record (Table 4.4).

**Table 4.4** Individual core  $\delta^{13}\text{C}$  and pH records compared with master records.

Records	Correlation coefficient $r$	Adjusted $r^{2*}$	$p$	$n$
<i><math>\delta^{13}\text{C}</math></i>				
Middle Pompey	0.58	0.33	<0.0001	66
Little Kindernar	0.81	0.65	<0.0001	81
Fitzroy Reef	0.93	0.86	<0.0001	54
Lady Musgrave Is.	0.93	0.86	<0.0001	74
Mean ( $1\sigma$ )	0.81 (0.16)	0.67 (0.25)		
<i>pH (Southern GBR)</i>				
Middle Pompey	0.75	0.55	<0.0001	66
Little Kindernar	0.77	0.59	<0.0001	81
Fitzroy Reef	0.39	0.14	<0.005	54
Lady Musgrave Is.	0.52	0.26	<0.0001	74
Mean ( $1\sigma$ )	0.61 (0.18)	0.39 (0.22)		
<i>pH (Southwest Pacific)</i>				
Southern GBR	0.58	0.33	<0.0001	85
Arlington Reef	0.41	0.16	<0.001	83
Fliders Reef	0.47	0.20	<0.001	56
Mean ( $1\sigma$ )	0.47 (0.11)	0.22 (0.10)		

\* The 'adjusted  $r^2$ ' value estimates the proportion of variance accounted for by the regression analysis.

#### 4.3.2 $\delta^{11}\text{B}$ coral records and $\delta^{11}\text{B}$ -derived seawater pH from the southern GBR

The  $\delta^{11}\text{B}$  records of the southern GBR corals are shown in Fig. 4.3, and the average  $\delta^{11}\text{B}$  compositions of the four cores over the full records and the common periods are summarized in Table 4.5.



**Table 4.5** Mean  $\delta^{11}\text{B}$  compositions (‰) and  $\delta^{11}\text{B}$ -derived seawater  $\text{pH}_T$  with their standard deviations ( $1\sigma$ ) for four *Porites* cores from the southern GBR. Values have been determined for the whole observation period (1837-2008) and the common period (1950-2005).

Sample	Period of record	Mean of full record	Number of samples	Mean of common period record	Number of samples
<i><math>\delta^{11}\text{B}</math></i>					
Middle Pompey	1907-2006	23.52 $\pm$ 0.61	73	23.32 $\pm$ 0.48	56
Little Kindermar	1834-2006	24.33 $\pm$ 0.73	87	24.18 $\pm$ 0.65	56
Fitzroy Reef	1950-2008	24.56 $\pm$ 0.45	59	24.59 $\pm$ 0.44	56
Lady Musgrave Is.	1890-2008	24.18 $\pm$ 0.52	79	24.26 $\pm$ 0.53	56
<i>Seawater <math>\text{pH}_T</math></i>					
Middle Pompey	1907-2006	7.97 $\pm$ 0.09	73	7.94 $\pm$ 0.07	56
Little Kindermar	1834-2006	8.08 $\pm$ 0.10	87	8.06 $\pm$ 0.09	56
Fitzroy Reef	1950-2008	8.16 $\pm$ 0.06	59	8.16 $\pm$ 0.06	56
Lady Musgrave Is.	1890-2008	8.11 $\pm$ 0.07	79	8.11 $\pm$ 0.07	56

The average  $\delta^{11}\text{B}$  compositions of the four cores are consistent, irrespective of their different age ranges (Table 4.5), and are consistent with previously determined  $\delta^{11}\text{B}$  compositions of *Porites* corals from the central GBR (23.33  $\pm$  0.81‰,  $1\sigma$ ; Wei et al., 2009) and Coral Sea (23.92  $\pm$  0.46‰,  $1\sigma$ ; Pelejero et al., 2005). These  $\delta^{11}\text{B}$  values translate to seawater  $\text{pH}_T$  values, which have averages that range from 7.97 to 8.16 for the full individual core records (Table 4.5). For the recent common period (1950-2005), the average core  $\delta^{11}\text{B}$  values are similar to or lowered by a small amount (to 0.03 pH units) relative to the full records. The latter may reflect to the effect of decadal scale fluctuations of the southern GBR  $\delta^{11}\text{B}$  records (Fig. 4.3). The two proxy estimates of average seawater  $\text{pH}_T$ , 8.14 and 7.94 for Fitzroy Reef and Lady Musgrave Island in 2008, compare well with an instrumental seawater  $\text{pH}_T$  value of 8.07  $\pm$  0.03 ( $1\sigma$ ) at the Heron Island mooring station in the southern GBR measured over the period 2009-2010.



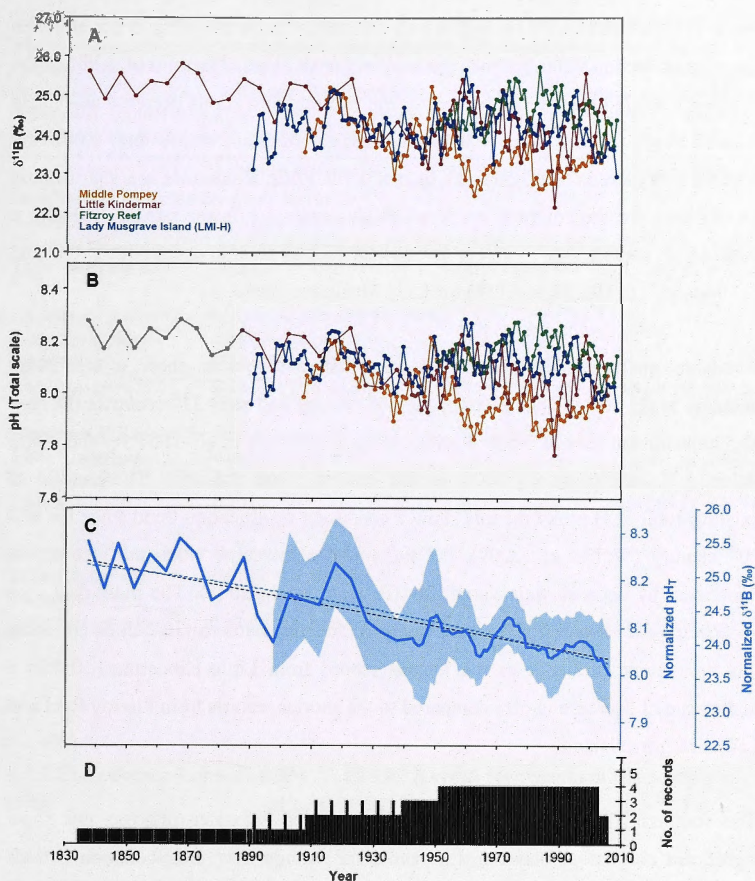


**Fig. 4.3** Time series of all  $\delta^{11}\text{B}$  and seawater  $\text{pH}_T$  records in the southern GBR. Absolute  $\delta^{11}\text{B}$  compositions (A) and seawater  $\text{pH}_T$  (B) for annual records except for Little Kindermar coral records prior to 1940 (5-year intervals). (C) Composite  $\delta^{11}\text{B}$  and seawater  $\text{pH}_T$  records with 95% confidence envelope calculated from 5-year running averages of normalized individual coral records to the period of 1950-2005. (D) Number of cores contributing to the  $\delta^{11}\text{B}$  and seawater  $\text{pH}_T$  composite records from each annual or 5-year period. Weighted linear regressions of each record and non-linear trends for the composite seawater  $\text{pH}_T$  record are represented by dotted lines over the whole observation period. The seawater  $\text{pH}_T$  records reconstruct ~40% of the common signal described by the composite record (Table 4.4).

All  $\delta^{11}\text{B}$  values and derived seawater  $\text{pH}_T$  estimates exhibit declining trends although the rates of decline differ between the southern GBR cores. The rates of acidification over each whole observations period for the two northern corals decrease at  $-0.0235 \pm 0.00246$   $\text{pH units yr}^{-1}$  ( $p < 0.0001$ ,  $n = 98$ ) for Middle Pompey and  $-0.00134 \pm 0.00201$   $\text{pH units yr}^{-1}$  ( $p < 0.0001$ ,  $n = 87$ ) for Little Kindermar are significantly greater than for the southern cores which decrease at a lower rate of  $-0.00009 \pm 0.00363$   $\text{pH units yr}^{-1}$  ( $p = 0.858$ ,  $n = 58$ ) for Fitzroy Reef and  $-0.00026 \pm 0.00203$   $\text{pH units yr}^{-1}$  ( $p = 0.173$ ,  $n = 118$ ) for Lady Musgrave Island.

Available multi-decadal instrumental seawater pH records show a significant decrease in pH over the latter part of the 20<sup>th</sup> century and early 21<sup>st</sup> centuries (Dore et al., 2009 for the central North Pacific; González-Dávila et al., 2007 for the North Atlantic; Takahashi et al., 2009 for the eastern North Atlantic). The handful of existing coral  $\delta^{11}\text{B}$  proxy records show a consistent acidification trend since the mid 20<sup>th</sup> century (Wei et al., 2009), but not prior to this time when the records are dominated by decadal scale variability (Pelejero et al., 2005). The individual core and composite seawater  $\text{pH}_T$  records derived for the southern GBR does not show this time frame influence as the longest record from Little Kindermar exhibits a higher rate of decrease in  $\text{pH}_T$  compared to the shorter records from Fitzroy Reef and Lady Musgrave Island.

The southern GBR  $\delta^{11}\text{B}$  values and  $\delta^{11}\text{B}$ -derived seawater  $\text{pH}_T$  do not show significant correlation between different coral records over their common periods (Table 4.6). The detrended  $\delta^{11}\text{B}$  and  $\text{pH}_T$  data also do not show any meaningful correlation between the individual coral cores. This is the first  $\delta^{11}\text{B}$  proxy study using multiple decadal-long cores and it is not clear as to the cause of the lack of relationship in closely located corals. The different rates of apparent acidification and lack of correlation between individual coral records may indicate that acidification and decadal scale climatic variation, which can be linked to physiological modification of reef water chemistry (Kleypas et al., 2012), affect the different coral  $\delta^{11}\text{B}$  compositions to a different extent.

**Table 4.6** Correlation between individual coral  $\delta^{11}\text{B}$  variations from the southern GBR for the whole and common observation periods using absolute  $\delta^{11}\text{B}$  compositions and detrended  $\delta^{11}\text{B}$  records. The correlations and significance were determined using Pearson Product-moment correlation at 95% confidential level. All correlation coefficients are given as  $r$ -values and all statistically significant values at 95% confidential level are shown in bold text. Correlations that are not significant are shown with  $p$ -values in brackets.

	Middle Pompey	Little Kindermar	Fitzroy Reef
<i>Absolute <math>\delta^{11}\text{B}</math> record for the whole period</i>			
Little Kindermar	0.01 (df=71, p=0.92)		
Fitzroy Reef	-0.11 (df=54, p=0.42)	<b>-0.34 (df=54, p&lt;0.05)</b>	
Lady Musgrave Is.	-0.12 (df=71, p=0.33)	0.16 (df=74, p=0.16)	0.15 (df=57, p=0.26)
<i>Absolute <math>\delta^{11}\text{B}</math> record for the common period (1950-2005)</i>			
Little Kindermar	0.01 (df=54, p=0.95)		
Fitzroy Reef	-0.11 (df=54, p=0.42)	<b>-0.34 (df=54, p&lt;0.05)</b>	
Lady Musgrave Is.	-0.14 (df=54, p=0.30)	0.08 (df=54, p=0.55)	0.09 (df=54, p=0.50)
<i>Detrended <math>\delta^{11}\text{B}</math> record for the whole period</i>			
Little Kindermar	-0.08 (df=71, p=0.52)		
Fitzroy Reef	0.20 (df=54, p=0.14)	-0.24 (df=54, p=0.08)	
Lady Musgrave Is.	-0.19 (df=71, p=0.11)	0.16 (df=74, p=0.17)	-0.04 (df=57, p=0.76)
<i>Detrended <math>\delta^{11}\text{B}</math> record for the common period (1950-2005)</i>			
Little Kindermar	-0.01 (df=54, p=0.94)		
Fitzroy Reef	0.20 (df=54, p=0.14)	-0.24 (df=54, p=0.08)	
Lady Musgrave Is.	<b>-0.27 (df=54, p&lt;0.05)</b>	0.02 (df=54, p=0.89)	-0.03 (df=54, p=0.85)

#### 4.3.3 The relationship between $\delta^{13}\text{C}$ and $\delta^{11}\text{B}$ coral records from the southern GBR

The  $\delta^{13}\text{C}$  and  $\delta^{11}\text{B}$  records from the southern GBR corals show positive correlations in all individual and composite records except for the negative correlation in the Middle Pompey coral (Table 4.7). The positive correlation between coral  $\delta^{13}\text{C}$  and  $\delta^{11}\text{B}$  indicates a link between seawater acidification and decreasing DIC  $\delta^{13}\text{C}$  in this region. The opposite correlation in the Middle Pompey coral records may be attributed to the higher effect of order of decadal fluctuations in the  $\delta^{11}\text{B}$  values (Fig. 4.3). It is notable that the correlation between detrended  $\delta^{13}\text{C}$  and  $\delta^{11}\text{B}$  values are far weaker than the absolute values, especially for the composite  $\delta^{13}\text{C}$  and  $\delta^{11}\text{B}$  records (Table 4.7 and Fig. 4.4). This indicates that the composite coral records may be

representative of the long-term  $\delta^{13}\text{C}$  and  $\delta^{11}\text{B}$  negative trends despite the lack of correlation between different  $\delta^{11}\text{B}$  records since 1837. Increasing anthropogenic emissions not only increase the atmospheric  $\text{CO}_2$  concentration but also decrease the  $\delta^{13}\text{C}$  composition of the atmosphere. The positive correlation between coral  $\delta^{11}\text{B}$  and  $\delta^{13}\text{C}$  records is consistent with acidification being closely linked to the anthropogenic  $\text{CO}_2$  emissions from burning of fossil fuels.

**Table 4.7** Correlation between individual coral  $\delta^{13}\text{C}$  and  $\delta^{11}\text{B}$  (or reconstructed seawater pH) variations from the southern GBR for the whole and common observation periods. Relationship between absolute  $\delta^{13}\text{C}$  and  $\delta^{11}\text{B}$  compositions and between depth effect corrected and detrended  $\delta^{13}\text{C}$  records and detrended  $\delta^{11}\text{B}$  records were also examined. The correlations and significance were determined using Pearson Product-moment correlation at 95% confidential level. All correlation coefficients are given as *r*-values and all statistically significant values at 95% confidential level are shown in bold text.

	<i>r</i>	<i>p</i>	<i>df</i>
<i>Absolute <math>\delta^{13}\text{C}</math> vs. <math>\delta^{11}\text{B}</math> (or pH) record for the whole period (1837-2008)</i>			
Middle Pompey	<b>-0.38</b>	< <b>0.01</b>	<b>71</b>
Little Kindermar	<b>0.55</b>	< <b>0.01</b>	<b>85</b>
Fitzroy Reef	0.21	0.12	57
Lady Musgrave Is.	<b>0.31</b>	< <b>0.01</b>	<b>77</b>
Composite record	<b>0.71</b>	< <b>0.01</b>	<b>88</b>
<i>Absolute <math>\delta^{13}\text{C}</math> vs. <math>\delta^{11}\text{B}</math> (or pH) record for the common period (1950-2005)</i>			
Middle Pompey	<b>-0.32</b>	< <b>0.05</b>	<b>54</b>
Little Kindermar	<b>0.54</b>	< <b>0.01</b>	<b>54</b>
Fitzroy Reef	0.14	0.30	54
Lady Musgrave Is.	<b>0.30</b>	< <b>0.05</b>	<b>54</b>
Composite record	<b>0.37</b>	< <b>0.01</b>	<b>54</b>
<i>Depth effect corrected and detrended <math>\delta^{13}\text{C}</math> vs. detrended <math>\delta^{11}\text{B}</math> (or pH) record for the whole period (1837-2008)</i>			
Middle Pompey	<b>-0.53</b>	< <b>0.01</b>	<b>71</b>
Little Kindermar	<b>0.36</b>	< <b>0.01</b>	<b>85</b>
Fitzroy Reef	0.17	0.21	57
Lady Musgrave Is.	0.11	0.33	77
Composite record	<b>0.17</b>	0.10	<b>88</b>
<i>Depth effect corrected and detrended <math>\delta^{13}\text{C}</math> vs. detrended <math>\delta^{11}\text{B}</math> (or pH) record for the common period (1950-2005)</i>			
Middle Pompey	<b>-0.55</b>	< <b>0.01</b>	<b>54</b>
Little Kindermar	<b>0.52</b>	< <b>0.01</b>	<b>54</b>
Fitzroy Reef	0.17	0.22	54
Lady Musgrave Is.	0.06	0.65	54
Composite record	<b>-0.18</b>	0.18	<b>54</b>



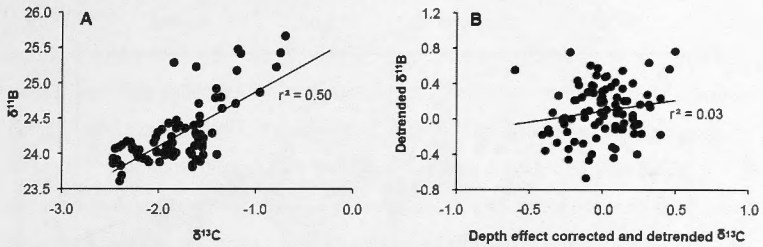
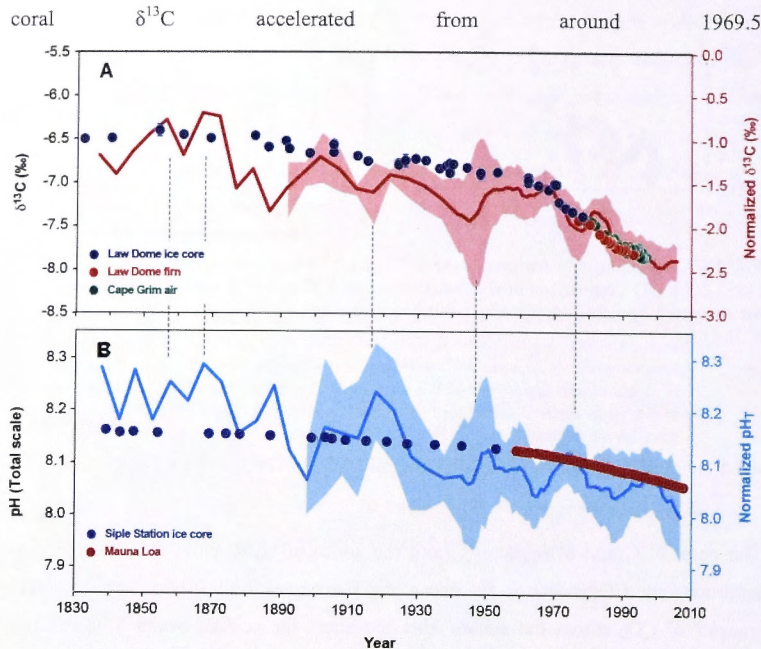


Fig 4.4 Correlation between composite  $\delta^{13}\text{C}$  and  $\delta^{11}\text{B}$  coral records for the whole period (1837-200). (A) Comparison of absolute composite  $\delta^{13}\text{C}$  and  $\delta^{11}\text{B}$  values. (B) Comparison of the corrected data from depth effect and decreasing trend in  $\delta^{13}\text{C}$  composition to detrended  $\delta^{11}\text{B}$ .

#### 4.3.4 Evidence for uptake of anthropogenic $\text{CO}_2$ in the southern GBR corals

The coral  $\delta^{13}\text{C}$  and  $\delta^{11}\text{B}$  records from the southern GBR show clear evidence of anthropogenic  $\text{CO}_2$  effect on the ocean chemistry over the last two centuries. Bulk transfer of  $\text{CO}_2$  across the air-sea interface alters the surface ocean  $\delta^{13}\text{C}$  because gaseous  $\text{CO}_2$  is strongly depleted in  $^{13}\text{C}$  relative to DIC (Broecker and Peng, 1974; Keeling et al., 2004). The  $\delta^{13}\text{C}$  of DIC in the mixed surface layer takes approximately a decade to equilibrate with the  $\delta^{13}\text{C}$  of atmospheric  $\text{CO}_2$  (Broecker and Peng, 1974). The GBR is on the western side of the southern west Pacific subtropical gyre, where the relatively stable mixed seawater layer of the subtropical gyre tends to closely follow changes in the atmospheric  $\delta^{13}\text{C}$  signal (Australian Bureau of Meteorology and CSIRO, 2011; Quay et al., 1992). Comparison of historical records of atmospheric  $\delta^{13}\text{C}$  from ice core, firm; and *in situ* air  $\text{CO}_2$  (Francey et al., 1999) with the master  $\delta^{13}\text{C}$  record from the southern GBR (Fig. 4.5A), reveal how closely the surface ocean in this region is equilibrated with atmospheric  $\text{CO}_2$ . The decreasing trends of the coral  $\delta^{13}\text{C}$  and atmospheric  $\text{CO}_2$   $\delta^{13}\text{C}$  are parallel up to ~1960, however, the acceleration of the  $\delta^{13}\text{C}$  of atmospheric  $\text{CO}_2$  depletion rate appears to precede the acceleration of the southern GBR coral  $\delta^{13}\text{C}$  depletion in the mid-20<sup>th</sup> century. The calculated acceleration of atmospheric  $\delta^{13}\text{C}$  depletion begins around 1958, within a range of 1956-1961, and the depletion of



**Fig. 4.5** (A) Comparison of coral master  $\delta^{13}\text{C}$  record (red line and shading) and  $\delta^{13}\text{C}$  records in atmospheric  $\text{CO}_2$  from the Law Dome ice core and firn samples in Antarctica (year 1832-1978 and year 1976-1993, respectively) and from the Cape Grim in Tasmania, Australia (year 1978-1996). (B) Comparison of reconstructed master seawater  $\text{pH}_T$  record from coral  $\delta^{11}\text{B}$  data (blue lines and shading) and calculated  $\text{pH}_T$  records based on atmospheric  $\text{CO}_2$  from the Siple Station ice core in Antarctica (year 1839-1953) and Mauna Loa in Hawaii (year 1959-2008).  $\text{pH}_T$  calculation based on  $\text{pCO}_2$  data from the Siple Station and Mauna Loa was computed by means of CO2SYS (Pierrot et al., 2006) assuming constant alkalinity of  $2300 \mu\text{mol/kg}$  and salinity of 35.3 PSU. Also constant phosphate and silicate concentrations of  $0.14$  and  $1 \mu\text{mol/kg}$  were assumed (Garcia et al., 2010). A southern GBR warming rate of  $0.0055 \text{ }^\circ\text{C}$  per year (see Chapter 3) was applied on the  $\text{pH}_T$  calculation. Coral master records are shown in normalized values to the period of 1950-2005 on the right axes with 95% confidence envelopes. Vertical lines represent negative IPO (or PDO) or positive SOI phases corresponding to low coral  $\delta^{13}\text{C}$  and high seawater  $\text{pH}_T$  periods in the southwestern Pacific.



within a range of 1967-1982 (Fig. 4.6). The observed offsets between coral  $\delta^{13}\text{C}$  values and atmospheric  $\text{CO}_2$  is also 0.4-0.5‰ for times between 0 to 10 years (Druffel and Griffin, 1993; Francey et al., 1999). The correspondence between the  $\delta^{13}\text{C}$  trends of atmospheric  $\text{CO}_2$  and the southern GBR coral composite record suggests that surface water in the southern GBR approaches isotopic equilibrium with the  $\delta^{13}\text{C}$  of atmospheric  $\text{CO}_2$  within 10 years (Fig.4.6).

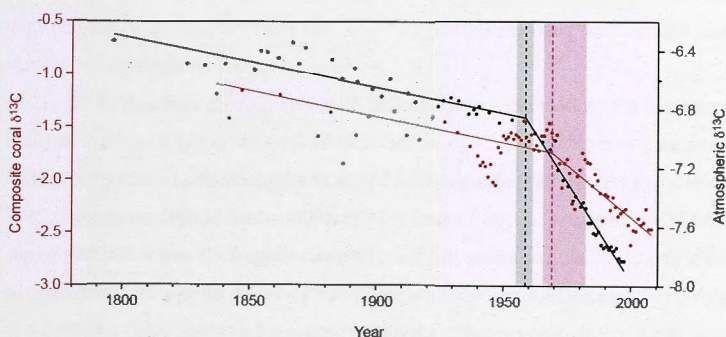


**Fig. 4.6** Break fits of the southern GBR composite  $\delta^{13}\text{C}$  (red) and  $\delta^{13}\text{C}$  records in atmospheric  $\text{CO}_2$  as in Fig. 4.5 (black) calculated using Matlab computing software (2010). The shaded areas represent the error range using a bootstrap resampling method with 1000 samples.

The  $\delta^{13}\text{C}$  composition of the southern GBR corals shows a statistically significant negative trend;  $-0.0077 \pm 0.0006\text{‰ yr}^{-1}$  ( $1\sigma$ ) over the period 1835-2008 (Figs 4.2B and 4.5A). This compares well to similar rates of  $\delta^{13}\text{C}$  decrease over the twentieth century reported from the southern Pacific ( $-0.0083 \pm 0.0022\text{‰ yr}^{-1}$ ,  $1\sigma$ ; derived from data in Swart et al. (2010) and  $\delta^{13}\text{C}$  regressions which are statistically significant at the 95% confidence limits are used) and from Atlantic Ocean corals ( $-0.0074 \pm 0.0065\text{‰ yr}^{-1}$ ,  $1\sigma$ , the period 1900-1990; Swart et al., 2010). These trends toward lighter  $\delta^{13}\text{C}$  compositions in both the Pacific and Atlantic Ocean basins can be ascribed to a global  $^{13}\text{C}$ -Suess effect (Druffel and Benavides, 1986). This

anthropogenic carbon emission signal in coral  $\delta^{13}\text{C}$  compositions has accelerated since 1960 to a rate of  $-0.0205 \pm 0.0014\text{‰ yr}^{-1}$  ( $1\sigma$ ) for the southern GBR. This rate corresponds to the global mean  $^{13}\text{C}$ -Suess effect ( $-0.015$  to  $-0.018\text{‰ yr}^{-1}$  from 1980 to 2000; Gruber et al., 1999; Keeling et al., 2004), and to the rate of change in  $\delta^{13}\text{C}$  composition of atmospheric  $\text{CO}_2$  in both the Northern ( $-0.023$  to  $-0.029\text{‰ yr}^{-1}$ , 1960-2008; Keeling et al., 2004) and Southern Hemisphere ( $-0.022\text{‰ yr}^{-1}$  for Law Dome firn (1830-1978) and Cape Grim air (1978-1997); Francey et al., 1999). The increasingly steep worldwide trend to, lower  $\delta^{13}\text{C}$  since the industrial revolution, is consistent with the increase in atmospheric carbon dioxide and is clearly manifest in surface waters of the southern GBR.

The seawater pH records derived from coral  $\delta^{11}\text{B}$  also provide evidence of the effect of increasing anthropogenic  $\text{CO}_2$  on the oceans. The averaged long-term surface ocean  $\text{pH}_\text{T}$  master record ranges from 7.95 to 8.29 and declines at a rate of  $-0.00123 \pm 0.00058$  pH unit  $\text{yr}^{-1}$  ( $1\sigma$ ) for the period 1835-2008, which is equivalent to a  $0.21 \pm 0.10$  pH unit ( $1\sigma$ ) decline during the last 170 years (Figs 4.4B and 4.5B). Although only one southern GBR coral core extends prior to 1890, no significant change in this particular coral proxy record is evident between 1834 and 1890 ( $-0.00097 \pm 0.00105$  pH unit  $\text{yr}^{-1}$ ,  $1\sigma$ ,  $p < 0.0001$  for the period 1890-2008, which is equivalent to a  $0.17 \pm 0.18$  pH unit decline over the last 170 years).

If atmospheric  $\text{CO}_2$  in the southern GBR reaches equilibrium with the surface ocean within 10 years, the seawater  $\text{pH}_\text{T}$  in this study might be expected to reflect the atmospheric  $\text{CO}_2$  concentrations in both ice core records (e.g. Siple ice core from Antarctica; year 1839-1953; Neftel et al., 1994) and atmospheric records (e.g. Mauna Loa station, Hawaii; year 1959-2008; Keeling et al., 2009). Given a southern GBR warming of  $0.0055^\circ\text{C yr}^{-1}$  (see Chapter 3), there is a good agreement between southern GBR seawater  $\text{pH}_\text{T}$  and these atmospheric  $\text{CO}_2$  records from 1890 to present (Fig. 4.5B). The coral  $\text{pH}_\text{T}$  record is 0.13 pH units lower than the seawater  $\text{pH}_\text{T}$  estimated from atmospheric  $\text{CO}_2$  record from 1830 to 1900 where only a single coral  $\text{pH}_\text{T}$  estimate has been obtained. However, this offset is within the range of 95% confidence levels when the largest observed uncertainty is applied.

The rate of acidification in the southern GBR is about double the mean rate of  $-0.00063 \pm 0.00028$  pH units  $\text{yr}^{-1}$  computed based on the surface ocean equilibrium with atmosphere  $\text{pCO}_2$  records from the Siple Station ice core and Station ALOHA for the period 1839-2008 (Fig. 4.5B). It is also notably less than the rate measured at the longest available instrumental time-series of  $-0.0019 \pm 0.0003$  pH units  $\text{yr}^{-1}$  (Station ALOHA in the central North Pacific 1988-2007; Dore et al., 2009) and the rate of the change in surface water  $\text{pH}_T$  in the southern GBR during the last 20 years ( $-0.0029 \pm 0.0015$  pH units  $\text{yr}^{-1}$ ). This probably reflects acceleration in the rate of acidification over the instrumental observation periods due to the accelerated increase in atmospheric  $\text{CO}_2$  concentration.

Until now, only two long-term seawater  $\text{pH}_T$  records have been reported based on the  $\delta^{11}\text{B}$  proxy in *Porites* corals, both from the southwest Pacific Ocean (Pelejero et al., 2005; Wei et al., 2009). A comparison of the coral  $\delta^{11}\text{B}$ - $\text{pH}_T$  master record from this study with those previous studies is shown in Fig. 4.7A. All three records share a general decreasing trend of  $\text{pH}_T$  from 1940 to present. The composite record from the southern GBR shows a higher  $\text{pH}_T$  than the other records to the north. This is unexpected and the reason for this difference is unclear. It could be due to the effect of greater metabolic  $\text{CO}_2$  build-up in reef waters at Arlington and Flinders reefs, which will be discussed further below. It is also notable that a large range of decadal variation in seawater  $\text{pH}_T$  occurs in the Arlington Reef coral, which has been attributed to possible river discharge and bleaching effects (Wei et al., 2009).

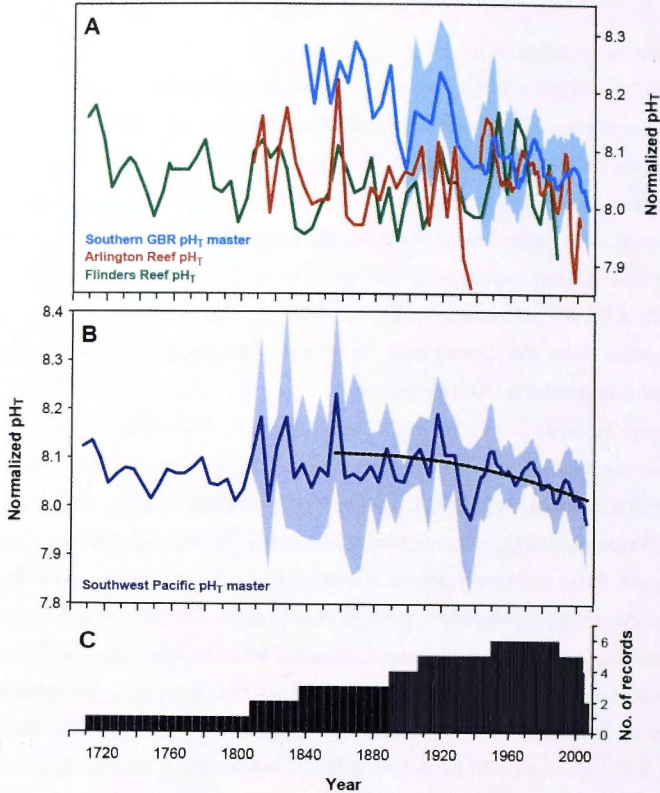


**Fig. 4.7** (A) Comparison of estimated seawater pH<sub>T</sub> from  $\delta^{11}\text{B}$  records of *Porites* from the southwest GBR (this study, the master record), Arlington Reef in the central GBR (Wei et al., 2009), and Flinders Reef in the Coral Sea (Pelejero et al., 2005). Seawater pH<sub>T</sub> was calculated from data in these previous studies using the calibration for the coral internal pH-up regulation (Trotter et al., 2011).  $\alpha_{\text{B3-B4}} = 1.0207$  (Klochko et al., 2006) was applied with  $pK_{\text{B}}$  adjusted for ambient temperature and salinity for the data from the southern GBR (this study). Fixed values of 25 °C and 35 PSU with  $\delta^{11}\text{B}$  of 39.5 ‰ were used for the calculation of published data. The Annual Arlington Reef pH<sub>T</sub> record has been converted using a 5-year running average since 1940. These three records share on average 22% of common variance (Table 4.4). (B) Master  $\delta^{11}\text{B}$ -derived pH<sub>T</sub> record for the southwest Pacific. Normalized individual records represented in (A) were used to derive the master  $\delta^{11}\text{B}$ -seawater pH<sub>T</sub> record. An exponential regression line (black dotted line) has been fitted and shown only over the period of high confidence (since 1837), where it is based on more than four samples. (C) Number of cores contributing to the southern Pacific pH<sub>T</sub> master record in (B).



To help understand long-term variability of the surface ocean pH in the southwest Pacific, all three long  $\delta^{11}\text{B}$ - $\text{pH}_T$  records from the Coral Sea (Pelejero et al., 2005), the Central GBR (Wei et al., 2009), and the southern GBR (this study) have been composited. The abnormally lower  $\text{pH}_T$  records than the more recent periods (e.g. 7.75 during 1940s and 7.57 in 1998) observed in the Arlington Reef were excluded from the composite record due to the potential for regional effects like coral bleaching on this record (Fig. 4.7A). The composite record shows a clear acceleration in  $\text{pH}_T$  decrease that follows the accelerating increase in the concentration of atmospheric  $\text{CO}_2$  (Fig. 4.7B).

The lowest recorded  $\delta^{11}\text{B}$ - $\text{pH}_T$  value before the twentieth century was 8.01, recorded in 1747, 1797, and 1802, whereas  $\text{pH}_T$  values below 8.01 occur from 2000 to present in the southwestern Pacific master record. This recent lower pH is almost certainly due to the increasingly dominant effect of ocean acidification in the southwest Pacific on surface ocean pH.

#### **4.3.5 Natural variability in the pH of reef waters of the Coral Sea and GBR**

##### ***4.3.5.1 Physical modification of reef water properties***

There appears to be an interdecadal oscillation in the seawater  $\text{pH}_T$  record of the southern Pacific that is superimposed upon the long-term acidification trend. To characterize this natural fluctuation, the data were detrended using linear fits to the reconstructed seawater  $\text{pH}_T$  records from Arlington reef, Flinders reef, and the southern GBR reef cores as well as the southwest Pacific composite record over the each observation period (hereafter referred to as  $\text{pH}_T^*$ ). Comparisons of these detrended seawater  $\text{pH}_T$  records to indices of natural climate variability are shown in Fig. 4.8.

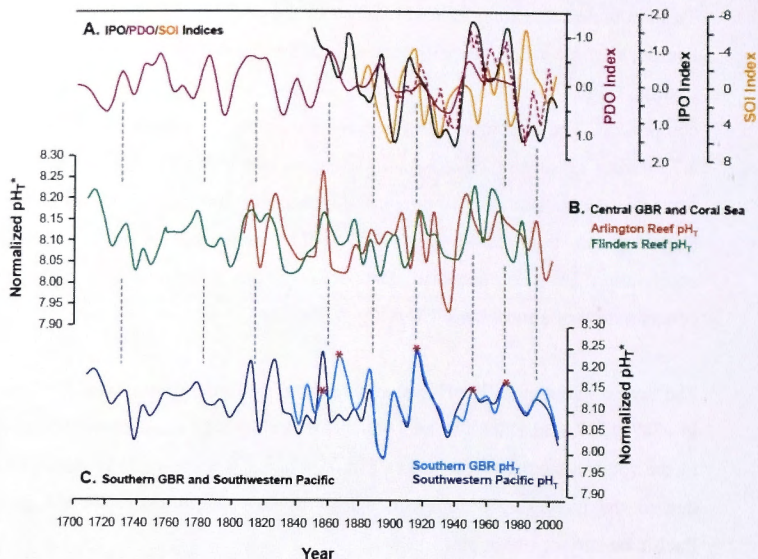


**Fig. 4.8** Comparison of interdecadal variability in reconstructed  $\text{pH}_T$  records from *Porites* corals from the southern GBR (this study, master records), Arlington Reef, the central GBR (Wei et al., 2009), and Flinders Reef, Coral Sea (Pelejero et al., 2005). The effect of ocean acidification for the each observation period was detrended in coral  $\delta^{13}\text{B}$ -derived  $\text{pH}_T$  ( $\text{pH}_T^*$ ), and then all records are normalized and averaged to 5-year intervals. (A) IPO (Folland et al., 2002), PDO (Mantua et al., 1997), North American tree-ring based PDO index back to 1700 (D'Arrigo et al., 2001), and SOI indices (Australian Bureau of Meteorology, National Climate Center). The annual IPO index is filtered values from the monthly resolution record. Positive phases of the IPO and PDO indices correspond to an El Niño-like mode and a negative phase corresponds to a La Niña-like mode. (B) The detrended  $\text{pH}_T$  records from the Central GBR (Arlington Reef; 16.5°S 146°E) and the Coral Sea (Flinders Reef; 17.5°S 148°E). (C) Detrended master  $\text{pH}_T$  records are for the Southern GBR cores and for the southwest Pacific cores includes cores from previous studies (Pelejero et al., 2005; Wei et al., 2009). Vertical lines represent negative IPO (or PDO) or positive SOI phases that correspond to high  $\text{pH}_T$  periods in the southwest Pacific. Red stars indicate depleted  $\delta^{13}\text{C}$  during negative IPO phases that correspond to vertical dotted lines in Fig. 4.5.



As previous studies reported (Pelejero et al., 2005; Wei et al., 2009), long-term coral  $\text{pH}_{\text{T}}^*$  records vary with the IPO (or PDO) and the Southern Oscillation Index (SOI). Negative covariations of the coral  $\text{pH}_{\text{T}}^*$  and the IPO are present in the southern GBR as well as both Flinders and Arlington Reefs from the Coral Sea and the central GBR. The occurrence of robust 20 year-cycles in the southern GBR master record are in agreement with those from Arlington Reef, whereas the coral pH record from Flinders Reef demonstrates a cyclicity of about 50 years. The latter may be due to the differing temporal resolution of the coral records in each study (5-year intervals from Flinders Reef vs. 1-year intervals from Arlington Reef and southern GBR; Wei et al., 2009; This study).

The IPO and ENSO exhibit similar climatic characteristics but on different timescales, with the positive IPO phases showing similarity to El Niño and the negative IPO index being similar to La Niña events (Folland et al., 2002). In the Southern Hemisphere extra-tropics the atmospheric circulation is dominated by strong mid-latitude westerly winds which oscillate between being stronger and more poleward, or weaker and more equatorward (Australian Bureau of Meteorology and CSIRO, 2011). While this feature primarily affects higher latitude oceans, it may directly impact the region of around 20°S via changes in the atmospheric circulation (Australian Bureau of Meteorology and CSIRO, 2011). In the subtropical southwest Pacific region, the East Australian Current (EAC), the western boundary of the South Pacific Gyre, as well as the South Equatorial Current (SEC) directly influence seawater properties in the southwestern Pacific. These currents are intensified during the negative IPO or the positive SOI phases due to a spin-up and southward shift of the Southern Hemisphere subtropical ocean circulation with the stronger westerly winds over the south Pacific (Holbrook et al., 2011; Pelejero et al., 2005; Power et al., 1999; Ridgway and Hill, 2009). The intrusion of the EAC during these La Niña-like periods into the southern GBR (Burrage et al., 1996) results in the surface seawater being less acidic and warmer than normal.

The full range of variability of reconstructed seawater  $\text{pH}_{\text{T}}^*$  is about 0.3 pH units in both the southern GBR and southwest Pacific  $\text{pH}_{\text{T}}$  master records, which is

consistent with the natural variability determined from tropical coral  $\delta^{11}\text{B}$  records (Pelejero et al., 2005). The changes in surface ocean  $\text{pH}_{\text{T}}^*$  and the apparent variation of the  $\text{pH}_{\text{T}}^*$  with the IPO suggest three possible physical mechanisms; vertical mixing of surface and/or subsurface waters, horizontal mixing of tropical and subtropical water masses, and/or a change in residence time of reef water (Pelejero et al., 2005). Each of these scenarios is discussed below.

The interdecadal changes in surface ocean  $\text{pH}_{\text{T}}^*$  recorded in southern GBR corals are unlikely to be due to vertical mixing by upwelling events during the positive IPO phases, as the relatively weak Pacific trade winds which occur in the positive IPO phases hinder strong upwelling episodes in the GBR. Furthermore, enhanced intrusion of subsurface deep waters to shallow depths during the negative IPO period should change the ocean chemistry to colder, more saline, and more acidic conditions (Pelejero et al., 2005). However, cold events recorded by coral Sr/Ca (see Chapter 3) and lower  $\text{pH}_{\text{T}}^*$  values during the periods of positive IPO show the opposite effects in our results (Fig. 4.8).

Horizontal mixing of tropical and subtropical water masses might explain the observed interdecadal variation in the ocean chemistry. During the negative IPO phases (vertical dotted lines in Fig. 4.8), the inflow of tropical water masses due to intensification of the EAC modifies the subtropical ocean chemistry. In addition to the positive correlation between the intensity of SEC and EAC and seawater  $\text{pH}_{\text{T}}^*$  values, the covariation of  $\text{pH}_{\text{T}}^*$  with reconstructed SSTs (see Chapter 3) reflects natural changes in SST that are associated with imposition of EAC and physical mixing in this region. Although a part of the range of  $\text{pH}_{\text{T}}^*$  variation in the southern GBR can be explained by this tropical and subtropical water mass exchange (up to 0.2 pH units), the subtropical region is less sensitive to the ENSO cycles compared to the tropical region (e.g. Niño 4 region). Thus other related influences, including biological modification, on reef water chemistry may still be significant.

It is noteworthy that  $\delta^{13}\text{C}$  compositions in the southern GBR show a cyclicity of about 20 years, which correlates with  $\text{pH}_{\text{T}}^*$  variability (Fig. 4.5). As reviewed by

Gruber et al. (1999), surface seawater enrichment in  $\delta^{13}\text{C}$  values occurs by kinetic fractionation of C isotopes during the air-sea exchange of  $\text{CO}_2$ . High wind velocity and temperature during the La Niña-like period in this region enhances this process such that  $\delta^{13}\text{C}$  increases in seawater and hence the coral skeleton records. It is finally noted that certain periods show negative covariation between the southern GBR  $\delta^{13}\text{C}$  and  $\text{pH}_T^*$  master records and these periods occur during negative IPO (La Niña-like) phases (represented with red stars in Fig. 4.8). However, a  $1^\circ\text{C}$  increase in ocean temperature would cause only a 0.1‰ change in oceanic  $\delta^{13}\text{C}$  when the surface ocean is in complete equilibrium (Gruber et al., 1999). Therefore, these periods of depleted  $\delta^{13}\text{C}$  compositions and higher  $\text{pH}_T^*$  values suggest that there may be controls other than thermodynamic factors that influence the coral record.

#### ***4.3.5.2 Biological controls on interdecadal variability in seawater $\text{pH}_T$***

It is well known that metabolic isotope effects cause  $\delta^{13}\text{C}$  enrichment in the coral skeleton as a result of the fractionation during  $\text{CO}_2$  uptake by photosynthesis. Increase in biological production with enhanced light intensity leads to higher calcification rates (Cohen and Holcomb, 2009; Reynaud-Vaganay et al., 2001). The results obtained from this study, however, show that  $\delta^{13}\text{C}$  is more depleted during warm IPO phases when enhanced solar irradiance by a lack of cloud cover should otherwise produce more enriched  $\delta^{13}\text{C}$  in coral records. Previous studies have revealed that heavier  $\delta^{13}\text{C}$  compositions can accompany a decrease in  $\text{pCO}_2$  in the ambient water due to increases in  $\text{CO}_2$  fixation by photosynthesis and thus that higher  $\text{pH}^*$  is associated with enriched  $\delta^{13}\text{C}$  values (Hemming et al., 1998; Krief et al., 2010). The results of this study show the opposite relationship (Fig. 4.5) and suggest that metabolic modification on skeletal  $\delta^{13}\text{C}$  may not be a dominant effect in the long-term southwest Pacific composite record.

Physiological processes (e.g. photosynthesis, calcification and respiration) could be a major cause of changing reef water chemistry through the transfer of  $\text{CO}_2$  between ambient seawater and calcification fluid. Anthony et al. (2011) and Kleypas et al.

(2011) have shown that coral dominated reef communities elevate  $p\text{CO}_2$  and reduce aragonite saturation state for reefs with long residence time compared to the open ocean, thereby compounding ocean acidification effects in the communities. As Pelejero et al. (2005) suggested, a decrease in reef water  $\text{pH}_T$  occurs due to a combination of faster accumulation of  $\text{CO}_2$  through calcification and limited flushing of reef waters by weak trade winds. The decreased rate of water mass exchange and/or sea to air  $\text{CO}_2$  flux during positive IPO periods is likely to play a role in acidifying reef water. Along with the changes in reef water  $\text{pH}_T^*$ , coral  $\delta^{13}\text{C}$  variation depends on the residence time of the reef water according to interdecadal natural climate variability. During the positive IPO periods with the low flushing rates due to weaker wind stress,  $\delta^{13}\text{C}$  could be enriched in reef water by photosynthetic activity of coral symbionts and other algae whereas depleted  $\delta^{13}\text{C}$  could be recorded in coral skeletons due to mixing with relatively light C isotopes derived from open ocean seawater during negative IPO phases. It follows that changes in biological process and the magnitude of flushing over IPO cycles defines reef water properties. This may explain the observation of lower historic pH values than modern seawater pH at times when there was no significant associated ocean acidification, for example, in years 1747 and 1802 (refer to Fig. 4.8).

#### 4.4 Conclusions

This study provides geochemical evidence for a long-term shift in seawater chemistry due to increases in atmospheric  $p\text{CO}_2$  that is overlaid with decadal-scale variability associated with ocean-atmosphere anomalies in the southern GBR and the southwestern Pacific. With respect to the  $\delta^{11}\text{B}$ -based reconstruction of seawater pH, we present the first study of high resolution and multiple coral approach, applying calibrations of physiological effects (i.e. coral pH-up regulation) on the  $\delta^{11}\text{B}$ -pH proxy. Reconstructed seawater  $\text{pH}_T$  from skeletal B isotope compositions provides direct evidence for significant ocean acidification over the last 170 years (i.e. a 0.21 pH units decrease), which is greater than the global average ocean acidification by a factor of two. The Suess effect is also evident in skeletal  $\delta^{13}\text{C}$  consistent with the



global ocean and atmospheric  $\delta^{13}\text{C}$  trend in particular since 1960. Furthermore, a composite record of all published southwestern Pacific *Porites* coral  $\delta^{11}\text{B}$ -derived seawater  $\text{pH}_\text{T}$  data from the Coral Sea (Pelejero et al., 2005), the central GBR (Wei et al., 2005), and the southern GBR (this study) indicates that ocean acidification has occurred at an accelerating rate since about 1840, in association with an increase in atmospheric  $\text{CO}_2$  concentrations. Skeletal  $\delta^{13}\text{C}$  and reconstructed seawater  $\text{pH}_\text{T}$  records also show decadal variations, suggesting correlation with natural ocean-atmospheric anomalies in the Pacific. Less acidic ( $>8.2$  pH unit) and warmer surface waters can be linked to an inflow of tropical water caused by intensification of the SEC and/or EAC during negative IPO phases with enhanced trade winds. Finally, the extent of ocean acidification and interdecadal variation evident in coral  $\text{pH}_\text{T}$  record is beyond the seawater  $\text{pH}_\text{T}$  range of water mass exchange ( $\sim 0.2$  pH unit) and suggests significant modification of reef water chemistry through the build-up of  $\text{CO}_2$  during the periods of positive IPO index. It follows that physical and biological processes need to be taken into account when considering the mechanisms which are producing large pH changes in reef water chemistry.





---

## Chapter 5.

### Coral calcification in the southern Great Barrier Reef

---

#### 5.1 Introduction

Coral reefs are one of the most biologically diverse and economically important ecosystems on Earth. However, the calcium carbonate ( $\text{CaCO}_3$ ) structures that they build are expected to be increasingly exposed in the future to progressive increase in sea surface temperature (SST) and decreases in seawater pH, associated with global warming and the oceanic uptake of carbon dioxide ( $\text{CO}_2$ ) produced by fossil fuel burning, deforestation, cement production, and other human activities. Since the mid-eighteenth century the rise in atmospheric carbon dioxide concentration ( $\text{pCO}_{2\text{atm}}$ ) exceeds any documented rate of change in geological history (Doney and Schimel, 2007). The elevated atmospheric  $\text{pCO}_2$  levels have so far contributed to a  $\sim 0.7^\circ\text{C}$  increase in the global average temperature of the oceans through the effects of  $\text{CO}_{2(\text{g})}$  as a greenhouse gas over the past hundred years (IPCC, 2007a). In addition to this, there has been an appreciable increase in the acidity of the surface oceans with an average decrease in the pH of seawater by  $\sim 0.1$  pH units, and a decrease in seawater carbonate ion concentrations ( $[\text{CO}_3^{2-}]$ ) by  $\sim 20\%$  or  $\sim 30 \mu\text{mol kg}^{-1}$  (IPCC, 2007b). Finally, the increasing  $\text{pCO}_{2\text{atm}}$  has contributed to a  $\sim 20$  cm rise in sea level due to thermal expansion by warming of the oceans since 1900 (IPCC, 2007a). In Chapter 3 and 4, the effects of increased atmospheric  $\text{CO}_2$  are shown to be apparent as a  $1.0^\circ\text{C}$  of ocean warming and 0.21 pH units of acidification in the southern GBR over the

last ~170 years. This study reports on the temporal trends and variability of coral calcification in response to change in SST and seawater pH in the southern GBR over the last ~170 years in the same region. It is based on estimates of changing SST and ocean acidification, derived from instrumental SST and coral Sr/Ca-SST (see Chapter 3) and to seawater pH estimates derived from coral boron isotopic compositions (see Chapter 4). This study investigates for the first time the combined long-term effects of ocean warming and acidification on the coral calcification based on proxy data recorded in the identical years.

### **5.1.1 Coral calcification, ocean warming and acidification**

#### ***5.1.1.1 Rising temperature of the ocean and coral calcification***

In theory, all chemical reaction rates increase exponentially with temperature (Tyrrell, 2008). Ectotherms, such as corals and coralline algae, do not regulate their internal temperature and therefore their metabolic reactions are likely to be affected by external changes in seawater temperature (Tyrrell, 2008). The photosynthetic rate of zooxanthellae, the symbiotic algae hosted by corals, is also enhanced by increasing seawater temperatures. This, in turn, accelerates the precipitation of coral aragonite through the active fixation of CO<sub>2</sub> (Gattuso et al., 1999).

Laboratory studies have shown that corals have an optimal temperature range (24°C to 27°C) for calcification and that calcification rates increase with temperature across this range (Coles and Jokiel, 1978; Marshall and Clode, 2004). Calcium ATPase (Ca<sup>2+</sup>-ATPase) transports calcium to and removes protons (H<sup>+</sup>) from the coral calcification site. The removal of H<sup>+</sup> increases pH within the site of calcification and promotes diffusion of CO<sub>2</sub> across the calcioblastic ectoderm and increased  $\Omega_{\text{arag}}$  and hence coral calcification (Cohen and McConnaughey, 2003). This enzyme-catalyzed reaction is temperature dependent (Marshall and Clode, 2004), such that calcification rates decrease outside of the optimal temperature range (Coles and Jokiel, 1978; Marshall and Clode, 2004).

When seawater temperature exceeds the optimal range for corals, it has been shown to cause stress in corals. This stress is associated with reduced calcification rates and can ultimately lead to coral bleaching. Bleaching has been documented in natural coral colonies by numerous studies including Glynn (1991), Hoegh-Guldberg (1999), Hoegh-Guldberg and Smith (1989), and Wilkinson and Hodgson (1999), and is characterized by the dissociation of the symbiotic relationship between corals and their zooxanthellae. Small increases ( $\geq 1^{\circ}\text{C}$ ) in SST over and above the long-term summer average have been shown to lead to bleaching events that have large-scale impacts on the distribution and abundance of reef-building corals (Hoegh-Guldberg, 2005). Large-scale bleaching events (referred as mass bleaching event) began to be recorded in the early 1980s and large areas (hundreds to thousand of kilometers of coral reef) bleached simultaneously (Hoegh-Guldberg, 2005). Almost 30% of coral cover has been lost from the GBR since the beginning of the 1980s in association with thermal events that exceed the  $1^{\circ}\text{C}$  threshold above the annual summer average maximum temperature (Wilkinson and Hodgson, 1999). Since 1995, most coral reefs worldwide have been affected by mass bleaching (Hoegh-Guldberg, 1999; Global Coral Reef Monitoring Network (GCRMN), 2000). In 1997-1998, 16% of corals in the world disappeared and 46% of corals were lost in the Western Indian Ocean alone by the end of the 1998 mass bleaching event (GCRMN, 2000). Two large-scale (2,000 km) bleaching events on the GBR were also observed in 1998 and 2002 (Berkelmans et al., 2004). Approximately 42% of reefs bleached in 1998, while in 2002, ~54% of reefs bleached with ~18% strongly bleached in the worst bleaching event on record for the GBR (Berkelmans et al., 2004).

Annually banded massive corals are widely used to measure coral growth and calcification rate. This is because coral growth occurs by vertical extension through the deposition of new material at the surface of the coral, and corals grow continuously throughout the year round but changes in the environmental conditions affect their calcification rates (Barnes and Lough, 1993). Field studies have found increasing coral calcification rates with increasing temperature beyond the optimal temperature range (Cooper et al., 2012; Lough and Barnes, 2000; Lough, 2008a). Average annual calcification rates of *Porites* from the GBR have increased by 0.33-



$0.39 \text{ g cm}^{-2} \text{ yr}^{-1}$  per  $1^\circ\text{C}$  rise in SST across an annual average temperature gradient ranging from  $23$  to  $29^\circ\text{C}$  (Lough and Barnes, 2000; Lough, 2008a). A recent study of *Porites* corals from the southeast Indian Ocean has shown a 24% increase in coral calcification across a temperature range from  $22$  to  $29^\circ\text{C}$  during the last century (Cooper et al., 2012). These studies suggested that changes in thermal environment are currently the dominant factor causing change in coral calcification rates.

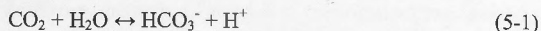
In contrast, coral growth rates have declined in the western Pacific, Indian, and North Atlantic Oceans despite increasing sea surface temperatures (Manzello, 2010). A study by Tanzil et al. (2009) compared the growth rate of eight *Porites lutea* from Phuket showed a 23.5% decrease in coral calcification from 1984 to 2003 ( $\sim 1.2\% \text{ yr}^{-1}$ ) due to a rate of  $0.16^\circ\text{C}$  per decade increase in SST. It was suggested corals in that part of the Andaman Sea may already be subjected to temperatures beyond their thermal optimum for skeletal growth. Cantin et al. (2010) also showed steadily rising SST, not ocean acidification, is already driving significant decline (30 % since 1998) in the growth of massive reef-building coral *Diploastrea heliopora* in the central Red Sea. Cooper et al. (2008) reported a  $1.02\% \text{ yr}^{-1}$  decline in coral calcification rate from 1988 to 1995 averaged across 38 colonies of *Porites* from two nearshore regions of the northern GBR. Manzello (2010) also showed the rate of decline in coral growth for *P. damicornis* from Pacific Panamá is  $0.9\% \text{ yr}^{-1}$  from 1974 to 2006 corresponding to massive *Porites* in the Indo-Pacific over the past 20–30 years ( $0.89\text{--}1.23\% \text{ yr}^{-1}$ ). The most extensive study to date, using 328 colonies of *Porites* throughout the GBR showed a 14.2% decrease in coral calcification from 1990 to 2005 (De'ath et al., 2009). The declines in the GBR region (Cooper et al. 2008; De'ath et al., 2009) and the Pacific (Manzello, 2010) have been attributed to the synergistic impact of environmental stress of high temperature and decreasing  $\Omega_{\text{arag}}$  due to ocean acidification. However, a limitation of these studies has been the lack of contemporaneous pH or aragonite saturation state data to compare with observed calcification rates.



### **5.1.1.2 Ocean acidification and coral calcification**

The oceans comprise the largest reservoir of carbon within Earth's short-term (month to century scale) carbon cycle. The oceans exchange carbon in the form of CO<sub>2</sub> with the atmosphere and act as a sink for anthropogenic CO<sub>2</sub> from the atmosphere. Between 30 and 50% of the CO<sub>2</sub> emitted by human activities in the past 200 years has been taken up by the oceans (Raven, 2005).

The CO<sub>2</sub> dissolved in the ocean exists mainly in three distinct inorganic forms which vary as a function of pH (Fig. 5.1); free aqueous carbon dioxide [CO<sub>2(aq)</sub>], bicarbonate ion [HCO<sub>3</sub><sup>-</sup>], and carbonate ion [CO<sub>3</sub><sup>2-</sup>]. A minor form is carbonic acid [H<sub>2</sub>CO<sub>3</sub>] whose concentration is less than 0.3% of [CO<sub>2(aq)</sub>] and the sum of [H<sub>2</sub>CO<sub>3</sub>] and [CO<sub>2(aq)</sub>] is denoted as [CO<sub>2</sub><sup>\*</sup>]. The dissolved carbonate species react with water, hydrogen and hydroxyl ions and are related by the following reactions.



Across the typical range of surface ocean pH (8.0 and 8.2), the concentration of HCO<sub>3</sub><sup>-</sup> is 6 to 10 times higher than [CO<sub>3</sub><sup>2-</sup>] (see Fig. 5.1). When additional CO<sub>2</sub> dissolves in seawater, it forces the equilibrium of reaction 5-1 to the right, generating more protons which in turn react with CO<sub>3</sub><sup>2-</sup> to form additional HCO<sub>3</sub><sup>-</sup>. This results in lowering of both the pH and the concentration of CO<sub>3</sub><sup>2-</sup> ions in seawater. The result of a doubling of atmospheric pCO<sub>2</sub> is expected to cause a drop in surface ocean pH of 0.2-0.3 units and a decline in [CO<sub>3</sub><sup>2-</sup>] of 25-53% relative to preindustrial concentrations (Langdon et al., 2000).

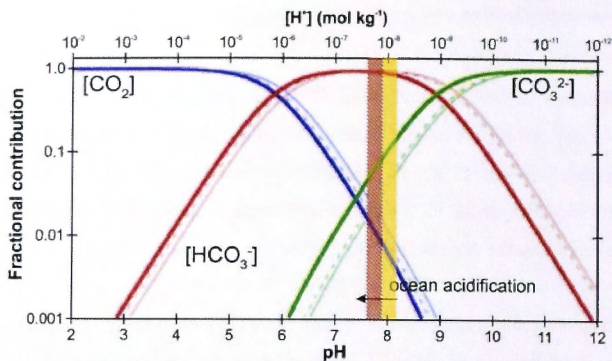
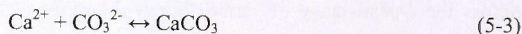


**Fig. 5.1** Bjerrum plot showing the relative proportions of the concentrations of the carbonate species ( $[\text{CO}_2]$ ,  $[\text{HCO}_3^-]$ , and  $[\text{CO}_3^{2-}]$ ) to dissolved inorganic carbon (DIC) in seawater as a function of pH. The effects of different temperature, salinity, and pressure are shown by thick lines ( $S = 35\text{‰}$ ,  $T = 25^\circ\text{C}$ ,  $P = 0$  bar), thin lines ( $S = 35\text{‰}$ ,  $T = 0^\circ\text{C}$ ,  $P = 0$  bar), and dashed lines ( $S = 35\text{‰}$ ,  $T = 0^\circ\text{C}$ ,  $P = 300$  bar). The yellow shaded region represents the range of modern (annual average) ocean surface pH, and the orange shaded region represents the projected ocean acidification by year 2100. Diagram from Barker and Ridgwell (2012).

The formation of calcium carbonate from solution is given by the reaction



and calcium carbonate saturation state ( $\Omega$ ) is defined as

$$\Omega = \frac{[\text{Ca}^{2+}][\text{CO}_3^{2-}]}{K'_{sp}} \quad (5-4)$$

where  $K'_{sp}$  is the stoichiometric solubility product of the relevant  $\text{CaCO}_3$  mineral polymorph (aragonite in the case of coral calcification).

Calcium is conservative in the ocean due to its long residence time ( $1.1 \times 10^6$  years) and therefore the aragonite saturation state ( $\Omega_{\text{arag}}$ ) of seawater varies as a function of  $[\text{CO}_3^{2-}]$ . Hence, reducing the concentration of  $\text{CO}_3^{2-}$  can affect the ability of corals to calcify by decreasing the calcium carbonate saturation state ( $\Omega$ ).

The tropical surface oceans are currently supersaturated with respect to aragonite with  $\Omega_{\text{arag}} \approx 4.0 \pm 0.2$  (Kleypas et al., 1999a). Studies indicate that net calcium carbonate accretion on coral reefs reaches zero or becomes negative at an aragonite saturation state  $\leq 3.3$  (Kleypas et al., 1999b; Hoegh-Guldberg et al., 2007). It is predicted that the surface oceans will reach this level when atmospheric  $\text{CO}_2$  attains 480 ppm, which may occur as soon as year 2065 (Hoegh-Guldberg et al., 2007; Raven, 2005)

A number of short-term coral culture studies (<4 years) have examined the relationship between  $\Omega_{\text{arag}}$  and coral calcification rate (see Table 5.1 and Fig. 5.2). Although calcification rates tend to increase with increasing  $\Omega_{\text{arag}}$  for all coral species and communities, there are differences in the sensitivity and form of the relationship (Fig. 5.2). These different degrees of sensitivity to declining seawater pH predict less or more dramatic changes in calcification rates over the probable range of future  $\text{pCO}_2$  scenarios (McCulloch et al., 2012). The reasons for these differences are unclear and could reflect different methods of measuring calcification, manipulating  $\Omega_{\text{arag}}$ , and treatment duration (Table 5.1). In addition, the proportion of sandy area in coral community studies could have increased potential for  $\text{CaCO}_3$  dissolution leading to discrepancies in such studies (Leclercq et al., 2000). The other limitation of using short-term experimental results for predicting future changes in calcification arises because these studies do not account for the potential interactive effects between saturation state and other factors controlling coral calcification such as temperature, light intensity, or nutrient levels (Langdon and Atkinson, 2005; Leclercq et al., 2002; Marubini et al., 2001).

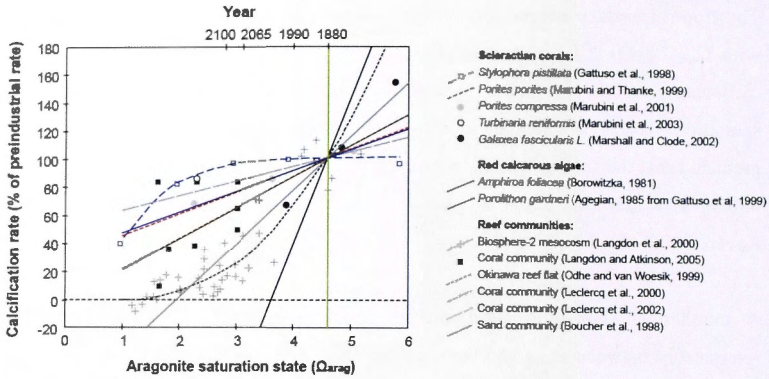


Fig. 5.2 Change in calcification rates plotted against seawater aragonite saturation state ( $\Omega_{\text{arag}}$ ). Calcification rate is expressed as a percentage of the preindustrial rate ( $\Omega_{\text{arag}} = 4.6$ ; green line) in order to facilitate this comparison. This figure is modified from Langdon and Atkinson (2005) and the plotted data are from the references cited in the figure legend.



Table 5.1 Previous experimental studies of the effect of aragonite saturation state ( $\Omega_{\text{arag}}$ ) on coral calcification

	Borowitzka (1981)	Boucher et al. (1998)	Gattuso et al. (1998)	Marubini and Thanke (1999)	Langdon et al. (2000)	Marubini et al. (2001)
Species	<i>Amphiroa foliacea</i>	Sand community collected from the southwest lagoon of New Caledonia	<i>Stylophora pistillata</i>	<i>Porites porites</i>	Biosphere-2 mesocosm: <i>Porites astreoides</i> , <i>Favia fragum</i> , <i>Agaricia sp.</i> , <i>Siderastrea sp.</i> , and <i>Acropora cervicornis</i>	<i>Porites compressa</i>
Method of manipulating $\Omega_{\text{arag}}$	Addition of HCl and NaOH	-	Addition of $\text{Na}_2\text{CO}_3$ and HCl	Addition of $\text{NaHCO}_3$ , $\text{KNO}_3$ , and $\text{NH}_4\text{Cl}$	Addition of $\text{NaHCO}_3$ , $\text{Na}_2\text{CO}_3$ , and $\text{CaCl}_2$	Addition of NaOH, HCl, $\text{NaHCO}_3$ , and $\text{Na}_2\text{CO}_3$
Method of measuring $\Omega_{\text{arag}}$	-	Calculation from pH and TA of water samples	Calculation from pH and TA of water samples	Calculation from pH and TA of water samples	Calculation from $\text{TCO}_2$ and TA of water samples	Calculation from DIC and TA of water samples
Method of measuring calcification	Buoyant weight technique	Alkalinity anomaly method	Alkalinity anomaly method	Buoyant weight technique	Alkalinity anomaly method	Buoyant weight technique
Duration of treatment	Not mentioned	1 day	2.5 hours	32 days	3.8 years	6 weeks
Calcification (%) relative to the rate at $\Omega_{\text{arag}} = 4.9$	$-1 + 21\Omega_{\text{arag}}^*$	$-287 + 79\Omega_{\text{arag}}^*$	$228(1 - \exp[-\Omega_{\text{arag}}/0.69]) - 128^*$	$51 + 10\Omega_{\text{arag}}^*$	$-67 + 34\Omega_{\text{arag}}^*$	$37 + 13\Omega_{\text{arag}}$



Table 5.1 (Continued)

	Leclercq (2000)	Leclercq (2002)	Marshall and Clode (2002)	Marubini et al. (2003)	Langdon and Atkinson (2005)	Marubini et al. (2008)
<b>Species</b>	Coral community: scleractinian corals ( <i>Acropora</i> spp., <i>Favia</i> sp., <i>Porites</i> sp., <i>Montipora</i> sp., <i>Galaxea fascicularis</i> , <i>trachiphyllia geoffroyi</i> , <i>Turbinaria mesenterina</i> ), calcareous red algae ( <i>Neogoniolithon</i> spp. and <i>Hydralothon</i> spp.), damselfish ( <i>Dascyllus trimaculatus</i> ), brown tang ( <i>Zebrasoma scopas</i> ), and microfauna (crustaceans, polychaetes, gastropods)		<i>Calaxea fascicularis</i> L.	<i>Turbinaria reniformis</i>	Coral community: <i>Porites compressa</i> and <i>montipora verucosa</i> (capitata)	<i>S.pistillata</i>
<b>Method of manipulating <math>\Omega_{\text{avg}}</math></b>	Use of a gas blender combined with a gas divider or a CO <sub>2</sub> scrubber filled with soda lime		Addition of CaCl <sub>2</sub> ·2H <sub>2</sub> O to see the impact of high-calcium seawater	Addition of HCl and NaOH	Addition of HCl and NaOH	Addition of HCl, NaHCO <sub>3</sub> , and NaOH
<b>Method of measuring <math>\Omega_{\text{avg}}</math></b>	Calculation from pH and TA of water samples		-	Calculation from pH and TA of water samples	Calculation from DIC and TA of water samples	Calculation from pH and TA of water samples
<b>Method of measuring calcification</b>	Alkalinity anomaly method		Buoyant weight technique	Buoyant weight technique	Alkalinity anomaly method	Buoyant weight technique
<b>Duration of treatment</b>	1 day	1 month	1.5 to 2 hours	8 days	7 days and 12 days under summer and winter condition, respectively	8 days
<b>Calcification (%) relative to the rate at <math>\Omega_{\text{avg}} = 4.9</math></b>	$31 + 14\Omega_{\text{avg}}^*$	$52 + 10\Omega_{\text{avg}}^*$ sand community: $-1533 + 333\Omega_{\text{avg}}^*$	$-110 + 43\Omega_{\text{avg}}$	$72 + 5.9\Omega_{\text{avg}}$	$-10.7 + 9\Omega_{\text{avg}}$ (before nutrient enrichment)	$66 + 7\Omega_{\text{avg}}$

\* Equations from Leclercq (2002)

### 5.1.1.3 Combined effects of increasing temperature and decreasing pH due to increasing $p\text{CO}_{2\text{atm}}$ on coral calcification

The combined effects of climate change and ocean acidification on biogenic calcifiers are still poorly constrained. This is because of (1) inherent limitations in experiments which simulate the impacts of high  $p\text{CO}_2$  and (2) the lack of knowledge about physiologically modified responses of calcification to seawater carbonate chemistry and rising temperature (McCulloch et al., 2012).

McNeil et al. (2004) estimated future changes in coral reef calcification by combining the empirical relationships between coral calcification rate,  $\Omega_{\text{arag}}$  and average annual SST from Langdon et al. (2000) and Lough and Barnes (2000) respectively. Their analysis suggests that annual average coral reef calcification rate will increase and exceed preindustrial rates by about 35% by 2100 as the effect of ocean warming far outweighs the impact from a decrease in  $\Omega_{\text{arag}}$ .

Recent  $\text{CO}_2$ -incubation experiments on a tropical coral, *Cladocora caespitose*, support the hypothesis above and suggest that increased  $p\text{CO}_2$  does not reduce its calcification rate (Rodolfo-Metalpa et al., 2010). The same study indicates seasonal temperature change is the predominant factor controlling photosynthesis, respiration, calcification, and symbiont density, and that an increase in  $p\text{CO}_2$  (or a decrease in ocean pH) had no significant effect on photosynthesis, photosynthetic efficiency and further calcification. It was concluded that the lack of sensitivity of temperate corals to elevated  $p\text{CO}_2$  would be more dependent on temperature than on the saturation state of calcium carbonate in the range projected for the end of the century.

A model study of ocean warming and acidification on coral calcification in combination with physiological pH up-regulation at calcification site has also shown a future increase in coral calcification (McCulloch et al., 2012). This study suggested that given the reduced sensitivity of coral calcification to ocean acidification as a result of pH up-regulation by corals, any decrease in coral calcification due to

declining seawater pH is more than compensated by the increase due to rising ocean temperature.

The complex and varied responses of coral calcification to seawater temperature and pH changes have produced large uncertainties and clearly require further investigation.

### 5.1.2 Adapting to rising temperature and ocean acidification

The response of coral calcification to long-term changes in SST and ocean carbonate chemistry depends on the ability and rate at which corals can adapt to such changes (Baker et al., 2004; Rodolfo-Metalpa et al., 2011). This aspect of coral calcification has been reviewed recently by Pandolfi et al. (2011) with emphasis on past rapid increases in temperature and ocean acidification that have occurred over millennial timescales. There is good evidence for adaptation and acclimatization of corals through the Phanerozoic period (~540 Ma to present) including the existence of shallow water tropical corals when surface temperature was 7°C higher than today and  $p\text{CO}_{2\text{atm}}$  exceeded 6000 ppm (Fig. 5.3). However, over such long geological timescales, there was substantial time for biodiversity recovery and the negative feedback system within the carbon cycle to increase the alkalinity in the oceans through increased rock weathering. Whilst the predicted future changes in SST and  $p\text{CO}_{2\text{atm}}$  due to anthropogenic  $\text{CO}_2$  emissions are, at most, half the magnitude of changes during the Phanerozoic, the rate of change that is occurring is much faster (Doney et al., 2009). It remains unclear whether corals will be able to adapt to this predicted rapid rate of environmental change.



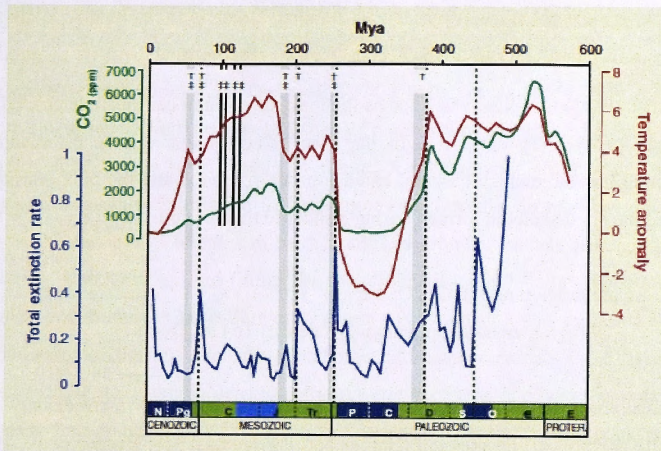


**Fig. 5.3** Summary of major episodes of physical and biological change of reefs across the Phanerozoic. Vertical dashed gray lines indicate global mass extinction events; vertical gray bars indicate reef crises; and short vertical black bars indicate ocean acidification events (Pandolfi et al., 2011).

## 5.2 Methods

### 5.2.1 Coral sampling and geochemical analysis

Corals were collected in March 2006 and October 2008 from four *Porites* colonies located in the southern Great Barrier Reef (GBR), Australia. The full lengths of these coral cores were sectioned and then scanned to obtain trace element data along their maximum growth axes using LA-ICPMS. Trace element seasonal cycles from LA-ICPMS profiles were used to determine core chronologies. Descriptions of all sample collection and preparations are given in chapter 2 and the reconstruction of coral chronologies is explained in chapter 2 and 3. Analysis of coral boron isotopic compositions and how these data have been converted to seawater pH are also described in chapter 4. Average annual sea surface temperature (SST) was derived from NOAA NCDC ERSST database (detailed in chapter 3).

### 5.2.2 Coral calcification rate

Calcification rate is typically defined as the mass of calcium carbonate deposited per unit area per year ( $\text{g cm}^{-2} \text{yr}^{-1}$ ). In the case of corals this can be estimated by combining measurements of annual extension rate ( $\text{cm yr}^{-1}$ ) and the bulk density ( $\text{g cm}^{-3}$ ) of the coral skeleton formed during a specific time period.

$$\text{Calcification rate (g CaCO}_3 \text{ cm}^{-2} \text{ yr}^{-1}) = \text{extension rate (cm yr}^{-1}) \times \text{density (g CaCO}_3 \text{ cm}^{-3}) \quad (5-5)$$

The density of coral skeletons varies with changes in both the 'micro-density' and the 'bulk density' of the skeleton (Barnes and Devereux, 1988; Bucher et al., 1998; Buddemeier et al., 1974). The micro density is related to the arrangement and organization of essentially acicular aragonite crystals within the various skeletal elements, whereas the bulk density is the amount of macro porosity created by variation in the arrangement of the skeletal elements (basal plates, thecae, septa, and dissepiments) that link adjacent corallites.

Variations in both micro-density and bulk density (porosity) can reflect environmental influences on calcification and growth. Eutrophication of seawater can affect micro-density without altering bulk density or porosity by interfering with the array of aragonite crystals (Bucher et al., 1998). On the other hand, wave exposure produces a significant increase in bulk density or porosity and no change in micro-density (Bucher et al., 1998). It is therefore desirable to measure both aspects of density to assess the different environmental impacts on coral growth.

Both the micro- and bulk density of coral skeletons can be measured simply and conveniently using Archimedes' Principle by either a water-displacement (Graus and Macintyre, 1982; Hughes, 1987) or mercury-displacement method (Dustan, 1975). These methods entail weighing cm-scale coral skeleton blocks with an analytical balance in air and then determining their volume by measuring the displacement of water or mercury. A significant advantage of this method is that it does not require



specialized equipment of alternate methods for measuring coral density. One of these methods is X-ray densitometry, which also known as photo-densitometry or microdensitometry (Dodge and Thomson, 1974; Chalker et al., 1985). This technique is convenient when the complete life span of coral can be determined from a single X-radiograph, or by overlapping multiple X-radiographs. Calibration of the procedure, especially calibration for the non-uniform irradiation of X-ray machines such as the anode heel effect, can be difficult and requires various assumptions for extracting, standardizing and fitting the data from different X-radiographs together (Chalker and Barnes, 1990). Similarly, gamma densitometry was proposed for the measurement of the bulk density of calcium carbonate materials by Chalker and Barnes (1990). The gamma densitometry of coral skeletons is quicker, simpler, and subject to fewer sources of variability than the measurement of coral skeletal density with X-radiographs, but it requires construction of specialized equipment for sources and counting (Lough and Cooper, 2011). Finally, computerized tomography (CT) has been used as a method of measuring coral bulk density which offers several major advantages (Cantin et al., 2010; Seander et al., 2009). These include (1) accurate measurement of three-dimensional matrix with a growth axis up to size of a human body (Bosscher, 1993), (2) direct conversion of CT density (Hounsfield units) to bulk density ( $\text{g cm}^{-3}$  unit) (Bessat and Buigues, 2001; Bosscher, 1993) and (3) fewer assumptions than needed for X-ray and gamma densitometry.

Two different density measurements have been used in this study to calculate calcification rate and porosity. The measurements are based on the Archimedean principle, whereby the difference in weight of an object when submerged in water is equivalent to the volume of displaced water. This buoyant-weight method has been chosen for this study as it is the only method able to measure both the micro- and bulk density. It is also simple and does not require pure standards (e.g. aluminum bars and aragonite wedges) for calibration. Unlike gamma and X-ray densitometry which use a 4 mm track to measure skeletal density, it can provide a more representative analysis of a coral colony. By using pieces of 25 mm width the measured density includes a large number of corallites, and thus can avoid fine scale variation across the skeleton due to changes in the orientation of growth axes and/or

seasonal density bands (D'Olivo et al., 2013). Lastly, it can be highly accurate (better than 1%; Spencer Davies, 1989).

### 5.2.2.1 Buoyant-weighing methods

Measurements of buoyant weight and calculation of density and porosity followed the methods described by Bucher et al. (1998) and Spencer Davies (1989) using a Mettler B6 electronic balance that is accurate to  $\pm 0.02$  mg. A 75 mm watchglass was used as a weighing platform and suspended using a triangular aluminum frame (70 mm sides). A 0.2 mm diameter hydrophobic nylon filament (fishing line) was used to attach the corner of the frame to a hook on the top of the balance. The watchglass was suspended in a 6 cm deep container of pure water, and the temperature of water was monitored using a  $N_2$  thermometer (a precision of  $\pm 0.05^\circ C$ ) to calculate the water density ( $\rho_{H_2O}$ ) from the following equation (Maidment, 1993).

$$\rho_{H_2O} \text{ (g cm}^{-3}\text{)} = 1000(1 - (T \text{ (}^\circ\text{C)} + 288.9414) / (508929.2 \times (T \text{ (}^\circ\text{C)} + 68.12963))) \times (T \text{ (}^\circ\text{C)} - 3.9863)^2 \quad (5-6)$$

The buoyant weight of the coral was then measured to a precision of  $\pm 0.5$  mg after the balance readout had stabilized. The measured density of each coral piece (~9 cm length) corresponded to the average density over a 5-year period. These density results were subsequently resampled at annual resolution by linear interpolation using the Analyseries program (Paillard et al., 1996). These annual density values were used to calculate annual calcification rate with annual extension rate (see the following section 5.2.3).

### 5.2.2.2 Skeletal 'bulk density'

Two different methods were used to determine the bulk density of coral samples. The first method estimated the bulk density of a coral piece by dividing the dry weight in

air by the volume based on the measured length, width, and thickness of each coral piece using a digital caliper that is accurate to  $\pm 0.01$  mm (hereafter referred as the caliper method). For non-rectangular coral pieces or irregular pieces, the area was calculated by combining multiple simple shapes that have readily calculated areas.

The second method estimated the bulk density of each coral piece by dividing the dry weight in air by the total enclosed volume (including the volume of skeletal voids) determined from its buoyant-weight (hereafter referred the enclosed-volume-buoyancy method; Bucher et al., 1998). The skeletal voids of coral pieces were enclosed by vacuum-plastic-shrink-wrapping in preference to plastic-shrink-wrapping which otherwise required the use of a hot iron that was found to be unable to seal the coral pieces tightly. A consumer vacuum seal system (Sunbeam VAC 420) was used to wrap the coral surface and a heat gun was used to seal the plastic shrink wrap onto the coral pieces. Excess plastic along the seal was then trimmed using scissors to minimize the contribution to the total weight. The weight of the plastic coated coral pieces was then determined in air and in water.

The two independent methods used for determining density should give the same values if sufficiently accurate measurements have been performed. However, the enclosed-volume-buoyancy method is consistently overestimated due to the excess volume that is included despite tight sealing (Fig. 5.4). In order to make accurate coral density determinations, the results of the enclosed-volume-buoyancy method were calibrated and corrected for the volume of the plastic shrink wrap used to cover each coral piece (hereafter calibrated enclosed-volume-buoyancy method). The required correction was estimated from the weight difference between the wrapped and unwrapped coral pieces divided by the density of the plastic ( $0.67 \text{ g cm}^{-3}$ ). A comparison of the density results obtained from the different calculations (i.e. the caliper method, enclosed-volume-buoyancy method, and calibrated enclosed-volume-buoyancy method) is shown in Fig. 5.4 (listed in appendix Tables E-1 and E-2).



The bulk density of the Middle Pompey coral samples estimated using the calibrated enclosed-volume-buoyancy method shows reasonable consistency with density determined using the caliper method ( $r^2 = 0.92$  following removal of 3 outliers, PSC-6, and -11;  $p < 0.001$ ) falling close to the 1:1 line (Fig. 5.4A). The density of Little Kindermar samples, on the other hand, show higher values when estimated using calibrated enclosed-volume-buoyancy method than the caliper method, and give a much weaker correlation between the methods ( $r^2 = 0.72$  following removal of 4 outliers, PSA-3, -13, -17, and -25; Fig. 5.4B). These inconsistencies are caused by volume estimation errors when dealing with more irregular coral pieces. For example, the density of the most irregular pieces PSA-17 and -25 from Little Kindermar measured using the caliper method are much lower than the values determined by the calibrated enclosed-volume-buoyancy method with a significant error of ~30%.

Determination of coral density by the calibrated enclosed-volume-buoyancy method was subsequently adopted for all core samples from the southern GBR in this study with the exception of Fitzroy Reef core. The density of the Fitzroy Reef coral samples was lower than pure water ( $<1 \text{ g cm}^{-3}$ ) making it impossible to use this approach. In this case density measurements were made via the caliper method using regular-shaped coral pieces (appendix Tables E-1 to E-6).

### 5.2.2.3 Skeletal 'micro-density'

In contrast to skeletal bulk density, the measurement of micro-density requires an estimation of the matrix volume. This can be obtained by filling all skeletal voids with water of the same density as the weighing medium. To achieve this, coral pieces for micro-density determination were placed in a  $26 \times 26 \times 30 \text{ cm}$  vacuum chamber (NAPCO model 5831) alongside an ultrapure water filled container, and the air was expelled from the coral skeleton by evacuating the chamber to a pressure of 28 mmHg. The coral pieces were then submerged in the water filled container and the container immediately removed from the chamber. Since the surface tension of water decreases with increasing air pressure, the container and immersed piece of

coral were left at atmospheric pressure until the voids with the coral pieces are saturated with the ultrapure water before being buoyant-weighted. Experiments revealed that void saturation was achieved in ~3-4 hours.

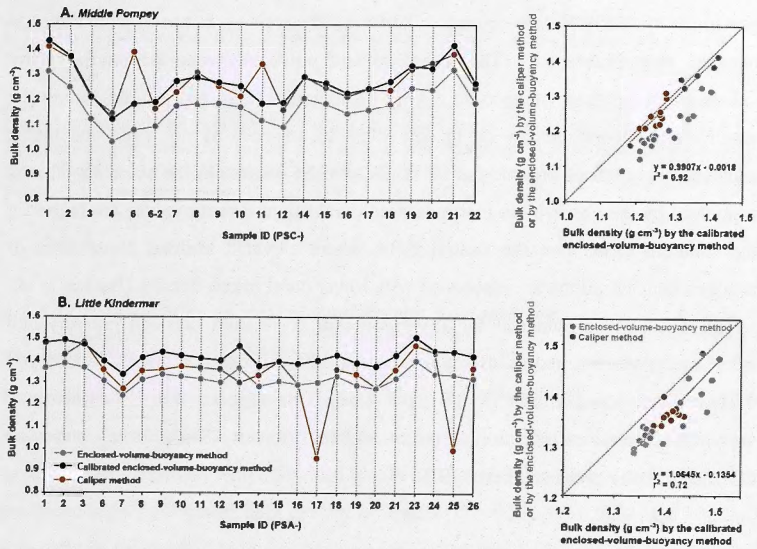


Fig. 5.4 Comparison of two different methods of bulk density measurement, the enclosed-volume-buoyancy method and the caliper method for (A) Middle Pompey and (B) Little Kindermar reefs. The result of the calibration for the volume of plastic wrap used to enclose coral pores (the calibrated enclosed-volume-buoyancy method) is also plotted. X axes represent sample ID of each piece. Linear relationship of the density from the calibrated enclosed-volume-buoyancy method to those from the enclosed-volume-buoyancy method and the caliper method is represented in the diagrams on the right side. Red dotted line indicates 1:1 line and linear regression between the calibrated enclosed-volume-buoyancy method and the caliper method is shown with black dotted line.

The effectiveness of the buoyancy weighing method was verified by examining the relationship between bulk density and porosity (Fig. 5.5). The linear regression coefficients ( $r^2$ ) obtained between these two measurements are  $>0.95$  and in excellent



agreement with previous measurements by Bucher et al. (1998). These results indicate the attainment of virtually complete sample void evacuation and re-filling with water using this method.

Comparison of micro-density results from Middle Pompey and Little Kindermar with previously published data reveals significant differences between colonies and between sites (Table 5.2). The measured and previously reported micro-density values are lower than the specific gravity of aragonite ( $2.94 \text{ g cm}^{-3}$ ), indicating the assumption of coral density being equivalent to aragonite is not valid and that a significant amount of organic matter is likely to be present in the skeleton. This is supported by the observation that measured coral micro-density values are higher in the southern GBR than the central GBR where elevated skeletal phosphorus or nitrogen concentrations are associated with lower coral micro-density (Bucher et al., 1998). There is no evidence for any significant correlation between porosity and calcification rate (see the following section) at either Middle Pompey ( $r^2 = 0.20$ ,  $p = 0.05$ ) or Little Kindermar ( $r^2 = 0.01$ ,  $p = 0.61$ ). This suggests that the influence of nutrients on coral calcification is minor and that porosity exerts little control on calcification rate in the southern GBR.

**Table 5.2** Micro-densities reported for *Porites* and other coral species. All literature values are from Bucher et al. (1998).

Species	Locality	Micro-density	Source
<i>Porites sp.</i>	Middle Pompey (southern GBR)	2.72-2.84	This study
<i>Porites sp.</i>	Little Kindermar (southern GBR)	2.77-2.84	This study
<i>Porites porites</i>	Jamaica	2.82	Edmunds and Davies (1986)
<i>Porites porites</i>	Barbados	2.72-2.77	Bucher (unpublished data)
<i>Porites lutea</i>	Pandora Reef (central GBR)	2.74-2.80	Barnes and Devereux (1988)
<i>Porites australiensis</i>	Pandora Reef (central GBR)	2.81-2.82	Barnes and Devereux (1988)
<i>Acropora sp.</i>	One Tree Island (southern GBR)	2.78-2.87	Bucher et al. (1998)
<i>Acropora sp.</i>	Solitary Island (New South Wales, Australia)	2.83	Bucher et al. (1998)
<i>Acropora humilis</i>	Jeddah	2.62	Davies (1989)
<i>Pocillopora verrucos</i>	Jeddah	2.79	Davies (1989)
<i>Pocillopora eydouxi</i>	Guam	2.78	Davies (1984)
<i>Pocillopora damicornis</i>	Solitary Island	2.7	Spinaze et al. (1996)

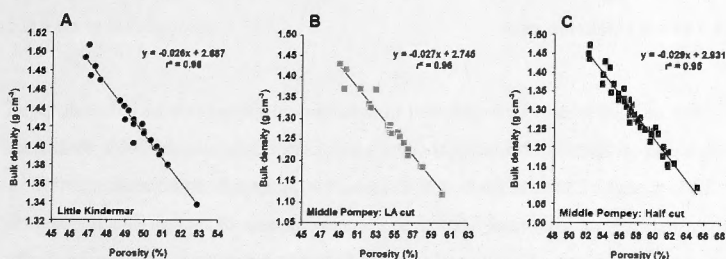


Fig. 5.5 Relationship of bulk density measured using the calibrated enclosed-volume-buoyancy method and porosity for *Porites* spp. coral cores from Little Kindermar and Middle Pompey. Little Kindermar (A) and Middle Pompey (B) core data determined from pieces used for LA analysis, and (C) Middle Pompey core data from half-length pieces (~4.5 cm) compared to the pieces for LA analysis.

#### 5.2.2.4 Reproducibility of coral skeletal density measurements

The reproducibility of the bulk density measurement method was determined by comparing difference size coral pieces from the Middle Pompey core. After measuring both the bulk and micro-density of typical 2.5 cm × 6.0 cm pieces, the procedure was repeated with half-sized pieces (2.5 cm × 3.0 cm in average). This test produced highly correlated bulk density estimates ( $r^2 = 0.93$ ,  $p < 0.0001$ ; see Fig. 5.6) that indicate the method produces results with accuracy of 1.5%.

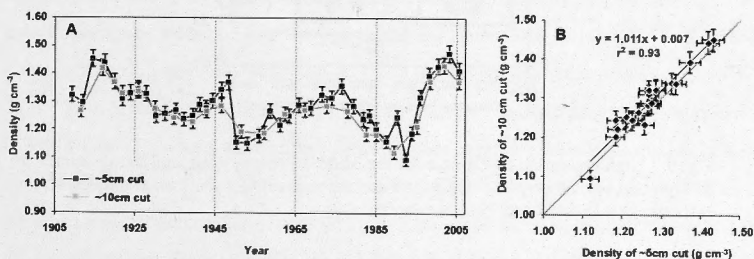


Fig. 5.6 Reproducibility of the calibrated enclosed-volume-buoyancy method between Middle Pompey coral skeletal pieces of two different sizes. (A) The close correspondence between the two records and (B) the clear correlation between the measured values based on two different size pieces. Red line represents 1:1 line and the regression of the data shown by the black line agrees with the 1:1 line. Error bars display 1.5% accuracy of measurements.

### 5.2.3 Annual extension rate

A number of studies have demonstrated that the annual extension rate of corals is the principle factor that determines coral calcification rate (De'ath et al., 2009; Helmle et al., 2011; Lough, 2008a; Lough and Barnes, 1997; Lough and Barnes, 2000). It follows that making high quality measurements of annual extension rate is essential for accurate estimation of calcification rates. This has been done by determining the linear distance between successive trace element/Ca maxima or minima (measured using LA-ICPMS) which correspond to growth at the lowest temperature in each year (approximately mid-August). Sr/Ca variations were employed in the case of cores from Middle Pompey (e.g. Fig. 5.7), Fitzroy Reef, and Lady Musgrave Island, whereas B/Ca was used for Little Kindermar core due to a lack of clear seasonal variations of Sr/Ca in this particular core.

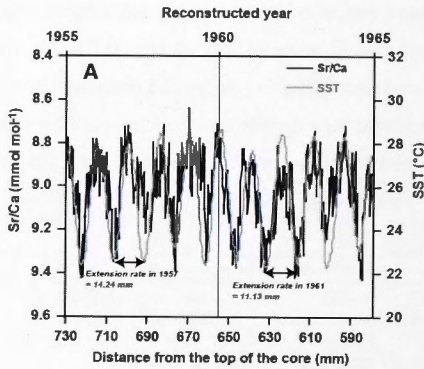


Fig. 5.7 High resolution Sr/Ca data for the Middle Pompey core and instrumental SST plotted against distance down core and reconstructed year. Two examples of extension rate in 1957 and 1961 are shown.

#### **5.2.4 Data manipulation**

A composite master record of extension, density, and calcification rate was calculated from the five southern GBR core records by normalizing the mean values of individual records to the mean values of all five cores relative to the coral records for the common period of all cores (i.e. 1950-2005). The methodology followed the data manipulation procedure outlined in Chapter 3.

The rates of variation of the southern GBR coral growth records were estimated with weighted least square linear regressions of the composite record due to different number of samples in each year (see Chapter 3 for more details). 95% confidence intervals are employed as weighting variables and the maximum confidence interval values obtained for each parameter were used for periods when only one record exists (i.e. the period of 1834-1889).

### **5.3 Results**

The annual extension rate, density, and calcification rate records for the Middle Pompey, Little Kindermar, Fitzroy Reef, and Lady Musgrave Island cores are presented in Fig. 5.8 and summarized in Table 5.4 (see appendix Tables E-7 to E-11 for the full dataset). The mean values and variability of extension rate, density, and calcification rate obtained for the individual southern GBR corals (Table 5.4) are consistent with a previous study on 45 colonies from the southern GBR (20.45°S-21.65°S; Lough and Barnes, 2000) except for one Lady Musgrave Island core (LMI08-C-a). This coral core comes from the most southern location sampled in this study and shows the lowest calcification rate ( $0.62 \pm 0.21 \text{ g cm}^{-3} \text{ yr}^{-1}$ ,  $1\sigma$ ) of the five coral records. However, there were no significant differences in the calcification rate of the other four *Porites* along the 3° latitudinal range which spans an average temperature gradient  $\sim 1.5^\circ\text{C}$  (Table 5.4 and Fig. 5.8) and none of the different annual coral calcification records are significantly correlated (Table 5.3). This result is inconsistent with results reported by Lough and Barnes (2000) who observed about a



10% decrease in the coral calcification across the same 3° increase in latitude.

**Table 5.3** Correlation between individual coral calcification rates from the southern GBR. The correlations and significance were determined using Pearson Product-moment correlation at 95% confidential level. All correlation coefficients are given as  $r$ -values.

	Middle Pompey	Little Kindermar	Fitzroy Reef	Lady Musgrave (H)
Little Kindermar	0.21 (df=94, p=0.04)			
Fitzroy Reef	0.06 (df=54, p=0.65)	0.19 (df=54, p=0.16)		
Lady Musgrave (H)	-0.04 (df=94, p=0.68)	-0.10 (df=114, p=0.31)	0.05 (df=57, p=0.70)	
Lady Musgrave (C-a)	0.08 (df=48, p=0.56)	0.18 (df=48, p=0.22)	0.18 (df=51, p=0.20)	0.14 (df=51, p=0.30)

Significant increases in coral calcification rate occur in all the sampled coral cores in the southern GBR with 1.2 %/decade for Little Kindermar from 1834 to 2005, 2.5 %/decade for Fitzroy Reef from 1950 to 2008, and 1.1 %/decade for Lady Musgrave Island (H) from 1890 to 2008, with an exception of changes in the calcification from the Middle Pompey Reef (-0.1 %/decade from 1909 to 2005; Fig. 5.8). Interannual variability of growth parameters, inferred from the coefficient of variation of results (CV; Table 5.4) ranges from 13 to 33% for extension rate, 3 to 6% for density, and 14 to 33% for calcification rates. The interannual variability of growth parameters is comparable to values obtained for *Porites* from the GBR by previous studies (Cooper et al., 2008; Lough and Barnes, 2000). These results indicate that the interannual variability of density is highly conservative whereas extension and calcification are much more variable. The correlations between these different growth parameters in Table 5.5 indicate that calcification rate is strongly determined by extension rate and that no significant relationship occurs between calcification and density. Again, this is consistent with previous coral calcification studies (Cooper et al., 2008; De'ath et al., 2009; Helmle et al., 2011; Lough and Barnes, 1997; Lough and Barnes, 2000). It follows that extension rate accounts for ~90% of the fluctuation of calcification rates in the southern GBR.

Weighted regression analysis of the composite record indicates significant increases in extension and calcification rate ( $p < 0.0001$ ,  $n = 125$ ) and no significant change in density over the last 125 years (1883 to present; Fig. 5.9). This long-term trend of



increasing coral calcification (about 0.7% per decade) is consistent with other recent studies in the subtropical region (Cooper et al., 2012). When the results of this study are considered over a shorter time scale since 1988, they are also comparable to the observations from the GBR, and indicate a ~20% decrease in the calcification rate since 1990 (Cooper et al., 2008; Cooper et al., 2012; De'ath et al., 2009; Helmle et al., 2011).

**Table 5.4** Summary of coral core sample latitude, observation periods, mean values and coefficients of variation of coral growth parameters for individual and composite master records from the southern GBR.

Sampled reef	Latitude	Periods	Mean values ( $\pm 1\sigma$ )			Coefficient of variation (CV; %)		
			Extension (mm yr <sup>-1</sup> )	Density (g cm <sup>-3</sup> )	Calcification (g cm <sup>-2</sup> yr <sup>-1</sup> )	Extension (mm yr <sup>-1</sup> )	Density (g cm <sup>-3</sup> )	Calcification (g cm <sup>-2</sup> yr <sup>-1</sup> )
Middle Pompey	20.99°S	2005-1909	13.72 ( $\pm 2.11$ )	1.28 ( $\pm 0.08$ )	1.75 ( $\pm 0.25$ )	15	7	14
Little Kindermar	21.10°S	2005-1834	8.69 ( $\pm 1.56$ )	1.43 ( $\pm 0.04$ )	1.24 ( $\pm 0.22$ )	18	3	17
Fitzroy Reef	23.38°S	2008-1950	16.11 ( $\pm 2.14$ )	1.01 ( $\pm 0.05$ )	1.62 ( $\pm 0.23$ )	13	5	14
Lady Musgrave (H)	23.54°S	2008-1890	11.70 ( $\pm 2.13$ )	1.24 ( $\pm 0.05$ )	1.43 ( $\pm 0.26$ )	18	4	18
Lady Musgrave (C-a)	23.54°S	2008-1956	6.24 ( $\pm 2.08$ )	1.52 ( $\pm 0.05$ )	0.62 ( $\pm 0.21$ )	33	3	33
Master record		2008-1834	11.42 ( $\pm 1.43$ )	1.26 ( $\pm 0.03$ )	1.41 ( $\pm 0.16$ )	12	3	11

**Table 5.5** Correlation coefficients ( $r$ ) of growth parameters for individual records and the composite master record comprising all 5 southern GBR coral cores. Significant relationships ( $p < 0.05$ ) are indicated in bold.

Sampled reef	No. of data	Extension vs Density	Extension vs Calcification	Density vs Calcification
Middle Pompey	95	$r = -0.34$ $p < 0.001$	$r = 0.93$ $p < 0.0001$	$r = 0.00$ $p = 1.000$
Little Kindermar	165	$r = -0.26$ $p < 0.001$	$r = 0.99$ $p < 0.0001$	$r = 0.12$ $p = 0.112$
Fitzroy Reef	58	$r = 0.13$ $p = 0.316$	$r = 0.95$ $p < 0.0001$	$r = 0.40$ $p = 0.002$
Lady Musgrave (H)	118	$r = -0.02$ $p = 0.844$	$r = 0.98$ $p < 0.0001$	$r = 0.18$ $p = 0.049$
Lady Musgrave (C-a)	52	$r = -0.47$ $p < 0.001$	$r = 1.00$ $p < 0.0001$	$r = 0.49$ $p < 0.001$
Master record	172	$r = -0.25$ $p < 0.001$	$r = 0.99$ $p < 0.0001$	$r = 0.11$ $p = 0.147$

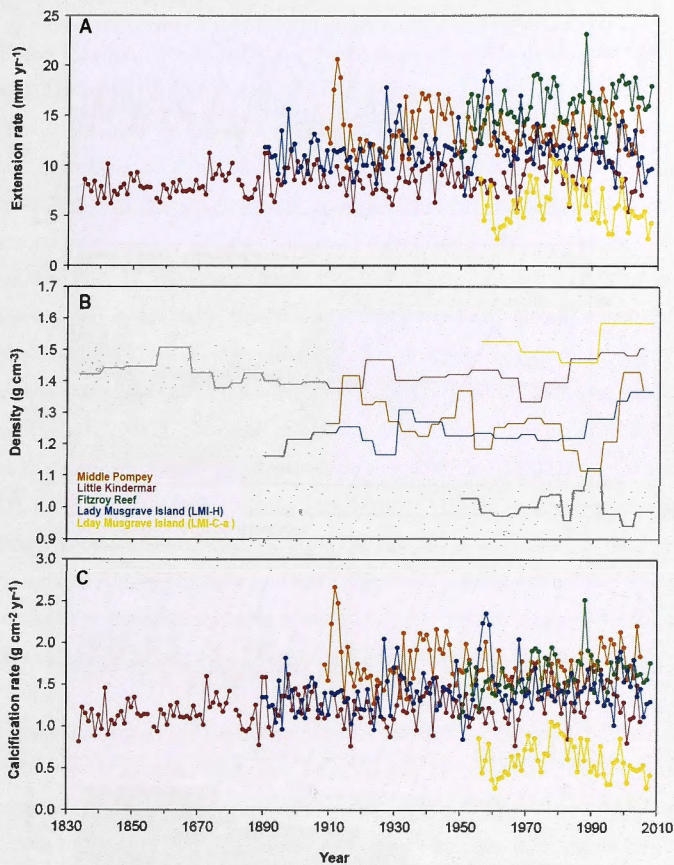


**Fig. 5.8** Comparison of (A) extension rate, (B) density, and (C) calcification rate records of individual coral cores from the southern GBR. Time series derived from trace element chronology (see Chapter 3.2.3). Extension rates were calculated annually from seasonal cycles of trace element records and density estimated by buoyant weighing for about 5-year periods. Calcification records are derived from these two measures.

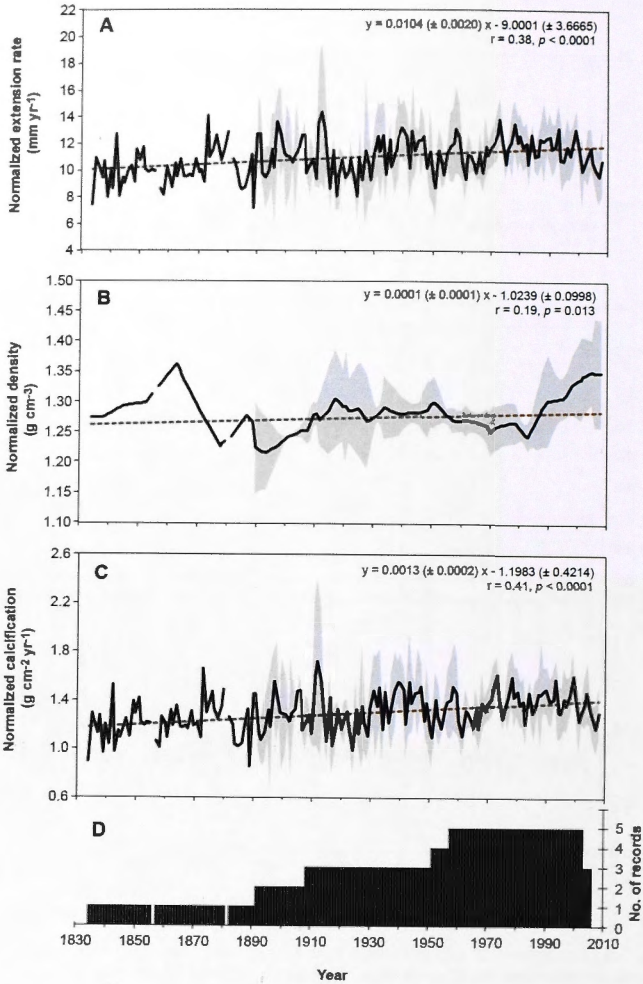


**Fig. 5.9** Time-series master records of normalized coral growth parameters shown with 95% confidence envelopes (gray areas) for (A) linear extension rate, (B) density, (C) calcification rate, and (D) number of samples contributing to the master records. The master record of each parameter was produced by averaging normalized individual records to the period of 1950 to 2005. The trends of coral growth parameter were determined by weighted linear regression and are shown as brown dotted lines along with fitted trends of the results.



## **5.4 Discussion**

Assessing long-term trends in *Porites* coral calcification records requires testing for possible age related artifacts whereby extension rates may increase and density may decrease from older to younger part of corals independent of other factors that include increasing SST and decreasing seawater pH (Lough, 2008a; Lough and Cooper, 2011). In this study, annual extension rate exhibits a significant increase with coral age, whereas density exhibits no significant variation over the 170-year period based on the fitted linear trends (Fig. 5.9). The possible age effect on growth parameters was tested with the 10-year average-trends of growth variables from Middle Pompey, Little Kindermar, and Lady Musgrave Island cores which have more than 100 year records following a published method for assessing age related effects (Lough, 2008a). The result indicates no significant evidence for an age effect in the southern GBR cores for extension rate ( $y = 0.0677x + 11.0921$ ,  $r^2 = 0.142$ ,  $p = 0.253$ ), density ( $y = 0.0016x + 1.2482$ ,  $r^2 = 0.048$ ,  $p = 0.518$ ) or calcification rate ( $y = 0.0089x + 1.3655$ ,  $r^2 = 0.251$ ,  $p = 0.116$ ). The absence of any change in coral growth characteristics with age in these southern GBR corals permits skeletal growth records to be used for determining changes associated with environmental trends, such as decreasing aragonite saturation state and warming water temperatures.

Most individual corals and the master coral record show increasing calcification rates over the last 170 years. This lack of a decline in coral calcification does not necessarily indicate that corals and reefs in the southern GBR are healthy (Edinger et al., 2000; Helmle et al., 2011). Rather, it demonstrates that these corals have been able to maintain and increase their rates of calcification over this period under a combination of environmental changes. The subtropical location of these reefs may contribute to their ability to persistently grow under less than optimal environmental conditions due to lower temperature and pH compared to tropical regions (Lough and Barnes, 2000; Orr et al., 2005). The trends in coral calcification rates raise important questions as to whether these corals are tolerant to changes in particular environmental conditions (such as increasing temperature and acidity), or whether such environmental variables are yet to exceed thresholds for calcification, and if so



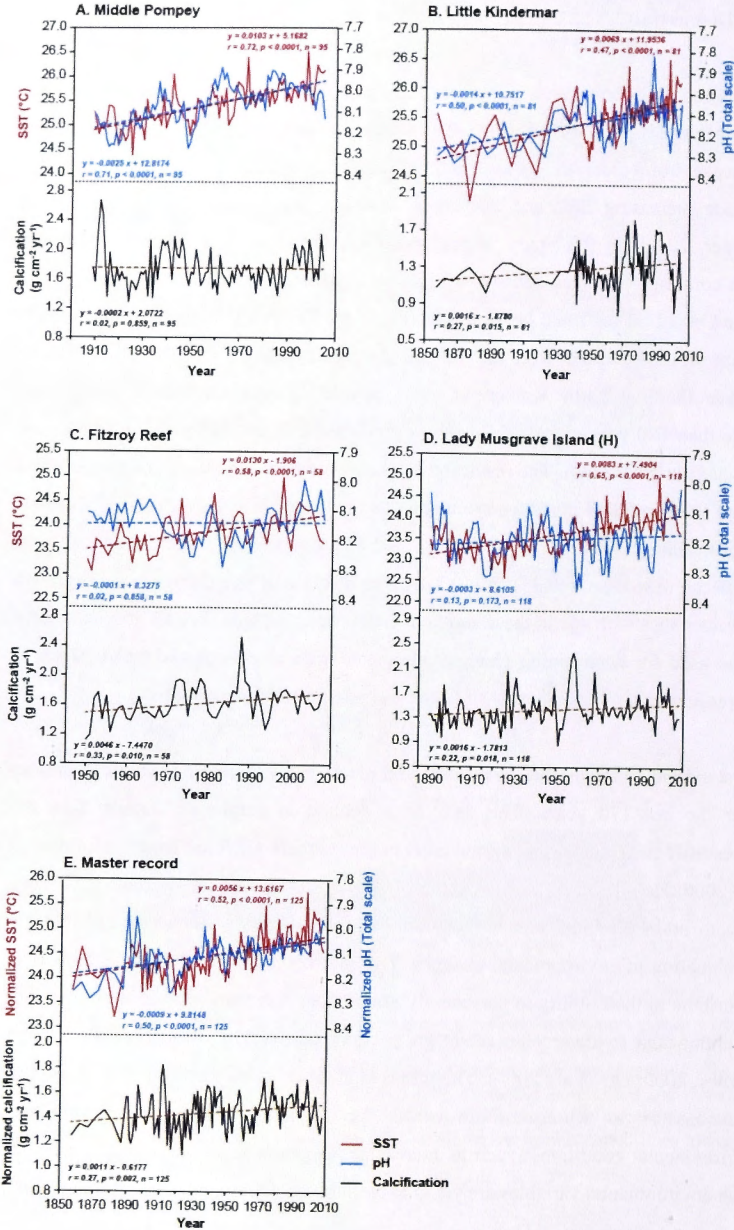


**Fig. 5.10** (*Opposite Page*) Comparison of individual (A to D) and master (E) records of coral calcification to SST and  $\delta^{11}\text{B}$ -derived seawater pH records from the southern GBR. Linear regressions for SST, pH, and calcification rate are shown in dotted red, blue, and brown lines, respectively. Also their corresponding equations,  $r$  and  $p$  values are presented with same color-coding. The uncertainty of instrumental SST during the period of 1857-1930 was complemented by the coral Sr/Ca-SST records in cases of Little Kindermar and composite records. Note that the y-axes for pH are inverted.

how far are they from these thresholds (Helmle et al., 2011). In an attempt to resolve some of these questions, the relevant long-term trends and decadal averages of SST and pH from each site have been assessed in the context of the equivalent trends in calcification rates. A comparison of decadal average values for temperature, pH, and calcification is conducted in order to determine the long-term trends with the deliberate exclusion of possible inter-annual variability of environmental factors such as weather.

Studies of the relationship between the *Porites* calcification and temperature have shown a linear relationship with annual average SST between 23°C to 30°C (Lough, 2008a; Lough and Barnes, 2000). Significant SST warming since the industrial revolution is confirmed by instrumental and coral based Sr/Ca-SST records for all coral core sites in the southern GBR (~1.0°C over the last 170 years; Fig. 5.10; see Chapter 3 for details about ocean warming in the southern GBR). The trend of increasing calcification is much more obvious against the average decadal SST data than against seawater pH (Fig. 5.11), however, correlations between SST and calcification rate are less statistically significant ( $p$ -values in Fig. 5.11).

A recent study showed that thermal stress associated with ocean warming occurs above an annual average SST of 26°C and results in significant calcification reduction in GBR corals (Carricart-Ganivet et al., 2012; De'ath et al., 2009). Carricart-Ganivet et al. (2012) also suggested calcification ceases at 30°C in *Porites spp.* corals. Such thermal stress levels are more likely to lead to the decreasing calcification in the recent years (since 1988) due to the observed rapid ocean warming in this region. However, there were no years when average SSTs exceeded

the 30°C threshold (Carricart-Ganivet et al., 2012) and the years when average SST is above 26°C is not linked to any significant reduction of calcification rates in the southern GBR. Moreover, no bleaching or disease outbreaks have been observed in the southern GBR (AIMS survey, see Chapter 2), hence it seems unlikely that this region has exceeded a thermal stress threshold for coral calcification.

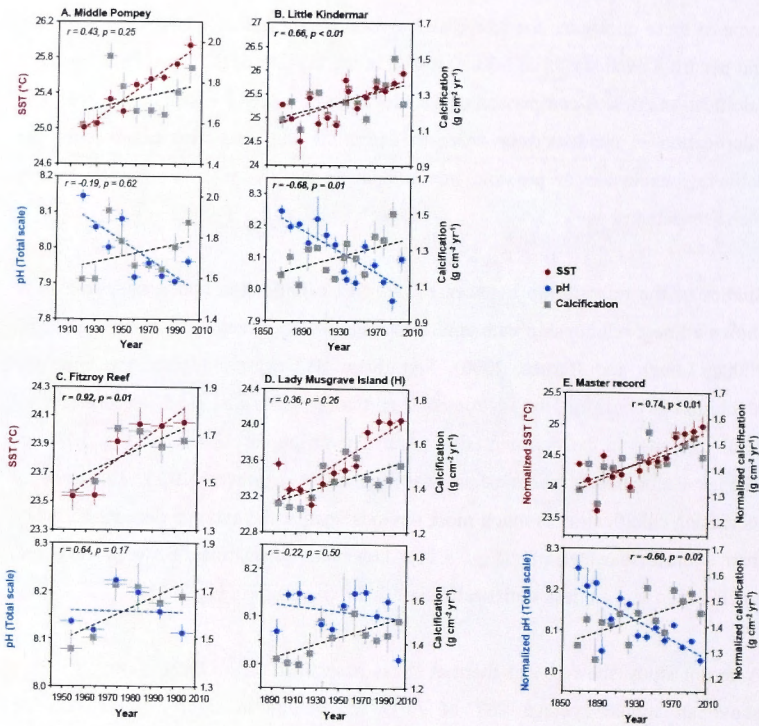


**Fig. 5.11** Comparison of decadal averages of calcification to decadal averages of SST and seawater pH for individual coral records (A to D) and for the southern GBR master record (E). Error bars for x-axes represent decadal ranges and y-axis error bars are  $\pm 1\sigma$ . Linear regressions for SST, pH, and calcification rate are shown in dotted red, blue, and black lines, respectively. Correlations between calcification and SST and between calcification and pH were analyzed and reported as the Pearson's correlation coefficient ( $r$ ) with  $p$ -values. Significant correlation ( $p < 0.05$ ) is indicated by bold characters.



The apparent temperature sensitivity of coral calcification rates ( $0.0542 \pm 0.0032 \text{ g cm}^{-3} \text{ yr}^{-1} \text{ }^{\circ}\text{C}^{-1}$ ,  $n = 86$ ) in the southern GBR is almost 7 times lower than previously observed for GBR corals as a whole ( $\sim 0.33 \text{ g cm}^{-3} \text{ yr}^{-1} \text{ }^{\circ}\text{C}^{-1}$ ,  $n = 49$ ; Lough, 2008a). It has been suggested that in the absence of thermal stress, that long-term or large-scale declines in coral calcification may occur with ocean acidification and decreasing aragonite saturation state (Cooper et al., 2012; De'ath et al., 2009). It follows that the suppression of the temperature sensitivity of coral calcification in the southern GBR may be due to the synchronous decrease in pH with rising temperature. The seawater pH records derived from coral  $\delta^{11}\text{B}$  compositions from the southern GBR master pH record show a  $0.21 \pm 0.10$  pH units decrease over the last 170 years which is equivalent to a decrease in aragonite saturation state of  $0.62 \pm 0.16$  (Fig. 5.10; see Chapter 4 for details about ocean acidification in the southern GBR).

The cumulative impact of these two competing influences (SST and seawater pH) on coral calcification can be gauged by comparison of the relative change per decade of these parameters and calcification rate. The average percent increases per decade in SST and calcification rate, and decreases in seawater pH derived by regression analysis of each coral core record are shown in Fig. 5.12. These results reveal a strong correlation between increasing coral calcification and increasing SST in the Little Kindermar, Fitzroy reef, and Lady Musgrave Island records with minimal if any obvious effect of decreasing pH. In contrast, this dominant effect of SST on calcification rate is not evident in the Middle Pompey coral, which has experienced a much higher rate of acidification than the other cores. The composite southern GBR record reflects the overall stronger response of calcification rate to temperature than ocean pH. This is consistent with evidence for a significant increase in calcification where SST warming is greatest at the same latitude in the southeast Indian Ocean (Cooper et al., 2012).

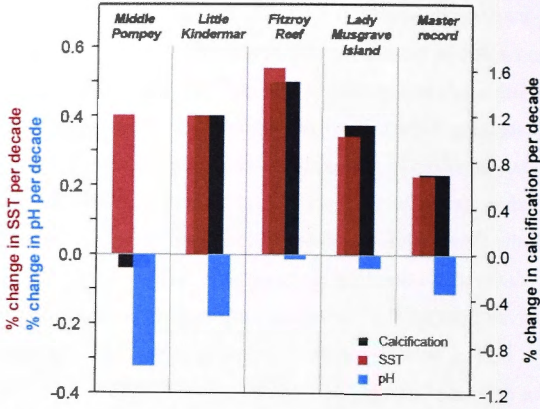
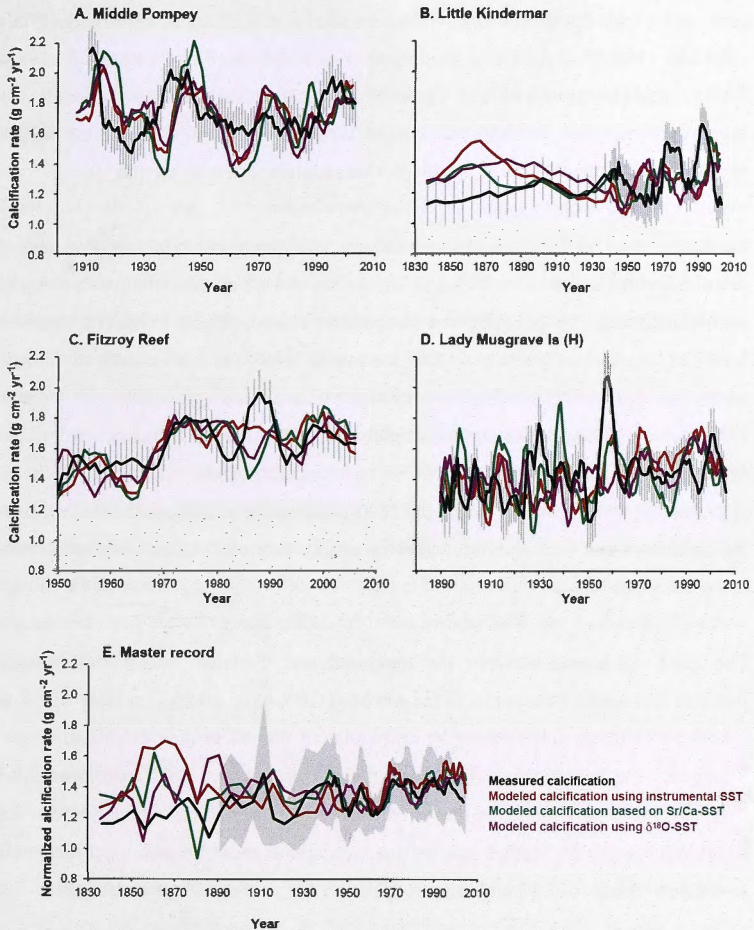


Fig. 5.12 Decadal percentage changes in SST, pH, and calcification rates for all the southern GBR core records.

To further assess the response of coral calcification in the southern GBR to ocean warming and acidification, we compared observed past calcification rates to three calcification reconstructions based on the IpHRAC coral calcification model which takes into account the kinetic effects of temperature and biological up-regulation of pH in the coral calcifying fluid (McCulloch et al., 2012). All parameters in this model are used following the methods by McCulloch et al. (2012), except the reaction order for the aragonite precipitation ( $n$ ) which have been empirically estimated. This was achieved by refitting  $n$  as a function of temperature to reproduce the measured calcification rates in the southern GBR cores. The resulting  $n$  values are between 2.1 to 2.2, and are consistent with the original range of the values ( $n = 1.8-2.4$ ) reported by Zhong and Mucci (1989).

The IpHRAC model results reproduce past calcification rates within an uncertainty level ( $\pm 1\sigma$  of the whole record in each cores) from individual southern GBR coral records and very similar results are obtained using the three different available temperature records (i.e. instrumental-, Sr/Ca-, and  $\delta^{18}\text{O}$ -derived SST; Figs 5.13A to D,  $p < 0.01$ ). However, the IpHRAC calcification model does not reproduce some





**Fig. 5.13** Comparison of calculated calcification rate using the IpHRAC coral calcification model (McCulloch et al., 2012) to measured annual coral calcification of the individual coral (A to D) and master coral records (E) from the southern GBR. All annual individual and master records are shown in 5-year running averages.  $\delta^{11}\text{B}$ -derived seawater  $\text{pH}_T$  record, calculated salinity and alkalinity (Lee et al., 2006), and satellite-, Sr/Ca-, and  $\delta^{18}\text{O}$ -derived SST were used for the modeling along with a higher order of reaction ( $n = 2.1\text{--}2.2$ ) than that used in the IpHRAC model (McCulloch et al., 2012). The calculation of aragonite saturation state at the site of calcification with elevated  $\text{pH}_T$ , DIC, and  $[\text{Ca}^{2+}]$  in calcifying fluid was conducted using the CO2SYS program (Pierrot et al., 2006). The uncertainty of the measured individual calcification records ( $\pm 1\sigma$ ) is shown as gray error bars in A to D, and a 95% confidence envelope for the composite measured calcification rate is presented by the gray area in E.

abnormally high calcification rate values measured in each coral record (e.g. 1969-1980 and 1990-1997 for Little Kindermar, 1985-1990 for Fitzroy Reef, and 1955-1960 for Lady Musgrave Island). These discrepancies occupy less than a decade and may be attributed to the high interannual variability in coral calcification due to regional environmental effects that are not taken into account by the model.

Similarly, the Iphrac model reproduces the southern GBR master record calcification rates within its 95 % confidence envelope, and very comparable results are obtained using the three different temperature records (Fig. 5.13E). The observed level of agreement between the measured and various calcification rate reconstructions is higher where the number of samples is greater ( $r = 0.74$ ,  $p < 0.0001$  since 1950), indicating the importance of multi-core composite record. In addition, no discrepancies occur between measured and calculated calcification rates of the master records during the period 1890-2008 unlike with the individual records. This indicates that local environmental variability may explain the observed offsets in the individual cores.

The good agreement between the measured and modeled calcification records suggests that most of the corals in the southern GBR have calcified at rates with low sensitivity to ocean acidification by up-regulating the pH in their calcification site. Moreover, the calcification increases due to increasing SST has more than compensated for any reduction due to concurrent seawater acidification. Some of the increase in coral calcification may be due to adaption or acclimation of these corals to the slow change of SST and seawater pH over the period of the reconstruction.

The contrasting and consistent decreases with time in both measured and modeled calcification rates from Middle Pompey suggest that a greater rates of ocean acidification may pose a threat to coral calcification rates despite their ability to regulate pH and the counteracting effect of increasing temperature. It is noteworthy that calcification rates measured in this study since 1988 show decreases that are comparable to the trends based on multiple coral observations from the GBR (Cooper et al., 2008; De'ath et al., 2009), Western Australia (Cooper et al., 2012),

and Florida Keys (Helmle et al., 2011). These common observations of declining calcification from the late twentieth century may imply a delayed response of corals to the synergistic impacts of increasing temperature and declining ocean pH, which may have reached a tipping point for calcification (De'ath et al., 2009).

This study shows that the relative contribution of rising temperature and ocean acidification accounts for changes in coral calcification. The general increasing trend of coral calcification from the southern GBR cores suggests ocean warming is the dominant controller of coral calcification due to the low sensitivity to pH in this region. However, the Middle Pompey coral records suggest that higher rates of increase in ocean acidity may counteract and overwhelm the enhanced calcification that is occurring due to ocean warming. Changes in ocean acidity will vary from region to region and some regions such as the Great Barrier Reef, the Coral Sea, and the Caribbean Sea, are attaining higher risk levels of seawater pH and aragonite saturation more rapidly than others (Hoegh-Guldberg et al., 2007). It follows that the regions which are more susceptible to ocean pH changes may deserve more attention to understanding the combined effects of rising temperature and ocean acidification on coral calcification.

## **5.5 Conclusion**

The results of this study show calcification rates in the southern GBR have increased during the last 170 years (~11.7 %) under the circumstances of ocean warming and acidification. A recent decrease in coral calcification since 1990 is also notable, which agrees with the earlier findings of Cooper et al. (2008) and De'ath et al. (2009) from the GBR. Comparison of calcification rates with synchronous SST and  $\delta^{11}\text{B}$ -derived seawater pH records reveals seawater temperature changes to be a primary controller of coral calcification rate, in agreement with previous studies of subtropical corals (Cooper et al., 2012). However, the apparent temperature sensitivity of coral calcification rates in the southern GBR is much lower than for the



GBR as a whole, indicating the possible suppression of the thermal sensitivity of calcification due to the decrease in seawater pH.

The cumulative impact of the two competing influences (SST and seawater pH) on coral calcification is estimated based on the percent decadal changes of each parameter and the IpHRAC coral calcification model (McCulloch et al., 2012). Our result shows that increasing in SST is a dominant limiting factor on coral calcification and that increasing anthropogenic CO<sub>2</sub> has resulted in a higher rate of calcification due to ocean warming despite concurrent ocean acidification during the last 170 years. However, the results from Middle Pompey show that enhanced rates of acidification accompanying ocean warming may result in reduced calcification rates. This indicates that more rapid increase in ocean acidity may counteract the effects of warming on coral calcification.

More rapid decrease in seawater pH may be expected in the future due to an exponential increase in atmospheric CO<sub>2</sub>. Given the predicted high level of ocean warming, the potential influence of a thermal upper limit for corals is also important. The synergistic effects of rising SST and ocean acidification on coral reefs clearly requires further investigation with an emphasis on the regions that are susceptible to seawater pH changes.







---

## Chapter 6.

### **Coral calcification response to increasing ocean temperature and acidity in the southern Great Barrier Reef**

---

Atmospheric carbon dioxide ( $\text{CO}_2$ ) concentrations have already increased by nearly 40% over preindustrial levels, resulting in global warming and ocean acidification due to increased dissolution of anthropogenic  $\text{CO}_2$  in surface waters (Caldeira and Wickett, 2005). The surface ocean is expected to become between 2 and 4°C warmer and between 0.2 and 0.4 pH units more acidic by 2100 AD (Caldeira and Wickett, 2005; IPCC, 2007b). These changes are affecting the rates at which calcifying organisms form their skeletons by altering thermal regulation of metabolic reactions and lowering carbonate ion concentration, and thereby calcium carbonate ( $\text{CaCO}_3$ ) saturation state of the ocean. Beyond short-term experiments that range from hours to months, little is known about more chronic effects of ocean pH on biogenic calcifiers and the impact of ocean warming.

In addition, such elevated  $\text{CO}_2$  response studies on marine biota in high-latitude areas are under-investigated although they have been identified as the regions potentially most sensitive to ocean acidification (Gattuso and Hansson, 2011). These subtropical organisms grow under lower (less optimum) temperatures and light levels, and more acidic seawater pH and therefore lower aragonite saturation state than tropical regions (Lough and Barnes, 2000; Orr et al., 2005). Thus, it remains to be established whether subtropical marine calcifiers will be more or less sensitive to the global environmental changes. Accordingly, a 170-year long record of changes in

ocean temperature and pH, and *Porites sp.* coral calcification has been reconstructed for the southernmost parts of the Great Barrier Reef (GBR), Australia, based on five coral cores from the Pompey complex (collected in March 2006), Lady Musgrave Island, and Fitzroy Reef (collected in October 2008; see Fig. 2.1 in Chapter 2). These reefs lie between 95 to 140 km from the coast, well beyond the effects of terrestrial runoff, and are near the southern limit of reef development (Lough and Barnes, 2000; Orr et al., 2005). The growth chronologies of the individual corals were determined from seasonal density banding and cross-checked against seasonal trace element ratio cycles determined by laser ablation inductively coupled plasma mass spectrometry analysis (Fallon et al., 1999; see Chapter 2 and 3 for the reconstruction of coral chronology). Annual calcification rates ( $\text{g cm}^{-2} \text{yr}^{-1}$ ) for each core were calculated from the measured annual extension rate ( $\text{cm yr}^{-1}$ ; linear distance between adjacent winter maxima of seasonal trace elements/Ca cycles) and skeletal bulk density ( $\text{g cm}^{-3}$ ; buoyant-weighting method; see Chapter 5 for detailed methods for calcification rates).

Strontium/Calcium ratios, stable isotope ( $\delta^{13}\text{C}$  and  $\delta^{18}\text{O}$ ), and boron isotope ( $\delta^{11}\text{B}$ ) compositions of annual growth increments were analyzed for each coral core, except the older part of the Little Kindermar core which was determined in 5-year increments from 1939 to 1834. The compositions of the individual coral cores were combined to produce composite records for each growth year and are presented as a 5-year spline fit in Fig. 6.1 with 95% confidence envelopes (see Chapter 2 for detailed information of methods and Chapter 3 for data manipulation). Only one coral core extends prior to 1890, but no significant change in this particular coral geochemical record is evident between 1834 and 1890.

The  $\delta^{13}\text{C}$  composition of the southern GBR corals has decreased at an average rate of  $-0.0068 \pm 0.0051\text{‰ yr}^{-1}$  ( $1\sigma$ ) from 1835 to 2008 (Fig. 6.1A; see Chapter 4 for individual coral  $\delta^{13}\text{C}$  records). This compares well to similar rates of  $\delta^{13}\text{C}$  decrease over the twentieth century reported for southern Pacific and Atlantic Ocean corals (Swart et al., 2010). These trends toward lighter  $\delta^{13}\text{C}$  compositions in both the Pacific and Atlantic Ocean basins can be ascribed to the depletion of the  $^{13}\text{C}$

composition of dissolved inorganic carbonate (DIC) in the ocean by uptake of anthropogenic CO<sub>2</sub> from the atmosphere that is enriched in <sup>12</sup>C (Druffell and Benavides, 1986; Swart et al., 2010). The coral records indicate acceleration in <sup>13</sup>C depletion since 1960, after which the average rate of  $\delta^{13}\text{C}$  change has been  $-0.0191 \pm 0.0066\text{‰ yr}^{-1}$  for the southern GBR. This change corresponds to the global mean <sup>13</sup>C-Suess effect (Gruber et al., 1999; Keeling et al., 2004) and the trend of changes in  $\delta^{13}\text{C}$  composition of atmospheric CO<sub>2</sub> in the Southern Hemisphere (Keeling et al., 2010).

The composite  $\delta^{11}\text{B}$  compositions of the southern GBR corals show significant variation ( $24.25 \pm 0.48\text{‰}$ ; Fig. 6.1B; see Chapter 4 for individual coral  $\delta^{11}\text{B}$  records) consistent with previously reported  $\delta^{11}\text{B}$  values of *Porites* corals from the central GBR (Wei et al., 2009) and Coral Sea (Pelejero et al., 2005). A recent study has shown that the  $\delta^{11}\text{B}$  composition of coral is modified from the  $\delta^{11}\text{B}$  values of borate ion in ambient seawater by the up-regulation of pH at the coral calcification site (Trotter et al., 2011). The  $\delta^{11}\text{B}$ -seawater pH proxy can be calibrated for this effect using the relationship between measured ambient seawater pH (pH<sub>T</sub>) and the pH at the site of calcification (pH<sub>cf</sub>) given by coral skeleton  $\delta^{11}\text{B}$  values. Accordingly, coral  $\delta^{11}\text{B}$  data from the southern GBR have been converted into seawater pH<sub>T</sub> estimates based on the relationship between pH<sub>T</sub> and pH<sub>cf</sub> reported for *Porites cylindrica* (Trotter et al., 2011; Fig. 4.1 in Chapter 4). The coral  $\delta^{11}\text{B}$  values indicate seawater pH<sub>T</sub> values of  $8.095 \pm 0.069$  consistent with an instrumental seawater pH<sub>T</sub> value of  $8.065 \pm 0.029$  (1 $\sigma$ ) at the mooring station near Heron Island in the southern GBR.

The composite seawater pH<sub>T</sub> record reconstructed from coral  $\delta^{11}\text{B}$  for the southern GBR decreases at an average rate of  $-0.00123 \pm 0.00058$  pH units yr<sup>-1</sup> for the period 1835-2008, which is equivalent to an overall decline of  $0.21 \pm 0.10$  pH units during the last 170 years (Fig. 6.1B; Chapter 4 for individual  $\delta^{11}\text{B}$ -derived seawater pH<sub>T</sub> records). This rate of acidification is about double the mean rate of  $-0.00063 \pm 0.00028$  pH unit yr<sup>-1</sup> computed based on surface ocean equilibrium with atmosphere pCO<sub>2</sub> records from the Siple Station ice core and Station ALOHA for the period 1839-2008 (Fig. 6.2; Chapter 4). It is also notably less than the rate measured at the



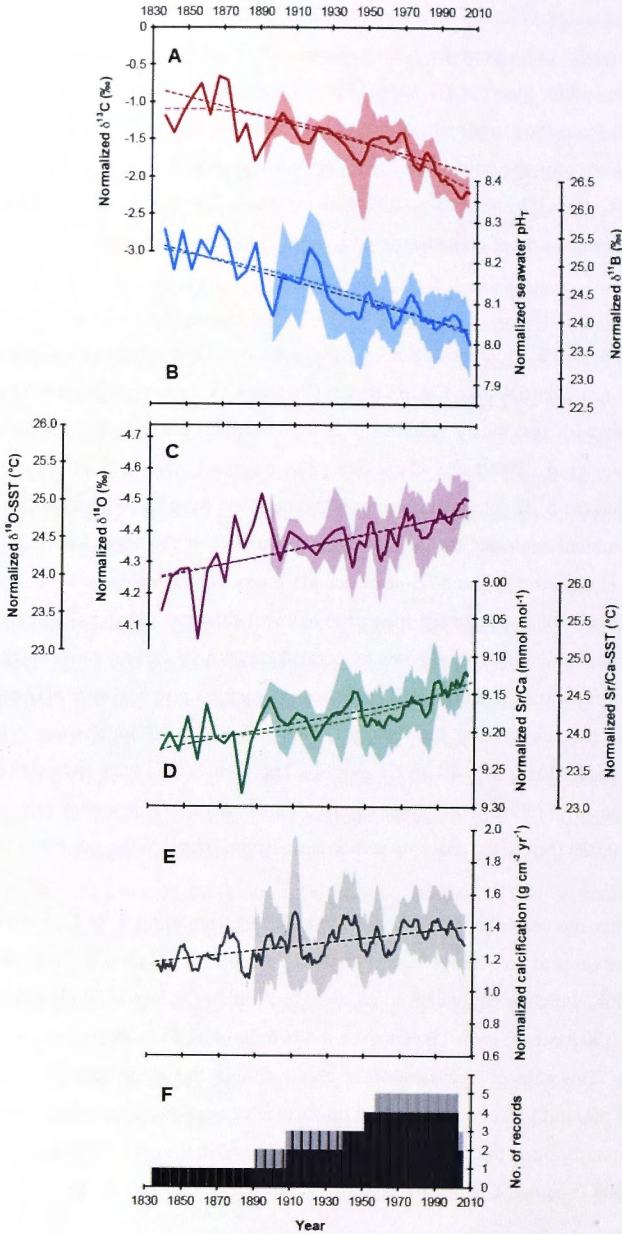




**Fig. 6.1** (*Opposite Page*) Composite coral geochemical and calcification records for the southern GBR. All records are plotted as 5-year splines. Individual annual resolution coral records were normalized to the period of 1950-2005 and then converted to continuous 5-year running average over the period of 1940-2008, whereas the normalized 5-year interval samples used the measured values which were composited with 5-year averages derived from the annual records for the period 1835-1939. The composite records for each geochemical proxy, (A)  $\delta^{13}\text{C}$ , (B)  $\delta^{11}\text{B}$ -derived  $\text{pH}_T$ , (C)  $\delta^{18}\text{O}$  with equivalent  $\delta^{18}\text{O}$ -derived temperature, (D) Sr/Ca with Sr/Ca-derived temperature, are based on four cores. The calcification rate composite (E) is constructed from five cores from the southern GBR. The color gradations indicate error bounds calculated using 95% confidence intervals. The number of records averaged at each time interval (annual or pentannual) is represented in (F). Weighted linear regressions of each composite record and non-linear trends for the ocean warming and acidification proxies are represented by dotted lines spanning the full observation period.

longest available instrumental time-series of  $-0.0019 \pm 0.0003$  pH unit  $\text{yr}^{-1}$  (Station ALOHA in the central North Pacific 1988-2007; Dore et al., 2009). This probably reflects acceleration in the rate of acidification over the instrumental observation periods due to an accelerating decrease of  $\text{pH}_T$  in association with an accelerating increase in atmospheric  $\text{CO}_2$  concentration.

The southern GBR coral  $\delta^{11}\text{B}$ -seawater  $\text{pH}_T$  records display interdecadal fluctuations that correlate negatively with the Interdecadal Pacific Oscillation (IPO) ocean atmosphere anomaly (correlation coefficient  $r = -0.67$ ,  $p < 0.001$ ,  $n = 120$ ). Similar interdecadal variation in coral  $\delta^{11}\text{B}$ -derived  $\text{pH}_T$  with the IPO has been documented previously in the GBR region (Pelejero et al., 2005; Wei et al., 2009). This relationship was attributed to the effect of wind stress and current strength on the flushing rate of reef waters. Slower flushing was linked to positive IPO index values and accelerated accumulation of  $\text{CO}_2$  in reef waters from community calcification and respiration, resulting in lower reef water  $\text{pH}_T$ . Given increasing coral calcification (Fig. 6.1E), this effect could explain the faster rate of decreases in ambient seawater  $\text{pH}_T$  in coral reefs in this region compared to the calculated  $\text{pH}_T$  from  $\text{pCO}_2$  records.

Coral  $\delta^{18}\text{O}$  and Sr/Ca proxies show decreasing trends (Figs 6.1C and D; see Chapter

3 for individual coral  $\delta^{18}\text{O}$  and Sr/Ca records) that reflect increasing SST over the last 170 years.  $\delta^{18}\text{O}$ -SST and Sr/Ca-SST were estimated with revised sensitivities ( $-0.23 \text{ ‰ } ^\circ\text{C}^{-1}$  and  $-0.084 \text{ mmol mol}^{-1} \text{ } ^\circ\text{C}^{-1}$  respectively; Gagan et al., 2012), taking into account the effect of bio-smoothing which attenuates coral  $\delta^{18}\text{O}$  and Sr/Ca records as they pass through the tissue layer (Gagan et al., 2012; see Chapter 2 and 3 for coral proxy-SST estimates and Chapter 2 for more information on the bio-smoothing effect). As coral  $\delta^{18}\text{O}$  compositions can also vary as a result of salinity changes, the residual  $\delta^{18}\text{O}$  signal record ( $\Delta\delta^{18}\text{O}$ ) determined by removing SST component of  $\delta^{18}\text{O}$  variation based on the Sr/Ca-SST record (Gagan et al., 1998; Chapter 3 for salinity estimate). The  $\Delta\delta^{18}\text{O}$  record shows no statistically significant change ( $0.00123 \pm 0.00054 \text{ ‰ yr}^{-1}$ ,  $p = 0.03$ ) and suggests negligible importance of salinity for reconstructed  $\delta^{18}\text{O}$ -SST estimates in the southern GBR. The rate of  $\Delta\delta^{18}\text{O}$  change is consistent with a reported low rate of increase in the study area relative to the global subtropics due to elevated precipitation offsetting enhanced evaporation from ocean warming in the southwest pacific (Durack and Wijffels, 2010).

The composite coral SST proxy records reveal the accumulated warming of the surface ocean in this region (Figs 6.1C and D; Chapter 3), correlating well with the instrumental record reconstructions of southern GBR warming over the period of 1890-2006 (NOAA ERSST version 3 from Smith and Reynolds, 2003;  $r = 0.62$ ,  $p < 0.001$ ,  $n = 114$  for  $\delta^{18}\text{O}$ -SST;  $r = 0.59$ ,  $p < 0.001$ ,  $n = 114$  for Sr/Ca-SST). The warming rates of the southern GBR from the composite  $\delta^{18}\text{O}$ -SST ( $0.0055 \pm 0.0052^\circ\text{C yr}^{-1}$ ), Sr/Ca-SST ( $0.0055 \pm 0.0055^\circ\text{C yr}^{-1}$ ), and instrumental SST of the southern GBR ( $0.0056 \pm 0.0064^\circ\text{C yr}^{-1}$ , 1875-2006) records are equivalent to approximately  $0.6^\circ\text{C}$  over the last century. The Sr/Ca-SST and instrumental SST records indicate that ocean warming is accelerated during the late twentieth century due to the exponential increase in the atmospheric  $\text{CO}_2$ . The accelerated warming rates ( $\sim 0.9 \pm 0.9^\circ\text{C/century}$  for  $\delta^{18}\text{O}$ -SST;  $\sim 1.5 \pm 0.6^\circ\text{C/century}$  for Sr/Ca-SST;  $\sim 1.2 \pm 0.7^\circ\text{C/century}$  for instrumental SST) since 1950 compares well with changes in SSTs of northern and central GBR regions and with global average SST ( $\sim 1.2 \text{ } ^\circ\text{C/century}$ ; Lough, 2008b). This indicates that the southern GBR has

experienced significant ocean warming due to anthropogenic CO<sub>2</sub> that is as rapid as warming in global and tropical regions.

*Porites* coral calcification has increased over the last 170 years at an average of  $0.0013 \pm 0.0016 \text{ g cm}^{-2} \text{ yr}^{-1}$  (Fig. 6.1E; see Chapter 5 for individual calcification records). This is consistent with reported increases since 1850 in coral calcification for the GBR based on an analysis of 328 colonies (De'ath et al., 2009) and an increase since 1900 in the subtropical corals of the North Atlantic (Helmle et al., 2011) and Indian Ocean (Cooper et al., 2012). These long-term trends in coral calcification are counter to changes that have taken place over much shorter recent periods such as a 21% decrease reported for a period from 1988 to 2002 (Cooper et al., 2008) and a 14.2% decline from 1990 to 2005 (De'ath et al., 2009) in the GBR. Moreover, long coral calcification records for the GBR (this study; De'ath et al., 2009) reveal past fluctuations of up to 30% over decadal time scales and indicate the potential for drawing misleading conclusions from short-term studies.

The apparent temperature sensitivity of coral calcification rates ( $0.0542 \pm 0.0032 \text{ g cm}^{-3} \text{ yr}^{-1} \text{ }^{\circ}\text{C}^{-1}$ ,  $n = 86$ ) in the southern GBR is almost 7 times slower than that previously observed across the whole GBR (Lough, 2008a). There were no years when average SSTs in the southern GBR exceeded the 30°C threshold in the GBR identified by (Carricart-Ganivet et al., 2012). Moreover, no bleaching or disease outbreaks have been observed in the southern GBR, hence it seems unlikely that this region has exceeded a thermal stress threshold for coral calcification. It has been suggested that in the absence of thermal stress, long-term or large-scale declines in coral calcification may occur with ocean acidification and decreasing aragonite saturation state (De'ath et al., 2009; Cooper et al., 2012). It follows that the suppression of the temperature sensitivity of coral calcification in the southern GBR may reflect a synchronous decrease in pH with rising temperature. Specifically, the seawater pH<sub>T</sub> records derived from the southern GBR coral δ<sup>11</sup>B compositions show a significant  $0.21 \pm 0.10$  pH units decrease over the last 170 years which is equivalent to a decrease in aragonite saturation state by  $0.62 \pm 0.16$  while  $0.95 \pm 0.95^{\circ}\text{C}$  warming occurred during the same period.

Two potential major competing influences on coral calcification (SST and pH) are consistent with the calcification model of McNeil et al. (2004) and McCulloch et al. (2012), which suggests the effect of ocean warming outweighs the impact of decreasing seawater pH, and that calcification rate has been increases with time. This is also consistent with evidence for a stronger calcification response to temperature than ocean pH changes in corals at the same latitude in the southeast Indian Ocean (Cooper et al., 2012).

A projection for future ocean acidification of coral reefs in the southwestern Pacific was generated by combining the southern GBR coral  $\delta^{11}\text{B-pH}_T$  records with those from two previous studies (Pelejero et al., 2005; Wei et al., 2009). The resulting master coral  $\delta^{11}\text{B-pH}_T$  record reveals an obvious decreasing trend that corresponds to anthropogenic  $\text{CO}_2$  increases in the atmosphere and a linear acidification rate of  $-0.00046 \pm 0.00092$  pH units  $\text{yr}^{-1}$  from the start of the industrial revolution to the present day. This record parallels and is offset by  $-0.05$  pH units from an estimate for the evolution of surface ocean  $\text{pH}_T$  based on atmospheric  $\text{pCO}_2$  data from Siple Station ice core and Mauna Loa (Fig. 7.2). The offset may reflect lower pH in coral reef ecosystems relative to open ocean sites due to enhancement of  $\text{pCO}_2$  in reef waters by coral calcification.

The future progress of ocean acidification in the southwest Pacific Ocean from 2000 to 2100 has been investigated under future  $\text{CO}_2$  scenarios (A2 for the high emission and B1 for the low emission scenarios; IPCC, 2007b). Under the A2 scenario surface ocean pH is projected to decrease by 0.28 pH units during the next century which is double the rate of pH changes over the last hundred years. Furthermore, future reef water pH is projected to undergo an even more significant decrease than the open surface ocean and reaching close to  $\text{pH}_T$  of 7.7 by the year 2100. This corresponds to more rapid changes in aragonite saturation state in the southern GBR compared to tropical regions (Hoegh-Guldberg et al., 2007), attaining a level of  $\sim 1.9$  at the end of this century.



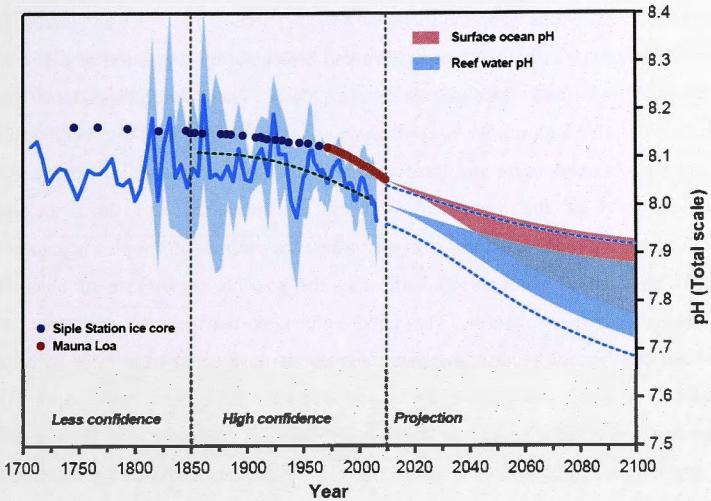


**Fig. 6.2** Comparison of past, present and future ocean acidification from a master  $\delta^{11}\text{B}$ -derived seawater  $\text{pH}_T$  for the southwest Pacific, calculated seawater  $\text{pH}_T$  based on  $\text{pCO}_2$  records from the Siple Station ice core (year 1744-1953) and Mauna Loa, Hawaii (year 1959-2008), and the IPCC marker scenarios (IPCC, 2007b; year 2000-2100; border lines represent A2 and B1 scenarios). Four southern GBR corals from this study, a central GBR coral from Arlington Reef (Wei et al., 2009), and a coral sea core from Flinders Reef (Pelejero et al., 2005) were compiled to produce the master  $\delta^{11}\text{B}$ -derived seawater  $\text{pH}_T$  record which is shown with a light blue line and 95% confidence envelope. Seawater  $\text{pH}_T$  calculation based on  $\text{pCO}_2$  data from the Siple Station and Mauna Loa was computed using CO2SYS (Pierrot et al., 2006) assuming a constant alkalinity of 2300  $\mu\text{mol}/\text{kg}$ , salinity of 35.3 PSU, and phosphate and silicate concentrations of 0.14 and 1  $\mu\text{mol}/\text{kg}$ . SST over the 21st century for surface ocean pH projection is calculated using the equation of a global warming response (McCulloch et al., 2012) whereas future SST for reef water pH projection is extracted from GFDL-CM 2.1 climate model centered 150.5°E, 21.0°S and 152.25°E, 23.5°S. The extracted future SST from the southern GBR is then adjusted to the reconstructed SST in this region over 1861-2000. Reef water pH then was projected by subtracting the offset ( $0.05 \pm 0.02$  pH units,  $1\sigma$ , 95% confidential interval shown as dotted light blue lines) between reconstructed surface ocean pH from atmospheric  $\text{pCO}_2$  and reef water pH from the southwest Pacific. The time scale for the period 2000 to 2100 is expanded.



To assess the possible future response of coral calcification in the southern GBR to ocean warming and acidification, we first compared observed past calcification rates to three reconstructions using the IpHRAC coral calcification model which takes into account the kinetic effects of temperature and biological up-regulation of pH in the coral calcifying fluid (McCulloch et al., 2012). The model reproduces past calcification rates within a 95 % confidence envelope (Fig. 6.3A), and very similar results are obtained using the three different available temperature records. The observed level of the agreement between the measured and three different calcification rate reconstructions is higher where the number of samples is greater ( $r = 0.74$ ,  $p < 0.0001$  since 1950), indicating the possible importance of obtaining multi-core composite records. The good agreement between the measured and modeled calcification records suggests these corals have calcified at rates with low sensitivity to ocean acidification by up-regulating the pH in their calcification site. Moreover, increased calcification due to increasing SST has more than compensated for any reduction due to concurrent seawater acidification. Some of the increase in coral calcification may be due to adaptation or acclimation of these corals in response to the slow variation of SST and seawater pH over the period of the reconstruction.

Future coral calcification in the southwest Pacific projected using the IpHRAC model based on modeled regional reef water  $\text{pH}_T$  and SST extracted from GFDL-CM 2.1 climate model (Data is available from Program for climate model diagnosis and intercomparison, PCMDI, <https://esg.llnl.gov:8443/index.jsp>). This regional calcification projection is compared to a global calcification model that has been estimated following the methods in McCulloch et al. (2012). All parameters used for the global calcification model are the same as in McCulloch et al. (2012) except for application of a higher empirical reaction order ( $n = \sim 2.1$ ) and use of the *Porites cylindrica* calibration (Trotter et al., 2011) for the physiological pH up-regulation.

Although the IpHRAC model enables future coral calcification rates to be quantified, it is based on the kinetics of inorganic calcification, albeit taking into account the enhanced pH up-regulation. It also does not include thermal stress as it assumes the adaptive potential of coral and their symbionts to elevating temperature (McCulloch

et al., 2012). Moreover, the additional impact of natural seawater pH variability (up to  $\sim 0.3$  pH units and  $\sim 0.24$  of aragonite saturation state) on future calcification rates is difficult to forecast with this model. As a result, the projections of this study which show only small changes in the future calcification compared to the past calcification variation are likely a best-case scenario. The results of the four future calcification projections are shown in Fig. 6.3B.

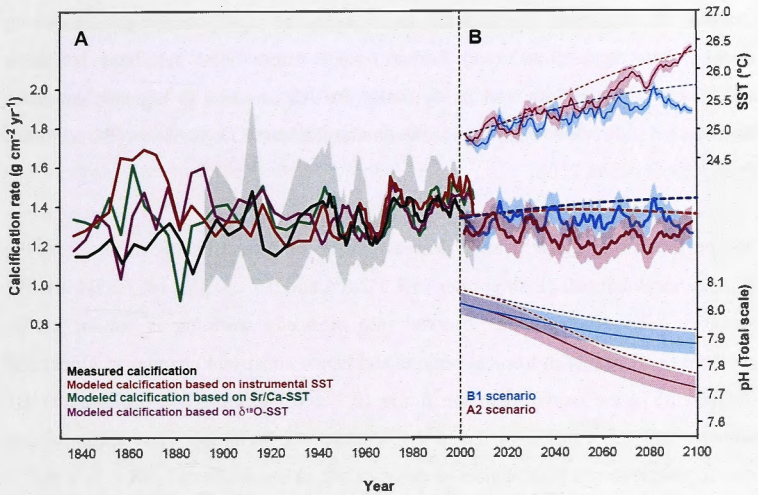


**Fig. 6.3** (A) Comparison of calculated calcification rate using the IpHRAC coral calcification model (McCulloch et al., 2012) to measured annual coral calcification master record from the southern GBR. Master  $\delta^{11}\text{B}$ -derived seawater  $\text{pH}_T$  record, calculated master salinity and alkalinity, and three SSTs master records (e.g. instrumental, Sr/Ca-derived, and  $\delta^{18}\text{O}$ -derived SSTs) were used for the modeling with higher order of reaction ( $n \sim 2.1$ ) than that used in the IpHRAC model (McCulloch et al., 2012). The calculation of aragonite saturation state at the site of calcification with elevated  $\text{pH}_T$ , DIC, and  $[\text{Ca}^{2+}]$  in calcifying fluid was conducted using CO2SYS program (Pierrot et al., 2006). 95% confidence envelope for the measured calcification rate is represented in gray area as shown in Fig. 1E. (B) Future coral calcification in the southwest Pacific projected using the IpHRAC model based on modeled reef water pH and SST extracted from GFDL-CM 2.1 climate model. This regional calcification projection is compared to global calcification model which is estimated by following the methods in (McCulloch et al., 2012) and shown as bold dotted lines.  $\sim 2.1$  of the empirical reaction order and pH up-regulation calibration of *Porites cylindrica* (Trotter et al., 2011) are applied to this model as used in the southwest Pacific projection. Future changes in SST and surface ocean and reef water  $\text{pH}_T$  are also represented; dotted lines are global changes and solid lines are the variations in the southwest Pacific reefs. The shaded areas represent 95% confidential envelopes.

Modeling suggests that an approximately constant or a slight decrease in coral calcification may occur by the end of this century in southwest Pacific reefs (Fig. 6.3B;  $-1.9 \pm 0.8\%$ ,  $1\sigma$ ,  $p = 0.62$  for B1 and  $-4.4 \pm 1.6\%$ ,  $p = 0.07$ , for A2 scenarios). This suggests that calcification, which has been increasing due to the effect of ocean warming that has overwhelmed concurrent seawater acidification to date, may decrease with the combination of declining seawater pH and frequent exposure to thermal stress, in particular, in summer (average seawater  $\text{pH}_T = 7.961 \pm 0.078$  and  $\text{SST} = 27.32 \pm 1.23^\circ\text{C}$ ,  $1\sigma$ , from southern GBR coral seasonal records, 2001-2008; Chapter 2). Moreover, the lack of the capacity to rapidly adapt to changes in environmental conditions could further reduce future coral calcification. These effects are more obvious and likely under the A2 scenario as higher changes in temperature and reef water pH occur than under the least  $\text{CO}_2$  variation (B1 scenario) from present day to 2100.

The projected future calcification decrease in the southwest Pacific differs from the increase in global calcification rates ( $6.7 \pm 2.6\%$  and  $0.7 \pm 0.3\%$ ,  $1\sigma$ , for B1 and A2 scenarios respectively). The observed rate of ocean warming is similar in the southern GBR to that in tropical regions and hence consistent changes in global and regional SSTs are expected in the future ( $0.9 \pm 0.3^\circ\text{C}$  vs.  $0.7 \pm 0.2^\circ\text{C}$  under B1 scenario and  $1.5 \pm 0.5^\circ\text{C}$  vs.  $1.5 \pm 0.4^\circ\text{C}$  under A2 scenario). Thus a comparable kinetic temperature effect applies to calcification in the southern GBR corals and to global calcification rates. The opposing results and offset in calcification values ( $\sim -0.1 \pm 0.1 \text{ g cm}^{-3} \text{ yr}^{-1}$ ) between the IpHRAC models for the global surface ocean and the southwest Pacific coral reefs can be attributed to the lower reef water  $\text{pH}_T$  (by  $\sim 0.05$  pH units) which arises from the increase in reef water  $\text{pCO}_2$  due to the effect of calcification, and leads to lower aragonite saturation state than surface ocean pH values predicted by the IPCC (2007b).

Thus far, the scarcity of coeval long-term seawater pH and calcification rate data for coral reefs has impeded rigorous assessment of relationships between changes in coral growth and ocean chemistry (Lough and Cooper, 2011). This study presents the first integrated long-term coral records of sea surface temperature and pH along with



calcification rates. The results confirm that significant ocean warming and acidification have occurred in the southern GBR due to uptake of anthropogenic CO<sub>2</sub> into the surface ocean. Calcification rates in the southern GBR have increased over the last 170 years as the positive effect of increasing SST has more than compensated for the negative influence of ocean acidification on reef water saturation state. This result indicates that despite rapid increases in SST and ocean acidification in the southern GBR, coral growth has persisted at history rates because such environmental variables are yet to cross thresholds for coral calcification. However, modeling demonstrates that intensified ocean acidification may prove a threat to coral and coral reef calcification in the near future. Given the high rate of ocean warming, temperature poses a significant potential threat to coral calcification. When future ocean acidification is combined with the thermal stress, the calcification rate will be even lower than the models presented here.





---

## References

---

- Adkins, J.F., Boyle, E.A., Curry, W.B., Lutringer, A., 2003. Stable isotopes in deep-sea corals and a new mechanism for "vital effects". *Geochimica et Cosmochimica Acta* 67, 1129-1143.
- Al-Horani, F.A., Al-Moghrabi, S.M., De Beer, D., 2003. Microsensor study of photosynthesis and calcification in the scleractinian coral, *Galaxea fascicularis*: Active internal carbon cycle. *Journal of Experimental Marine Biology and Ecology* 288, 1-15.
- Alibert, C., McCulloch, M.T., 1997. Strontium/calcium ratios in modern *Porites* corals from the Great Barrier Reef as a proxy for sea surface temperature: Calibration of the thermometer and monitoring of ENSO. *Paleoceanography* 12, 345-363.
- Allison, N., Finch, A.A., EIMF, 2010.  $\delta^{11}\text{B}$ , Sr, Mg and B in a modern *Porites* coral: the relationship between calcification site pH and skeletal chemistry. *Geochimica et Cosmochimica Acta* 74, 1790-1800.
- Anthony, K.R.N., A. Kleypas, J., Gattuso, J.P., 2011. Coral reefs modify their seawater carbon chemistry - implications for impacts of ocean acidification. *Global Change Biology* 17, 3655-3666.
- Australian Bureau of Meteorology and CSIRO, 2011. *Climate Change in the Pacific: Scientific Assessment and New Research. Volume 1: Regional Overview.*
- Ayling, B.F., McCulloch, M.T., Gagan, M.K., Stirling, C.H., Andersen, M.B., Blake, S.G., 2006. Sr/Ca and  $\delta^{18}\text{O}$  seasonality in a *Porites* coral from the MIS 9 (339-303 ka) interglacial. *Earth and Planetary Science Letters* 248, 447-460.
- Baker, A.C., Starger, C.J., McClanahan, T.R., Glynn, P.W., 2004. Corals' adaptive response to climate change: Shifting to new algal symbionts may safeguard devastated reefs from extinction. *Nature* 430, 741.

- Barker, S., Ridgwell, A., 2012. Ocean Acidification. Nature Education Knowledge 3, 21.
- Barnes, D.J., Devereux, M.J., 1988. Variations in skeletal architecture associated with density banding in the hard coral *Porites*. Journal of Experimental Marine Biology and Ecology 121, 37-54.
- Barnes, D.J., Taylor, R.B., Lough, J.M., 1995. On the inclusion of trace materials into massive coral skeletons. Part II: Distortions in skeletal records of annual climate cycles due to growth processes. Journal of Experimental Marine Biology and Ecology 194, 251-275.
- Bates, N.R., 2009. Bermuda Institute of Ocean Sciences (BIOS; <http://www.bios.edu>).
- Bates, N.R., Amat, A., Andersson, A.J., 2010. Feedbacks and responses of coral calcification on the Bermuda reef system to seasonal changes in biological processes and ocean acidification. Biogeosciences 7, 2509-2530.
- Bessat, F., Buigues, D., 2001. Two centuries of variation in coral growth in a massive *Porites* colony from Moorea (French Polynesia): A response of ocean-atmosphere variability from south central Pacific. Palaeogeography, Palaeoclimatology, Palaeoecology 175, 381-392.
- Blamart, D., Rollion-Bard, C., Meibom, A., Cuif, J.P., Juillet-Leclerc, A., Dauphin, Y., 2007. Correlation of boron isotopic composition with ultrastructure in the deep-sea coral *Lophelia pertusa*: Implications for biomineralization and paleo-pH. Geochemistry, Geophysics, Geosystems 8.
- Böhm, F., Haase-Schramm, A., Eisenhauer, A., Dullo, W.C., Joachimski, M.M., Lehnert, H., Reitner, J., 2002. Evidence for preindustrial variations in the marine surface water carbonate system from coralline sponges. Geochem. Geophys. Geosyst. 3, 1019.
- Borowitzka, M.A., 1981. Algae and grazing in coral reef ecosystems. Endeavour 5, 99-106.
- Bosscher, H., 1993. Computerized tomography and skeletal density of coral skeletons. Coral Reefs 12, 97-103.
- Boucher, G., Clavier, J., Hily, C., Gattuso, J.P., 1998. Contribution of soft-bottoms to the community metabolism (primary production and calcification) of a barrier reef flat (Moorea, French Polynesia). Journal of Experimental Marine Biology and Ecology 225, 269-283.
- Broecker, W.S., Peng, T.H., 1974. Gas exchange rates between air and sea. Tellus 26, 21-35.
- Bucher, D.J., Harriott, V.J., Roberts, L.G., 1998. Skeletal micro-density, porosity and bulk density of acroporid corals. Journal of Experimental Marine Biology and Ecology 228, 117-136.

- Buddemeier, R.W., Maragos, J.E., Knutson, D.W., 1974. Radiographic studies of reef coral exoskeletons: Rates and patterns of coral growth. *Journal of Experimental Marine Biology and Ecology* 14, 179-199.
- Burrage, D.M., Steinberg, C.R., Skirving, W.J., Kleypas, J.A., 1996. Mesoscale circulation features of the Great Barrier Reef region inferred from NOAA satellite imagery. *Remote Sensing of Environment* 56, 21-41.
- Caldeira, K., Wickett, M., 2005. Ocean model predictions of chemistry changes from carbon dioxide emissions to the atmosphere and ocean. *Journal of Geophysical Research C: Oceans* 110, 1-12.
- Calvo, E., Marshall, J.F., Pelejero, C., McCulloch, M.T., Gagan, M.K., Lough, J.M., 2007. Interdecadal climate variability in the Coral Sea since 1708 A.D. *Palaeogeography, Palaeoclimatology, Palaeoecology* 248, 190-201.
- Carricart-Ganivet, J.P., Cabanillas-Terán, N., Cruz-Ortega, I., Blanchon, P., 2012. Sensitivity of calcification to thermal stress varies among genera of massive reef-building corals. *PLoS ONE* 7, e32859.
- Castillo, K.D., Lima, F.P., 2010. Comparison of in situ and satellite-derived (MODIS-Aqua/Terra) methods for assessing temperatures on coral reefs. *Limnology and Oceanography: Methods* 8, 107-117.
- Catanzaro, E.J., Champion, G.E., Garner, E.L., Marinenko, G., Sappenfield, K.M., Shields, W.R., 1970. Boric Assay; Isotopic, and Assay Standard Reference Materials. National Bureau of Standards. Special Publication.
- Cayan, D.R., 1992. Latent and sensible heat flux anomalies over the northern oceans: driving the sea surface temperature. *Journal of Physical Oceanography* 22, 859-881.
- Chalker, B., Barnes, D., Isdale, P., 1985. Calibration of x-ray densitometry for the measurement of coral skeletal density. *Coral Reefs* 4, 95-100.
- Chalker, B.E., Barnes, D.J., 1990. Gamma densitometry for the measurement of skeletal density. *Coral Reefs* 9, 11-23.
- Cohen, A.L., and T.A. McConnaughey 2003. Geochemical perspectives on coral mineralization, in: P.M. Dove, S.W., and J.J. deYoreo (Ed.), *Biom mineralization*. The Mineralogical Society of America Washington, DC., pp. 151-187.
- Cohen, A.L., Gaetani, G.A., Lundälv, T., Corliss, B.H., George, R.Y., 2006. Compositional variability in a cold-water scleractinian, *Lophelia pertusa*: New insights into "vital effects". *Geochemistry, Geophysics, Geosystems* 7.
- Cohen, A.L., Holcomb, M., 2009. Why corals care about ocean acidification : uncovering the mechanism. *Oceanography* 22, 118-127.

- Cohen, A.L., Layne, G.D., Hart, S.R., Lobel, P.S., 2001. Kinetic control of skeletal Sr/Ca in a symbiotic coral: Implications for the paleotemperature proxy. *Paleoceanography* 16, 20-26.
- Cohen, A.L., McConnaughey, T.A., 2003. Geochemical perspectives on coral mineralization, in *Biom mineralization*: P.M. Dove, S.W., and J.J. de Yoreo (Ed.). The Mineralogical Society of America Washington, DC., pp. 151-187.
- Cohen, A.L., Owens, K.E., Layne, G.D., Shimizu, N., 2002. The effect of algal symbionts on the accuracy of Sr/Ca paleotemperatures from coral. *Science* 296, 331-333.
- Coles, S.L., Jokiel, P.L., 1978. Synergistic effects of temperature, salinity and light on the hermatypic coral *Montipora verrucosa*. *Marine Biology* 49, 187-195.
- Collins, M., An, S.-I., Cai, W., Ganachaud, A., Guilyardi, E., Jin, F.-F., Jochum, M., Lengaigne, M., Power, S., Timmermann, A., Vecchi, G., Wittenberg, A., 2010. The impact of global warming on the tropical Pacific Ocean and El Niño. *Nature Geoscience* 3, 391-397.
- Cooper, T.F., De'ath, G., Fabricius, K.E., Lough, J.M., 2008. Declining coral calcification in massive *Porites* in two nearshore regions of the northern Great Barrier Reef. *Global Change Biology* 14, 529-538.
- Cooper, T.F., O'Leary, R.A., Lough, J.M., 2012. Growth of Western Australian Corals in the Anthropocene. *Science* 335, 593-596.
- Corrège, T., 2006. Sea surface temperature and salinity reconstruction from coral geochemical tracers. *Palaeogeography, Palaeoclimatology, Palaeoecology* 232, 408-428.
- D'Arrigo, R., Villalba, R., Wiles, G., 2001. Tree-ring estimates of Pacific decadal climate variability. *Climate Dynamics* 18, 219-224.
- de Villiers, S., Shen, G.T., Nelson, B.K., 1994. The Sr/Ca-temperature relationship in coralline aragonite: Influence of variability in  $(\text{Sr}/\text{Ca})_{\text{seawater}}$  and skeletal growth parameters. *Geochimica et Cosmochimica Acta* 58, 197-208.
- De'ath, G., Lough, J.M., Fabricius, K.E., 2009. Declining coral calcification on the Great Barrier Reef. *Science* 323, 116-119.
- Dickson, A.G., 1990. Thermodynamics of the dissociation of boric acid in synthetic seawater from 273.15 to 318.15K. *Deep Sea Research* 37, 755-766.
- Dodge, R.E., Thomson, J., 1974. The natural radiochemical and growth records in contemporary hermatypic corals from the Atlantic and Caribbean. *Earth and Planetary Science Letters* 23, 313-322.
- DOE, 1994. *Handbook of Methods for the Analysis of the Various Parameters of the Carbon Dioxide System in Seawater*.



- Doney, S.C., Fabry, V.J., Feely, R.A., Kleypas, J.A., 2009. Ocean Acidification: The Other CO<sub>2</sub> Problem. *Annual Review of Marine Science* 1, 196-192.
- Doney, S.C., Schimel, D.S., 2007. Carbon and climate system coupling on timescales from the Precambrian to the anthropocene. *Annual Review of Environment and Resources* 32, 31-66.
- Dore, J.E., Lukas, R., Sadler, D.W., Church, M.J., Karl, D.M., 2009. Physical and biogeochemical modulation of ocean acidification in the central North Pacific. *Proceedings of the National Academy of Sciences of the United States of America* 106, 12235-12240.
- Dr. Pieter Tans, NOAA/ESRL ([www.esrl.noaa.gov/gmd/ccgg/trends/](http://www.esrl.noaa.gov/gmd/ccgg/trends/)) and Dr. Ralph Keeling, Scripps Institution of Oceanography ([scrippsco2.ucsd.edu/](http://scrippsco2.ucsd.edu/))
- Druffel, E.R.M., Benavides, L.M., 1986. Input of excess CO<sub>2</sub> to the surface ocean based on <sup>13</sup>C/<sup>12</sup>C ratios in a banded Jamaican sclerosponge. *Nature* 321, 58-61.
- Druffel, E.R.M., Griffin, S., 1993. Large variations of surface ocean radiocarbon: evidence of circulation changes in the southwestern Pacific. *Journal of Geophysical Research* 98, 20,249-220,259.
- Druffel, E.R.M., Griffin, S., 1999. Variability of surface ocean radiocarbon and stable isotopes in the southwestern Pacific. *Journal of Geophysical Research C: Oceans* 104, 23607-23613.
- CSIRO, Australian Bureau of Meteorology. 2007. *Climate change in Australia: technical report 2007*. CSIRO. 148 pp.
- Durack, P.J., Wijffels, S.E., 2010. Fifty-Year trends in global ocean salinities and their relationship to broad-scale warming. *Journal of Climate* 23, 4342-4362.
- Dustan, P., 1975. Growth and form in the reef-building coral *Montastrea annularis*. *Marine Biology* 33, 101-107.
- Edinger, E.N., Limmon, G.V., Jompa, J., Widjatmoko, W., Heikoop, J.M., Risk, M.J., 2000. Normal coral growth rates on dying reefs: Are coral growth rates good indicators of reef health? *Marine Pollution Bulletin* 40, 404-425.
- Fallon, S.J., Guilderson, T.P., Caldeira, K., 2003a. Carbon isotope constraints on vertical mixing and air-sea CO<sub>2</sub> exchange. *Geophysical Research Letters* 30, OCE 9-1 - OCE 9-4.
- Fallon, S.J., McCulloch, M.T., Alibert, C., 2003b. Examining water temperature proxies in *Porites* corals from the Great Barrier Reef: A cross-shelf comparison. *Coral Reefs* 22, 389-404.
- Fallon, S.J., McCulloch, M.T., Van Woesik, R., Sinclair, D.J., 1999. Corals at their latitudinal limits: Laser ablation trace element systematics in *Porites* from Shirigai Bay, Japan. *Earth and Planetary Science Letters* 172, 221-238.



- Farkaš, J., Böhm, F., Wallmann, K., Blenkinsop, J., Eisenhauer, A., van Geldern, R., Munneke, A., Voigt, S., Veizer, J., 2007. Calcium isotope record of Phanerozoic oceans: Implications for chemical evolution of seawater and its causative mechanisms. *Geochimica et Cosmochimica Acta* 71, 5117-5134.
- Feely, R.A., Doney, S.C., Cooley, S.R., 2009. Ocean acidification: Present conditions and future changes in a high-CO<sub>2</sub> world. *Oceanography* 22, 36-47.
- Folland, C.K., Renwick, J.A., Salinger, M.J., Mullan, A.B., 2002. Relative influences of the Interdecadal Pacific Oscillation and ENSO on the South Pacific Convergence Zone. *Geophysical Research Letters* 29.
- Foster, G.L., 2008. Seawater pH, pCO<sub>2</sub> and [CO<sub>2</sub><sup>-3</sup>] variations in the Caribbean Sea over the last 130-kyr: A boron isotope and B/Ca study of planktic foraminifera. *Earth and Planetary Science Letters* 271, 254-266.
- Francey, R.J., Allison, C.E., Etheridge, D.M., Trudinger, C.M., Enting, I.G., Leuenberger, M., Langenfelds, R.L., Michel, E., Steele, L.P., 1999. A 1000-year high precision record of δ<sup>13</sup>C in atmospheric CO<sub>2</sub>. *Tellus, Series B: Chemical and Physical Meteorology* 51, 170-193.
- Gaetani, G.A., Cohen, A.L., 2006. Element partitioning during precipitation of aragonite from seawater: A framework for understanding paleoproxies. *Geochimica et Cosmochimica Acta* 70, 4617-4634.
- Gagan, M.K., Ayliffe, L.K., Beck, J.W., Cole, J.E., Druffel, E.R.M., Dunbar, R.B., Schrag, D.P., 2000. New views of tropical paleoclimates from corals. *Quaternary Science Reviews* 19, 45-64.
- Gagan, M.K., Ayliffe, L.K., Hopley, D., Cali, J.A., Mortimer, G.E., Chappell, J., McCulloch, M.T., Head, M.J., 1998. Temperature and surface-ocean water balance of the mid-Holocene tropical western Pacific. *Science* 279, 1014-1017.
- Gagan, M.K., Chivas, A.R., Isdale, P.J., 1994. High-resolution isotopic records from corals using ocean temperature and mass-spawning chronometers. *Earth and Planetary Science Letters* 121, 549-558.
- Gagan, M.K., Dunbar, G.B., Suzuki, A., 2012. The effect of skeletal mass accumulation in *Porites* on coral Sr/Ca and δ<sup>18</sup>O paleothermometry. *Paleoceanography* 27, PA1203.
- Garcia, H.E., R. A. Locamini, T. P. Boyer, J. I. Antonov, M. M. Zweng, O. K. Baranova, Johnson, D.R., 2010. *World Ocean Atlas 2009, Volume 4: Nutrients (phosphate, nitrate, and silicate)*. S. Levitus, Ed., NOAA Atlas NESDIS 71, U.S. Government Printing Office, Washington, D.C.
- Gattuso, J.-P., Allemand, D., Frankignoulle, M., 1999. Photosynthesis and calcification at cellular, organismal and community levels in coral reefs: A review on interactions and control by carbonate chemistry. *American Zoologist* 39, 160-183.

- Gattuso, J.-P., Frankignoulle, M., Bourge, I., Romaine, S., Buddemeier, R.W., 1998. Effect of calcium carbonate saturation of seawater on coral calcification. *Global and Planetary Change* 18, 37-46.
- Gattuso, J.-P., Hansson, L., 2011. *Ocean acidification*. Oxford University Press.
- Gledhill, D.K., Wanninkhof, R., Eakin, C.M., 2009. Observing ocean acidification from space. *Oceanography* 22, 48-59.
- Global Coral Reef Monitoring Network (GCRMN), 2000. *Global Coral Monitoring Network: Status of Coral Reef of the World in 2000*, edited by C. R. Wilkinson, Aust. Inst. of Mar. Sci., Townsville, Queensland.
- Glynn, P.W., 1991. Coral reef bleaching in the 1980s and possible connections with global warming. *Trends in Ecology and Evolution* 6, 175-179.
- Graus, R.R., Macintyre, I.G., 1982. Variation in growth forms of the reef coral *Montastrea annularis* (Ellis and Solander): a quantitative evaluation of growth response to light distribution using computer simulation. The Atlantic barrier reef ecosystem at Carrie Bow Cay, Belize, I: structure and communities, 441-464.
- Grottoli, A.G., Wellington, G.M., 1999. Effect of light and zooplankton on skeletal  $\delta^{13}\text{C}$  values in the eastern Pacific corals *Pavona clavus* and *Pavona gigantea*. *Coral Reefs* 18, 29-41.
- Gruber, N., Keeling, C.D., Bacastow, R.B., Guenther, P.R., Lueker, T.J., Wahlen, M., Meijer, H.A.J., Mook, W.G., Stocker, T.F., 1999. Spatiotemporal patterns of carbon-13 in the global surface oceans and the oceanic Suess effect. *Global Biogeochemical Cycles* 13, 307-335.
- Helmle, K.P., Dodge, R.E., Swart, P.K., Gledhill, D.K., Eakin, C.M., 2011. Growth rates of Florida corals from 1937 to 1996 and their response to climate change. *Nature Communication* 2, 215.
- Hemming, N.G., Guilderson, T.P., Fairbanks, R.G., 1998. Seasonal variations in the boron isotopic composition of coral: A productivity signal? *Global Biogeochemical Cycles* 12, 581-586.
- Hemming, N.G., Hanson, G.N., 1992. Boron isotopic composition and concentration in modern marine carbonates. *Geochimica et Cosmochimica Acta* 56, 537-543.
- Hendy, E.J., 2003. *Coral reconstructions of decadal-to-centennial climate variability in the Great Barrier Reef since 1565 AD*. Australian National University, 2003.
- Hendy, E.J., Gagan, M.K., Alibert, C.A., McCulloch, M.T., Lough, J.M., Isdale, P.J., 2002. Abrupt decrease in tropical pacific sea surface salinity at end of little ice age. *Science* 295, 1511-1514.

- Hoegh-Guldberg, O., 1999. Climate change, coral bleaching and the future of the world's coral reefs. *Marine and Freshwater Research* 50, 839-866.
- Hoegh-Guldberg, O., 2005. Low coral cover in a high-CO<sub>2</sub> world. *Journal of Geophysical Research C: Oceans* 110, 1-11.
- Hoegh-Guldberg, O., 2006. Complexities of coral reef recovery. *Science* 311, 42-43.
- Hoegh-Guldberg, O., Mumby, P.J., Hooten, A.J., Steneck, R.S., Greenfield, P., Gomez, E., Harvell, C.D., Sale, P.F., Edwards, A.J., Caldeira, K., Knowlton, N., Eakin, C.M., Iglesias-Prieto, R., Muthiga, N., Bradbury, R.H., Dubi, A., Hatzioiols, M.E., 2007. Coral reefs under rapid climate change and ocean acidification. *Science* 318, 1737-1742.
- Hoegh-Guldberg, O., Smith, G.J., 1989. The effect of sudden changes in temperature, light and salinity on the population density and export of zooxanthellae from the reef corals *Stylophora pistillata* Esper and *Seriatopora hystrix* Dana. *Journal of Experimental Marine Biology and Ecology* 129, 279-303.
- Hoerling, M.P., Hurrell, J.W., Xu, T., Bates, G.T., Phillips, A.S., 2004. Twentieth century North Atlantic climate change. Part II: Understanding the effect of Indian Ocean warming. *Climate Dynamics* 23, 391-405.
- Holbrook, N.J., Goodwin, I.D., McGregor, S., Molina, E., Power, S.B., 2011. ENSO to multi-decadal time scale changes in East Australian Current transports and Fort Denison sea level: Oceanic Rossby waves as the connecting mechanism. *Deep-Sea Research Part II: Topical Studies in Oceanography* 58, 547-558.
- Hönisch, B., Hemming, N.G., Archer, D., Siddall, M., McManus, J.F., 2009. Atmospheric carbon dioxide concentration across the mid-pleistocene transition. *Science* 324, 1551-1554.
- Hönisch, B., Hemming, N.G., Grottoli, A.G., Amat, A., Hanson, G.N., Bijma, J., 2004. Assessing scleractinian corals as recorders for paleo-pH: Empirical calibration and vital effects. *Geochimica et Cosmochimica Acta* 68, 3675-3685.
- Hönisch, B., Hemming, N.G., Loose, B., 2007. Comment on "A critical evaluation of the boron isotope-pH proxy: The accuracy of ancient ocean pH estimates" by M. Pagani, D. Lemarchand, A. Spivack and J. Gaillardet. *Geochimica et Cosmochimica Acta* 71, 1636-1641.
- Hopley, D., Smithers, S.G., Parnell, K.E., 2007. *The geomorphology of the Great Barrier Reef*. Cambridge University Press, New York.
- Hughes, T.P., 1987. Skeletal density and growth form of corals. *Marine Ecology-Progress Series* 35, 259-266.
- IBM Corp. Released 2011. *IBM SPSS Statistics for Windows, Version 20.0*. Armonk, NY: IBM Corp.

- IBM Corp. Released 2011. IBM SPSS Statistics for Windows, Version 20.0. Armonk, NY: IBM Corp.
- Inoue, M., Suzuki, A., Nohara, M., Hibino, K., Kawahata, H., 2007. Empirical assessment of coral Sr/Ca and Mg/Ca ratios as climate proxies using colonies grown at different temperatures. *Geophysical Research Letters* 34.
- IPCC, 2007a: Climate Change 2007: Synthesis Report. Contribution of Working Groups I, II and III to the Fourth Assessment Report of the Intergovernmental Panel on Climate Change [Core Writing Team, Pachauri, R.K and Reisinger, A. (eds.)]. IPCC, Geneva, Switzerland, 104 pp.
- IPCC, 2007b. Climate Change 2007: The Physical Science Basis. Contribution of Working Group I to the Fourth Assessment Report of the Intergovernmental Panel on Climate Change [Solomon, S., D. Qin, M. Manning, Z. Chen, M. Marquis, K.B. Averyt, M.Tignor and H.L. Miller (eds.)]. Cambridge University Press, Cambridge, United Kingdom and New York, NY, USA.
- Jones, P.D., Parker, D.E., Osborn, T.J., K.R., B., 2011. Global and hemispheric temperature anomalies—land and marine instrumental records. In *Trends: A Compendium of Data on Global Change*. Carbon Dioxide Information Analysis Center, Oak Ridge National Laboratory, U.S. Department of Energy, Oak Ridge, Tenn., U.S.A. .
- Kakihana, H., Kotaka, M., Satoh, S., Nomura, M., Okamoto, M., 1977. Fundamental studies on ion-exchanges sepeation of boron isotopes. *Bulletin of the Chemical Society of Japan* 50, 158-163.
- Keeling, C.D., Brix, H., Gruber, N., 2004. Seasonal and long-term dynamics of the upper ocean carbon cycle at Station ALOHA near Hawaii. *Global Biogeochemical Cycles* 18, 1-26.
- Keeling, R.F., Piper, S.C., Bollenbacher, A.F., Walker, J.S., 2009. Atmospheric CO<sub>2</sub> records from sites in the SIO air sampling network. In *Trends: A Compendium of Data on Global Change*. Carbon Dioxide Information Analysis Center, Oak Ridge National Laboratory, U.S. Department of Energy, Oak Ridge, Tenn., U.S.A.
- Kleypas, J.A., Anthony, K.R.N., Gattuso, J.P., 2011. Coral reefs modify their seawater carbon chemistry - case study from a barrier reef (Moorea, French Polynesia). *Global Change Biology* 17, 3667-3678.
- Kleypas, J.A., Buddemeier, R.W., Archer, D., Gattuso, J.P., Langdon, C., Opdyke, B.N., 1999a. Geochemical consequences of increased atmospheric carbon dioxide on coral reefs. *Science* 284, 118-120.
- Kleypas, J.A., Burrage, D.M., 1994. Satellite observations of circulation in the southern Great Barrier Reef, Australia. *International Journal of Remote Sensing* 15, 2051-2063.



- Kleypas, J.A., McManu, J.W., Mene, L.A.B., 1999b. Environmental limits to coral reef development: Where do we draw the line? *American Zoologist* 39, 146-159.
- Klochko, K., Kaufman, A.J., Yao, W., Byrne, R.H., Tossell, J.A., 2006. Experimental measurement of boron isotope fractionation in seawater. *Earth and Planetary Science Letters* 248, 261-270.
- Krief, S., Hendy, E.J., Fine, M., Yam, R., Meibom, A., Foster, G.L., Shemesh, A., 2010. Physiological and isotopic responses of scleractinian corals to ocean acidification. *Geochimica et Cosmochimica Acta* 74, 4988-5001.
- Langdon, C., Atkinson, M.J., 2005. Effect of elevated pCO<sub>2</sub> on photosynthesis and calcification of corals and interactions with seasonal change in temperature/irradiance and nutrient enrichment. *Journal of Geophysical Research C: Oceans* 110, 1-16.
- Langdon, C., Takahashi, T., Sweeney, C., Chipman, D., Goddard, J., Marubini, F., Aceves, H., Barnett, H., Atkinson, M.J., 2000. Effect of calcium carbonate saturation state on the calcification rate of an experimental coral reef. *Global Biogeochemical Cycles* 14, 639-654.
- Leclercq, N., Gattuso, J.P., Jaubert, J., 2000. CO<sub>2</sub> partial pressure controls the calcification rate of a coral community. *Global Change Biology* 6, 329-334.
- Leclercq, N., Gattuso, J.P., Jaubert, J., 2002. Primary production, respiration, and calcification of a coral reef mesocosm under increased CO<sub>2</sub> partial pressure. *Limnology and Oceanography* 47, 558-564.
- Lee, K., Tong, L.T., Millero, F.J., Sabine, C.L., Dickson, A.G., Goyet, C., Park, G.H., Wanninkhof, R., Feely, R.A., Key, R.M., 2006. Global relationships of total alkalinity with salinity and temperature in surface waters of the world's oceans. *Geophysical Research Letters* 33.
- Lemarchand, D., Gaillardet, J., Lewin, É., Allègre, C.J., 2002. Boron isotope systematics in large rivers: Implications for the marine boron budget and paleo-pH reconstruction over the Cenozoic. *Chemical Geology* 190, 123-140.
- Linsley, B.K., Messier, R.G., Dunbar, R.B., 1999. Assessing between-colony oxygen isotope variability in the coral *Porites lobata* at Clipperton Atoll. *Coral Reefs* 18, 13-27.
- Linsley, B.K., Wellington, G.M., Schrag, D.P., 2000. Decadal sea surface temperature variability in the subtropical south Pacific from 1726 to 1997 A.D. *Science* 290, 1145-1148.
- Linsley, B.K., Wellington, G.M., Schrag, D.P., Ren, L., Salinger, M.J., Tudhope, A.W., 2004. Geochemical evidence from corals for changes in the amplitude and spatial pattern of South Pacific interdecadal climate variability over the last 300 years. *Climate Dynamics* 22, 1-11.



- Liu, Y., Liu, W., Peng, Z., Xiao, Y., Wei, G., Sun, W., He, J., Liu, G., Chou, C.L., 2009. Instability of seawater pH in the South China Sea during the mid-late Holocene: Evidence from boron isotopic composition of corals. *Geochimica et Cosmochimica Acta* 73, 1264-1272.
- Lough, J.M., 2008a. Coral calcification from skeletal records revisited. *Marine Ecology Progress Series* 373, 257-264.
- Lough, J.M., 2008b. Shifting climate zones for Australia's tropical marine ecosystems. *Geophysical Research Letters* 35, L14708.
- Lough, J.M., Barnes, D.J., 1997. Several centuries of variation in skeletal extension, density and calcification in massive *Porites* colonies from the Great Barrier Reef: A proxy for seawater temperature and a background of variability against which to identify unnatural change. *Journal of Experimental Marine Biology and Ecology* 211, 29-67.
- Lough, J.M., Barnes, D.J., 2000. Environmental controls on growth of the massive coral *Porites*. *Journal of Experimental Marine Biology and Ecology* 245, 225-243.
- Lough, J.M., Cooper, T.F., 2011. New insights from coral growth band studies in an era of rapid environmental change. *Earth-Science Reviews* 108, 170-184.
- Maidment, D.R., 1993. *Handbook of hydrology*. McGraw-Hill, New York.
- Mantua, N.J., Hare, S.R., 2002. The Pacific Decadal Oscillation. *Journal of Oceanography* 58, 35-44.
- Mantua, N.J., Hare, S.R., Zhang, Y., Wallace, J.M., Francis, R.C., 1997. A Pacific Interdecadal Climate Oscillation with impacts on salmon production. *Bulletin of the American Meteorological Society* 78, 1069-1079.
- Marshall, A.T., Clode, P., 2004. Calcification rate and the effect of temperature in a zooxanthellate and an azooxanthellate scleractinian reef coral. *Coral Reefs* 23, 218-224.
- Marshall, A.T., Clode, P.L., 2002. Effect of increased calcium concentration in sea water on calcification and photosynthesis in the scleractinian coral *Galaxea fascicularis*. *Journal of Experimental Biology* 205, 2107-2113.
- Marubini, F., Barnett, H., Langdon, C., Atkinson, M.J., 2001. Dependence of calcification on light and carbonate ion concentration for the hermatypic coral *Porites compressa*. *Marine Ecology Progress Series* 220, 153-162.
- Marubini, F., Ferrier-Pagès, C., Cuif, J.P., 2003. Suppression of skeletal growth in scleractinian corals by decreasing ambient carbonate-ion concentration: A cross-family comparison. *Proceedings of the Royal Society B: Biological Sciences* 270, 179-184.

- Marubini, F., Ferrier-Pagès, C., Furla, P., Allemand, D., 2008. Coral calcification responds to seawater acidification: A working hypothesis towards a physiological mechanism. *Coral Reefs* 27, 491-499.
- Marubini, F., Thake, B., 1999. Bicarbonate addition promotes coral growth. *Limnology and Oceanography* 44, 716-720.
- MATLAB 7.11 R2010b, 2010. The MathWorks, Inc., Natick, Massachusetts, United States.
- McConnaughey, T., 1989a.  $^{13}\text{C}$  and  $^{18}\text{O}$  isotopic disequilibrium in biological carbonates: I. Patterns. *Geochimica et Cosmochimica Acta* 53, 151-162.
- McConnaughey, T., 1989b.  $^{13}\text{C}$  and  $^{18}\text{O}$  isotopic disequilibrium in biological carbonates: II. In vitro simulation of kinetic isotope effects. *Geochimica et Cosmochimica Acta* 53, 163-171.
- McConnaughey, T.A., Burdett, J., Whelan, J.F., Paull, C.K., 1997. Carbon isotopes in biological carbonates: Respiration and photosynthesis. *Geochimica et Cosmochimica Acta* 61, 611-622.
- McConnaughey, T.A., Whelan, J.F., 1997. Calcification generates protons for nutrient and bicarbonate uptake. *Earth-Science Reviews* 42, 95-117.
- McCulloch, M., Falter, J., Trotter, J., Montagna, P., 2012. Coral resilience to ocean acidification and global warming through pH up-regulation. *Nature Clim. Change* 2, 623-627.
- McCulloch, M.T., Gagan, M.K., Mortimer, G.E., Chivas, A.R., Isdale, P.J., 1994. A high-resolution Sr/Ca and  $\delta^{18}\text{O}$  coral record from the Great Barrier Reef, Australia, and the 1982-1983 El Niño. *Geochimica et Cosmochimica Acta* 58, 2747-2754.
- McCulloch, M.T., Tudhope, A.W., Esat, T.M., Mortimer, G.E., Chappell, J., Pillans, B., Chivas, A.R., Omura, A., 1999. Coral record of equatorial sea-surface temperatures during the penultimate deglaciation at Huon Peninsula. *Science* 283, 202-204.
- McNeil, B.I., Matear, R.J., Barnes, D.J., 2004. Coral reef calcification and climate change: The effect of ocean warming. *Geophysical Research Letters* 31, 1-4.
- Middleton, J.H., 1994. Circulation and water mass characteristics of the southern Great Barrier Reef. *Australian Journal of Marine & Freshwater Research* 45, 1-18.
- Mitsuguchi, T., Matsumoto, E., Abe, O., Uchida, T., Isdale, P.J., 1996. Mg/Ca thermometry in coral skeletons. *Science* 274, 961-963.
- Mitsuguchi, T., Matsumoto, E., Uchida, T., 2003. Mg/Ca and Sr/Ca ratios of *Porites* coral skeleton: Evaluation of the effect of skeletal growth rate. *Coral Reefs* 22, 381-388.

- Neftel, A., Friedli, H., Moor, E., Lötscher, H., Oeschger, H., Siegenthaler, U., Stauffer, B., 1994. Historical CO<sub>2</sub> record from the Siple Station ice core. In *Trends: A Compendium of Data on Global Change*. Carbon Dioxide Information Analysis Center, Oak Ridge National Laboratory, U.S. Department of Energy, Oak Ridge, Tenn., U.S.A.
- Ni, Y., Foster, G.L., Bailey, T., Boyer, P., Elliott, T., Schmidt, D.N., Pearson, P., Haley, N.B., C., C., 2007. A core top assessment of proxies for the ocean carbonate system in surface-dwelling foraminifers. *Paleoceanography* 22, PA3212.
- Ohde, S., Van Woesik, R., 1999. Carbon dioxide flux and metabolic processes of a coral reef, Okinawa. *Bulletin of Marine Science* 65, 559-576.
- Omata, T., Suzuki, A., Kawahat, H., Okamoto, M., 2005. Annual fluctuation in the stable carbon isotope ratio of coral skeletons: The relative intensities of kinetic and metabolic isotope effects. *Geochimica et Cosmochimica Acta* 69, 3007-3016.
- Opdyke, B.N., Walker, J.C.G., 1992. Return of the coral reef hypothesis: basin to shelf partitioning of CaCO<sub>3</sub> and its effect on atmospheric CO<sub>2</sub>. *Geology* 20, 733-736.
- Orr, J.C., Fabry, V.J., Aumont, O., Bopp, L., Doney, S.C., Feely, R.A., Gnanadesikan, A., Gruber, N., Ishida, A., Joos, F., Key, R.M., Lindsay, K., Maier-Reimer, E., Matear, R., Monfray, P., Mouchet, A., Najjar, R.G., Plattner, G.K., Rodgers, K.B., Sabine, C.L., Sarmiento, J.L., Schlitzer, R., Slater, R.D., Totterdell, I.J., Weirig, M.F., Yamanaka, Y., Yool, A., 2005. Anthropogenic ocean acidification over the twenty-first century and its impact on calcifying organisms. *Nature* 437, 681-686.
- Pagani, M., Lemarchand, D., Spivack, A., Gaillardet, J., 2005. A critical evaluation of the boron isotope-pH proxy: The accuracy of ancient ocean pH estimates. *Geochimica et Cosmochimica Acta* 69, 953-961.
- Paillard, D., Labeyrie, L., Yiou, P., 1996. Macintosh program performs time-series analysis. *Eos Trans. AGU* 77, 379.
- Pandolfi, J.M., Connolly, S.R., Marshall, D.J., Cohen, A.L., 2011. Projecting coral reef futures under global warming and ocean acidification. *Science* 333, 418-422.
- Pelejero, C., Calvo, E., Hoegh-Guldberg, O., 2010. Paleo-perspectives on ocean acidification. *Trends in Ecology and Evolution* 25, 332-344.
- Pelejero, C., Calvo, E., McCulloch, M.T., Marshall, J.F., Gagan, M.K., Lough, J.M., Opdyke, B.N., 2005. Preindustrial to modern interdecadal variability in coral reef pH. *Science* 309, 2204-2207.
- Petit, J.R., Jouzel, J., Raynaud, D., Barkov, N.I., Barnola, J.M., Basile, I., Bender, M., Chappellaz, J., Davis, M., Delaygue, G., Delmotte, M., Kotiyakov, V.M.,



- Legrand, M., Lipenkov, V.Y., Lorius, C., Pépin, L., Ritz, C., Saltzman, E., Stevenard, M., 1999. Climate and atmospheric history of the past 420,000 years from the Vostok ice core, Antarctica. *Nature* 399, 429-436.
- Pfeiffer, M., Timm, O., Dullo, W.C., Garbe-Schönberg, D., 2006. Paired coral Sr/Ca and  $\delta^{18}\text{O}$  records from the Chagos Archipelago: Late twentieth century warming affects rainfall variability in the tropical Indian Ocean. *Geology* 34, 1069-1072.
- Pierrot, D., Lewis E., Wallace, D.W.R., 2006. MS Excel Program Developed for CO<sub>2</sub> System Calculations. ORNL/CDIAC-105a. (Ed.). Carbon Dioxide Information Analysis Center, Oak Ridge National Laboratory, U.S. Department of Energy, Oak Ridge, Tennessee.
- Power, S., Casey, T., Folland, C., Colman, A., Mehta, V., 1999. Inter-decadal modulation of the impact of ENSO on Australia. *Climate Dynamics* 15, 319-324.
- Quay, P., Sonnerup, R., Westby, T., Stutsman, J., McNichol, A., 2003. Changes in the  $^{13}\text{C}/^{12}\text{C}$  of dissolved inorganic carbon in the ocean as a tracer of anthropogenic CO<sub>2</sub> uptake. *Global Biogeochemical Cycles* 17, 4-1.
- Quay, P.D., Tilbrook, B., Wong, C.S., 1992. Oceanic uptake of fossil fuel CO<sub>2</sub>: Carbon-13 evidence. *Science* 256, 74-79.
- Quinn, T.M., Crowley, T.J., Taylor, F.W., 1996. New stable isotope results from a 173-year coral from Espiritu Santo, Vanuatu. *Geophysical Research Letters* 23, 3413-3416.
- Quinn, T.M., Crowley, T.J., Taylor, F.W., Henin, C., Joannot, P., Join, Y., 1998. A multicentury stable isotope record from a New Caledonia coral: Interannual and decadal sea surface temperature variability in the southwest Pacific since 1657 A.D. *Paleoceanography* 13, 412-426.
- Quinn, T.M., Taylor, F.W., Crowley, T.J., 1993. A 173 year stable isotope record from a tropical south pacific coral. *Quaternary Science Reviews* 12, 407-418.
- Raven, J., 2005. Ocean acidification due to increasing atmospheric carbon dioxide. The Royal Society, London.
- Rayner, N.A., Horton, E.B., Parker, D.E., Folland, C.K., Hackett, R.B., 1996. Version 2.2 of the global sea ice and sea surface temperature data set, 1903 – 1994, in: Hadley Centre for Climate Prediction and Research, M.O. (Ed.). Climate Research Technical Note Bracknell, UK.
- Rayner, N.A., Parker, D.E., Horton, E.B., Folland, C.K., Alexander, L.V., Rowell, D.P., Kent, E.C., Kaplan, A., 2003. Global analyses of sea surface temperature, sea ice, and night marine air temperature since the late nineteenth century. *Journal of Geophysical Research D: Atmospheres* 108, ACL 2-1 - ACL 2-29.

- Ren, L., Linsley, B.K., Wellington, G.M., Schrag, D.P., Hoegh-guldberg, O., 2003. Deconvolving the  $\delta^{18}\text{O}$  seawater component from subseasonal coral  $\delta^{18}\text{O}$  and Sr/Ca at Rarotonga in the southwestern subtropical Pacific for the period 1726 to 1997. *Geochimica et Cosmochimica Acta* 67, 1609-1621.
- Reynaud-Vaganay, S., Juillet-Leclerc, A., Jaubert, J., Gattuso, J.-P., 2001. Effect of light on skeletal  $\delta^{13}\text{C}$  and  $\delta^{18}\text{O}$ , and interaction with photosynthesis, respiration and calcification in two zooxanthellate scleractinian corals. *Palaeogeography, Palaeoclimatology, Palaeoecology* 175, 393-404.
- Reynolds, R.W., Rayner, N.A., Smith, T.M., Stokes, D.C., Wang, W., 2002. An improved in situ and satellite SST analysis for climate. *Journal of Climate* 15, 1609-1625.
- Ridgway, K., Hill, K., 2009. The East Australian Current. A Marine Climate Change Impacts and Adaptation Report Card for Australia 2009
- Ries, J.B., 2011. A physicochemical framework for interpreting the biological calcification response to  $\text{CO}_2$ -induced ocean acidification. *Geochimica et Cosmochimica Acta* 75, 4053-4064.
- Rodolfo-Metalpa, R., Houlbrequé, F., Tambutte, E., Boisson, F., Baggini, C., Patti, F.P., Jeffree, R., Fine, M., Foggo, A., Gattuso, J.-P., Hall-Spencer, J.M., 2011. Coral and mollusc resistance to ocean acidification adversely affected by warming. *Nature Climate Change* 1, 308-312.
- Rodolfo-Metalpa, R., Martin, S., Ferrier-Pagès, C., Gattuso, J.-P., 2010. Response of the temperate coral *Cladocora caespitosa* to mid- and long-term exposure to  $\text{pCO}_2$  and temperature levels projected for the year 2100 AD. *Biogeosciences* 7, 289-300.
- Rollion-Bard, C., Chaussidon, M., France-Lanord, C., 2003. pH control on oxygen isotopic composition of symbiotic corals. *Earth and Planetary Science Letters* 215, 275-288.
- Sabine, C.L., Feely, R.A., Gruber, N., Key, R.M., Lee, K., Bullister, J.L., Wanninkhof, R., Wong, C.S., Wallace, D.W.R., Tilbrook, B., Millero, F.J., Peng, T.H., Kozyr, A., Ono, T., Rios, A.F., 2004. The oceanic sink for anthropogenic  $\text{CO}_2$ . *Science* 305, 367-371.
- Sanchez-Valle, C., Reynard, B., Daniel, I., Lecuyer, C., Martinez, I., Chervin, J.C., 2005. Boron isotopic fractionation between minerals and fluids: New insights from in situ high pressure-high temperature vibrational spectroscopic data. *Geochimica et Cosmochimica Acta* 69, 4301-4313.
- Santana-Casiano, J.M., González-Dávila, M., Rueda, M.J., Llinás, O., González-Dávila, E.F., 2007. The interannual variability of oceanic  $\text{CO}_2$  parameters in the northeast Atlantic subtropical gyre at the ESTOC site. *Global Biogeochemical Cycles* 21.



- Santos, I.R., Glud, R.N., Maher, D., Erler, D., Eyre, B.D., 2011. Diel coral reef acidification driven by porewater advection in permeable carbonate sands, Heron Island, Great Barrier Reef. *Geophysical Research Letters* 38.
- Sanyal, A., Nugent, M., Reeder, R.J., Bijma, J., 2000. Seawater pH control on the boron isotopic composition of calcite: Evidence from inorganic calcite precipitation experiments. *Geochimica et Cosmochimica Acta* 64, 1551-1555.
- Schrag, D.P., 1999. Rapid analysis of high-precision Sr/Ca ratios in corals and other marine carbonates. *Paleoceanography* 14, 97-102.
- Shaw, E.C., McNeil, B.I., Tilbrook, B., 2012. Impacts of ocean acidification in naturally variable coral reef flat ecosystems. *Journal of Geophysical Research C: Oceans* 117.
- Shen, C.C., Lee, T., Chen, C.Y., Wang, C.H., Dai, C.F., Li, L.A., 1996. The calibration of D[Sr/Ca] versus sea surface temperature relationship for *Porites* corals. *Geochimica et Cosmochimica Acta* 60, 3849-3858.
- Silverman, J., Lazar, B., Erez, J., 2007. Effect of aragonite saturation, temperature, and nutrients on the community calcification rate of a coral reef. *Journal of Geophysical Research C: Oceans* 112.
- Sinclair, D.J., 2005. Correlated trace element "vital effects" in tropical corals: A new geochemical tool for probing biomineralization. *Geochimica et Cosmochimica Acta* 69, 3265-3284.
- Sinclair, D.J., Kinsley, L.P.J., McCulloch, M.T., 1998. High resolution analysis of trace elements in corals by laser ablation ICP-MS. *Geochimica et Cosmochimica Acta* 62, 1889-1901.
- Smith, T.M., Reynolds, R.W., 2003. Extended reconstruction of global sea surface temperatures based on COADS data (1854-1997). *Journal of Climate* 16, 1495-1510.
- Spencer Davies, P., 1989. Short-term growth measurements of corals using an accurate buoyant weighing technique. *Marine Biology* 101, 389-395.
- Spivack, A.J., Edmond, J.M., 1986. Determination of boron isotope ratios by thermal ionization mass spectrometry of the dicesium metaborate cation. *Analytical Chemistry* 58, 31-35.
- Spivack, A.J., Edmond, J.M., 1987. Boron isotope exchange between seawater and the oceanic crust. *Geochimica et Cosmochimica Acta* 51, 1033-1043.
- Swart, P.K., Greer, L., Rosenheim, B.E., Moses, C.S., Waite, A.J., Winter, A., Dodge, R.E., Helmle, K., 2010. The  $^{13}\text{C}$  Suess effect in scleractinian corals mirror changes in the anthropogenic  $\text{CO}_2$  inventory of the surface oceans. *Geophysical Research Letters* 37, L05604.
- Swart, P.K., Greer, L., Rosenheim, B.E., Moses, C.S., Waite, A.J., Winter, A., Dodge, R.E., Helmle, K., 2010. The  $^{13}\text{C}$  Suess effect in scleractinian corals

- mirror changes in the anthropogenic CO<sub>2</sub> inventory of the surface oceans. *Geophysical Research Letters* 37, L05604.
- Taft, B.A., Kessler, W.S., 1991. Variations of zonal currents in the central tropical Pacific during 1970 to 1987: Sea level and dynamic height measurements. *Journal of Geophysical Research-Oceans* 96, 12599-12618.
- Tans, P., Keeling, R., 2012. NOAA/ESRL (<http://www.esrl.noaa.gov/gmd/ccgg/trends/>). Scripps Institution of Oceanography.
- Taylor, R.B., Barnes, D.J., Lough, J.M., 1993. Simple models of density band formation in massive corals. *Journal of Experimental Marine Biology and Ecology* 167, 109-125.
- Trotter, J., Montagna, P., McCulloch, M., Silenzi, S., Reynaud, S., Mortimer, G., Martin, S., Ferrier-Pagès, C., Gattuso, J.P., Rodolfo-Metalpa, R., 2011. Quantifying the pH 'vital effect' in the temperate zooxanthellate coral *Cladocora caespitosa*: Validation of the boron seawater pH proxy. *Earth and Planetary Science Letters* 303, 163-173.
- Tyrrell, T., 2008. Calcium carbonate cycling in future oceans and its influence on future climates. *Journal of Plankton Research* 30, 141-156.
- Vengosh, A., Kolodny, Y., Starinsky, A., Chivas, A.R., McCulloch, M.T., 1991. Coprecipitation and isotopic fractionation of boron in modern biogenic carbonates. *Geochimica et Cosmochimica Acta* 55, 2901-2910.
- Venn, A., Tambutté, E., Holcomb, M., Allemand, D., Tambutté, S., 2011. Live tissue imaging shows reef corals elevate pH under their calcifying tissue relative to seawater. *PLoS ONE* 6.
- Veron, J.E.N., 2000a. Corals of Australia and Indo-Pacific. Australian Institute of Marine Science, London.
- Veron, J.E.N., 2000b. Corals of the world. Australian Institute of Marine Science, Townsville, Qld.
- Wei, G., Deng, W., Yu, K., Li, X.H., Sun, W., Zhao, J.X., 2007. Sea surface temperature records in the northern South China Sea from mid-Holocene coral Sr/Ca ratios. *Paleoceanography* 22.
- Wei, G., McCulloch, M.T., Mortimer, G., Deng, W., Xie, L., 2009. Evidence for ocean acidification in the Great Barrier Reef of Australia. *Geochimica et Cosmochimica Acta* 73, 2332-2346.
- Wellington, G.M., Dunbar, R.B., Merlen, G., 1996. Calibration of stable oxygen isotope signatures in Galápagos corals. *Paleoceanography* 11, 467-480.
- Wilkinson, C., Hodgson, G., 1999. Coral reefs and the 1997-1998 mass bleaching and mortality. *Nature and Resources* 35, 16-25.

- Wootton, J.T., Pfister, C.A., Forester, J.D., 2008. Dynamic patterns and ecological impacts of declining ocean pH in a high-resolution multi-year dataset. *Proceedings of the National Academy of Sciences*.
- Xiao, Y.K., Shirodkar, P.V., Zhang, C.G., Wei, H.Z., Liu, W.G., Zhou, W.J., 2006. Isotopic fractionation of boron in growing corals and its palaeoenvironmental implication. *Current Science* 90, 414-420.
- Yates, K.K., Halley, R.B., 2006.  $\text{CO}_3^{2-}$  concentration and  $\text{pCO}_2$  thresholds for calcification and dissolution on the Molokai reef flat, Hawaii. *Biogeosciences* 3, 357-369.
- Yu, J., Elderfield, H., Hönisch, B., 2007. B/Ca in planktonic foraminifera as a proxy for surface seawater pH. *Paleoceanography* 22.
- Zeebe, R.E., 2005. Stable boron isotope fractionation between dissolved  $\text{B}(\text{OH})_3$  and  $\text{aB}(\text{OH})_4^-$ . *Geochimica et Cosmochimica Acta* 69, 2753-2766.
- Zeebe, R.E., Wolf-Gladrow, D.A., 2001.  $\text{CO}_2$  in seawater : equilibrium, kinetics, isotopes. Elsevier, Amsterdam ; New York.
- Zhong, S., Mucci, A., 1989. Calcite and aragonite precipitation from seawater solutions of various salinities: Precipitation rates and overgrowth compositions. *Chemical Geology* 78, 283-299.
- Zhu, X., Liu, Z., 2009. Tropical SST response to global warming in the twentieth century. *Journal of Climate* 22, 1305-1312.









---

## Appendices

---

### **Appendix A. Details of all collected coral cores from the southern GBR**

Fig. A-1 Map of sampling locations of this study

Fig. A-2 An example of bioerosion

Table A-1. Collected southern GBR coral core details

### **Appendix B. Positive X-radiography of coral slabs**

Fig. B-1 Positive X-radiography of Middle Pompey (PSC) coral slabs

Fig. B-2 Positive X-radiography from Little Kindermar (PSA) coral slabs

Fig. B-3 Positive X-radiography of Fitzroy Reef (FYR) coral slabs

Fig. B-4 Positive X-radiography of Lady Musgrave Island (LHI08-H) coral slabs

Fig. B-5 Positive X-radiography of Lady Musgrave Island (LHI08-C-a) coral slabs

### **Appendix C. Boron isotope as a proxy for seawater pH**

### **Appendix D. Coral geochemical records**

Table D-1. Seasonal data for four *Porites* corals from the southern GBR

Table D-2. Long-term annual coral geochemical and isotopic records from Middle Pompey over 1905-2005

Table D-3. Long-term coral geochemical and isotopic records from Little Kindermar over 1835-2005.

Table D-4. Long-term annual coral geochemical and isotopic records from Fitzroy Reef over 1950-2008

Table D-5. Long-term annual coral geochemical and isotopic records from Lady Musgrave Island over 1890-2008

**Appendix E. Measured density, extension rate, and calcification records in the southern GBR**

Table E-1. Density data by three methods and porosity data from a Middle Pompey (PSC) core

Table E-2. Density data by three methods and porosity data from a Little Kindermar (PSA) core

Table E-3. Extension, density, calcification, and porosity data of pieces from LA-ICPMS analysis and half-sized pieces from a Middle Pompey (PSC) core

Table E-4. Density data from a Fitzroy Reef (FYR) core

Table E-5. Density data from a Lady Musgrave Island (LMI08-H) core

Table E-6. Density data from a Lady Musgrave Island (LMI08-C-a) core

Table E-7. Annual extension, density, and calcification data from a Middle Pompey (PSC) core

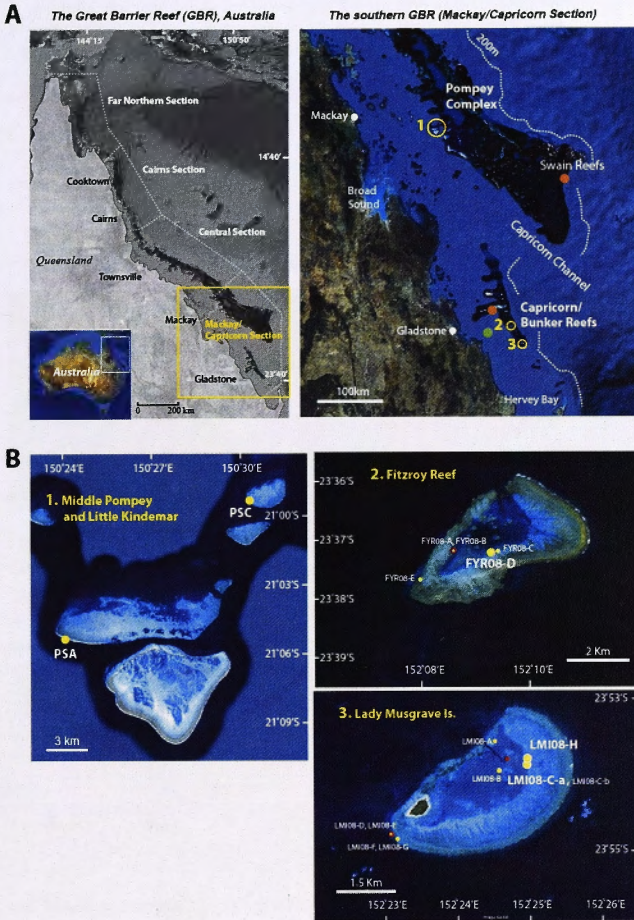
Table E-8. Annual extension, density, and calcification data from a Little Kindermar (PSA) core

Table E-9. Annual extension, density, and calcification data from a Fitzroy Reef (FYR) core

Table E-10. Annual extension, density, and calcification data from a Lady Musgrave Island (LMI08-H) core

Table E-11. Annual extension, density, and calcification data from a Lady Musgrave Island (LMI08-C-a) core

## Appendix A. Details of all collected coral cores from the southern GBR



**Fig. A-1** (A) Map of northeastern Australia showing the locations of the Great Barrier Reef (GBR) in Australia (left) and the southern GBR or Mackey/Capricorn Section (right). Orange and green circles represent in situ SST and pH measurement locations respectively. (B) Maps showing the location of *Porites* coral core sampling sites in the southern GBR. Yellow circles in the main map are enlarged and exhibit (1) Middle Pompey and Little



Kindermar in Pompey Complex, (2) Fitzroy Reef, and (3) Lady Musgrave Island. Yellow dots represent coral collection sites and red dots show seawater-sampling sites. Two sample IDs on one mark indicate the collection of two coral cores from proximal coral colonies. Coral cores represented by large yellow dots are subject to chemical and isotopic analyses in this study. Images from Google maps.



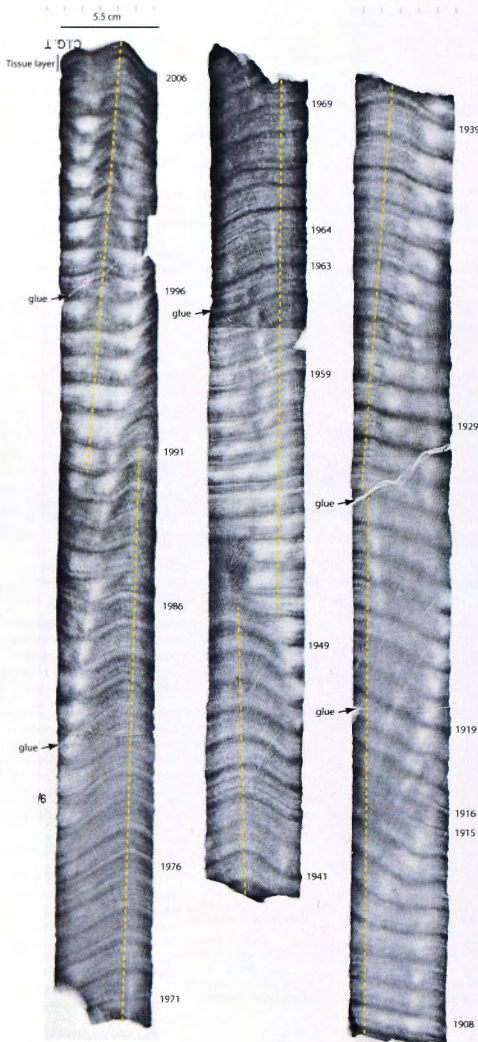
**Fig. A-2** An example of bioerosion and dead part from Lady Mugarve Island (LMI08-D).

Table A-1. Collected southern GBR coral core details

Reef	Sample ID	Latitude (°S)	Longitude (°E)	Core collecting depth (m)	Core length (cm)	Date collected	Sampling location of reef lagoon	Description
Middle Pompey	PSC	20.99	150.51	5	150	10/03/2006	outside	
Little Kindermar	PSA	21.10	150.40	5	186	9/03/2006	outside	
Fitzry Reef	FYR08-A	23.37	152.08	5.6	113.0	23/10/2008	inside	Poor core. Top and bottom pieces look good. But the middle part is dead and broken.
Fitzry Reef	FYR08-B	23.37	152.08	6.2	124.5	23/10/2008	inside	Nice core. Taken from neighboring bummie to FYR08-A. Good condition. But lots of missing and broken parts exist.
Fitzry Reef	FYR08-C	23.37	152.10	1.2	93.0	24/10/2008	inside	Nice clean core with two long pieces. Sampled by only air drill.
Fitzry Reef	FYR08-D	23.37	152.10	0.5	96.5	24/10/2008	inside	Taken from neighboring bummie to FYR08-C. Sampled by only air drill.
Fitzry Reef	FYR08-E	23.38	152.08	7.1	175.5	24/10/2008	outside	Nice longest core. But multiple growth observed from X-ray.
Lady Musgrave Is.	LMI08-A	23.52	152.24	7.9	118.0	20/10/2008	inside	Poor core, presence of dead part in the piece #6 and fissuring.
Lady Musgrave Is.	LMI08-B	23.54	152.25	5.1	117.5	21/10/2008	inside	Very nice core. Little bio-erosion. But multiple growth observed from X-ray.
Lady Musgrave Is.	LMI08-C-a	23.54	152.25	4.5	130.0	21/10/2008	inside	Nice core. Little bio-erosion and a tiny dead part in the piece #2.
Lady Musgrave Is.	LMI08-C-b	23.54	152.25	4.5	136.5	21/10/2008	inside	Poor core. Same coral colony with LMI-C08-a (30 cm away from core a). Any dead parts among the pieces - not suitable for continuous dating.
Lady Musgrave Is.	LMI08-D	23.55	152.23	-	124.5	22/10/2008	outside	Poor core. Two top pieces have dead parts (big hole in the center of the core). Bottom half looks good but has brown spots on the core wall.
Lady Musgrave Is.	LMI08-E	23.55	152.23	-	125.0	22/10/2008	outside	Poor core. Taken from neighboring bummie to LMI-D08. Most of the upper parts dead (pieces #1, 2, 3). Bottom half looks good.
Lady Musgrave Is.	LMI08-F	23.55	152.23	4.4	166.5	22/10/2008	outside	Nice clean core - looks to be cut to growth axis. But multiple growth observed from X-ray.
Lady Musgrave Is.	LMI08-G	23.55	152.23	5.5	98.5	22/10/2008	outside	Nice clean core. Sampled from bummy part, ~2m from LMI08-F. But multiple growth observed from X-ray.
Lady Musgrave Is.	LMI08-H	23.54	152.25	7.9	143	22/10/2008	inside	OK core. Top and bottom look good. But the middle part of the core has dead part.



Appendix B. Positive X-radiography of coral slabs



**Fig. B-1** Positive print from X-radiography of coral slabs from Middle Pompey over the period 1907-2006. Chronology was reconstructed by cross checking of high density bands and Sr/Ca ratios from LA-ICPMS. Yellow dashed lines indicate the maximum growth axes which agree with tracks of LA-ICPMS and milling for the isotope analyses.

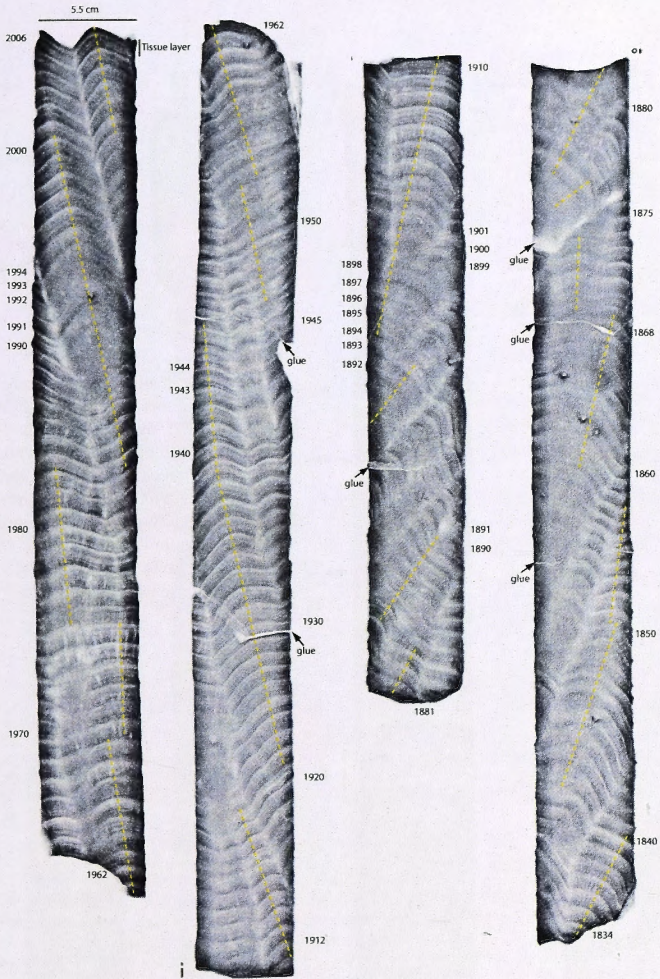


**Fig. B-2** Positive print from X-radiography of coral slabs from Little Kindermar over the period 1834-2006. Chronology was reconstructed by cross checking of high density bands and B/Ca ratios from LA-ICPMS. Yellow dashed lines indicate the maximum growth axes which agree with tracks of LA-ICPMS and milling for the isotope analyses.



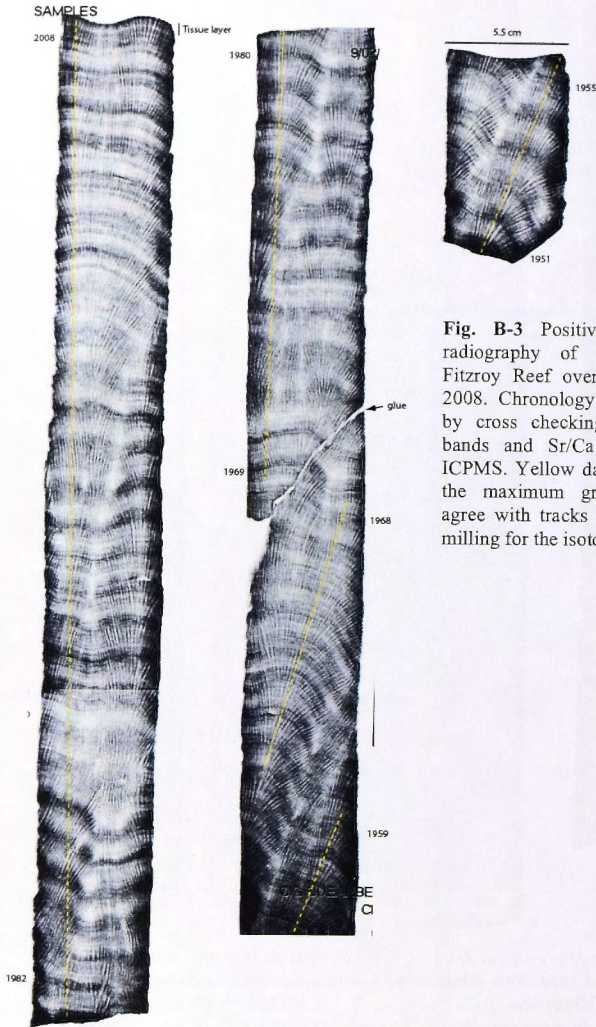
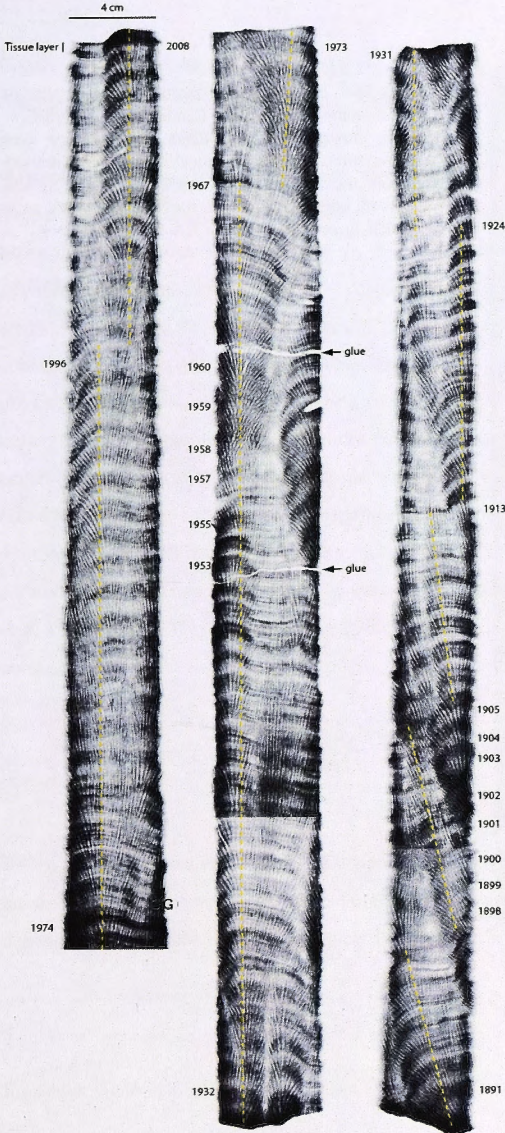


Fig. B-3 Positive print from X-radiography of coral slabs from Fitzroy Reef over the period 1950-2008. Chronology was reconstructed by cross checking of high density bands and Sr/Ca ratios from LA-ICPMS. Yellow dashed lines indicate the maximum growth axes which agree with tracks of LA-ICPMS and milling for the isotope analyses.



**Fig. B-4** Positive print from X-radiography of coral slabs from Lady Musgrave Island (LMI08-H) over the period 1890-2008. Chronology was reconstructed by cross checking of high density bands and Sr/Ca ratios from LA-ICPMS. Yellow dashed lines indicate the maximum growth axes which agree with tracks of LA-ICPMS and milling for the isotope analyses.





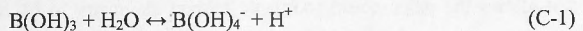
**Fig. B-5** Positive print from X-radiography of coral slabs from Little Kindermar (LMI08-C-a) over the period 1956-2008. Chronology was reconstructed by cross checking of high density bands and Sr/Ca ratios from LA-ICPMS. Yellow dashed lines indicate the maximum growth axes which agree with tracks of LA-ICPMS.

**Appendix C. Boron isotope as a proxy for seawater pH**

Corals provide an ideal material for recording the paleo-pH of surface water (Hemming et al., 1998; Vengosh et al., 1991). They precipitate an aragonite skeleton into which trace elements and stable isotopes are co-precipitated from the surrounding seawater controlled by a number of factors, including the composition, temperature, and salinity of the seawater. Coral boron concentrations are typically 5 times that in foraminifera (>50 ppm vs. 5-15 ppm, respectively; Hemming et al., 1998; Vengosh et al., 1991), providing ample sample for high resolution (~monthly) analysis. This can be particularly useful for reconstructing past changes in the context of the lack of instrumental data. Using a range of isotopic, elemental and physiological tracers, coral-based paleoclimate research has the ability to produce a network of subannually resolved, multi-century records of temperature, salinity, ocean circulation and other changes in the surface ocean (see review by Gagan et al. (2000) and Corrège (2006)). These capabilities have been expanded by the recently demonstrated ability of boron concentrations and isotope systematics in biogenic carbonates to constrain past changes in seawater pH and carbonate system equilibria (e.g. Liu et al., 2009; Pelejero et al., 2005; Wei et al., 2009; Xiao et al., 2006 for coral studies)

***Boron in seawater***

Boron exists in seawater primarily as trigonally coordinated boric acid ( $B(OH)_3$ ) and tetrahedrally coordinated borate ion ( $B(OH)_4^-$ ), the proportions of which are pH dependent as defined by the following equilibrium:



for which the stoichiometric equilibrium constant is:

$$K_B^* = \frac{[H^+][B(OH)_4^-]}{[B(OH)_3]} \quad (C-2)$$

The  $K_B^*$  of seawater has been determined experimentally and  $pK_B$  is 8.5975 at 25°C and a salinity of 35 PSU (DOE, 1994).

The abundance of boron in biologically precipitated and inorganic carbonates increases with increasing pH (Fig. 1.4a; Hemming and Hanson, 1992; Sanyal et al., 2000). This is consistent with a model in which only the charged species,  $B(OH)_4^-$ , attaches to and is incorporated into growing calcium carbonate (Vengosh et al., 2001). Hemming and Hanson (1992) proposed the following mechanism for the substitution of boron into calcium carbonate:



for which the exchange distribution coefficient,  $K_D$ , can be expressed as:

$$K_D = \frac{[B/Ca]_{CaCO_3}}{[B(OH)_4^- / HCO_3^-]_{seawater}} \quad (C-4)$$

The ratio of  $[B(OH)_4^-]/[HCO_3^-]$  in seawater is pH dependent as the concentration of  $B(OH)_4^-$  increases, and  $HCO_3^-$  decreases with increasing seawater pH (Zeebe and Wolf-Gladrow, 2001). Given sufficiently precise empirical calibration of  $K_D$ , it should be possible to use measured B/Ca of marine carbonates to reconstruct seawater  $[B(OH)_4^-]/[HCO_3^-]$  ratio values (Foster, 2008; Yu et al., 2007). Importantly, if  $[B(OH)_4^-]/[HCO_3^-]$  is known from an independent reconstruction of pH, as is possible using boron isotopes (see next section), an estimate of  $[HCO_3^-]$  can be made that allows the paleo-ocean inorganic carbon chemistry to be fully constrained. In this way Foster (2008) and Yu et al. (2007) have reconstructed pH and  $pCO_2$  in the North Atlantic Ocean and the Southern Ocean using B/Ca ratios from planktonic foraminifera back to 500 ka.

The above model unfortunately cannot be used to reconstruct modern (<200 years BP) surface seawater pH, due to the long oceanic residence times of both boron (20 Myr; Spivack and Edmond, 1987) and calcium (~1 Myr; Farkaš et al., 2007), which makes fluctuations of the B/Ca ratio of seawater unlikely on time-scales shorter than a few million years (Lemarchand et al., 2002; Yu et al., 2007). Furthermore, this has not been possible in corals as the  $K_D$  is dependent on changes in growth rate (Ni et al., 2007), temperature and/or carbonate ion concentration (Trotter et al., 2011; Yu et al., 2007). The effects of temperature and pH on  $K_D$  and B/Ca are also still not well constrained (Foster, 2008; Trotter et al., 2011). A recent study has shown that B/Ca profiles are correlated with temperature and  $[B(OH)_4^-]/[CO_3^{2-}]$  ratios rather than ambient seawater pH and  $[B(OH)_4^-]/[HCO_3^-]$  ratios (Trotter et al., 2011). These uncertainties require an alternative and robust method to reconstruct paleo-seawater pH.

### ***Boron isotopes seawater pH proxy***

The boron isotope-pH proxy is based on the change in boron speciation in seawater with pH, the isotopic fractionation between the two boron species, and the assumption that only the charged borate species is incorporated into calcium carbonate (equation 1-7 and Fig. 1.4a). Boron has two isotopes,  $^{10}B$  and  $^{11}B$ , and variations in the composition of which are expressed in a delta notation relative to the standard, NIST SRM 951 boric acid ( $^{11}B/^{10}B = 4.04367$ ; Catanzaro et al., 1970), as follows:

$$\delta^{11}B = \left[ \left( \frac{^{11}B/^{10}B_{\text{sample}}}{^{11}B/^{10}B_{\text{SRM951}}} \right) - 1 \right] \times 1000 \quad (C-5)$$

Due to differences in coordination and consequent B–O vibrational frequencies there is a large isotopic fractionation ( $\alpha_{B3-B4}$ ) between the two aqueous species of boron (Fig. 1.4b; Kakihana et al., 1977). The magnitude of this isotopic fractionation has been debated in the literature (e.g. Pagani et al., 2005; Zeebe, 2005) with empirical



and theoretical estimates of  $\alpha_{B3-B4}$  ranging from 1.0176 (Sanchez-Valle et al., 2005) to more than 1.030 (Zeebe, 2005). Uncertainty in the value of  $\alpha_{B3-B4}$  has been cited as a limiting factor in the applicability of this proxy (Pagani et al., 2005), however, recent determination of  $\alpha_{B3-B4}$  in seawater using a spectrophotometric approach has constrained  $\alpha_{B3-B4}$  in seawater to a value of  $1.0272 \pm 0.0006$  that is largely independent of temperature (Klochko et al., 2006). This value is significantly different from the theoretically estimated values (e.g. 1.0194 from Kakihana et al. (1977)) or empirically derived values (Liu et al., 2009; Pelejero et al., 2005; Wei et al., 2009; Xiao et al., 2006), which are both commonly used in earlier  $\delta^{11}\text{B}$  studies.

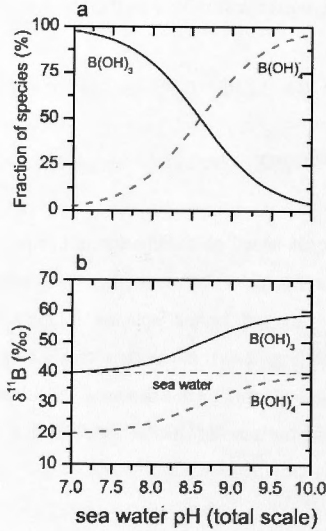


Fig. C-1 (a) Fraction and (b) boron isotopic composition of dissolved boron species as a function of pH. Adopted from Yu et al. (2007).

The theory behind the boron isotope seawater pH proxy is based on the assumption that corals precipitate aragonite in equilibrium with seawater. However, biological modification of coral aragonite  $\delta^{11}\text{B}$  from the  $\delta^{11}\text{B}$  value of  $\text{B(OH)}_4^-$  at a given

seawater pH remains a limiting factor for accurate seawater pH reconstruction. Biogenic calcification takes place within a physiologically controlled environment, with corals precipitating their calcium carbonate skeleton from an extracellular calcifying fluid that is located in the semi-isolated space between the skeleton and the calcicoblastic ectoderm (Al-Horani et al., 2003; Cohen and McConnaughey, 2003; Cohen and Holcomb, 2009; Ries, 2011). During active calcification, the pH of the calcifying fluid ( $\text{pH}_{\text{c}}$ ) is elevated by 0.2-0.5 pH units above ambient seawater (Al-Horani et al., 2003; Venn et al., 2011), resulting in the equilibrium composition of dissolved inorganic carbon (DIC) being shifted in favor of  $\text{CO}_3^{2-}$  relative to  $\text{HCO}_3^-$ , thus promoting the reaction 1-3 via the  $\text{Ca}^{2+}$ -ATPase pump which removes two  $\text{H}^+$  ions from the calcifying fluid in exchange for every  $\text{Ca}^{2+}$  ions (Al-Horani et al., 2003; Cohen and McConnaughey, 2003).

Micron-scale variations of  $\delta^{11}\text{B}$  in coral skeletons indicate pH variation at the calcification site of *Porites* ranging from 7.1 to 9.0 over a 6 months period (Allison et al., 2010; Blamart et al., 2007; Rollion-Bard et al., 2003). More recent studies of coral bulk  $\delta^{11}\text{B}$  analysis have shown the difference between  $\delta^{11}\text{B}$ -derived calcification pH and external seawater pH to be between  $\sim 0.3$  to  $\sim 1.0$  depending on species and ambient seawater pH (Krief et al., 2010; Trotter et al., 2011). This offset between the seawater pH and pH at the coral calcification site can be corrected using the species-dependent linear calibration of Trotter et al. (2011). These corrections allow the boron isotopic composition of corals to be used to accurately reconstruct surface water pH (more details about the calibration of physiological pH up-regulation are given in Chapter 4).

Appendix D. Coral geochemical records

Table D-1. Seasonal data for four *Porites* corals from the southern GBR. All coral cores are approximately 5-year geochemical proxy records at 2-month resolution.

Decimal year	$\delta^{13}\text{C}$ (‰)	$\delta^{18}\text{O}$ (‰)	Sr/Ca ( $\text{mmol mol}^{-1}$ )	Mg/Ca ( $\text{mmol mol}^{-1}$ )	$\delta^{21}\text{B}$ (‰)	$\pm 2\sigma$	$\text{pH}_T^a$	$\pm 1\sigma$
<i>Middle Pompey</i>								
2006.08	-2.21	-5.15	9.002	5.240	22.69	0.05	7.83	0.05
2005.92	-2.00	-4.84	-	-	23.40	0.06	7.92	0.05
2005.63	-2.46	-4.26	9.191	4.240	24.85	0.04	8.27	0.04
2005.29	-2.32	-4.59	-	-	24.04	0.04	8.06	0.04
2005.23	-2.17	-4.86	9.011	4.478	24.15	0.04	8.03	0.04
2005.10	-1.89	-4.94	9.007	4.362	23.83	0.04	7.97	0.04
2004.85	-1.88	-4.60	9.079	4.208	23.76	0.04	8.01	0.04
2004.56	-2.25	-4.25	9.193	4.079	26.42	0.04	8.47	0.03
2004.31	-2.42	-4.53	9.156	4.185	24.42	0.05	8.12	0.04
2004.23	-2.11	-4.87	9.020	4.364	23.05	0.04	7.89	0.04
2004.06	-1.95	-4.99	8.958	4.352	24.23	0.07	8.02	0.04
2003.85	-1.85	-4.61	9.097	4.144	25.35	0.04	8.25	0.03
2003.57	-2.13	-4.36	9.139	4.230	25.51	0.02	8.35	0.03
2003.28	-1.81	-4.84	9.005	4.331	23.59	0.05	7.97	0.04
2003.15	-1.73	-4.89	9.001	4.313	23.48	0.04	7.92	0.04
2002.90	-1.79	-4.70	9.081	4.179	23.77	0.04	8.01	0.04
2002.71	-2.07	-4.29	9.195	3.994	23.99	0.07	8.11	0.04
2002.54	-2.25	-4.19	9.196	4.010	24.67	0.04	8.25	0.04
2002.40	-2.23	-4.56	9.096	4.210	23.30	0.04	7.98	0.04
2002.21	-2.24	-4.94	8.989	4.416	22.33	0.05	7.78	0.05
2002.02	-2.09	-5.14	8.960	4.424	23.12	0.04	7.86	0.04
2001.94	-2.00	-5.03	8.969	4.438	23.82	0.05	7.98	0.04
2001.85	-2.13	-4.61	9.057	4.209	23.91	0.04	8.03	0.04
2001.63	-2.20	-4.32	9.193	4.025	24.58	0.03	8.21	0.03
2001.40	-2.14	-4.40	9.126	4.204	24.15	0.04	8.10	0.04
2001.25	-2.08	-4.76	8.976	4.355	23.49	0.04	7.94	0.05
2001.21	-2.10	-4.90	8.935	4.535	23.59	0.05	7.93	0.05
2000.98	-2.18	-4.84	9.002	4.468	24.21	0.04	8.06	0.04
2000.81	-2.30	-4.47	9.087	4.285	24.33	0.04	8.09	0.04
2000.58	-2.41	-4.11	9.219	3.950	24.61	0.04	8.23	0.04
2000.33	-2.60	-4.37	9.157	4.112	24.77	0.04	8.16	0.04
2000.06	-2.58	-4.66	9.044	4.232	24.08	0.04	8.01	0.04
<i>Little Kindermar</i>								
2006.08	-1.91	-4.67	9.040	5.542	23.31	0.06	7.87	0.05
2005.66	-2.42	-4.31	9.152	4.850	23.71	0.07	7.98	0.05
2005.49	-2.25	-4.44	9.101	4.694	23.91	0.04	8.12	0.04
2005.32	-1.99	-4.60	9.018	4.824	23.11	0.07	7.96	0.05
2005.16	-2.16	-4.79	9.048	4.843	24.42	0.04	8.07	0.04
2004.99	-1.92	-4.64	9.077	4.961	24.68	0.05	8.08	0.04
2004.82	-1.78	-4.35	9.059	4.882	24.36	0.05	8.05	0.04
2004.74	-2.01	-4.38	9.129	4.655	24.64	0.04	8.15	0.04
2004.57	-1.92	-4.21	9.108	4.433	24.91	0.04	8.24	0.04
2004.41	-1.98	-4.12	9.099	4.354	24.57	0.04	8.19	0.04
2004.24	-2.07	-4.16	9.106	4.289	24.57	0.04	8.11	0.04

Table D-1. (Continued)

Decimal year	$\delta^{13}\text{C}$ (‰)	$\delta^{18}\text{O}$ (‰)	Str/Ca (mmol mol <sup>-1</sup> )	Mg/Ca (mmol mol <sup>-1</sup> )	$\delta^{11}\text{B}$ (‰)	$\pm 2\sigma$	pH <sub>T</sub> <sup>a</sup>	$\pm 1\sigma$
2004.07	-2.04	-4.45	9.010	4.341	24.03	0.07	7.95	0.04
2003.90	-1.82	-4.58	9.014	4.423	24.79	0.07	8.06	0.04
2003.74	-1.21	-4.41	9.117	4.117	24.97	0.04	8.15	0.04
2003.57	-1.33	-4.12	9.197	3.970	25.20	0.04	8.28	0.03
2003.40	-1.85	-4.18	9.161	4.099	25.34	0.04	8.29	0.03
2003.23	-1.81	-4.39	9.097	4.217	25.11	0.04	8.17	0.04
2003.06	-1.65	-4.45	9.042	4.256	24.29	0.04	8.01	0.04
2002.89	-1.52	-4.53	9.108	4.132	24.46	0.04	8.07	0.04
2002.72	-1.49	-4.40	9.231	3.931	24.77	0.03	8.18	0.03
2002.55	-1.58	-4.17	9.218	4.062	24.90	0.04	8.26	0.04
2002.38	-1.83	-4.09	9.123	4.263	24.39	0.04	8.14	0.04
2002.21	-1.81	-4.16	9.071	4.300	24.36	0.05	8.04	0.04
2002.04	-1.72	-4.36	9.021	4.449	24.99	0.05	8.08	0.04
2001.87	-1.58	-4.55	9.070	4.479	24.10	0.04	8.00	0.04
2001.70	-1.55	-4.52	9.139	4.278	24.18	0.04	8.10	0.04
2001.53	-1.31	-4.22	9.159	4.329	24.38	0.04	8.17	0.04
2001.36	-1.63	-4.03	9.138	4.405	25.06	0.04	8.22	0.03
<i>Lady Musgrave Island</i>								
2008.73	-2.78	-4.12	9.408	4.625	23.34	0.04	8.06	0.04
2008.51	-3.02	-4.34	9.253	5.122	22.78	0.05	7.98	0.06
2008.29	-2.62	-4.65	8.988	5.237	22.77	0.04	7.89	0.05
2008.06	-2.61	-4.82	8.935	5.369	22.83	0.04	7.87	0.05
2007.81	-2.51	-4.52	9.119	4.757	23.67	0.03	8.07	0.05
2007.56	-2.49	-4.26	9.301	4.409	24.41	0.03	8.20	0.04
2007.36	-2.84	-4.22	9.243	4.692	23.96	0.04	8.06	0.04
2007.16	-2.67	-4.62	8.960	5.248	23.16	0.04	7.90	0.05
2006.96	-2.45	-4.74	8.932	5.012	22.85	0.04	7.88	0.05
2006.76	-2.37	-4.80	9.129	4.539	23.78	0.04	8.10	0.04
2006.56	-2.30	-4.04	9.256	4.284	24.36	0.03	8.18	0.03
2006.43	-2.67	-4.17	9.196	4.710	24.47	0.03	8.17	0.04
2006.30	-2.84	-4.48	9.053	5.124	23.81	0.03	8.02	0.04
2006.17	-2.68	-4.89	8.930	5.267	23.33	0.04	7.93	0.04
2006.04	-2.53	-4.89	8.916	5.070	22.91	0.03	7.85	0.05
2005.91	-2.29	-4.68	8.937	4.784	22.83	0.04	7.86	0.05
2005.78	-2.13	-4.37	9.103	4.159	24.52	0.03	8.16	0.04
2005.65	-2.70	-4.19	9.264	4.031	24.36	0.03	8.17	0.04
2005.45	-2.20	-4.27	9.214	4.275	23.72	0.03	8.08	0.04
2005.25	-2.46	-4.75	8.954	4.760	23.39	0.03	7.96	0.05
2005.05	-2.63	-4.78	8.933	4.556	23.20	0.03	7.90	0.05
2004.85	-2.44	-4.35	9.184	4.022	23.59	0.03	8.01	0.04
2004.65	-2.88	-4.19	9.225	4.101	24.42	0.03	8.19	0.04
2004.47	-3.13	-4.44	9.089	4.600	23.90	0.03	8.10	0.04
2004.29	-3.06	-4.90	8.937	4.903	22.74	0.04	7.88	0.05
2004.10	-2.84	-4.97	8.874	4.730	22.71	0.03	7.82	0.05
2003.92	-2.54	-4.71	9.074	4.329	23.47	0.03	7.98	0.04
2003.74	-2.40	-4.52	9.156	4.179	24.15	0.03	8.14	0.04



Table D-1. (Continued)

Decadal year	$\delta^{13}\text{C}$ (‰)	$\delta^{18}\text{O}$ (‰)	Sr/Ca ( $\text{mmol mol}^{-1}$ )	Mg/Ca ( $\text{mmol mol}^{-1}$ )	$\delta^{11}\text{B}$ (‰)	$\pm 2\sigma$	$\text{pH}_T^a$	$\pm 1\sigma$
2003.56	-2.65	-4.26	9.163	4.337	23.96	0.03	8.13	0.04
2003.40	-2.84	-4.59	9.092	4.680	23.66	0.03	8.05	0.04
<i>Fitzroy Reef</i>								
2008.77	-2.36	-4.01	9.691	6.823	25.44	0.03	8.30	0.03
2008.54	-2.77	-4.44	9.329	5.812	24.25	0.04	8.19	0.04
2008.38	-2.44	-4.91	9.080	5.235	23.79	0.06	8.04	0.03
2008.02	-2.09	-4.88	9.033	4.971	23.79	0.03	8.01	0.04
2007.81	-1.87	-4.37	9.233	4.533	24.59	0.03	8.18	0.03
2007.60	-2.52	-3.86	9.481	4.227	24.65	0.03	8.24	0.03
2007.42	-3.18	-4.28	9.229	4.692	23.77	0.03	8.07	0.04
2007.24	-2.45	-4.81	9.065	4.842	23.15	0.05	7.93	0.05
2007.05	-2.15	-4.79	9.086	4.838	23.24	0.06	7.93	0.05
2006.87	-1.92	-4.48	9.175	4.488	23.75	0.04	8.04	0.04
2006.69	-2.16	-4.11	9.325	4.173	24.55	0.04	8.21	0.03
2006.53	-2.72	-4.00	9.327	4.368	24.45	0.05	8.20	0.04
2006.38	-2.54	-4.38	9.162	4.731	24.52	0.03	8.16	0.04
2006.22	-1.97	-4.82	9.037	4.796	24.07	0.06	8.04	0.04
2006.07	-1.42	-4.81	9.031	4.530	23.47	0.10	7.93	0.07
2005.91	-1.61	-4.75	9.148	4.524	23.97	0.04	8.03	0.03
2005.76	-2.24	-4.05	9.343	4.177	24.92	0.04	8.23	0.03
2005.60	-2.67	-3.89	9.423	4.258	24.51	0.04	8.20	0.04
2005.45	-2.71	-4.27	9.230	4.679	24.47	0.04	8.15	0.03
2005.30	-2.27	-4.74	9.074	4.879	23.85	0.08	8.01	0.05
2005.14	-1.84	-4.87	9.002	4.845	24.14	0.05	8.03	0.04
2004.99	-1.78	-4.59	9.132	4.711	24.03	0.04	8.06	0.04
2004.84	-1.81	-4.10	9.352	4.228	25.09	0.05	8.25	0.04
2004.69	-2.27	-3.90	9.392	4.170	24.67	0.03	8.23	0.04
2004.50	-2.54	-4.35	9.203	4.636	24.03	0.03	8.12	0.04
2004.32	-2.32	-4.84	9.060	4.798	24.37	0.03	8.10	0.04
2004.14	-2.03	-4.89	9.063	4.847	23.26	0.04	7.90	0.04
2003.96	-2.08	-4.76	9.103	4.871	23.53	0.04	7.96	0.04
2003.78	-1.95	-4.19	9.235	4.454	24.27	0.04	8.12	0.03
2003.60	-2.39	-3.98	9.392	4.311	24.71	0.05	8.23	0.04
2003.35	-2.88	-4.46	9.263	4.703	23.92	0.05	8.10	0.04

<sup>a</sup>  $\text{pH}_T$  = Calculated  $\delta^{11}\text{B}$ -derived seawater pH in total scale taking into account of physiological pH up-regulation

Table D-2. Long-term annual coral geochemical and isotopic records from Middle Pompey over 1905-2005

<i>Middle Pompey</i>										
Sample ID	year	$\delta^{13}\text{C}$ (‰)	$\delta^{18}\text{O}$ (‰)	Sr/Ca ( $\text{mmol mol}^{-1}$ )	Mg/Ca ( $\text{mmol mol}^{-1}$ )	$\delta^{11}\text{B}$ (‰)	$\pm 2\sigma$	pH <sub>T</sub> <sup>a</sup>	$\pm 1\sigma$	
PSC-1	2005	-2.10	-4.65	9.048	4.732	24.33	0.04	8.07	0.03	
PSC-2	2004	-2.09	-4.67	9.121	4.148	23.44	0.03	7.95	0.04	
PSC-3	2003	-1.85	-4.68	9.117	4.078	23.29	0.04	7.93	0.04	
PSC-4	2002	-2.16	-4.69	9.110	4.068	23.45	0.04	7.95	0.03	
PSC-5	2001	-2.20	-4.58	9.135	4.170	23.95	0.02	8.03	0.03	
PSC-6	2000	-2.50	-4.54	9.135	4.138	23.31	0.05	7.95	0.04	
PSC-7	1999	-2.12	-4.60	9.043	4.124	23.44	0.04	7.95	0.05	
PSC-8	1998	-2.14	-4.68	9.077	4.227	23.21	0.04	7.91	0.04	
PSC-9	1997	-2.10	-4.70	9.135	4.388	23.28	0.04	7.95	0.04	
PSC-10	1996	-2.18	-4.72	9.129	4.182	23.20	0.04	7.93	0.05	
PSC-11	1995	-2.20	-4.70	9.114	4.199	23.10	0.07	7.91	0.05	
PSC-12	1994	-2.22	-4.61	9.108	4.238	23.33	0.05	7.95	0.04	
PSC-13	1993	-1.87	-4.50	9.123	4.099	23.14	0.04	7.91	0.04	
PSC-14	1992	-2.10	-4.63	9.126	4.253	23.13	0.04	7.92	0.04	
PSC-15	1991	-1.67	-4.62	9.131	4.001	22.92	0.05	7.89	0.04	
PSC-16	1990	-1.91	-4.44	9.119	4.070	23.07	0.04	7.90	0.05	
PSC-17	1989	-1.99	-4.69	9.056	4.203	23.46	0.05	7.97	0.04	
PSC-18	1988	-1.76	-4.76	9.044	4.248	22.76	0.04	7.86	0.04	
PSC-19	1987	-1.91	-4.55	9.037	4.182	22.77	0.04	7.85	0.04	
PSC-20	1986	-1.81	-4.65	9.073	4.185	23.07	0.03	7.90	0.04	
PSC-21	1985	-1.89	-4.60	9.107	4.166	22.74	0.07	7.86	0.06	
PSC-22	1984	-1.71	-4.45	9.132	4.111	22.62	0.06	7.84	0.05	
PSC-23	1983	-1.71	-4.45	9.137	4.111	22.63	0.05	7.84	0.04	
PSC-24	1982	-1.67	-4.53	9.137	4.035	22.90	0.04	7.89	0.04	
PSC-25	1981	-1.66	-4.63	9.124	4.131	22.75	0.03	7.86	0.04	
PSC-26	1980	-1.77	-4.45	9.193	4.198	23.97	0.05	8.03	0.04	
PSC-27	1979	-1.73	-4.52	9.128	4.239	23.39	0.06	7.95	0.04	
PSC-28	1978	-2.00	-4.46	9.132	4.177	23.70	0.05	7.99	0.04	
PSC-29	1977	-1.74	-4.65	9.097	4.147	23.31	0.08	7.95	0.05	
PSC-30	1976	-1.68	-4.57	9.099	4.103	23.67	0.05	8.00	0.05	
PSC-31	1975	-1.60	-4.64	9.140	4.095	23.56	0.06	7.98	0.04	
PSC-32	1974	-1.68	-4.69	9.076	4.093	23.27	0.05	7.94	0.04	
PSC-33	1973	-1.66	-4.64	9.114	4.13	23.86	0.05	8.00	0.04	
PSC-34	1972	-1.58	-4.64	9.146	4.14	23.83	0.08	8.03	0.04	
PSC-35	1971	-1.66	-4.69	9.163	4.141	23.56	0.04	7.98	0.04	
PSC-36	1970	-1.74	-4.81	9.137	4.076	23.24	0.06	7.94	0.04	
PSC-37	1969	-1.62	-4.61	9.149	4.033	23.33	0.07	7.94	0.04	
PSC-38	1968	-1.45	-4.56	9.170	3.953	23.04	0.07	7.91	0.06	
PSC-39	1967	-1.57	-4.55	9.200	3.976	23.21	0.04	7.94	0.03	
PSC-40	1966	-1.44	-4.47	9.206	3.985	23.11	0.04	7.93	0.06	
PSC-41	1965	-1.51	-4.51	9.141	3.963	23.00	0.05	7.91	0.05	
PSC-42	1964	-1.62	-4.72	9.140	4.031	22.61	0.06	7.85	0.06	
PSC-43	1963	-1.60	-4.53	9.173	3.988	22.83	0.06	7.88	0.06	
PSC-44	1962	-1.69	-4.53	9.191	4.021	22.45	0.06	7.82	0.06	
PSC-45	1961	-1.59	-4.60	9.181	3.983	22.69	0.08	7.87	0.07	
PSC-46	1960	-1.80	-4.35	9.155	4.168	23.33	0.21	7.94	0.05	
PSC-47	1959	-1.81	-4.51	9.155	4.148	22.85	0.17	7.88	0.05	

Table D-2. (Continued)

Sample ID	year	$\delta^{13}\text{C}$ (‰)	$\delta^{18}\text{O}$ (‰)	Sr/Ca ( $\text{mmol mol}^{-1}$ )	Mg/Ca ( $\text{mmol mol}^{-1}$ )	$\delta^{11}\text{B}$ (‰)	$\pm 2\sigma$	$\text{pH}_T^a$	$\pm 1\sigma$
PSC-48	1958	-1.62	-4.35	9.163	4.061	23.26	0.05	7.92	0.04
PSC-49	1957	-1.75	-4.64	9.152	4.153	23.47	0.05	7.98	0.04
PSC-50	1956	-1.71	-4.58	9.163	4.162	23.44	0.05	7.97	0.03
PSC-51	1955	-1.96	-4.54	9.096	4.189	24.13	0.05	8.06	0.04
PSC-52	1954	-2.00	-4.53	9.148	4.145	23.64	0.05	8.00	0.04
PSC-53	1953	-1.86	-4.64	9.149	4.217	23.50	0.03	7.98	0.04
PSC-54	1952	-1.99	-4.61	9.151	4.265	24.25	0.04	8.08	0.03
PSC-55	1951	-2.13	-4.50	9.172	4.329	24.38	0.08	8.11	0.03
PSC-56	1950	-2.05	-4.31	9.163	4.247	24.65	0.05	8.13	0.03
PSC-57	1949	-2.24	-4.54	9.104	4.385	24.94	0.05	8.18	0.03
PSC-58	1948	-2.28	-4.51	9.114	4.369	25.22	0.04	8.21	0.03
PSC-59	1947	-2.60	-4.51	9.112	4.547	24.41	0.06	8.10	0.03
PSC-60	1946	-2.41	-4.59	9.063	4.522	23.59	0.08	7.99	0.04
PSC-61	1945	-2.04	-4.56	9.079	4.463	23.92	0.07	8.03	0.03
PSC-62	1944	-2.10	-4.61	9.140	4.413	24.24	0.06	8.08	0.03
PSC-63	1943	-2.08	-4.47	9.141	4.312	24.40	0.15	8.09	0.03
PSC-64	1942	-2.10	-4.49	9.108	4.391	24.04	0.06	8.03	0.04
PSC-65	1941	-2.00	-4.45	9.104	4.332	24.02	0.04	8.04	0.04
PSC-66	1940	-2.01	-4.53	9.200	4.281	23.46	0.04	7.98	0.04
PSC-67	1939	-1.80	-4.58	9.176	4.261	23.48	0.05	7.99	0.04
PSC-68	1938	-1.88	-4.42	9.220	4.099	23.19	0.03	7.93	0.04
PSC-69	1937	-1.87	-4.62	9.174	4.259	23.47	0.11	7.99	0.04
PSC-70	1936	-1.87	-4.50	9.192	4.180	22.86	0.10	7.89	0.06
PSC-71	1935	-1.87	-4.55	9.224	4.182	23.54	0.07	7.99	0.06
PSC-72	1934	-1.71	-4.62	9.152	4.212	23.80	0.09	8.03	0.03
PSC-73	1933	-1.93	-4.62	9.179	4.241	23.61	0.03	8.00	0.03
PSC-74	1932	-1.88	-4.69	9.167	4.318	23.96	0.07	8.05	0.04
PSC-75	1931	-1.63	-4.62	9.146	4.163	24.22	0.06	8.07	0.03
PSC-76	1930	-1.65	-4.44	9.173	4.163	23.67	0.05	8.01	0.03
PSC-77	1929	-1.89	-4.45	9.178	4.189	24.12	0.03	8.07	0.03
PSC-78	1928	-1.76	-4.55	9.124	4.167	24.52	0.07	8.12	0.03
PSC-79	1927	-1.70	-4.47	9.186	4.261	24.25	0.06	8.09	0.03
PSC-80	1926	-1.62	-4.56	9.151	4.190	24.40	0.06	8.10	0.03
PSC-81	1925	-1.60	-4.46	9.169	4.187	23.69	0.05	8.02	0.03
PSC-82	1924	-1.52	-4.47	9.190	4.038	24.07	0.05	8.06	0.03
PSC-83	1923	-1.49	-4.45	9.183	4.103	24.32	0.05	8.10	0.03
PSC-84	1922	-1.14	-4.37	9.138	4.224	24.40	0.03	8.11	0.03
PSC-85	1921	-1.70	-4.51	9.142	4.251	24.27	0.04	8.09	0.03
PSC-86	1920	-1.88	-4.44	9.089	4.315	24.93	0.03	8.17	0.03
PSC-87	1919	-1.91	-4.39	9.119	4.286	25.03	0.05	8.20	0.03
PSC-88	1918	-1.83	-4.44	9.172	4.498	24.57	0.04	8.13	0.03
PSC-89	1917	-1.81	-4.56	9.166	4.164	25.09	0.04	8.20	0.04
PSC-90	1916	-2.09	-4.52	9.147	4.201	25.07	0.03	8.19	0.03
PSC-91	1915	-1.99	-4.59	9.086	4.266	25.20	0.04	8.20	0.03
PSC-92	1914	-1.76	-4.51	9.101	4.268	24.88	0.03	8.17	0.03
PSC-93	1913	-1.65	-4.55	9.197	4.178	24.18	0.05	8.09	0.03
PSC-94	1912	-1.52	-4.49	9.158	4.108	24.31	0.04	8.09	0.03

Table D-2. (Continued)

Sample ID	year	$\delta^{13}\text{C}$ (‰)	$\delta^{18}\text{O}$ (‰)	Sr/Ca ( $\text{mmol mol}^{-1}$ )	Mg/Ca ( $\text{mmol mol}^{-1}$ )	$\delta^{11}\text{B}$ (‰)	$\pm 2\sigma$	$\text{pH}_T^a$	$\pm 1\sigma$
PSC-95	1911	-1.75	-4.47	9.120	4.149	24.38	0.08	8.10	0.04
PSC-96	1910	-1.97	-4.56	9.145	4.179	24.03	0.12	8.06	0.07
PSC-97	1909	-1.84	-4.66	9.130	4.224	23.93	0.08	8.04	0.04
PSC-98	1908	-1.61	-4.38	9.170	4.127	24.15	0.05	8.07	0.03
PSC-99	1907	-1.57	-4.56	9.136	4.098	23.55	0.06	7.98	0.04

<sup>a</sup>  $\text{pH}_T$  = Calculated  $\delta^{11}\text{B}$ -derived seawater pH in total scale taking into account of physiological pH up-regulation



**Table D-3.** Long-term coral geochemical and isotopic records from Little Kindermar over 1835-2005. Annual records are resolved from 1940 to 2005 and 5-year interval coral records are obtained from 1835 to 1939.

*Little Kindermar*

Sample ID	year	$\delta^{13}\text{C}$ (‰)	$\delta^{18}\text{O}$ (‰)	Sr/Ca (mmol mol <sup>-1</sup> )	Mg/Ca (mmol mol <sup>-1</sup> )	$\delta^{11}\text{B}$ (‰)	$\pm 2\sigma$	pH <sub>T</sub> <sup>a</sup>	$\pm 1\sigma$
	2005 <sup>b</sup>	-2.00	-4.44	9.080	4.803	23.79	0.06	7.99	0.05
	2004 <sup>b</sup>	-1.69	-4.34	9.075	4.542	24.57	0.06	8.10	0.05
	2003 <sup>b</sup>	-1.68	-4.32	9.120	4.132	24.89	0.06	8.15	0.04
	2002 <sup>b</sup>	-1.60	-4.31	9.122	4.247	24.58	0.05	8.10	0.04
PSA-1	2001	-1.43	-4.41	9.081	4.514	23.96	0.06	8.02	0.07
PSA-2	2000	-1.42	-4.31	9.161	4.452	23.44	0.06	7.96	0.06
PSA-3	1999	-1.50	-4.18	9.131	4.164	24.74	0.06	8.13	0.05
PSA-4	1998	-1.51	-4.32	9.029	4.454	25.55	0.04	8.22	0.04
PSA-5	1997	-1.26	-4.34	9.155	4.323	24.79	0.05	8.15	0.05
PSA-6	1996	-1.45	-4.27	9.117	4.325	24.75	0.03	8.13	0.04
PSA-7	1995	-1.62	-4.25	9.107	4.527	23.78	0.05	8.00	0.05
PSA-8	1994	-1.27	-4.16	9.117	4.360	24.45	0.05	8.10	0.05
PSA-9	1993	-1.48	-4.40	9.101	4.558	23.14	0.05	7.91	0.04
PSA-10	1992	-1.60	-4.42	9.109	4.579	23.45	0.04	7.96	0.04
PSA-11	1991	-1.75	-4.50	9.131	4.385	24.21	0.04	8.07	0.04
PSA-12	1990	-1.64	-4.22	9.126	4.414	23.78	0.06	8.00	0.05
PSA-13	1989	-1.64	-4.25	9.057	4.311	23.15	0.05	7.92	0.06
PSA-14	1988	-1.79	-4.54	9.001	4.569	22.15	0.08	7.76	0.07
PSA-15	1987	-2.19	-4.19	9.132	4.354	23.07	0.10	7.90	0.07
PSA-16	1986	-1.92	-4.44	9.066	4.296	24.07	0.05	8.04	0.05
PSA-17	1985	-1.86	-4.36	9.137	3.989	24.04	0.03	8.04	0.04
PSA-18	1984	-1.42	-4.32	9.120	4.070	23.67	0.05	7.99	0.05
PSA-19	1983	-1.58	-4.37	9.187	4.106	24.29	0.10	8.07	0.06
PSA-20	1982	-1.20	-4.10	9.157	4.176	23.61	0.04	7.98	0.05
PSA-21	1981	-1.45	-4.22	9.113	4.157	23.59	0.05	7.97	0.04
PSA-22	1980	-1.31	-4.22	9.089	4.186	24.43	0.04	8.09	0.04
PSA-23	1979	-1.69	-4.09	9.123	4.141	24.10	0.04	8.05	0.05
PSA-24	1978	-2.14	-4.14	9.131	4.286	23.76	0.05	8.00	0.04
PSA-25	1977	-1.99	-4.35	9.111	4.178	23.29	0.04	7.94	0.05
PSA-26	1976	-1.68	-4.28	9.152	4.035	24.40	0.04	8.10	0.04
PSA-27	1975	-1.43	-4.26	9.116	4.129	24.44	0.04	8.09	0.04
PSA-28	1974	-1.46	-4.35	9.184	3.940	24.49	0.05	8.11	0.04
PSA-29	1973	-1.75	-4.42	9.136	4.218	23.61	0.04	7.96	0.04
PSA-30	1972	-1.42	-4.33	9.187	4.150	23.70	0.05	8.00	0.05
PSA-31	1971	-1.00	-4.25	9.102	4.477	25.14	0.07	8.18	0.05
PSA-32	1970	-1.03	-4.36	9.092	4.811	24.06	0.06	8.03	0.05
PSA-33	1969	-1.25	-4.38	9.130	4.704	24.07	0.06	8.04	0.05
PSA-34	1968	-1.01	-4.24	9.151	4.420	24.64	0.05	8.12	0.04
PSA-35	1967	-0.94	-4.25	9.130	4.449	24.68	0.07	8.14	0.05
PSA-36	1966	-1.44	-4.26	9.129	4.771	24.23	0.04	8.08	0.04
PSA-37	1965	-1.03	-4.13	9.156	4.568	23.81	0.04	8.02	0.04
PSA-38	1964	-1.06	-4.32	9.126	4.549	24.31	0.03	8.07	0.04
PSA-39	1963	-0.78	-4.39	9.101	4.822	25.09	0.09	8.19	0.05
PSA-40	1962	-0.87	-4.29	9.140	4.531	24.55	0.04	8.11	0.04
PSA-41	1961	-0.67	-4.36	9.153	4.124	24.58	0.04	8.13	0.04
PSA-42	1960	-0.70	-4.39	9.213	3.927	24.83	0.04	8.15	0.04
PSA-43	1959	-0.43	-4.24	9.198	3.880	24.95	0.03	8.17	0.03

Table D-3. (Continued)

Sample ID	year	$\delta^{13}\text{C}$ (‰)	$\delta^{18}\text{O}$ (‰)	Sr/Ca ( $\text{mmol mol}^{-1}$ )	Mg/Ca ( $\text{mmol mol}^{-1}$ )	$\delta^{11}\text{B}$ (‰)	$\pm 2\sigma$	$\text{pH}_T^a$	$\pm 1\sigma$
PSA-44	1958	-0.59	-4.21	9.244	3.816	25.40	0.05	8.22	0.04
PSA-45	1957	-0.70	-4.37	9.201	3.988	25.07	0.05	8.19	0.04
PSA-46	1956	-1.03	-4.22	9.135	4.238	23.95	0.04	8.03	0.04
PSA-47	1955	-1.01	-4.30	9.195	4.153	24.87	0.04	8.17	0.04
PSA-48	1954	-1.00	-4.21	9.198	4.060	24.61	0.03	8.13	0.03
PSA-49	1953	-1.00	-4.36	9.211	4.053	24.39	0.05	8.10	0.04
PSA-50	1952	-0.94	-4.36	9.128	4.478	23.67	0.04	7.99	0.05
PSA-51	1951	-0.87	-4.29	9.096	4.536	23.26	0.04	7.95	0.05
PSA-52	1950	-0.74	-4.34	9.164	4.412	24.27	0.04	8.09	0.04
PSA-53	1949	-0.57	-4.16	9.205	4.465	23.98	0.03	8.05	0.04
PSA-54	1948	-0.32	-4.18	9.197	4.243	24.14	0.03	8.07	0.04
PSA-55	1947	-0.84	-4.17	9.126	4.418	23.15	0.04	7.93	0.04
PSA-56	1946	-0.78	-4.22	9.111	4.408	23.45	0.07	7.97	0.05
PSA-57	1945	-1.08	-4.29	9.094	4.433	23.26	0.04	7.94	0.05
PSA-58	1944	-1.04	-4.34	9.156	4.534	23.69	0.04	8.00	0.04
PSA-59	1943	-1.05	-4.17	9.117	4.739	23.68	0.03	7.99	0.04
PSA-60	1942	-0.73	-4.23	9.093	4.757	23.80	0.03	7.99	0.03
PSA-61	1941	-1.03	-4.10	9.106	4.742	24.26	0.03	8.08	0.04
PSA-62	1940	-0.78	-4.20	9.144	4.669	23.91	0.05	8.03	0.04
PSA-63	1937	-1.01	-4.34	9.110	4.670	24.32	0.04	8.09	0.04
PSA-64	1932	-1.05	-4.35	9.115	4.881	23.81	0.04	8.02	0.04
PSA-65	1927	-0.69	-4.27	9.164	4.165	23.84	0.08	8.03	0.05
PSA-66	1922	-0.89	-4.26	9.219	4.112	25.42	0.04	8.25	0.03
PSA-67	1917	-0.87	-4.27	9.191	3.933	25.10	0.06	8.20	0.04
PSA-68	1912	-1.04	-4.26	9.164	4.168	24.65	0.07	8.14	0.04
PSA-69	1907	-0.54	-4.31	9.207	3.944	25.22	0.04	8.22	0.04
PSA-70	1902	-0.46	-4.20	9.175	3.992	25.30	0.03	8.23	0.03
PSA-71	1897	-0.77	-4.25	9.135	4.132	24.31	0.04	8.09	0.04
PSA-72	1892	-1.23	-4.43	9.154	4.074	25.18	0.04	8.20	0.04
PSA-73	1887	-1.31	-4.30	9.186	3.794	25.40	0.05	8.24	0.04
PSA-74	1882	-0.78	-4.25	9.259	3.893	24.88	0.04	8.17	0.04
PSA-75	1877	-1.04	-4.32	9.172	4.243	24.79	0.04	8.14	0.03
PSA-76	1872	-0.15	-4.17	9.188	3.945	25.54	0.05	8.25	0.04
PSA-77	1867	-0.09	-4.23	9.179	4.324	25.80	0.05	8.28	0.04
PSA-78	1862	-0.65	-4.20	9.133	4.195	25.28	0.04	8.21	0.04
PSA-79	1857	-0.20	-4.05	9.212	4.531	25.34	0.05	8.25	0.04
PSA-80	1852	-0.40	-4.20	9.151	4.220	24.96	0.05	8.17	0.04
PSA-81	1847	-0.62	-4.20	9.199	4.292	25.53	0.04	8.27	0.04
PSA-82	1842	-0.91	-4.18	9.174	4.552	24.88	0.06	8.17	0.04
PSA-83	1837	-0.67	-4.11	9.199	4.501	25.59	0.05	8.28	0.04

<sup>a</sup>  $\text{pH}_T$  = Calculated  $\delta^{11}\text{B}$ -derived seawater pH in total scale taking into account of physiological pH up-regulation

<sup>c</sup> averaged values from high resolution (i.e. bimonthly) data in each year

Appendices

Table D-4. Long-term annual coral geochemical and isotopic records from Fitzroy Reef over 1950-2008

Fitzroy Reef									
Sample ID	year	$\delta^{13}\text{C}$ (‰)	$\delta^{18}\text{O}$ (‰)	Sr/Ca (mmol mol <sup>-2</sup> )	Mg/Ca (mmol mol <sup>-1</sup> )	$\delta^{11}\text{B}$ (‰)	$\pm 2\sigma$	pH <sub>T</sub> <sup>a</sup>	$\pm 1\sigma$
	2008 <sup>b</sup>	-2.31	-4.52	9.273	5.475	24.37	0.04	8.14	0.03
	2007 <sup>b</sup>	-2.44	-4.44	9.207	4.617	23.71	0.04	8.04	0.04
	2006 <sup>b</sup>	-2.10	-4.42	9.196	4.471	24.28	0.05	8.11	0.04
	2005 <sup>b</sup>	-2.18	-4.41	9.202	4.600	24.35	0.05	8.11	0.04
	2004 <sup>b</sup>	-2.20	-4.49	9.176	4.629	24.02	0.04	8.07	0.04
FYR08-D-1	2003	-2.25	-4.60	9.232	4.749	23.53	0.04	8.01	0.04
FYR08-D-2	2002	-2.13	-4.42	9.180	4.687	24.35	0.04	8.11	0.04
FYR08-D-3	2001	-2.36	-4.47	9.222	4.828	24.56	0.03	8.15	0.04
FYR08-D-4	2000	-2.31	-4.52	9.188	4.850	24.69	0.04	8.18	0.04
FYR08-D-5	1999	-2.27	-4.46	9.155	4.944	24.86	0.03	8.19	0.04
FYR08-D-6	1998	-1.85	-4.11	9.309	4.515	24.78	0.03	8.16	0.04
FYR08-D-7	1997	-2.13	-4.28	9.292	4.634	24.62	0.03	8.17	0.03
FYR08-D-8	1996	-2.08	-4.34	9.180	4.683	24.39	0.03	8.12	0.03
FYR08-D-9	1995	-2.06	-4.47	9.207	4.654	24.23	0.04	8.10	0.04
FYR08-D-10	1994	-2.05	-4.20	9.297	4.623	24.18	0.04	8.11	0.04
FYR08-D-11	1993	-1.91	-4.26	9.244	4.769	24.81	0.03	8.19	0.03
FYR08-D-12	1992	-2.01	-4.43	9.217	4.716	24.54	0.04	8.15	0.04
FYR08-D-13	1991	-2.04	-4.46	9.210	4.721	24.49	0.04	8.15	0.04
FYR08-D-14	1990	-1.77	-4.45	9.257	4.608	25.26	0.04	8.26	0.03
FYR08-D-15	1989	-2.50	-4.32	9.190	4.886	24.71	0.03	8.18	0.03
FYR08-D-16	1988	-1.99	-4.29	9.327	4.685	25.22	0.04	8.24	0.03
FYR08-D-17	1987	-1.08	-4.32	9.344	4.517	25.03	0.04	8.22	0.03
FYR08-D-18	1986	-1.21	-4.16	9.347	4.193	24.77	0.06	8.18	0.05
FYR08-D-19	1985	-1.63	-4.25	9.323	4.421	25.12	0.05	8.24	0.03
FYR08-D-20	1984	-1.56	-4.36	9.241	4.582	25.03	0.06	8.23	0.03
FYR08-D-21	1983	-1.38	-4.36	9.224	4.576	25.72	0.04	8.31	0.03
FYR08-D-22	1982	-1.83	-4.37	9.215	4.973	24.80	0.05	8.19	0.04
FYR08-D-23	1981	-1.39	-4.33	9.260	5.325	24.61	0.03	8.14	0.03
FYR08-D-24	1980	-1.80	-4.60	9.211	4.757	24.11	0.03	8.10	0.03
FYR08-D-25	1979	-1.83	-4.50	9.201	4.859	24.34	0.03	8.13	0.03
FYR08-D-26	1978	-2.15	-4.47	9.216	5.242	25.13	0.04	8.24	0.03
FYR08-D-27	1977	-2.34	-4.35	9.261	5.019	24.91	0.03	8.21	0.03
FYR08-D-28	1976	-1.48	-4.22	9.310	4.758	25.36	0.03	8.27	0.03
FYR08-D-29	1975	-1.11	-4.28	9.258	4.674	25.43	0.03	8.27	0.03
FYR08-D-30	1974	-1.55	-4.64	9.172	5.119	24.81	0.03	8.20	0.03
FYR08-D-31	1973	-2.42	-4.39	9.201	5.125	25.36	0.04	8.25	0.03
FYR08-D-32	1972	-1.63	-4.24	9.285	4.804	24.79	0.03	8.19	0.03
FYR08-D-33	1971	-1.19	-4.29	9.321	4.683	24.91	0.03	8.21	0.03
FYR08-D-34	1970	-1.13	-4.59	9.258	5.015	24.86	0.03	8.20	0.03
FYR08-D-35	1969	-1.42	-4.34	9.215	4.888	24.90	0.04	8.19	0.03
FYR08-D-36	1968	-1.29	-4.19	9.246	4.650	24.65	0.04	8.17	0.04
FYR08-D-37	1967	-1.50	-4.18	9.280	4.488	24.32	0.03	8.13	0.04
FYR08-D-38	1966	-1.42	-4.35	9.286	4.408	24.05	0.03	8.10	0.04
FYR08-D-39	1965	-1.58	-4.47	9.289	4.406	23.82	0.04	8.08	0.04
FYR08-D-40	1964	-1.61	-4.33	9.249	4.412	24.17	0.04	8.10	0.04
FYR08-D-41	1963	-1.79	-4.23	9.374	4.261	24.14	0.03	8.12	0.04
FYR08-D-42	1962	-1.58	-4.43	9.268	4.404	23.96	0.04	8.08	0.04

Table D-4. (Continued)

Sample ID	year	$\delta^{13}\text{C}$ (‰)	$\delta^{18}\text{O}$ (‰)	Sr/Ca (mmol mol <sup>-1</sup> )	Mg/Ca (mmol mol <sup>-1</sup> )	$\delta^{11}\text{B}$ (‰)	$\pm 2\sigma$	$\text{pH}_{\text{T}}^{\text{a}}$	$\pm 1\sigma$
FYR08-D-43	1961	-1.51	-4.29	9.274	4.518	24.27	0.04	8.13	0.04
FYR08-D-44	1960	-1.34	-4.28	9.272	4.416	24.66	0.03	8.17	0.03
FYR08-D-45	1959	-1.59	-4.07	9.261	4.554	24.13	0.03	8.09	0.04
FYR08-D-46	1958	-1.80	-4.39	9.264	4.733	24.35	0.03	8.13	0.03
FYR08-D-47	1957	-1.65	-4.25	9.185	5.596	24.15	0.03	8.10	0.04
FYR08-D-48	1956	-1.35	-3.88	9.331	6.229	24.80	0.03	8.19	0.03
FYR08-D-49	1955	-1.12	-4.05	9.248	5.010	24.20	0.04	8.11	0.04
FYR08-D-50	1954	-1.30	-4.37	9.269	4.564	24.52	0.03	8.16	0.03
FYR08-D-51	1953	-1.27	-4.57	9.218	4.523	24.39	0.03	8.14	0.04
FYR08-D-52	1952	-1.08	-4.47	9.300	4.636	24.44	0.04	8.15	0.04
FYR08-D-53	1951	-1.04	-4.37	9.289	4.632	24.16	0.04	8.13	0.04
FYR08-D-54	1950	-1.40	-4.38	9.292	4.765	24.16	0.03	8.12	0.04

<sup>a</sup>  $\text{pH}_{\text{T}}$  = Calculated  $\delta^{11}\text{B}$ -derived seawater pH in total scale taking into account of physiological pH up-regulation

<sup>c</sup> averaged values from high resolution (i.e. bimonthly) data in each year



Appendices

**Table D-5.** Long-term annual coral geochemical and isotopic records from Lady Musgrave Island over 1890-2008

*Lady Musgrave Island*

Sample ID	year	$\delta^{13}\text{C}$ (‰)	$\delta^{18}\text{O}$ (‰)	Sr/Ca (mmol mol <sup>-1</sup> )	Mg/Ca (mmol mol <sup>-1</sup> )	$\delta^{\text{H}}\text{B}$ (‰)	$\pm 2\sigma$	pH <sub>T</sub> <sup>a</sup>	$\pm 1\sigma$
	2008 <sup>b</sup>	-2.76	-4.48	9.146	5.088	22.93	0.04	7.94	0.05
	2007 <sup>b</sup>	-2.59	-4.47	9.111	4.824	23.61	0.03	8.03	0.04
	2006 <sup>b</sup>	-2.52	-4.56	9.060	4.825	23.64	0.03	8.03	0.04
	2005 <sup>b</sup>	-2.43	-4.45	9.109	4.301	23.80	0.03	8.04	0.04
	2004 <sup>b</sup>	-2.89	-4.64	9.040	4.533	23.45	0.03	7.99	0.04
LMI08-H-1	2003	-3.11	-4.52	9.148	4.532	23.34	0.06	7.98	0.06
LMI08-H-2	2002	-3.32	-4.55	9.131	4.684	23.55	0.04	8.01	0.04
LMI08-H-3	2001	-3.06	-4.53	9.156	4.521	23.31	0.05	7.98	0.04
LMI08-H-4	2000	-3.25	-4.43	9.100	4.658	23.73	0.05	8.05	0.04
LMI08-H-5	1999	-3.06	-4.88	9.041	4.741	23.84	0.04	8.07	0.04
LMI08-H-6	1998	-2.75	-4.55	9.086	4.381	24.15	0.04	8.07	0.04
LMI08-H-7	1997	-2.92	-4.51	9.168	4.364	23.78	0.03	8.05	0.04
LMI08-H-8	1996	-2.70	-4.49	9.092	4.557	24.25	0.05	8.10	0.04
LMI08-H-9	1995	-2.63	-4.36	9.117	4.351	25.12	0.03	8.22	0.03
LMI08-H-10	1994	-2.54	-4.39	9.139	4.500	24.97	0.04	8.21	0.03
LMI08-H-11	1993	-2.81	-4.67	9.101	4.641	24.77	0.04	8.19	0.03
LMI08-H-12	1992	-2.66	-4.43	9.094	4.653	24.38	0.04	8.12	0.03
LMI08-H-13	1991	-2.72	-4.61	9.090	4.960	24.57	0.04	8.16	0.03
LMI08-H-14	1990	-2.56	-4.52	9.128	4.919	24.16	0.03	8.11	0.04
LMI08-H-15	1989	-2.79	-4.44	9.074	4.921	23.97	0.04	8.07	0.03
LMI08-H-16	1988	-2.39	-4.36	9.151	4.632	24.76	0.04	8.17	0.04
LMI08-H-17	1987	-2.10	-4.44	9.102	4.614	24.07	0.04	8.07	0.04
LMI08-H-18	1986	-2.18	-4.49	9.125	4.804	23.82	0.05	8.05	0.05
LMI08-H-19	1985	-2.12	-4.37	9.191	4.593	23.75	0.06	8.05	0.04
LMI08-H-20	1984	-2.07	-4.32	9.223	4.610	24.23	0.04	8.12	0.03
LMI08-H-21	1983	-2.06	-4.39	9.263	4.560	24.53	0.05	8.15	0.04
LMI08-H-22	1982	-1.92	-4.50	9.138	4.751	23.98	0.09	8.08	0.05
LMI08-H-23	1981	-1.88	-4.42	9.186	4.564	24.03	0.04	8.07	0.03
LMI08-H-24	1980	-2.12	-4.44	9.138	4.657	24.27	0.04	8.11	0.04
LMI08-H-25	1979	-2.03	-4.40	9.214	4.257	24.37	0.06	8.14	0.04
LMI08-H-26	1978	-2.11	-4.59	9.125	4.590	24.07	0.03	8.10	0.03
LMI08-H-27	1977	-2.37	-4.52	9.179	4.934	23.91	0.07	8.07	0.04
LMI08-H-28	1976	-2.50	-4.60	9.120	4.866	24.21	0.03	8.12	0.03
LMI08-H-29	1975	-2.77	-4.39	9.107	5.052	24.56	0.04	8.15	0.04
LMI08-H-30	1974	-2.20	-4.34	9.206	4.634	25.07	0.04	8.23	0.03
LMI08-H-31	1973	-2.03	-4.52	9.021	5.095	24.41	0.04	8.11	0.04
LMI08-H-32	1972	-2.42	-4.40	9.164	4.373	25.01	0.05	8.22	0.03
LMI08-H-33	1971	-1.89	-4.29	9.195	4.312	25.09	0.03	8.22	0.03
LMI08-H-34	1970	-2.04	-4.60	9.130	4.298	24.52	0.04	8.15	0.03
LMI08-H-35	1969	-1.28	-4.24	9.176	3.976	24.44	0.03	8.12	0.03
LMI08-H-36	1968	-1.69	-4.51	9.144	4.050	23.25	0.04	7.98	0.05
LMI08-H-37	1967	-1.56	-4.29	9.213	3.885	24.66	0.04	8.18	0.03
LMI08-H-38	1966	-1.65	-4.27	9.200	3.993	24.72	0.04	8.19	0.03
LMI08-H-39	1965	-1.82	-4.28	9.080	4.272	24.16	0.04	8.10	0.04
LMI08-H-40	1964	-2.27	-4.43	9.061	4.386	24.02	0.04	8.07	0.04
LMI08-H-41	1963	-2.15	-4.46	9.108	4.327	24.14	0.06	8.11	0.04
LMI08-H-42	1962	-2.34	-4.38	9.139	4.156	23.96	0.05	8.07	0.04

Table D-5. (Continued)

Sample ID	year	$\delta^{13}\text{C}$ (‰)	$\delta^{18}\text{O}$ (‰)	Sr/Ca (mmol mol <sup>-1</sup> )	Mg/Ca (mmol mol <sup>-1</sup> )	$\delta^{11}\text{B}$ (‰)	$\pm 2\sigma$	pH <sub>T</sub> <sup>a</sup>	$\pm 1\sigma$
LMI08-H-43	1961	-2.16	-4.39	9.178	4.465	25.27	0.05	8.27	0.03
LMI08-H-44	1960	-2.20	-4.29	9.109	4.039	25.09	0.04	8.22	0.03
LMI08-H-45	1959	-1.99	-4.15	9.052	4.884	25.65	0.05	8.28	0.03
LMI08-H-46	1958	-1.19	-4.03	9.233	4.770	24.89	0.10	8.18	0.04
LMI08-H-47	1957	-1.93	-4.38	9.165	3.826	23.65	0.04	8.03	0.04
LMI08-H-48	1956	-1.82	-4.37	9.103	3.904	23.85	0.04	8.06	0.03
LMI08-H-49	1955	-1.48	-4.60	9.142	3.852	24.34	0.04	8.15	0.03
LMI08-H-50	1954	-1.40	-4.40	9.178	4.505	24.22	0.04	8.12	0.04
LMI08-H-51	1953	-1.46	-4.44	9.190	3.774	24.29	0.05	8.13	0.04
LMI08-H-52	1952	-1.67	-4.51	9.139	3.827	24.53	0.06	8.16	0.04
LMI08-H-53	1951	-1.63	-4.60	9.102	4.138	23.49	0.04	8.03	0.05
LMI08-H-54	1950	-1.35	-4.47	9.231	3.739	24.32	0.02	8.15	0.04
LMI08-H-55	1949	-1.69	-4.44	9.238	3.747	24.81	0.03	8.22	0.03
LMI08-H-56	1948	-1.71	-4.24	9.177	3.962	24.07	0.03	8.10	0.04
LMI08-H-57	1947	-1.74	-4.46	9.103	3.901	23.79	0.04	8.07	0.04
LMI08-H-58	1946	-2.13	-4.69	9.152	3.917	23.91	0.04	8.10	0.04
LMI08-H-59	1945	-1.96	-4.37	9.106	4.102	23.41	0.04	8.00	0.05
LMI08-H-60	1944	-2.33	-4.22	9.135	4.173	23.65	0.03	8.03	0.04
LMI08-H-61	1943	-1.98	-4.17	9.143	4.048	23.98	0.04	8.07	0.04
LMI08-H-62	1942	-2.21	-4.08	9.150	4.243	23.88	0.03	8.04	0.04
LMI08-H-63	1941	-2.17	-4.36	9.075	4.236	23.95	0.03	8.07	0.04
LMI08-H-64	1940	-2.12	-4.30	9.060	4.292	24.14	0.05	8.09	0.04
LMI08-H-65	1939	-2.09	-4.40	9.025	4.283	24.69	0.03	8.18	0.04
LMI08-H-66	1938	-1.70	-4.32	9.099	3.945	23.99	0.03	8.07	0.04
LMI08-H-67	1937	-1.92	-4.27	9.133	3.929	23.54	0.04	8.02	0.04
LMI08-H-68	1936	-1.51	-4.43	9.106	3.929	23.35	0.04	8.00	0.04
LMI08-H-69	1935	-1.59	-4.60	9.146	3.847	24.06	0.03	8.11	0.04
LMI08-H-70	1934	-1.69	-4.22	9.202	3.834	24.28	0.03	8.13	0.03
LMI08-H-71	1933	-1.32	-4.24	9.185	3.852	24.42	0.03	8.14	0.04
LMI08-H-72	1932	-1.28	-4.42	9.013	4.262	23.71	0.03	8.04	0.04
LMI08-H-73	1931	-1.57	-4.22	9.187	4.969	24.26	0.02	8.11	0.04
LMI08-H-74	1930	-1.51	-4.23	9.179	4.361	24.13	0.03	8.11	0.04
LMI08-H-75	1929	-1.41	-4.40	9.258	4.188	23.95	0.05	8.10	0.04
LMI08-H-76	1928	-1.52	-4.41	9.223	4.199	23.92	0.03	8.09	0.04
LMI08-H-77	1927	-1.56	-4.33	9.161	4.112	24.14	0.04	8.11	0.04
LMI08-H-78	1926	-1.76	-4.58	9.056	4.226	24.42	0.04	8.15	0.04
LMI08-H-79	1925	-2.05	-4.48	9.068	4.251	24.47	0.05	8.17	0.04
LMI08-H-80	1924	-1.62	-4.39	9.189	4.378	24.22	0.03	8.12	0.04
LMI08-H-81	1923	-1.40	-4.40	9.191	4.106	24.37	0.03	8.15	0.04
LMI08-H-82	1922	-1.69	-4.30	9.218	4.132	24.38	0.03	8.16	0.04
LMI08-H-83	1921	-1.80	-4.47	9.152	4.196	24.41	0.05	8.16	0.04
LMI08-H-84	1920	-1.73	-4.28	9.157	4.212	24.36	0.04	8.14	0.04
LMI08-H-85	1919	-1.77	-4.42	9.099	4.375	24.37	0.04	8.15	0.04
LMI08-H-86	1918	-1.54	-4.33	9.118	4.047	25.03	0.03	8.23	0.03
LMI08-H-87	1917	-1.82	-4.50	9.145	4.195	25.03	0.04	8.24	0.03
LMI08-H-88	1916	-1.64	-4.32	9.123	4.228	25.13	0.05	8.24	0.04
LMI08-H-89	1915	-1.62	-4.34	9.147	4.257	25.08	0.04	8.23	0.03

Table D-5. (Continued)

Sample ID	year	$\delta^{13}\text{C}$ (‰)	$\delta^{18}\text{O}$ (‰)	Sr/Ca (mmol mol <sup>-1</sup> )	Mg/Ca (mmol mol <sup>-1</sup> )	$\delta^{11}\text{B}$ (‰)	$\pm 2\sigma$	pH <sub>T</sub> <sup>a</sup>	$\pm 1\sigma$
LM108-H-90	1914	-1.70	-4.28	9.096	4.267	24.67	0.03	8.17	0.03
LM108-H-91	1913	-1.54	-4.44	9.095	4.357	24.22	0.03	8.12	0.04
LM108-H-92	1912	-1.94	-4.59	9.125	4.729	23.65	0.04	8.05	0.04
LM108-H-93	1911	-1.81	-4.41	9.177	4.535	23.67	0.04	8.06	0.04
LM108-H-94	1910	-2.12	-4.58	9.148	4.595	23.62	0.03	8.05	0.04
LM108-H-95	1909	-1.81	-4.52	9.124	4.248	23.95	0.04	8.09	0.04
LM108-H-96	1908	-1.73	-4.39	9.152	4.212	24.12	0.04	8.11	0.04
LM108-H-97	1907	-1.65	-4.43	9.126	4.199	24.58	0.04	8.16	0.04
LM108-H-98	1906	-1.67	-4.43	9.150	4.513	24.41	0.04	8.15	0.04
LM108-H-99	1905	-1.60	-4.36	9.125	4.285	24.29	0.04	8.13	0.04
LM108-H-100	1904	-1.48	-4.40	9.130	4.188	24.09	0.03	8.11	0.04
LM108-H-101	1903	-1.42	-4.20	9.201	4.069	24.20	0.03	8.11	0.04
LM108-H-102	1902	-1.53	-4.32	9.110	4.091	24.74	0.04	8.19	0.03
LM108-H-103	1901	-1.88	-4.42	9.143	4.169	24.25	0.05	8.12	0.04
LM108-H-104	1900	-1.61	-4.41	9.104	4.178	24.75	0.04	8.18	0.03
LM108-H-105	1899	-2.15	-4.43	9.064	4.272	24.60	0.03	8.18	0.04
LM108-H-106	1898	-1.66	-4.30	9.123	4.153	24.78	0.03	8.19	0.03
LM108-H-107	1897	-1.55	-4.48	9.119	4.290	23.51	0.04	8.01	0.05
LM108-H-108	1896	-1.74	-4.84	9.126	4.300	23.42	0.03	8.03	0.04
LM108-H-109	1895	-1.69	-4.44	9.153	4.347	23.26	0.05	7.99	0.06
LM108-H-110	1894	-1.91	-4.70	9.069	4.379	23.88	0.04	8.08	0.04
LM108-H-111	1893	-1.81	-4.38	9.132	4.178	24.52	0.03	8.15	0.04
LM108-H-112	1892	-1.58	-4.39	9.165	4.028	24.49	0.03	8.15	0.04
LM108-H-113	1891	-1.51	-4.49	9.213	4.200	23.76	0.05	8.07	0.04
LM108-H-114	1890	-1.67	-4.26	9.162	4.701	23.10	0.04	7.96	0.05

<sup>a</sup> pH<sub>T</sub> = Calculated  $\delta^{11}\text{B}$ -derived seawater pH in total scale taking into account of physiological pH up-regulation

<sup>b</sup> averaged values from high resolution (i.e. bimonthly) data in each year

**Appendix E. Measured density, extension rate, and calcification records  
in the southern GBR**



**Table E-1.** Density data by three methods and porosity data from a Middle Pompey core. Pieces from LA-ICPMS analysis were used. Method 1 and 2 is for the bulk density measurement, whereas Method 3 is for skeletal density. Method 1 is done by estimating volume of coral pieces with calipers and buoyant-weighing measurement with enclosed volume by plastic wrapping is applied for the Method 2.

piece	Reconstructed year <sup>a</sup>			Method 1		Method 2								Method 3					Porosity(%) <sup>h</sup>	
				Bulk density by calipers		Bulk density				Calibration of bulk density				Skeletal density						
	Year_start	Year_end	Year_mid	V(cm <sup>3</sup> )	ρ(g cm <sup>-3</sup> ) <sup>b</sup>	W <sub>air</sub> (g)	W <sub>H<sub>2</sub>O</sub> (g)	ρ <sub>H<sub>2</sub>O</sub> (g cm <sup>-3</sup> )	V(cm <sup>3</sup> )	ρ(g cm <sup>-3</sup> )	W <sub>wrap</sub> (g) <sup>c</sup>	V <sub>wrap</sub> (cm <sup>3</sup> ) <sup>d</sup>	V <sub>coral</sub> (cm <sup>3</sup> ) <sup>e</sup>	ρ(g cm <sup>-3</sup> ) <sup>f</sup>	W <sub>air</sub> (g)	W <sub>H<sub>2</sub>O</sub> (g)	ρ <sub>H<sub>2</sub>O</sub> (g cm <sup>-3</sup> )	V(cm <sup>3</sup> )		ρ(g cm <sup>-3</sup> )
PSC-1-tissue	2006.17	2004.73	2005.45	-	-	-	-	-	-	-	-	-	-	-	-	-	-	-	-	-
PSC-1	2004.73	1999.10	2001.91	8.94	1.41	13.14	0.73	0.998	2.39	1.24	0.15	0.22	2.16	1.37	2.97	1.92	0.997	1.05	2.82	
PSC-2	1999.10	1997.55	1998.32	3.06	1.36	4.38	1.04	0.998	9.60	1.31	0.33	0.79	8.82	1.43	12.61	8.14	0.997	4.49	2.81	
PSC-3	1997.55	1992.91	1995.23	8.43	1.21	10.66	1.57	0.998	9.10	1.12	0.21	0.31	3.04	1.37	4.17	2.64	0.997	1.53	2.72	
PSC-4	1992.91	1986.22	1989.57	9.33	1.14	11.24	0.88	0.998	10.37	1.03	0.55	0.82	9.55	1.12	10.20	6.55	0.997	3.67	2.78	
PSC-6	1986.22	1984.04	1985.13	2.88	1.39	4.22	0.51	0.998	3.71	1.08	0.23	0.34	3.38	1.18	3.99	6.90	0.997	3.80	2.82	
PSC-6-2	1984.04	1980.90	1982.47	5.53	1.16	6.74	0.85	0.998	5.90	1.09	0.32	0.48	5.42	1.18	6.42	4.16	0.997	1.42	2.82	
PSC-7	1980.90	1974.98	1977.94	10.57	1.22	13.50	2.48	0.998	11.05	1.17	0.56	0.84	10.20	1.27	12.94	8.31	0.997	4.64	2.79	
PSC-8	1974.98	1970.17	1972.57	8.19	1.31	11.19	2.16	0.998	9.04	1.18	0.48	0.71	8.33	1.28	10.71	6.90	0.997	3.81	2.81	
PSC-9	1970.17	1964.50	1967.33	12.84	1.26	16.70	3.14	0.998	13.57	1.19	0.59	0.87	12.70	1.27	16.11	10.42	0.997	5.70	2.82	
PSC-10	1964.50	1960.07	1962.28	11.62	1.22	14.67	2.65	0.998	12.04	1.18	0.52	0.77	11.27	1.26	14.15	9.15	0.997	5.01	2.82	
PSC-11	1960.07	1954.35	1957.21	12.96	1.34	18.05	2.46	0.998	15.62	1.12	0.63	0.94	14.67	1.19	17.42	11.25	0.998	6.18	2.82	
PSC-12	1954.35	1948.56	1951.45	16.27	1.16	19.61	2.30	0.998	17.34	1.09	0.63	0.94	14.19	1.37	18.90	12.24	0.998	6.67	2.83	
PSC-14	1948.56	1944.26	1946.41	12.55	1.29	16.79	1.35	0.998	14.47	1.24	0.51	0.83	11.78	1.24	14.63	9.46	0.998	4.27	2.80	
PSC-15	1944.26	1941.45	1942.86	8.00	1.25	10.36	1.33	0.998	11.33	1.16	0.55	0.76	10.58	1.23	11.94	7.58	0.998	4.34	2.80	
PSC-16	1941.45	1937.34	1939.40	10.72	1.21	13.48	2.17	0.998	10.10	1.18	0.48	0.72	9.38	1.27	11.94	7.82	0.998	4.54	2.80	
PSC-17	1937.34	1932.17	1934.76	11.77	1.24	15.18	2.60	0.998	12.61	1.16	0.55	0.83	11.78	1.24	14.63	9.46	0.998	4.27	2.80	
PSC-18	1932.17	1927.53	1929.85	9.65	1.24	12.43	2.34	0.998	10.10	1.18	0.48	0.72	9.38	1.27	11.94	7.82	0.998	4.54	2.80	
PSC-19	1927.53	1923.89	1925.71	9.18	1.32	12.60	2.86	0.998	9.76	1.25	0.44	0.66	9.10	1.34	12.15	7.82	0.998	4.27	2.79	
PSC-20	1923.89	1919.82	1921.85	8.84	1.35	12.34	2.73	0.998	9.63	1.24	0.44	0.65	8.98	1.33	11.90	7.64	0.998	4.27	2.79	
PSC-21	1919.82	1914.07	1916.94	12.70	1.38	18.16	4.91	0.998	13.28	1.32	0.60	0.89	12.39	1.42	17.57	11.36	0.998	6.22	2.82	
PSC-22	1914.07	1908.84	1911.46	14.24	1.25	18.38	3.45	0.998	14.95	1.19	0.64	0.95	14.00	1.27	17.74	11.51	0.998	6.25	2.84	

Notations: V = volume, ρ = density of a piece, ρ<sub>H<sub>2</sub>O</sub> = density of ultrapure water, W<sub>air</sub> = weight in air, and W<sub>H<sub>2</sub>O</sub> = weight in ultrapure water, measured by each method.

<sup>a</sup> Reconstructed year from LA-ICPMS trace elements data. 'Year\_start' means the first year in a piece and 'Year\_end' represent the last year in a piece. Middle of a year ('Year\_mid') was used for representing the year of a piece.

<sup>b</sup> Calculated by the equation, density = weight of an unwrapped sample / volume by calipers

<sup>c</sup> W<sub>wrap</sub> = weight of plastic wrap. Calculated by the subtraction equation, weight of plastic wrap = weight of a wrapped sample - weight of an unwrapped sample

<sup>d</sup> V<sub>wrap</sub> = volume of plastic wrap. Calculated by the equation, volume of plastic wrap = weight of plastic wrap / density of plastic wrap = W<sub>wrap</sub> / 0.67 g cm<sup>-3</sup>

<sup>e</sup> V<sub>coral</sub> = volume of a coral piece. Calculated by the subtraction equation, volume of a coral piece = volume of a wrapped sample - volume of plastic wrap

<sup>f</sup> Calculated by the equation, density = weight of an unwrapped sample / volume of a coral piece

<sup>h</sup> Calculated by the equation, porosity = 100 × (volume of a wrapped sample - volume of an unwrapped sample) / volume of a wrapped sample

**Table E-2.** Density data by all methods and porosity data from a Little Kindermar core. Pieces from LA-ICPMS analysis were used. Method 1 and 2 is for the bulk density measurement, whereas Method 3 is for skeletal density. Method 1 is done by estimating volume of coral pieces with calipers and buoyant-weighting measurement with enclosed volume by plastic wrapping is applied for the Method 2.

piece	Reconstructed year <sup>a</sup>			Method 1		Method 2								Method 3					Porosity(%) <sup>b</sup>	
				Bulk density by calipers		Bulk density				Calibration of bulk density				Skeletal density						
	Year_start	Year_end	Year_mid	V(cm <sup>3</sup> )	$\rho(g\ cm^{-3})^c$	W <sub>air</sub> (g)	W <sub>H<sub>2</sub>O</sub> (g)	$\rho_{H_2O}(g\ cm^{-3})^d$	V(cm <sup>3</sup> )	$\rho(g\ cm^{-3})^e$	W <sub>wrap</sub> (g) <sup>f</sup>	V <sub>wrap</sub> (cm <sup>3</sup> ) <sup>g</sup>	V <sub>cored</sub> (cm <sup>3</sup> ) <sup>h</sup>	$\rho(g\ cm^{-3})^i$	W <sub>air</sub> (g)	W <sub>H<sub>2</sub>O</sub> (g)	$\rho_{H_2O}(g\ cm^{-3})^j$	V(cm <sup>3</sup> )		$\rho(g\ cm^{-3})^k$
PSA-1-tissue	2006.17	2004.13	2005.15	-	-	3.62	1.08	0.998	2.55	1.35	0.17	0.26	2.29	1.51	3.45	2.17	0.997	1.29	2.68	43.8
PSA-1	2004.13	1999.71	2001.92	-	-	8.34	2.48	0.998	5.87	1.37	0.30	0.45	5.42	1.48	8.04	5.19	0.997	2.85	2.82	47.3
PSA-2 & PSA-3*	1999.71	1991.54	1995.63	7.21	1.43	10.67	3.24	0.998	7.44	1.39	0.36	0.54	6.90	1.49	10.31	6.64	0.997	3.67	2.81	46.8
PSA-3-1 & PSA-4*	1991.54	1982.98	1987.26	9.27	1.48	14.24	4.20	0.998	10.06	1.37	0.49	0.73	9.33	1.47	13.75	8.63	0.997	4.94	2.78	47.0
PSA-6	1982.98	1974.75	1978.86	12.10	1.36	16.96	4.42	0.998	12.57	1.31	0.56	0.83	11.74	1.40	16.41	10.63	0.997	5.79	2.83	50.7
PSA-7	1974.75	1968.14	1971.45	10.63	1.27	14.03	3.17	0.998	10.88	1.24	0.51	0.77	10.11	1.34	13.52	8.76	0.997	4.77	2.84	52.9
PSA-8	1968.14	1962.08	1965.11	7.24	1.35	10.13	2.69	0.998	7.46	1.31	0.36	0.54	6.92	1.41	9.77	6.32	0.997	3.46	2.82	49.9
PSA-9	1962.08	1952.57	1957.33	13.37	1.36	18.79	5.25	0.998	13.57	1.34	0.62	0.92	12.65	1.44	18.17	11.76	0.997	6.43	2.82	49.1
PSA-10	1952.57	1945.84	1949.21	10.52	1.37	14.94	4.07	0.998	10.89	1.33	0.49	0.73	10.16	1.42	14.45	9.33	0.997	5.13	2.81	49.5
PSA-11	1945.84	1937.58	1941.71	12.26	1.37	17.38	4.65	0.998	12.76	1.32	0.59	0.89	11.87	1.41	16.79	10.87	0.997	5.94	2.83	50.0
PSA-12 & PSA-12-1*	1937.58	1929.53	1933.55	5.93	1.36	8.39	2.19	0.998	6.21	1.30	0.31	0.46	5.76	1.40	8.08	5.23	0.997	2.86	2.83	50.3
PSA-13	1929.53	1920.50	1925.01	11.39	1.30	15.31	4.51	0.998	10.82	1.37	0.49	0.74	10.08	1.47	14.81	9.54	0.997	5.29	2.80	47.6
PSA-14	1920.50	1910.02	1915.26	12.57	1.34	17.43	4.36	0.998	13.10	1.29	0.59	0.88	12.22	1.38	16.84	10.91	0.997	5.95	2.83	51.3
PSA-15	1910.02	1901.80	1905.91	12.16	1.40	17.54	4.58	0.998	13.00	1.31	0.57	0.85	12.15	1.40	16.98	10.99	0.997	6.01	2.83	50.6
PSA-16	1901.80	1894.69	1898.25	12.04	1.29	16.12	4.12	0.998	12.02	1.29	0.55	0.83	11.20	1.39	15.56	10.07	0.997	5.51	2.82	50.8
PSA-17	1894.69	1890.23	1892.46	9.98	0.96	9.90	2.57	0.998	7.34	1.30	0.35	0.53	6.81	1.40	9.54	6.11	0.998	3.44	2.77	49.4
PSA-18	1890.23	1884.00	1887.11	8.70	1.36	12.26	3.37	0.998	8.90	1.33	0.40	0.59	8.32	1.43	11.86	7.66	0.998	4.21	2.82	50.9
PSA-19	1884.00	1880.29	1882.14	6.00	1.34	8.34	2.13	0.998	6.23	1.29	0.31	0.46	5.77	1.39	8.04	5.21	0.997	2.83	2.83	51.3
PSA-20	1880.29	1875.35	1877.82	7.29	1.28	9.70	2.41	0.998	7.31	1.28	0.36	0.53	6.77	1.38	9.34	6.05	0.997	3.30	2.83	48.9
PSA-21 & PSA-22*	1875.35	1868.00	1871.68	7.75	1.36	10.96	2.98	0.998	8.00	1.32	0.40	0.60	7.40	1.43	10.56	6.79	0.997	3.78	2.79	48.9
PSA-23	1868.00	1858.09	1863.05	13.76	1.47	20.91	6.52	0.998	14.43	1.40	0.66	0.99	13.44	1.51	20.25	13.14	0.997	7.13	2.84	46.9
PSA-24	1858.09	1848.33	1853.21	11.96	1.44	17.79	5.02	0.998	12.80	1.34	0.63	0.94	11.86	1.45	17.16	11.09	0.997	6.09	2.82	48.7
PSA-25	1848.33	1841.39	1844.86	13.62	1.00	14.07	3.95	0.998	10.14	1.34	0.48	0.71	9.43	1.44	13.59	8.79	0.997	4.82	2.82	48.9
PSA-26	1841.39	1833.73	1837.56	8.99	1.37	12.73	3.45	0.998	9.30	1.32	0.44	0.66	8.64	1.42	12.29	7.97	0.997	4.33	2.84	49.9

Notations: V = volume,  $\rho$  = density of a piece,  $\rho_{H_2O}$  = density of ultrapure water, W<sub>air</sub> = weight in air, and W<sub>H<sub>2</sub>O</sub> = weight in ultrapure water, measured by each method.

<sup>a</sup> Two pieces were measured at once due to excellent joint between the pieces

<sup>b</sup> Reconstructed year from LA-ICPMS trace elements data. 'Year\_start' means the first year in a piece and 'Year\_end' represent the last year in a piece. Middle of a year ('Year\_mid') was used for representing the year of a piece.

<sup>c</sup> Calculated by the equation, density = weight of an unwrapped sample / volume by calipers

<sup>d</sup> W<sub>wrap</sub> = weight of plastic wrap. Calculated by the subtraction equation, weight of plastic wrap = weight of a wrapped sample - weight of an unwrapped sample

<sup>e</sup> V<sub>wrap</sub> = volume of plastic wrap. Calculated by the equation, volume of plastic wrap = weight of plastic wrap / density of plastic wrap = W<sub>wrap</sub> / 0.67 g cm<sup>-3</sup>

<sup>f</sup> V<sub>cored</sub> = volume of a coral piece. Calculated by the subtraction equation, volume of a coral piece = volume of a wrapped sample - volume of plastic wrap

<sup>g</sup> Calculated by the equation, density = weight of an unwrapped sample / volume of a coral piece

<sup>h</sup> Calculated by the equation, porosity = 100 × (volume of a wrapped sample - volume of an unwrapped sample) / volume of a wrapped sample



**Table E-4.** Density data from a Fitzroy Reef core. Pieces from LA-ICPMS analysis were used. Method 1 using calipers was chosen for the bulk density measurement due to lower density than ultrapure water.

piece	Reconstructed year <sup>a</sup>			Method 1		
				Bulk density by calipers		
	Year_start	Year_end	Year_mid	W <sub>air</sub> (g)	V(cm <sup>3</sup> )	ρ(g cm <sup>-3</sup> ) <sup>c</sup>
FYR08-D-1	2008.78	2003.33	2006.05	15.13	15.34	0.99
FYR08-D-2	2003.33	1998.53	2000.93	14.55	15.44	0.94
FYR08-D-3	1998.53	1993.00	1995.76	14.96	15.24	0.98
FYR08-D-4	1992.99	1987.95	1990.47	16.27	14.43	1.13
FYR08-D-5	1987.92	1984.15	1986.04	10.51	9.97	1.05
FYR08-D-6	1984.15	1981.05	1982.60	8.94	9.31	0.96
FYR08-D-7	1981.04	1976.93	1978.99	12.13	11.64	1.04
FYR08-D-8	1976.91	1974.11	1975.51	7.46	7.20	1.04
FYR08-D-9	1974.11	1968.32	1971.21	17.01	16.98	1.00
FYR08-D-10	1968.30	1964.57	1966.44	9.54	9.71	0.98
FYR08-D-11	1964.56	1960.30	1962.43	10.73	11.02	0.97
FYR08-D-12	1960.29	1956.17	1958.23	10.70	10.87	0.98
FYR08-D-13	1956.15	1949.83	1952.99	15.63	15.18	1.03

Notations: W<sub>air</sub> = weight in air, V = volume, and ρ = density of a piece

<sup>a</sup> Reconstructed year from LA-ICPMS trace elements data. 'Year\_start' means the first year in a piece and 'year\_end' represent the last year in a piece. Middle of a year (Year\_mid) was used for representing the year of a piece.

<sup>c</sup> Calculated by the equation, density = weight of a sample in air / volume by calipers

**Table E-5.** Density data from a Lady Musgrave Island (LMI08-H) core. Pieces from LA-ICPMS analysis were used. Method 2, buoyant-weighing, was chosen for the bulk density measurement.

piece	Reconstructed year <sup>a</sup>			Method 2									
				Bulk density					Calibration of bulk density				
	Year_start	Year_end	Year_mid	W <sub>air</sub> (g)	W <sub>wrap</sub> (g)	W <sub>H<sub>2</sub>O</sub> (g)	ρ <sub>H<sub>2</sub>O</sub> (g cm <sup>-3</sup> )	V(cm <sup>3</sup> )	ρ(g cm <sup>-3</sup> )	W <sub>wrap</sub> (g) <sup>b</sup>	V <sub>wrap</sub> (cm <sup>3</sup> ) <sup>c</sup>	V <sub>corr</sub> (cm <sup>3</sup> ) <sup>d</sup>	ρ(g cm <sup>-3</sup> ) <sup>e</sup>
LMI08-H-1	2008.74	2001.37	2005.05	17.62	18.21	4.48	0.997	13.769	1.32	0.59	0.89	12.88	1.37
LMI08-H-2	2001.36	1996.86	1999.11	13.33	13.80	3.18	0.997	10.655	1.30	0.47	0.71	9.95	1.34
LMI08-H-3	1996.70	1988.13	1992.42	20.14	20.82	4.16	0.997	16.711	1.25	0.67	1.00	15.71	1.28
LMI08-H-4	1988.12	1980.34	1984.23	19.21	19.91	3.19	0.997	16.773	1.19	0.70	1.04	15.73	1.22
LMI08-H-5	1980.33	1973.12	1976.72	17.82	18.48	2.86	0.997	15.661	1.18	0.66	0.99	14.68	1.21
LMI08-H-6	1973.10	1967.70	1970.40	13.93	14.45	2.42	0.997	12.059	1.20	0.52	0.77	11.29	1.23
LMI08-H-7	1967.69	1959.56	1963.62	18.76	19.44	3.11	0.997	16.382	1.19	0.69	1.03	15.36	1.22
LMI08-H-8	1959.55	1953.67	1956.61	16.28	16.89	2.85	0.997	14.077	1.20	0.61	0.91	13.17	1.24
LMI08-H-9	1953.66	1944.97	1949.31	20.92	21.68	3.57	0.997	18.160	1.19	0.76	1.13	17.03	1.23
LMI08-H-10	1944.96	1936.39	1940.68	21.67	22.40	4.32	0.997	18.136	1.24	0.74	1.10	17.03	1.27
LMI08-H-11	1936.36	1931.12	1933.74	14.01	14.51	3.10	0.997	11.442	1.27	0.50	0.75	10.70	1.31
LMI08-H-12	1931.12	1924.33	1927.73	15.95	16.61	2.02	0.997	14.636	1.13	0.66	0.98	13.66	1.17
LMI08-H-13	1924.27	1919.82	1922.05	9.27	9.67	1.45	0.997	8.245	1.17	0.40	0.60	7.65	1.21
LMI08-H-14	1919.80	1913.21	1916.50	13.54	14.05	2.54	0.997	11.545	1.22	0.52	0.77	10.77	1.26
LMI08-H-15	1913.20	1905.36	1909.28	19.24	19.93	3.40	0.997	16.578	1.20	0.70	1.04	15.54	1.24
LMI08-H-16	1905.19	1897.46	1901.33	18.55	19.24	2.98	0.997	16.302	1.18	0.69	1.03	15.27	1.21
LMI08-H-17	1897.40	1889.81	1893.61	17.79	18.48	2.19	0.997	16.336	1.13	0.68	1.02	15.32	1.16

Notations: V = volume, ρ = density of a piece. ρ<sub>H<sub>2</sub>O</sub> = density of ultrapure water, W<sub>air</sub> = weight of a coral piece in air, W<sub>wrap</sub> = weight of a plastic wrapped coral piece in air, and W<sub>H<sub>2</sub>O</sub> = weight in ultrapure water

<sup>a</sup> Reconstructed year from LA-ICPMS trace elements data. 'Year\_start' means the first year in a piece and 'year\_end' represent the last year in a piece. Middle of a year ('Year\_mid') was used for representing the year of a piece.

<sup>b</sup> W<sub>wrap</sub> = weight of plastic wrap. Calculated by the subtraction equation, weight of plastic wrap = weight of a wrapped sample - weight of an unwrapped sample

<sup>c</sup> V<sub>wrap</sub> = volume of plastic wrap. Calculated by the equation, volume of plastic wrap = weight of plastic wrap / density of plastic wrap = W<sub>wrap</sub> / 0.67 g cm<sup>-3</sup>

<sup>d</sup> V<sub>corr</sub> = volume of a coral piece. Calculated by the subtraction equation, volume of a coral piece = volume of a wrapped sample - volume of plastic wrap

<sup>e</sup> Calculated by the equation, density = weight of a coral sample / volume of a coral piece



**Table E-6.** Density data from a Lady Musgrave Island (LMI08-C-a) core. Pieces from LA-ICPMS analysis were used. Method 2, buoyant-weighing, was chosen for the bulk density measurement.

piece	Reconstructed year*			Method 2									
				Bulk density					Calibration of bulk density				
	Year_start	Year_end	Year_mid	W <sub>air</sub> (g)	W <sub>wrap</sub> (g)	W <sub>H<sub>2</sub>O</sub> (g)	ρ <sub>H<sub>2</sub>O</sub> (g cm <sup>-3</sup> )	V(cm <sup>3</sup> )	ρ(g cm <sup>-3</sup> )	W <sub>wrap</sub> (g) <sup>b</sup>	V <sub>wrap</sub> (cm <sup>3</sup> ) <sup>c</sup>	V <sub>coral</sub> (cm <sup>3</sup> ) <sup>d</sup>	ρ(g cm <sup>-3</sup> ) <sup>e</sup>
LMI08-C-a-1	2008.68	1992.46	2000.37	20.919	21.575	7.443	0.997	14.173	1.52	0.66	0.98	13.19	1.59
LMI08-C-a-2	1992.38	1979.67	1986.03	20.181	20.893	6.064	0.997	14.873	1.40	0.71	1.06	13.81	1.46
LMI08-C-a-3	1979.66	1967.99	1973.83	16.86	17.492	5.303	0.997	12.225	1.43	0.63	0.94	11.28	1.49
LMI08-C-a-4	1967.98	1955.65	1961.81	14.247	14.741	4.704	0.997	10.066	1.46	0.49	0.74	9.33	1.53

Notations: V = volume, ρ = density of a piece, ρ<sub>H<sub>2</sub>O</sub> = density of ultrapure water, W<sub>coral</sub> = weight of a coral piece in air, W<sub>wrap</sub> = weight of a plastic wrapped coral piece in air, and W<sub>H<sub>2</sub>O</sub> = weight in ultrapure water

\* Reconstructed year from LA-ICPMS trace elements data. 'Year\_start' means the first year in a piece and 'year\_end' represent the last year in a piece. Middle of a year (Year\_mid) was used for representing the year of a piece.

<sup>b</sup> W<sub>wrap</sub> = weight of plastic wrap. Calculated by the subtraction equation, weight of plastic wrap = weight of a wrapped sample - weight of an unwrapped sample

<sup>c</sup> V<sub>wrap</sub> = volume of plastic wrap. Calculated by the equation, volume of plastic wrap = weight of plastic wrap / density of plastic wrap = W<sub>wrap</sub> / 0.67 g cm<sup>-3</sup>

<sup>d</sup> V<sub>coral</sub> = volume of a coral piece. Calculated by the subtraction equation, volume of a coral piece = volume of a wrapped sample - volume of plastic wrap

<sup>e</sup> Calculated by the equation, density = weight of a coral sample / volume of a coral piece

Appendices

Table E-7. Annual extension, density, and calcification data from a Middle Pompey core.

Middle Pompey (PSC)							
Year	Annual extension (mm yr <sup>-1</sup> ) <sup>a</sup>	Annual density (g cm <sup>-3</sup> ) <sup>b</sup>	Annual calcification (g cm <sup>-2</sup> yr <sup>-1</sup> ) <sup>c</sup>	Year	Annual extension (mm yr <sup>-1</sup> ) <sup>a</sup>	Annual density (g cm <sup>-3</sup> ) <sup>b</sup>	Annual calcification (g cm <sup>-2</sup> yr <sup>-1</sup> ) <sup>c</sup>
2005	13.50	1.37	1.85	1957	14.24	1.19	1.69
2004	15.92	1.39	2.22	1956	13.82	1.22	1.68
2003	11.33	1.41	1.60	1955	12.59	1.25	1.57
2002	12.19	1.43	1.74	1954	11.79	1.28	1.51
2001	11.14	1.42	1.58	1953	13.80	1.31	1.81
2000	13.98	1.40	1.96	1952	14.90	1.34	2.00
1999	15.45	1.39	2.14	1951	12.10	1.37	1.66
1998	11.61	1.37	1.59	1950	12.47	1.35	1.69
1997	15.17	1.32	2.00	1949	11.27	1.34	1.51
1996	16.27	1.26	2.06	1948	12.45	1.32	1.64
1995	14.69	1.21	1.78	1947	15.27	1.30	1.99
1994	16.47	1.19	1.96	1946	16.71	1.29	2.15
1993	17.71	1.17	2.08	1945	14.72	1.28	1.88
1992	15.14	1.16	1.75	1944	15.20	1.27	1.93
1991	15.40	1.14	1.75	1943	17.16	1.27	2.17
1990	16.76	1.12	1.88	1942	12.64	1.26	1.59
1989	13.96	1.13	1.58	1941	15.46	1.25	1.93
1988	12.92	1.14	1.48	1940	17.03	1.24	2.11
1987	16.36	1.16	1.89	1939	16.69	1.23	2.05
1986	11.80	1.17	1.38	1938	17.25	1.23	2.12
1985	13.09	1.18	1.55	1937	15.58	1.23	1.92
1984	15.25	1.18	1.80	1936	12.82	1.24	1.59
1983	12.76	1.18	1.51	1935	15.42	1.24	1.91
1982	14.24	1.18	1.69	1934	10.73	1.25	1.34
1981	14.37	1.21	1.73	1933	16.93	1.25	2.12
1980	14.68	1.23	1.80	1932	10.77	1.26	1.36
1979	12.13	1.25	1.51	1931	13.52	1.27	1.71
1978	13.92	1.27	1.76	1930	12.98	1.27	1.65
1977	11.06	1.27	1.41	1929	13.07	1.29	1.68
1976	13.14	1.27	1.67	1928	11.89	1.30	1.55
1975	12.43	1.28	1.59	1927	10.92	1.32	1.44
1974	13.97	1.28	1.79	1926	11.43	1.34	1.53
1973	13.41	1.28	1.72	1925	11.75	1.33	1.57
1972	13.93	1.28	1.79	1924	9.63	1.33	1.28
1971	12.78	1.28	1.63	1923	12.16	1.33	1.62
1970	-	-	-	1922	12.00	1.33	1.59
1969	14.06	1.27	1.79	1921	12.57	1.34	1.69
1968	12.19	1.27	1.55	1920	11.52	1.36	1.57
1967	13.48	1.27	1.71	1919	12.71	1.38	1.76
1966	11.80	1.27	1.49	1918	10.63	1.40	1.49
1965	12.43	1.26	1.57	1917	11.60	1.42	1.65
1964	12.83	1.26	1.62	1916	14.05	1.39	1.96
1963	13.28	1.26	1.67	1915	9.89	1.37	1.35
1962	15.30	1.26	1.92	1914	14.13	1.34	1.90
1961	11.13	1.24	1.38	1913	18.82	1.32	2.48
1960	12.91	1.23	1.59	1912	20.66	1.29	2.67
1959	12.09	1.21	1.47	1911	17.62	1.27	2.23
1958	16.85	1.20	2.02	1910	12.29	1.27	1.56
				1909	13.78	1.27	1.75

<sup>a</sup> Calculated from Sr/Ca maxima

<sup>b</sup> Annual resampling of density was done by Analyseries program (Paillard et al., 1996)

<sup>c</sup> Calculated with annual extension rate and annually resampled density data.

- Joins between core sections or distortion of growth along the LA-ICPMS tracks

Table E-8. Annual extension, density, and calcification data from a Little Kindermar core.

<i>Little Kindermar (PSA)</i>							
Year	Annual extension (mm yr <sup>-1</sup> ) <sup>a</sup>	Annual density (g cm <sup>-3</sup> ) <sup>b</sup>	Annual calcification (g cm <sup>-2</sup> yr <sup>-1</sup> ) <sup>c</sup>	Year	Annual extension (mm yr <sup>-1</sup> ) <sup>a</sup>	Annual density (g cm <sup>-3</sup> ) <sup>b</sup>	Annual calcification (g cm <sup>-2</sup> yr <sup>-1</sup> ) <sup>c</sup>
2005	7.14	1.51	1.08	1956	8.27	1.43	1.19
2004	10.07	1.50	1.51	1955	8.77	1.43	1.26
2003	7.57	1.49	1.13	1954	7.75	1.43	1.11
2002	7.46	1.48	1.11	1953	7.07	1.43	1.01
2001	5.52	1.48	0.82	1952	9.82	1.43	1.40
2000	8.77	1.49	1.30	1951	8.97	1.43	1.28
1999	7.98	1.49	1.19	1950	7.98	1.42	1.14
1998	9.27	1.49	1.38	1949	9.28	1.42	1.32
1997	9.42	1.49	1.41	1948	7.98	1.42	1.13
1996	10.39	1.49	1.55	1947	10.58	1.42	1.50
1995	10.56	1.49	1.58	1946	8.31	1.42	1.18
1994	9.93	1.49	1.48	1945	10.11	1.42	1.43
1993	11.41	1.49	1.70	1944	9.14	1.42	1.29
1992	11.43	1.48	1.70	1943	11.28	1.42	1.60
1991	11.30	1.48	1.67	1942	6.39	1.41	0.90
1990	11.64	1.48	1.72	1941	10.84	1.41	1.53
1989	8.77	1.48	1.30	1940	10.04	1.41	1.42
1988	7.68	1.48	1.13	1939	9.73	1.41	1.37
1987	8.06	1.47	1.19	1938	9.58	1.41	1.35
1986	10.64	1.46	1.56	1937	6.87	1.41	0.97
1985	8.24	1.45	1.20	1936	8.55	1.41	1.20
1984	9.01	1.45	1.30	1935	9.71	1.41	1.37
1983	6.02	1.44	0.86	1934	8.37	1.40	1.17
1982	10.80	1.43	1.54	1933	8.48	1.41	1.20
1981	8.28	1.42	1.17	1932	11.06	1.42	1.57
1980	10.50	1.41	1.48	1931	8.86	1.43	1.26
1979	9.47	1.40	1.32	1930	7.66	1.43	1.10
1978	11.96	1.39	1.66	1929	6.15	1.44	0.89
1977	13.19	1.38	1.82	1928	6.92	1.45	1.00
1976	8.54	1.37	1.17	1927	7.55	1.45	1.10
1975	9.97	1.37	1.36	1926	7.73	1.46	1.13
1974	9.86	1.36	1.34	1925	10.16	1.47	1.49
1973	13.06	1.35	1.77	1924	7.68	1.46	1.12
1972	12.51	1.34	1.68	1923	7.29	1.45	1.06
1971	10.71	1.34	1.43	1922	9.06	1.44	1.31
1970	10.55	1.35	1.42	1921	-	-	-
1969	9.18	1.36	1.25	1920	7.81	1.42	1.11
1968	7.97	1.37	1.10	1919	8.60	1.41	1.22
1967	5.65	1.39	0.78	1918	9.36	1.41	1.31
1966	11.48	1.40	1.61	1917	5.55	1.40	0.77
1965	7.44	1.41	1.05	1916	9.71	1.39	1.35
1964	7.91	1.41	1.12	1915	7.11	1.38	0.98
1963	9.37	1.42	1.33	1914	8.78	1.38	1.21
1962	-	-	-	1913	8.20	1.38	1.13
1961	6.95	1.42	0.99	1912	10.00	1.38	1.38
1960	8.26	1.43	1.18	1911	-	-	-
1959	8.62	1.43	1.23	1910	-	-	-
1958	7.35	1.43	1.05	1909	7.95	1.39	1.11
1957	8.53	1.44	1.23	1908	9.14	1.39	1.27

Appendices

Table E-8. (continued)

Year	Annual extension (mm yr <sup>-1</sup> ) <sup>a</sup>	Annual density (g cm <sup>-3</sup> ) <sup>b</sup>	Annual calcification (g cm <sup>-2</sup> yr <sup>-1</sup> ) <sup>c</sup>	Year	Annual extension (mm yr <sup>-1</sup> ) <sup>a</sup>	Annual density (g cm <sup>-3</sup> ) <sup>b</sup>	Annual calcification (g cm <sup>-2</sup> yr <sup>-1</sup> ) <sup>c</sup>
1907	7.95	1.40	1.11	1858	6.40	1.48	0.94
1906	10.66	1.40	1.49	1857	6.79	1.47	1.00
1905	10.17	1.40	1.42	1856	-	-	-
1904	8.66	1.40	1.21	1855	7.88	1.46	1.15
1903	10.56	1.39	1.47	1854	7.92	1.45	1.15
1902	8.34	1.39	1.16	1853	7.80	1.45	1.13
1901	9.96	1.39	1.39	1852	7.99	1.45	1.15
1900	10.49	1.39	1.46	1851	9.36	1.45	1.35
1899	8.64	1.39	1.20	1850	8.53	1.44	1.23
1898	11.72	1.39	1.63	1849	9.23	1.44	1.33
1897	9.85	1.39	1.37	1848	7.18	1.44	1.04
1896	9.84	1.39	1.37	1847	8.20	1.44	1.18
1895	8.14	1.40	1.14	1846	7.85	1.44	1.13
1894	8.65	1.40	1.21	1845	7.15	1.44	1.03
1893	6.45	1.40	0.90	1844	7.49	1.44	1.08
1892	7.12	1.40	1.00	1843	6.30	1.44	0.90
1891	11.33	1.41	1.59	1842	10.22	1.43	1.46
1890	11.30	1.41	1.59	1841	6.80	1.43	0.97
1889	5.55	1.42	0.79	1840	7.98	1.43	1.14
1888	8.89	1.42	1.26	1839	6.27	1.42	0.89
1887	7.70	1.43	1.10	1838	8.50	1.42	1.21
1886	6.88	1.42	0.98	1837	7.48	1.42	1.06
1885	6.73	1.41	0.95	1836	8.16	1.42	1.16
1884	6.91	1.41	0.97	1835	8.67	1.43	1.23
1883	8.11	1.40	1.14	1834	5.78	1.42	0.82
1882	8.64	1.39	1.20				
1881	-	-	-				
1880	10.31	1.39	1.43				
1879	9.29	1.38	1.28				
1878	8.57	1.38	1.18				
1877	9.11	1.39	1.26				
1876	10.13	1.39	1.41				
1875	9.20	1.40	1.29				
1874	8.75	1.41	1.23				
1873	11.31	1.42	1.60				
1872	7.19	1.43	1.03				
1871	7.97	1.44	1.14				
1870	7.82	1.44	1.13				
1869	8.61	1.45	1.25				
1868	7.51	1.46	1.10				
1867	7.66	1.47	1.13				
1866	7.51	1.48	1.11				
1865	7.51	1.49	1.12				
1864	8.60	1.50	1.29				
1863	7.51	1.51	1.13				
1862	8.37	1.50	1.26				
1861	6.85	1.49	1.02				
1860	7.72	1.49	1.15				
1859	8.12	1.48	1.20				

<sup>a</sup> Calculated from B/Ca maxima

<sup>b</sup> Annual resampling of density was done by Analyseries program (Paillard et al., 1996)

<sup>c</sup> Calculated with annual extension rate and annually resampled density data.

- Joins between core sections or distortion of growth along the LA-ICPMS tracks

Table E-9. Annual extension, density, and calcification data from a Fitzroy Reef core.

*Fitzroy Reef (FYR08-D)*

Year	Annual extension (mm yr <sup>-1</sup> ) <sup>a</sup>	Annual density (g cm <sup>-3</sup> ) <sup>b</sup>	Annual calcification (g cm <sup>-2</sup> yr <sup>-1</sup> ) <sup>c</sup>
2008	17.98	0.99	1.77
2007	16.00	0.99	1.58
2006	15.67	0.99	1.55
2005	16.83	0.98	1.65
2004	16.83	0.97	1.63
2003	18.83	0.96	1.81
2002	15.70	0.95	1.49
2001	18.34	0.94	1.73
2000	18.18	0.95	1.73
1999	19.00	0.96	1.82
1998	18.51	0.97	1.79
1997	16.86	0.97	1.64
1996	18.18	0.98	1.78
1995	14.22	1.01	1.43
1994	12.40	1.03	1.28
1993	14.87	1.05	1.57
1992	16.69	1.08	1.80
1991	12.89	1.10	1.42
1990	16.52	1.13	1.86
1989	17.35	1.11	1.92
1988	23.14	1.09	2.52
1987	16.40	1.07	1.76
1986	17.06	1.05	1.80
1985	15.41	1.02	1.58
1984	16.72	0.99	1.66
1983	16.21	0.96	1.56
1982	14.56	0.98	1.43
1981	14.39	1.00	1.44
1980	14.88	1.02	1.52
1979	18.02	1.04	1.88
1978	18.85	1.04	1.96
1977	16.87	1.04	1.75
1976	17.72	1.04	1.84
1975	14.07	1.03	1.45
1974	18.69	1.02	1.91
1973	19.17	1.02	1.95
1972	19.01	1.01	1.92
1971	15.87	1.00	1.59
1970	14.71	1.00	1.47
1969	14.38	0.99	1.43
1968	15.72	0.99	1.56
1967	14.40	0.99	1.42
1966	14.90	0.98	1.46
1965	15.40	0.98	1.51
1964	15.20	0.98	1.49
1963	17.51	0.98	1.71
1962	15.53	0.97	1.51
1961	14.21	0.98	1.39
1960	14.41	0.98	1.41
1959	16.08	0.98	1.58
1958	15.74	0.98	1.55
1957	14.58	0.99	1.45
1956	12.24	1.00	1.23
1955	17.00	1.01	1.72
1954	13.70	1.02	1.40
1953	17.17	1.03	1.77
1952	16.34	1.03	1.68
1951	11.55	1.03	1.19
1950	10.89	1.03	1.12

<sup>a</sup> Calculated from Sr/Cu maxima

<sup>b</sup> Annual resampling of density was done by Analyserics program (Paillard et al., 1996)

<sup>c</sup> Calculated with annual extension rate and annually resampled density data.



Appendices

**Table E-10.** Annual extension, density, and calcification data from a Lady Musgrave Island (LMI08-H).

*Lady Musgrave Island (LMI08-H)*

Year	Annual extension (mm yr <sup>-1</sup> ) <sup>a</sup>	Annual density (g cm <sup>-3</sup> ) <sup>b</sup>	Annual calcification (g cm <sup>-2</sup> yr <sup>-1</sup> ) <sup>c</sup>	Year	Annual extension (mm yr <sup>-1</sup> ) <sup>a</sup>	Annual density (g cm <sup>-3</sup> ) <sup>b</sup>	Annual calcification (g cm <sup>-2</sup> yr <sup>-1</sup> ) <sup>c</sup>
2008	9.76	1.34	1.31	1949	14.87	1.21	1.79
2007	9.59	1.34	1.29	1948	11.07	1.21	1.34
2006	8.44	1.34	1.13	1947	11.73	1.22	1.43
2005	10.92	1.34	1.47	1946	11.89	1.22	1.45
2004	10.26	1.34	1.37	1945	12.06	1.23	1.48
2003	13.57	1.34	1.81	1944	10.25	1.23	1.26
2002	11.25	1.33	1.50	1943	9.75	1.24	1.21
2001	12.71	1.33	1.69	1942	12.73	1.25	1.58
2000	11.72	1.32	1.55	1941	11.24	1.25	1.41
1999	14.53	1.32	1.91	1940	11.74	1.26	1.47
1998	14.03	1.31	1.84	1939	13.06	1.26	1.65
1997	7.92	1.30	1.03	1938	10.41	1.27	1.32
1996	9.91	1.29	1.28	1937	11.24	1.27	1.43
1995	10.41	1.29	1.34	1936	10.09	1.28	1.29
1994	9.91	1.28	1.27	1935	11.91	1.28	1.53
1993	12.88	1.27	1.64	1934	11.25	1.29	1.45
1992	10.41	1.26	1.31	1933	12.57	1.26	1.59
1991	12.22	1.25	1.53	1932	13.07	1.24	1.62
1990	11.73	1.25	1.46	1931	16.03	1.22	1.95
1989	13.71	1.24	1.70	1930	14.37	1.19	1.71
1988	12.07	1.23	1.49	1929	9.74	1.17	1.14
1987	11.74	1.22	1.44	1928	13.54	1.14	1.55
1986	11.58	1.21	1.41	1927	17.84	1.15	2.05
1985	10.75	1.21	1.30	1926	9.74	1.16	1.13
1984	13.73	1.20	1.65	1925	11.56	1.17	1.35
1983	11.91	1.20	1.43	1924	8.27	1.17	0.97
1982	10.75	1.20	1.29	1923	10.26	1.18	1.21
1981	12.08	1.20	1.44	1922	12.25	1.19	1.45
1980	11.90	1.20	1.42	1921	10.09	1.20	1.21
1979	11.07	1.19	1.32	1920	10.09	1.21	1.22
1978	11.56	1.19	1.38	1919	11.74	1.21	1.43
1977	12.55	1.19	1.50	1918	9.42	1.22	1.15
1976	12.22	1.19	1.46	1917	8.43	1.23	1.04
1975	11.23	1.20	1.35	1916	10.91	1.23	1.34
1974	11.89	1.20	1.43	1915	10.58	1.23	1.30
1973	14.20	1.20	1.71	1914	11.74	1.23	1.44
1972	10.24	1.21	1.23	1913	11.57	1.22	1.42
1971	11.72	1.21	1.42	1912	11.41	1.22	1.39
1970	11.39	1.21	1.38	1911	11.57	1.22	1.41
1969	13.04	1.21	1.58	1910	9.42	1.22	1.15
1968	17.00	1.21	2.05	1909	11.57	1.22	1.41
1967	10.73	1.21	1.29	1908	9.59	1.21	1.16
1966	11.06	1.20	1.33	1907	9.92	1.21	1.20
1965	10.07	1.20	1.21	1906	12.56	1.21	1.52
1964	11.56	1.20	1.39	1905	13.22	1.20	1.59
1963	11.06	1.20	1.33	1904	12.39	1.20	1.49
1962	11.89	1.20	1.43	1903	9.25	1.20	1.11
1961	12.55	1.21	1.51	1902	11.07	1.20	1.32
1960	13.38	1.21	1.62	1901	9.91	1.19	1.18
1959	18.41	1.21	2.23	1900	9.41	1.18	1.12
1958	19.47	1.21	2.36	1899	12.22	1.18	1.44
1957	18.50	1.21	2.24	1898	11.56	1.17	1.35
1956	15.97	1.21	1.94	1897	15.69	1.16	1.82
1955	12.46	1.21	1.51	1896	8.43	1.15	0.97
1954	11.01	1.21	1.33	1895	13.55	1.15	1.55
1953	9.25	1.21	1.12	1894	9.25	1.14	1.05
1952	9.41	1.21	1.14	1893	11.07	1.14	1.26
1951	7.10	1.21	0.86	1892	10.90	1.14	1.24
1950	11.40	1.21	1.38	1891	11.89	1.14	1.36
				1890	11.89	1.14	1.36

<sup>a</sup> Calculated from Sr/Ca maxima

<sup>b</sup> Annual resampling of density was done by Analyserics program (Paillard et al., 1996)

<sup>c</sup> Calculated with annual extension rate and annually resampled density data.

Appendices

**Table E-11.** Annual extension, density, and calcification data from a Lady Musgrave Island (LMI08-H).

<i>Lady Musgrave Island (LMI08-C-a)</i>			
Year	Annual extension (mm yr <sup>-1</sup> ) <sup>a</sup>	Annual density (g cm <sup>-2</sup> ) <sup>b</sup>	Annual calcification (g cm <sup>-2</sup> yr <sup>-1</sup> ) <sup>c</sup>
2008	4.37	1.56	0.44
2007	2.86	1.56	0.29
2006	5.57	1.56	0.56
2005	5.12	1.56	0.51
2004	4.97	1.56	0.50
2003	5.12	1.56	0.51
2002	5.57	1.56	0.56
2001	3.46	1.56	0.35
2000	5.87	1.55	0.59
1999	8.73	1.54	0.87
1998	6.17	1.54	0.62
1997	5.87	1.53	0.59
1996	3.31	1.52	0.33
1995	3.31	1.51	0.33
1994	4.52	1.50	0.45
1993	7.83	1.49	0.78
1992	4.43	1.49	0.44
1991	5.45	1.48	0.55
1990	4.79	1.47	0.48
1989	8.59	1.46	0.86
1988	6.11	1.45	0.61
1987	8.76	1.44	0.88
1986	4.79	1.44	0.48
1985	7.77	1.44	0.78
1984	8.59	1.44	0.86
1983	6.28	1.44	0.63
1982	9.09	1.45	0.91
1981	9.42	1.45	0.94
1980	10.41	1.45	1.04
1979	10.24	1.45	1.02
1978	10.73	1.46	1.07
1977	6.77	1.46	0.68
1976	6.93	1.46	0.69
1975	4.79	1.46	0.48
1974	6.11	1.47	0.61
1973	8.75	1.47	0.87
1972	7.43	1.47	0.74
1971	9.08	1.48	0.91
1970	7.43	1.48	0.74
1969	4.95	1.48	0.50
1968	6.77	1.48	0.68
1967	5.44	1.49	0.54
1966	6.60	1.49	0.66
1965	4.45	1.49	0.45
1964	4.78	1.50	0.48
1963	4.12	1.50	0.41
1962	3.96	1.50	0.40
1961	2.80	1.50	0.28
1960	3.79	1.50	0.38
1959	8.08	1.50	0.81
1958	6.10	1.50	0.61
1957	4.62	1.50	0.46
1956	8.74	1.50	0.87

<sup>a</sup> Calculated from Sr/Ca maxima

<sup>b</sup> Annual resampling of density was done by Analyseries program (Paillard et al., 1996)

<sup>c</sup> Calculated with annual extension rate and annually resampled density data.